

Multi-Photon Phosphor Feasibility Research

Advanced Light Source Development
U.S. Dept. of Energy Contract with
EPRI: DE-FC26-00NT40987
Reporting Period 10/01/00 to 3/31/02

1007799

Final Report, May 2003

Cosponsors
U.S. Department of Energy
National Energy Technology Laboratory
3610 Collins Ferry Road
P.O. Box 10940, M/S E06
Morgantown, WV 26507-0080

Project Manager
C. Christy

Osram Sylvania, Inc.
71 Cherry Hill Drive
Beverly, MA 01915
Research Manager
D. Bay

EPRI Project Managers
R. Graham
W. Chow

DISCLAIMER OF WARRANTIES AND LIMITATION OF LIABILITIES

THIS DOCUMENT WAS PREPARED BY THE ORGANIZATION(S) NAMED BELOW AS AN ACCOUNT OF WORK SPONSORED OR COSPONSORED BY THE ELECTRIC POWER RESEARCH INSTITUTE, INC. (EPRI). NEITHER EPRI, ANY MEMBER OF EPRI, ANY COSPONSOR, THE ORGANIZATION(S) BELOW, NOR ANY PERSON ACTING ON BEHALF OF ANY OF THEM:

(A) MAKES ANY WARRANTY OR REPRESENTATION WHATSOEVER, EXPRESS OR IMPLIED, (I) WITH RESPECT TO THE USE OF ANY INFORMATION, APPARATUS, METHOD, PROCESS, OR SIMILAR ITEM DISCLOSED IN THIS DOCUMENT, INCLUDING MERCHANTABILITY AND FITNESS FOR A PARTICULAR PURPOSE, OR (II) THAT SUCH USE DOES NOT INFRINGE ON OR INTERFERE WITH PRIVATELY OWNED RIGHTS, INCLUDING ANY PARTY'S INTELLECTUAL PROPERTY, OR (III) THAT THIS DOCUMENT IS SUITABLE TO ANY PARTICULAR USER'S CIRCUMSTANCE; OR

(B) ASSUMES RESPONSIBILITY FOR ANY DAMAGES OR OTHER LIABILITY WHATSOEVER (INCLUDING ANY CONSEQUENTIAL DAMAGES, EVEN IF EPRI OR ANY EPRI REPRESENTATIVE HAS BEEN ADVISED OF THE POSSIBILITY OF SUCH DAMAGES) RESULTING FROM YOUR SELECTION OR USE OF THIS DOCUMENT OR ANY INFORMATION, APPARATUS, METHOD, PROCESS, OR SIMILAR ITEM DISCLOSED IN THIS DOCUMENT.

ORGANIZATION(S) THAT PREPARED THIS DOCUMENT

Gough & Associates, Inc.

Osram Sylvania, Inc.

NOTICE: THIS REPORT WAS PREPARED AS AN ACCOUNT OF WORK SPONSORED BY AN AGENCY OF THE UNITED STATES GOVERNMENT. NEITHER THE UNITED STATES GOVERNMENT NOR ANY AGENCY THEREOF, NOR ANY OF THEIR EMPLOYEES, MAKES ANY WARRANTY, EXPRESS OR IMPLIED, OR ASSUMES ANY LEGAL LIABILITY OR RESPONSIBILITY FOR THE ACCURACY, COMPLETENESS, OR USEFULNESS OF ANY INFORMATION, APPARATUS, PRODUCT, OR PROCESS DISCLOSED, OR REPRESENTS THAT ITS USE WOULD NOT INFRINGE PRIVATELY OWNED RIGHTS. REFERENCE HEREIN TO ANY SPECIFIC COMMERCIAL PRODUCT, PROCESS, OR SERVICE BY TRADE NAME, TRADEMARK, MANUFACTURER, OR OTHERWISE DOES NOT NECESSARILY CONSTITUTE OR IMPLY ITS ENDORSEMENT, RECOMMENDATION, OR FAVORING BY THE UNITED STATES GOVERNMENT OR ANY AGENCY THEREOF. THE VIEWS AND OPINIONS OF AUTHORS EXPRESSED HEREIN DO NOT NECESSARILY STATE OR REFLECT THOSE OF THE UNITED STATES GOVERNMENT OR ANY AGENCY THEREOF.

ORDERING INFORMATION

Requests for copies of this report should be directed to EPRI Orders and Conferences, 1355 Willow Way, Suite 278, Concord, CA 94520, (800) 313-3774, press 2 or internally x5379, (925) 609-9169, (925) 609-1310 (fax).

Electric Power Research Institute and EPRI are registered service marks of the Electric Power Research Institute, Inc. EPRI. ELECTRIFY THE WORLD is a service mark of the Electric Power Research Institute, Inc.

Copyright © 2003 Electric Power Research Institute, Inc. All rights reserved. This paper was written with support of the U.S. Department of Energy under Contract No. DE-FC26-00NT40987. The Government reserves for itself and others acting on its behalf a royalty-free, nonexclusive, irrevocable, worldwide license for Governmental purposes to publish, distribute, translate, duplicate, exhibit, and perform this copyrighted paper.

CITATIONS

This report was prepared by

Gough & Associates, Inc.
2626 Laurel Park Highway
Hendersonville, NC 28739

Principal Investigator
A. Gough

Osram Sylvania, Inc.
71 Cherry Hill Drive
Beverly, MA 01915

Principal Investigator
K. Mishra

This report describes research sponsored by EPRI, U.S. Department of Energy
and Osram Sylvania, Inc.

The report is a corporate document that should be cited in the literature in the following manner:

Multi-Photon Phosphor Feasibility Research: Advanced Light Source Development, U.S. Dept. of Energy Contract with EPRI: DE-FC26-00NT40987, Reporting Period 10/01/00 to 3/31/02, EPRI, Palo Alto, CA, U.S. Department of Energy, Morgantown, WV, and Osram Sylvania, Inc., Beverly, MA: 2003. 1007799.

PRODUCT DESCRIPTION

Development of multi-photon phosphor materials for discharge lamps represents a goal that would achieve up to a doubling of discharge (fluorescent) lamp efficacy. This report reviews the existing literature on multi-photon phosphors, identifies obstacles in developing such phosphors, and recommends directions for future research to address these obstacles. To critically examine issues involved in developing a multi-photon phosphor, the project brought together a team of experts from universities, national laboratories, and an industrial lamp manufacturer.

Results & Findings

Results and findings are organized into three categories: (1) Multi-Photon Systems and Processes, (2) Chemistry and Materials Issues, and (3) Concepts and Models.

Multi-Photon Systems and Processes: This category focuses on how to use our current understanding of multi-photon phosphor systems to design new phosphor systems for application in fluorescent lamps. The quickest way to develop multi-photon lamp phosphors lies in finding sensitizer ions for Gd^{3+} and identifying activator ions to red shift the blue emission from Pr^{3+} due to the $^1\text{S}_0 \rightarrow ^1\text{I}_6$ transition associated with the first cascading step. Success in either of these developments would lead to more efficient fluorescent lamps.

Chemistry and Materials Issues: The most promising multi-photon phosphors are found in fluoride hosts. However, stability of fluorides in environments typically found in fluorescent lamps needs to be greatly improved. Experimental investigation of fluorides in actual lamp environments needs to be undertaken while working on oxide and oxyfluoride alternative systems for backup.

Concepts and Models: Successful design of a multi-photon phosphor system based on cascading transitions of Gd^{3+} and Pr^{3+} depends critically on how the former can be sensitized and the latter can sensitize an activator ion. Methods to predict energy level diagrams and Judd-Ofelt parameters of multi-photon transitions are needed to help guide the experimental material selection.

Challenges & Objectives

This report provides the theoretical basis for leading knowledgeable researchers along the path to develop multi-photon phosphor systems. The ultimate goal, a doubling of fluorescent lamp efficacy, is not going to be easily obtained. This report begins the process and should be followed with detailed experimental and theoretical research to continue the development process.

Applications, Values & Use

The evolving research to improve discharge lamp efficacy will need to be done in an orderly, precise manner. The results described here lay out the next steps to follow.

EPRI Perspective

The team that was assembled to perform this feasibility research represents a unique approach to solving this difficult problem. It is important to continue this effort, with the team intact, to reach the research goals.

Approach

The team that was selected was divided into twelve small groups, with some researchers serving in more than one group. Each group was given a specific task and then wrote a report with their findings. The findings appear under Results & Findings.

Keywords

Discharge lamps

Fluorescent lamps

Phosphors

Multi-photon phosphors

Rare earth materials

ABSTRACT

This Final Report provides the background, process, and results from the feasibility research of developing a multi-photon phosphor material for use in discharge (fluorescent) lamps. The research program culminated in a two-day Workshop held in Peabody, MA on February 27-28, 2002. At this meeting, Feasibility Research Plans for 12 tasks related to the identification, preparation, and testing of multi-photon phosphor candidate materials were presented. The Feasibility Research Plans were prepared by a team of experts from universities, national laboratories, and an industrial lamp manufacturer to critically examine the issues involved in developing a multi-photon phosphor. Recommendations for the next steps in this process are given for each of the 12 tasks.

ACKNOWLEDGMENTS

U.S. Department of Energy

This Final Report for the Multi-Photon Phosphor Feasibility Research project was prepared with the support of the U.S. Department of Energy, under Award No. DE-FC26-00NT40987. However, any opinions, findings, conclusions, or recommendations expressed herein are those of the authors and do not necessarily reflect the views of DOE. The goal of the DOE's competitive Lighting Research and Development (LR&D) Program is to develop viable technologies having the technical potential to conserve 50% of lighting consumption by 2010. The Program partners with industry, utilities, universities, and research institutions to create energy efficient lighting technologies in pursuit of this goal.

Multi-Photon Phosphor Feasibility Research Project Participants

EPRI thanks the many participants in the Multi-Photon Phosphor (MPP) Feasibility Research Project for their leadership, expertise and contributions in making this project successful. The complete list of these participants is provided on the following page as a continuation of this Acknowledgements section. Thanks also go to Prof. B. Di Bartolo and Prof. D. Keszler for their efforts as technology group leaders in organizing Workshop-I. Also, Prof. Di Bartolo is recognized for his continuing support in organizing Workshop-II.

A major portion of the feasibility research efforts during the June 2001 to February 2002 period was carried out by twelve task teams. Each of these task team leaders and their members are particularly thanked for their extensive work in completing the feasibility research and the final task team reports. A listing of these task teams is provided on pages 3-2 and 3-3 of this report. The individual team reports are provided in Appendix B.

EPRI particularly thanks and recognizes Osram Sylvania, Inc. (OSI) as its co-sponsor for the MPP Project. In particular, EPRI acknowledges the OSI management leadership and support from Drs. John Gustafson, Gus Bandyopadhyay, Voitek Byszewski and Mr. David Bay. OSI's Dr. Kailash Mishra is recognized for his key role in integrating and leading the scientific focus of the program among the many participants.

EPRI and the Project Team thank Mr. Alfred Gough, the MPP Project Manager, for his successful leadership of the entire project and the workshops.

EPRI has had the opportunity to respond to the U.S. Department of Energy (DOE) public solicitations for proposals that included research in the areas of energy efficient products. EPRI applauds and fully supports the DOE for establishing this open and equitable process, and also commends the personnel at the National Energy Technology Laboratory for their professional management of the program.

As part of the process in responding to the DOE Public Solicitations, EPRI and its proposal partners expended significant manpower in preparing their proposals. In 1999 and 2000 EPRI responded with two separate proposals. The 1999 proposal was not accepted, but the 2000 proposal on “Multi-Photon Phosphor Feasibility Research” was accepted. Recognition goes to EPRI’s Roger Bedard for his coordination and production of both proposals, and the “first in EPRI’s history competitive award from DOE”. Recognition for the Multi-Photon Phosphor Feasibility Research project award also goes to Osram Sylvania, Inc. (OSI) for its participation and technical leadership in preparing the proposal.

Multi-Photon Phosphor Feasibility Research Project Participants

Affiliation	Location	Name
EPRI Prime Contract with USDOE Project Co-funder	Palo Alto, CA	Dr. John P. Kesselring
Gough & Associates, Inc. Research Agreement with EPRI	Hendersonville, NC	Alfred B. Gough
Los Alamos National Laboratory CRADA with EPRI	Los Alamos, NM	Dr. Jeff Hay Dr. Joel Kress
Osram Sylvania, Inc. Project Co-funder	Beverly, MA Towanda, PA	David Bay Dr. Voitek Byszewski Earnest Dale Dr. Arun Dutta Roger B. Hunt, Jr. Dr. Kailash C. Mishra Dr. Madis Raukas Dr. Barry G. DeBoer
Osram GmbH	Munich, Germany	Dr. Ard Ellens Dr. Martin Zachau
Independent Researchers		
Research Subcontracts with Gough & Associates, Inc		
Boston College	Newton, MA	Prof. B. Di Bartolo
College of the Holy Cross	Worcester, MA	Prof. R. S. Rana
Consultant (OSI Retired)	Wrentham, MA	Dr. Charles W. Struck
Lawrence Berkeley National Lab.	Berkeley, CA	Dr. Marvin J. Weber
Massachusetts Institute of Technology	Cambridge, MA	Prof. Keith Johnson
NASA LaRC	Hampton, VA	Dr. Norman P. Barnes
Oregon State University	Corvallis, OR	Prof. Douglas Keszler
Penn State University	University Park, PA	Prof. William B. White
Univ. of California at San Diego	San Diego, CA	Prof. Joanna McKittrick
Univ. of Georgia	Athens, GA	Prof. Richard S. Meltzer
Utrecht University	Utrecht, The Netherlands	Prof. Andries Meijerink
Wheaton College	Norton, MA	Prof. John Collins

CONTENTS

1 BACKGROUND.....	1-1
Lighting Importance.....	1-1
The Problem to be Addressed	1-1
The Potential	1-2
The Approach.....	1-2
Program 1: Non-Equilibrium, Low Pressure Electric Discharge Light Sources	1-2
Program 2: Multiphoton Phosphors (“Quantum Splitters”).....	1-3
2 FEASIBILITY RESEARCH PROCESS	2-1
Research Participants	2-1
Research Process Outline	2-2
Step 1: Preparation for Initial Workshop (Workshop-I)	2-2
Step 2: Initial Workshop (Workshop-I).....	2-2
Step 3: Feasibility Research	2-2
Step 4: Second Workshop (Workshop-II)	2-2
Step 5: Final Report.....	2-2
3 FEASIBILITY RESEARCH PLANNING	3-1
Workshop-I.....	3-1
Individual Task Planning.....	3-1
4 AGENDA	4-1
Multi-Photon Phosphor	4-1
5 FINAL REPORT SUMMARY – CONCLUSIONS AND RECOMMENDATIONS	5-1
Workshop-II.....	5-1
Final Report Overview	5-1
Project Organization	5-2
Conclusions and Recommendations	5-2

Multi-Photon Systems and Processes.....	5-2
Chemistry and Material Issues.....	5-3
Concepts and Models	5-4
A FEASIBILITY RESEARCH PLANS.....	A-1
Task 1 Research Plan: Optical/Plasma Testing of Fluorides.....	A-1
Task 2 Research Plan: Bulk and Surface Defects	A-4
Task 3 Research Plan: New Oxides for Pr^{3+} Cascading	A-5
Task 4 Research Plan: Sensitizer for Gd^{3+}	A-7
Task 5 Research Plan: Cascading from Gd^{3+} in Oxides	A-9
Task 6 Research Plan: Modeling.....	A-11
Task 7 Research Plan: Sugano-Tanabe Diagram for Transition Metal Candidates.....	A-13
Task 8 Research Plan: Conversion of 407 nm to Red or Green	A-14
Task 9 Research Plan: New Green	A-16
Task 10 Research Plan: Search for New Cascading Ions.....	A-17
Task 11 Research Plan: Two Photon Emission from Hg 254 nm Excitation.....	A-19
Task 12 Research Plan: Synthesis and Chemical Stability of Fluorides.....	A-20
B FINAL RESEARCH TASK REPORTS	B-1
Task 1: Optical/Plasma Testing of Fluorides.....	B-1
Introduction.....	B-1
Defect Formation in Fluorides.....	B-2
Influence of Impurities and Surface.....	B-4
Optical Testing.....	B-6
Conclusions and Recommendations.....	B-10
High Quality Fluoride Single Crystals	B-10
Crystalline Fluoride Materials with Impurities.....	B-10
Optical Testing	B-10
Recommendations	B-10
Task 2: Bulk and Surface Defects in Fluorides	B-12
Part I (D. Keszler)	B-12
Conclusions and Recommendations	B-14
Part II (M. Raukas).....	B-15
Introduction	B-15
Phosphor Degradation in Lamps	B-15

Defect Formation.....	B-17
Conclusions	B-21
Recommendations	B-22
Part III (W. White)	B-22
Task 3: New Oxides for Pr^{3+} Cascading	B-24
Subtask A: New Oxide Systems for Pr^{3+} (Low-lying $^1\text{S}_0$)	B-24
Subtask B Maximize Radiative $^1\text{S}_0 \rightarrow ^1\text{I}_6$ Transition	B-26
Subtask C Minimize Nonradiative $^3\text{P}_0$ -to- $^1\text{D}_2$ Transitions	B-28
Conclusions and Recommendations	B-31
Task 4: Sensitizer for Gd^{3+}	B-32
Introduction.....	B-32
Charge Transfer.....	B-34
s^2 Ions.....	B-38
fd Transitions	B-42
Host Lattice Excitation	B-45
Conclusions	B-46
Charge Transfer Transitions.....	B-47
s^2 Ions.....	B-47
$4f^{n-1}5d$ Luminescence	B-47
Host Lattice	B-47
Task 5: $\text{Gd}^{3+} \text{ } ^6\text{G}$ Based 2 Photon Generation in Oxide Solids	B-48
Introduction.....	B-48
Possible Oxide Hosts for $\text{Gd}^{3+} \text{ } ^6\text{G}_{7/2}$ Sensitized Phosphors	B-48
The Activator for Visible Emissions	B-49
Eu^{3+}	B-49
Other Activators than Eu^{3+}	B-53
Recommendations.....	B-53
Bibliography.....	B-53
Appendix.....	B-54
Barnes 5-30-01	B-54
Task 6: Modeling.....	B-58
Objective.....	B-58
Subtask A.....	B-58
Subtask B.....	B-59

Subtask C	B-59
Subtask D	B-60
Subtask E.....	B-60
Final Task.....	B-61
Background and Elaboration.....	B-61
Judd-Ofelt Parameters	B-61
Multiphonon Relaxation.....	B-62
Computing Electronic-Structure-Properties of Potential Activators	B-62
Task 7: Sugano-Tanabe Diagram for Transition Metal Candidates.....	B-64
Conclusions	B-64
Recommendations for Future Research	B-76
Report on Cascade Phosphors.....	B-76
Free Ion Parameters	B-76
Tanabe-Sugano Diagrams	B-77
Data for Crystal Field Parameters	B-78
Interpretation and Conclusions.....	B-81
Task 8: Conversion of 407 nm to Red or Green.....	B-89
Introduction.....	B-89
Subtask A: Potential Rare Earth Candidates for Energy Transfer	B-90
Subtask B: Energy Transfer Rates.....	B-92
Subtask C: Spectral Output of the Systems	B-94
Subtask D: Transition Metal Activators for Energy Transfer	B-95
Sensitization of $3d^n$ Transition Metal Ions	B-95
Sensitization of $4d^n$ and $5d^n$ Transition Metal Ions	B-98
Conclusions and Recommendations.....	B-101
Conclusions: Subtasks A-C.....	B-101
Recommendations: Subtasks A-C.....	B-102
Conclusions: Subtask D	B-102
Recommendations – Subtask D	B-103
Task 9: New Green	B-104
Recommendations.....	B-104
Summary of Investigation	B-104
Introduction	B-104
Spectral Requirements of a Green Emitting Activator Ion.....	B-105

Lamp Requirements for Generating White Light.....	B-105
Review of Green Emitting Phosphors	B-106
Transitions within the f^N Manifold.....	B-109
5d→4f Transitions.....	B-112
Task 10: New Cascading Ions.....	B-113
Purpose of Task 10	B-113
Subtask A	B-113
Subtask B	B-113
Subtask A	B-113
Conclusions	B-113
Recommendations.....	B-114
Subtask B	B-114
Conclusions	B-114
Recommendations.....	B-114
Appendices.....	B-115
Appendix 10A: Potential Lanthanide Series Atoms for a 2:1 Quantum Efficiency.....	B-115
Introduction	B-115
Technical Discussion	B-116
Appendix 10B: High Efficiency Lighting Quantum Efficiency Greater than Unity Prospects.....	B-119
Potential Discharges.....	B-120
Phosphors.....	B-121
Quantum Efficiency Physics	B-123
Appendix 10C: A Computer Program to Calculate Energy Mismatches	B-126
Pr to REI Energy Transfer.....	B-127
Gd to REI Energy Transfer	B-133
Task 11: Two-Photon Emission from Hg 254 nm Excitation	B-139
Quantum Cutting by Energy Transfer.....	B-139
Introduction	B-139
Limitations Imposed by the Physics of Energy Cascade Processes	B-139
Absorption of Excitation	B-140
Host Excitonic Absorptions	B-141
Quantum Cutter Schemes Involving Energy Transfer	B-141
Recommendations for Approach Using Energy Transfer	B-144
General Bibliography for Section I	B-144

Mishra. 12-13-01 Tm ³⁺ as an Activator or Sensitizer Ion for Designing Multi-Photon Phosphors for 254 nm Emission.....	B-145
Introduction	B-145
Multi-Photon Scheme for Tm ³⁺	B-146
Conclusion	B-147
Recommendation.....	B-147
Bibliography	B-148
Raukas MPP for 254 nm Emission from Hg-Discharge: Experimental.....	B-148
Discussion	B-148
Recommendations.....	B-150
Additional Bibliography Regarding Tm ³⁺	B-151
Task 12: Phosphor Synthesis and Processing.....	B-152
Conclusions from Original Objectives.....	B-152
Recommendations of Promising Research Topics.....	B-152
Background	B-153
Multiple Task Report: Los Alamos National Laboratory	B-154
Task 2: Bulk and Surface Defects in Fluorides.....	B-154
Empirical Potential Modeling.....	B-155
Ab Initio Simulations	B-155
Tasks 6 and 7: Multiplet States of Transition Metal and Lanthanide Ions in Fluoride and Oxide Lattices.....	B-156
Details of the Calculation	B-156
Cluster Models.....	B-156
Basis Sets and Effective Core Potentials.....	B-157
Self-Consistent Field and Configuration Interaction Calculations	B-157
Results.....	B-157
Ni ²⁺ in 6-Fold Fluoride Site (KNiF ₃)	B-157
Nb ³⁺ in 6-Fold Oxide Site (ABO ₃) and 7-Fold Oxide Site (La ₂ O ₃).....	B-157
Pr ³⁺ in 7-Fold Oxide Site (La ₂ O ₃)	B-158
Discussion	B-158
References	B-162

LIST OF FIGURES

Figure B-1 Transmission Spectra of CaF_2 Crystals at 295 K. (a) Freshly Cleaved (1) and Polished (2) Samples. (b) Polished Samples before (2) and after (1) a Thermal Treatment. (c) Freshly Cleaved (1), Aged (2), Polished (3), Polished and Chemically Etched (4) Surface of Samples Cleaved from the Same CaF_2 Crystal. Reproduced from Reference [25].	B-5
Figure B-2 (a) Emission Spectrum of a $\text{LiGdF}_4:\text{Eu}^{3+}$ 0.1% Polycrystalline Sample before VUV Irradiation, (b) Time Evolution of the Emission Intensity During VUV Irradiation and (c) Emission Spectrum after Irradiation. The Gradual Increase in the Emission Intensity is due to the Slow Removal of Trace Amounts of Oxygen in the Spectrofluorometer. The Periodic Structure is due to Periodic Variations in the Lamp Intensity.	B-8
Figure B-3 (a) Emission Spectrum of $\text{LiYF}_4:\text{Er}^{3+}$ 4% Single before VUV Irradiation, (b) Time Evolution of the Emission Intensity During VUV Irradiation and (c) Emission Spectrum after Irradiation. The Periodic Structure is due to Periodic Variations in the Lamp Intensity.	B-9
Figure B-4 Quantum Cutting through Downconversion for the Gd-Eu Couple in $\text{LiGdF}_4:\text{Eu}^{3+}$	B-32
Figure B-5 Schematic Picture of Energy Transfer from an Ideal Sensitizer to the ^6G Level of Gd^{3+}	B-34
Figure B-6 Emission (exc=140 nm) and Excitation (em=270 nm) Spectra of Yb^{3+} in ScPO_4 at 10 K. in the Emission Spectrum the Broken and Drawn line are Emission Spectra Recorded with Different Detection Set-up (VUV/UV Broken Line, UV/VIS Drawn).	B-35
Figure B-7 Energy Level Diagram for s^2 Ions	B-39
Figure B-8 Excitation Spectrum (Solid) of $\text{CaF}_2:\text{Pb}^{2+}$ for the A-band Emission at 220 nm and Emission Spectrum (Dotted) upon Excitation in the C-band at 152 nm (T=10 K)	B-40
Figure B-9 Excitation Spectrum of the A-band Emission at 217 nm (Drawn Line) and Emission Spectrum for 135 nm Excitation (Broken Line) for $\text{KMgF}_3:\text{Pb}^{2+}$ at 10 K	B-42
Figure B-10 Emission Spectra of (a) Ce^{3+} (1%), (b) Pr^{3+} (2%), (c) Nd^{3+} (5%), (d) Er^{3+} (1%) and (e) Tm^{3+} (1%) Incorporated in LiYF_4 , Recorded upon Excitation the $4f^{n-1}5d$ Levels	B-44
Figure B-11 $\text{Gd} f^8$ States and Offset Feeding State	B-49
Figure B-12 Diagram from Meijerink Showing the Sequence of Energy Transfers from Gd to Two Eu Ions	B-50

Figure B-13 Extension of the Dicke Diagram in the VUV Region. For the Ions in the Middle of the Series (Sm through Dy) Only the Strongest Experimentally Observed Lines are Included. Assignments for Sm and Dy are Lacking Since Energy Level Calculations have not been Performed Yet.....	B-51
Figure B-14 Defining Color: CIE Chromaticity Diagram.....	B-106
Figure B-15 Absorption Spectrum of Ag ⁺ at 77 K in KCL	B-108
Figure B-16 Excitation and Emission Spectra of Mn ²⁺ in LaAl ₁₁ O ₁₈	B-109
Figure B-17 Energy Level Diagram for Ln ³⁺ in LaCl ₃ . Transitions up to Energies Slightly Higher than that of ⁵ D ₄ State of Tb ³⁺ are Indicated.....	B-110
Figure B-18	B-142
Figure B-19	B-143
Figure B-20 Energy Level Diagram of Tm ³⁺ in Y ₂ O ₃ and Pr ³⁺ in LaF ₃ . Since the Energy Levels of Pr ³⁺ in Y ₂ O ₃ are not well Resolved, those in LaF ₃ are used.	B-145
Figure B-21 Variation of Quantum Efficiency (QE) for the ³ P ₂ to ¹ G ₄ Transition with Ω_2 , Ω_4 and Ω_6 Note the Strong Dependence of QE on Ω_2 (Red Line)	B-146
Figure B-22 Excitation Spectra of Y ₂ O ₃ :Tm for 453, 771, 778 and 780 nm Emissions at 22K.....	B-149

LIST OF TABLES

Table 2-1 Participants in the Multiphoton Phosphor Feasibility Research Project (MPP Project)	2-1
Table 3-1 Task Outline: Leaders, Members and Description	3-2
Table B-1 Literature Studies on Defect Formation and Optical Testing of Undoped Fluorides	B-3
Table B-2 Literature Studies on Defect Formation and Optical Testing of Doped Fluoride Crystals	B-6
Table B-3 Approximate Energy Values of Defect Formation in Solids	B-18
Table B-4 Formation Energies of a Neutral Oxygen Vacancy in MgO [65]	B-20
Table B-5 Properties of Demonstrated Oxide Pr^{3+} Phosphors with Low-lying $^1\text{S}_0$	B-25
Table B-6 Demonstrated and Potential Oxide Hosts with Low-lying $^1\text{S}_0$ Level and some of their Optical Properties. (Bold Indicates Observation of Low-lying $^1\text{S}_0$.)	B-27
Table B-7 Experimental Judd-Ofelt Parameters for Pr^{3+}	B-28
Table B-8 Approximate Frequencies of the Highest Energy Phonons in Oxide and Fluoride Hosts	B-30
Table B-9 Charge Transfer Luminescence Properties for Yb^{3+} in Various Host Lattices [118]	B-37
Table B-10 Position of Absorption and Emission Bands of Pb^{2+} in Various Fluoride Host Lattices. Most Data are from Unpublished Results of Oskam et al.	B-41
Table B-11 Data on Host Lattice Luminescence in some Oxides and Fluorides (Data from References [118, 157])	B-46
Table B-12 Racah Parameters for Free Ions of the First Transition Series	B-77
Table B-13 Racah Parameters for M^{4+} Ions	B-77
Table B-14 Crystal Field Parameters for Ti^{3+}	B-78
Table B-15 Crystal Field Parameters for V^{3+}	B-78
Table B-16 Crystal Field Parameters for Cr^{3+}	B-79
Table B-17 Crystal Field Parameters for Cr^{2+}	B-79
Table B-18 Crystal Field Parameters for Mn^{3+}	B-79
Table B-19 Crystal Field Parameters for Mn^{2+}	B-80
Table B-20 Crystal Field Parameters for Fe^{3+}	B-80
Table B-21 Crystal Field Parameters for Fe^{2+}	B-80
Table B-22 Crystal Field Parameters for Co^{2+}	B-81
Table B-23 Crystal Field Parameters for Ni^{2+}	B-81

Table B-24 Candidate Rare Earth Ions for Energy Transfer from Pr^{3+} Corresponding to the $^1\text{S}_0 \rightarrow ^1\text{I}_6$ Transition. In Order to Obtain some Typical Numerical Energies, Values are taken from the Example of Rare Earths in LaF_3 where the Energy Levels are Well-known.....	B-90
Table B-25 Selection Rules for Energy Transfer Between Two Rare Earth Ions Involving States within the f-manifold	B-91
Table B-26 Emission from Third and Fourth Row Transition Metal Ions.....	B-100
Table B-27 Experimentally Observed Terms of Zr^{2+} , Nb^{3+} and Mo^{4+}	B-101
Table B-28 Racah Parameters (cm^{-1}) of Zr^{2+} , Nb^{3+} and Mo^{4+}	B-101
Table B-29 Crystal Field Parameters (Theory) for Mo^{4+} and Nb^{3+}	B-101
Table B-30 Mn^{2+} Sites and Luminescence Properties.....	B-109
Table B-31 Transitions from Candidate Green Emitting Rare Earth Ions	B-111
Table B-32 Emission Spectra in Electric Discharges.....	B-120
Table B-33 Properties of Host Materials	B-123
Table B-34 Pr to Nd Transfer Paths.....	B-127
Table B-35 Pr to Sm Transfer Paths.....	B-128
Table B-36 Pr to Eu Transfer Paths.....	B-129
Table B-37 Pr to Tb Transfer Paths	B-130
Table B-38 Pr to Dy Transfer Paths.....	B-130
Table B-39 Pr to Ho Transfer Paths.....	B-131
Table B-40 Pr to Er Transfer Paths.....	B-132
Table B-41 Pr to Tm Transfer Paths	B-133
Table B-42 Gd to Pr Transfer Paths	B-133
Table B-43 Gd to Nd Transfer Paths	B-134
Table B-44 Gd to Sm Transfer Paths.....	B-135
Table B-45 Gd to Eu Transfer Paths.....	B-135
Table B-46 Gd to Dy Transfer Paths.....	B-136
Table B-47 Gd to Ho Transfer Paths	B-137
Table B-48 Gd to Er Transfer Paths	B-138
Table B-49 Gd to Tm Transfer Paths.....	B-138
Table B-50 Judd-Ofelt Parameters (in 10^{-20} cm^2) for Tm^{3+}	B-147
Table B-51 Modeling & Simulation Needs for Multi-Photon Phosphors.....	B-159
Table B-52 Electronic States of Ni^{2+} (d^8) in Octahedral site in KNiF_3	B-160
Table B-53 Calculated Electronic States of Nb^{3+} (d^2) in Six-Fold Oxide Site in ABO_3 Perovskite and in Seven-Fold Oxide Site in La_2O_3	B-160
Table B-54 Results of Pr^{3+} (f^2) in 7-Fold Oxide Site (C_{3v} Symmetry) in La_2O_3	B-161

1

BACKGROUND

Lighting Importance

Lighting consumes about 20 to 23% of the electric power production of the nation.

Development of significantly more efficient “white” light sources (suitable for general lighting applications) has the potential to reduce substantially the electric power consumption for lighting. This would limit the rate-of-increase of electric power consumption, permit avoidance of costs for new generating capacity, and result in less greenhouse gas (and other pollutant) emission. In fact, reduction of energy consumption by lighting and other current uses is the most efficient and environmentally sound way that the nation’s power system can absorb (without new generating capacity) the added loads.

A large number of studies have been completed and published on the potential of energy savings through energy conservation measures. The U.S. Department of Energy’s Energy Information Agency (EIA) continues to implement a broad array of surveys and related reports regarding the potential for energy savings and the current and potential results of various measures. For example, the commercial building sector accounts for approximately 30 to 35% of the U.S. electrical demand, and is estimated to utilize approximately 35 to 40% of its energy for lighting, and another five to ten percent for air-conditioning driven by cooling of the lighting heat generation. Various estimates have indicated a potential of 25 to 50% potential of energy savings in the commercial sector utilizing existing technology. From a lighting standpoint, the main focus has been on moving the average efficiency from the 40 to 50 lumens per watt (older fluorescent technology) upward toward the newer fluorescent systems now beginning to approach 100 lumens per watt. The future programs which are described in this report are aimed at breakthrough basic research to achieve approximately 200 lumens per watt for commercially applicable light sources.

The Problem to be Addressed

Efficiencies of Commercial Light Sources have reached a plateau.

After increasing steadily throughout the previous seventy-five years, efficiency of conversion of electric energy into light by commercial light sources appears to have reached a plateau, about 33% maximum. No truly revolutionary light sources have been introduced since the mid-1960s, marked by the debut of metal halide and high-pressure-sodium arc discharge lamps. Light source developments since then have been primarily evolutionary, with incremental improvements in efficiency. Overall system gains in lighting efficiency have in the last decade primarily resulted from the substitution of more efficient sources for less efficient ones (viz. Compact fluorescent replacing incandescent).

The Potential

To *achieve* the continued energy savings challenges that will be required in the future, ***much greater efficiency improvements, of about a factor of two***, will be required. That such an increase is not ruled out by thermodynamic considerations is explained by the fact that the fluorescent lamp generates radiation at greater than 50% efficiency, even if ultraviolet instead of visible. Then conversion of UV to visible by phosphors results in reduction of the overall efficiency to 25%. An ideal multi-colored spectrum of principally visible light which, taken as a whole, is “white” in visual color, will be comprised of red, green and blue emission lines near 610, 555 and 450 nm, respectively, and have no emission lines longer than 650 nm or shorter than 450 nm. Such a spectrum would have a luminous efficacy of 300 lumens per radiant watt and would be suitable for most lighting applications.

The Approach

Technology assessment, research agenda development, research program prioritization:

Two major programs have been identified, further developed and prioritized by the EPRI consortium. These programs are more completely described in the collaborative technology planning work and the culminating workshop report EPRI TR-106022 entitled “***ALITE ‘95 Industry and Government Co-Sponsored Workshop-Pre-competitive Research in the Basic Science of Commercial Light Sources to Achieve Major Breakthroughs in Performance and Efficiency.***”

- Program 1: Non-Equilibrium, Low Pressure Electric Discharge Light Sources
- Program 2: Multiphoton Phosphors (“Quantum Splitters”)

This workshop established the basis for the formation of an advanced light source research consortium. The consortium addresses the fact that the efficiency of current light sources has reached a plateau with no new higher efficiency light sources being introduced since metal halide and high-pressure sodium arc discharge lamps in the 1960s. Since lighting use consumes 20 to 23% of U.S. electricity production and 35 to 40% of the electricity use in commercial buildings, significantly improved lighting efficiency is crucial to an energy efficient future.

Program 1: Non-Equilibrium, Low Pressure Electric Discharge Light Sources

The Advanced Light Source Consortium (ALITE) formed in 1997 has completed its first three years of research focused primarily in this low pressure gaseous discharge area. The results were published in 2001 in EPRI Report 1006630 entitled:

ALITE – Advanced Light Source Research: Research in the Basic Science of Commercial Light Sources to Achieve Major Breakthroughs in Performance and Efficiency, EPRI, Palo Alto, CA, and Osram Sylvania, Inc., Danvers, MA: 2001. 1006630.

Program 2: Multiphoton Phosphors (“Quantum Splitters”)

While Program 1 is addressing the basic gaseous discharge research, Program 2 is focusing on developing multiphoton phosphors for application to fluorescent lamps that emit two visible photons for each absorbed ultraviolet photon.

In 2000 EPRI and its cofunding partner, Osram Sylvania, Inc., responded to the U.S. Department of Energy (USDOE) Public Solicitation with a proposal to embark upon a multiphoton phosphor feasibility research project. The effort resulted in a cooperative agreement award from USDOE. This report documents this multiphoton phosphor feasibility research project.

2

FEASIBILITY RESEARCH PROCESS

Research Participants

The EPRI and Osram Sylvania project co-sponsors completed the development of the complete research team and established appropriate contracts and subcontracts with each of the participants as shown in Table 2-1.

Table 2-1
Participants in the Multiphoton Phosphor Feasibility Research Project (MPP Project)

Affiliation	Location	Name
EPRI-Prime Contract with USDOE Project Co-funder	Palo Alto, CA	Dr. John P. Kesselring
Gough & Associates, Inc. Research Agreement with EPRI	Hendersonville, NC	Alfred B. Gough
Los Alamos National Laboratory CRADA with EPRI	Los Alamos, NM	Dr. Jeff Hay Dr. Joel Kress
Osram Sylvania, Inc. Project Co-funder	Beverly, MA	David Bay Dr. Voitek Byszewski Earnest Dale Dr. Arun Dutta Roger B. Hunt, Jr. Dr. Kailash C. Mishra Dr. Madis Raukas Dr. Barry G. DeBoer
	Towanda, PA	
Osram GmbH	Munich, Germany	Dr. Ard Ellens Dr. Martin Zachau

Independent Researchers

Research Subcontracts with Gough & Associates, Inc.

Boston College	Newton, MA	Prof. B. Di Bartolo
College of the Holy Cross	Worcester, MA	Prof. R. S. Rana
Consultant (OSI Retired)	Wrentham, MA	Dr. Charles W. Struck
Lawrence Berkeley National Lab.	Berkeley, CA	Dr. Marvin J. Weber
Massachusetts Institute of Technology	Cambridge, MA	Prof. Keith Johnson
NASA LaRC	Hampton, VA	Dr. Norman P. Barnes
Oregon State University	Corvallis, OR	Prof. Douglas Keszler
Penn State University	University Park, PA	Prof. William B. White
Univ. of California at San Diego	San Diego, CA	Prof. Joanna McKittrick
Univ. of Georgia	Athens, GA	Prof. Richard S. Meltzer
Utrecht University	Utrecht, The Netherlands	Prof. Andries Meijerink
Wheaton College	Norton, MA	Prof. John Collins

Research Process Outline

Step 1: Preparation for Initial Workshop (Workshop-I)

Each of the participants in the project prepared an update and tutorial in luminescence and multi-photon phosphor research from their own viewpoint. These “viewpoint” papers and their composite bibliographies were shared with all participants prior to the workshop in order to expedite getting all participants up to the same general level of understanding.

Step 2: Initial Workshop (Workshop-I)

This initial workshop was divided into three sessions. During the first session each of the participants briefly highlighted their viewpoint papers, then responded to questions and requests for clarification. The second session focused on achieving an initial consensus as to the most promising directions to pursue multi-photon phosphor feasibility research. Major barriers to achieving research success were categorized, along with the kinds of breakthroughs that would be required to overcome the specific barriers. The third session was used to establish and agree upon: the feasibility research agenda that would be conducted in the next five to seven months; the team and/or the individual assigned to the specific research areas; and the key milestones that would be achieved for each area over the research period.

Step 3: Feasibility Research

During this period the assigned teams and/or individuals implemented the feasibility research agenda outlined in Step 2. Additional integration across teams and individuals was achieved by holding working and reporting sessions at selected key milestone points during the period. At the conclusion of this work interim written reports were prepared for each of the tasks. These interim reports were compiled and shared with all participants.

Step 4: Second Workshop (Workshop-II)

All participants and task teams highlighted their interim reports prepared at the end of Step 3. These presentations were followed by discussion sessions where merits of the different findings and recommendations were evaluated. The workshop participants then developed consensus findings and recommendations. Where additional research is part of the recommendations, proposed research efforts were also developed.

Step 5: Final Report

A final report was prepared that included a compilation of the individual findings and the findings of the team as a whole including recommendations for future research.

3

FEASIBILITY RESEARCH PLANNING

Workshop-I

In order to assess the possibility of developing new multi-photon phosphors for lamp applications, Workshop-I was organized and held to allow the research participants to prepare and present their viewpoints regarding aspects of luminescence and multi-photon phosphor research. Workshop-I was held May 8 through May 10, 2001 in Peabody, Massachusetts. Presenters at the workshop discussed the major barriers that must be overcome and the potential breakthroughs that are required for success in developing new multi-photon phosphors for lamp applications. Participants drafted a feasibility research agenda and divided the feasibility research work into twelve tasks. This task outline with task leaders, members and descriptions is shown in Table 3-1 (two pages). As part of the concluding session of Workshop-I a review was held with the U.S. DOE representatives. Based upon the positive results of Workshop-I, and following the review, the representatives of the U.S. DOE authorized proceeding with the second stage of the contract. An interim EPRI report summarizing Workshop-I presentations was provided to the U.S. DOE:

“Multi-photon Phosphor Feasibility Research: Scientific Viewpoints, EPRI, Palo Alto, CA: 2001. 1006238.”

Individual Task Planning

An initial steering committee group composed of K. Mishra, OSI’s Principal Investigator, A. Gough, EPRI’s Principal Investigator, Prof. B. Di Bartolo (Boston College) leading the team of outside physics researchers, and Prof. D. Keszler (Oregon State University) leading the chemistry and materials research team, developed the forms and procedures for more completely documenting the individual task assignments. The individual task documentation included:

- Scope: short and longer range research scope
- Subtasks: description; deliverables; start/finish dates
- Inputs required from other tasks
- Outputs required to other tasks

These twelve Task Research Plans were documented, refined, and then distributed to all researchers during the June and July, 2001 period. These Task Research Plans are provided in Appendix A.

Table 3-1
Task Outline: Leaders, Members and Description

#	Task Leader	Task Members	Task Description
1	Meijerink	DeBoer	<i>Optical/Plasma Testing of Fluorides</i> <ul style="list-style-type: none"> • Test single crystals in Xe- (Other discharges) • Blackening of fluorides in Hg- discharge <ul style="list-style-type: none"> - Why? - What about Xe- discharge? • Identify the nature of broad band absorption in LiGdF_4
2	Raukas	Keszler; White (PTCOE)	<i>Bulk and Surface Defects</i> <ul style="list-style-type: none"> • Color Centers (fluorides) <ul style="list-style-type: none"> - Literature search - PTCOE info on surface losses - Talk to Baldacchini • Effects of oxygen contamination
3	Meltzer	Weber; Rana; Meijerink	<i>New Oxides for Pr^{3+} Cascading</i> <ul style="list-style-type: none"> • New systems for Pr^{3+} <ul style="list-style-type: none"> - Maximize $^1\text{S}_0$-to-$^1\text{I}_6$ transition - Minimize $^3\text{P}_0$ - to- $^1\text{D}_2$ transition • materials with low frequency phonon modes
4	Meijerink	Struck; Weber	<i>Sensitizer for Gd^{3+}</i> <ul style="list-style-type: none"> • Identify sensitizers for Gd^{3+}
5	Struck	Keszler; Meijerink; Barnes	<i>Cascading from Gd^{3+} in Oxides</i> <ul style="list-style-type: none"> • can it happen with/without Eu^{3+} in the material? • compile a list of potential systems
6	Weber	Johnson; White; Rana; Meijerink	<i>Modeling - I</i> <ul style="list-style-type: none"> • assemble information <ul style="list-style-type: none"> - reduce matrix elements for rare earth ions for excited states - literature search for Judd-Ofelt parameters - calculate and extend Dieke diagram • organize crystal structure properties versus luminescence properties <ul style="list-style-type: none"> - correlations - selection rules - pre-screening rules
7	Johnson	Struck; Mishra; White	<i>Sugano-Tanabe diagram for transition metal candidates</i> <ul style="list-style-type: none"> • 3d (White); 4d & 5d <ul style="list-style-type: none"> - literature search • Calculations
8	Meltzer	Mishra; Meijerink	<i>Conversion of 407 nm to red or green</i> <ul style="list-style-type: none"> • Energy transfer from Pr^{3+} to other ions for conversion of 407 nm transition to green or red
9	Mishra	Raukas; Ellens; Meijerink; Zachau	<i>New Green</i>
10	Di Bartolo	Barnes; Collins	<i>New Cascading Ions</i> <ul style="list-style-type: none"> • Literature search
11	Struck	Mishra; Raukas; Hunt	<i>MPP for 254 nm emission from Hg- discharge</i>
12	McKittrick	Keszler; Dutta; Hunt	<i>Synthesis and chemical stability of fluorides</i> <ul style="list-style-type: none"> • stability of fluorides in water based suspension • synthesis issues • purity of samples <ul style="list-style-type: none"> - reducing oxygen contamination

4

AGENDA

Multi-Photon Phosphor

Final Agenda

February 27, 2002: Day 1

8:00 a.m.	Opening Welcome	
8:20	Welcome & Introductions	Dr. J. Gustafson, OSI Dr. J. Kesselring, EPRI Dr. J. Brodrick, DOE
8:40	Workshop Organization	Dr. K. Mishra & A. Gough
9:00	Session I – Multi-photon System and Processes (30 minutes each)	Chair: Prof. B. DiBartolo
	Task 4: Sensitizers for Gd^{3+}	Prof. A. Meijerink
	Task 3: New Oxides for Pr^{3+}	Prof. R. Meltzer
	Task 5: Cascading from Gd^{3+} in oxides	Dr. C. Struck
	Task 8: Conversion of 407 nm to red or green	Prof. R. Meltzer
11:00	Break	
11:10	Session II – Chemistry and Materials Issues (30 minutes each)	Chair: Prof. D. Keszler
	Task 12: Synthesis and chemical stability of fluorides	Prof. J. McKittrick
	Task 1: Optical/plasma testing of fluorides	Prof. A. Meijerink
12:10	Lunch	
1:10 p.m.	Task 2: Bulk and surface defects	
1:40	Session III – Concepts and Models (30 minutes each)	Chair: Mr. D. Bay
	Task 10: New cascading ions	Prof. B. Di Bartolo
	Task 11: MPP for 254 nm emission of Hg-discharge	Dr. C. Struck
	Task 9: New green	Dr. K. Mishra
3:10	Break	
3:20	Task 6: Modeling I	Dr. M. Weber
3:50	Task 7: Modeling II	Prof. K. Johnson
4:20	LANL MPP modeling, simulation and computations	Drs. J. Hay & J. Kress
4:50	Day 2 Plans & Workshop Organization	Dr. K. Mishra and A. Gough
5:15	Adjourn	

Final Agenda
February 28, 2002: Day 2

8:20 a.m.	Opening Welcome	
8:30	Session IV – Discussion & Evaluation of Recommendations: Projections for Future Research Summary of objectives, achievements and recommendations of the feasibility study	Chair: Dr. K. Mishra Dr. K. Mishra
9:20	Multiphoton Systems and Processes: Tasks 3, 4, 5, 8	Prof. A. Meijerink & Prof. R. Meltzer
10:30	Chemistry and Materials Issues: Tasks 1, 2, 12	Prof. D. Keszler & Dr. M. Raukas
11:40	Concepts and Modeling: Tasks 6, 7, 9, 10, 11	Prof. B. Di Bartolo & Dr. M. Webber
12:10 p.m.	Lunch	
1:00	Concepts and Modeling: Tasks 6, 7, 9, 10, 11	Prof. B. Di Bartolo & Dr. M. Weber
1:40	Summary	Prof. Di Bartolo
2:20	Discussion with DOE	Prof. Di Bartolo
2:50	Wrap-up	Mr. D. Bay & Mr. A. Gough
3:30	Adjourn	

5

FINAL REPORT SUMMARY – CONCLUSIONS AND RECOMMENDATIONS

Workshop-II

As shown in Chapter 4, Workshop-II individual task reports, presentations and discussions were organized under three general categories:

Multi-photon Systems and Processes

Chemistry and Materials Issues

Concepts and Models

During Day 1 of the workshop each of the task team leaders presented highlights of their reports. The individual Task Team reports are provided in Appendix B. These task team reports include conclusions and recommendations pertinent to the specific area of feasibility research.

Day 2 of the workshop was devoted to developing overall conclusions and recommendations.

Final Report Overview

The multi-photon phosphor feasibility study brought together experts from universities and national and industrial research laboratories to critically examine a newly emerging science that has the potential for technological breakthroughs. With such a diverse group of independent researchers, significant technical and organizational integration was required to achieve the full success of the project.

In the present context, the recent breakthroughs in the area of multi-photon transitions of rare earth ions in ionic hosts led to creation of this feasibility research study to explore possibilities of designing new phosphor systems for application in fluorescent lamps. This study was supported in part by a Cooperative Research Agreement with the U.S. Department of Energy and was cosponsored by EPRI and OSRAM Sylvania Inc. Experts from various areas of luminescence evaluated the recent developments in multi-photon luminescence, and examined the available data, luminescence processes and underlying theories to identify routes for developing multi-photon phosphors for energy efficiency in lighting. This report summarizes their conclusions and identifies the most promising routes to develop multi-photon lamp phosphors.

Project Organization

The main objectives of the ‘Feasibility Study’ following Workshop I were to review the existing literature on multi-photon phosphors, identify obstacles to developing such phosphors, and recommend directions for future research to address these issues in order to develop new phosphor systems for application in fluorescent lamps. Twelve task teams were created to address various topical issues identified at Workshop I for further investigation. Each task team was led by a team leader who was responsible for organizing research activities allotted to his/her task team and for generating the final report based on the conclusions and recommendations. In this report, we have compiled results, conclusions and recommendations from this feasibility study.

Conclusions and Recommendations

The conclusions and recommendations of the various task teams are organized into three categories: Multi-photon Systems and Processes (Tasks 3, 4, 5 and 8), Chemistry and Materials Issues (Tasks 1, 2, and 12) and Concepts and Models (Tasks 6, 7, 9, 10, and 11). Some of the conclusions and recommendations that are significant from the perspective of designing multiphoton lamp phosphors are described below. For more details, please refer to individual reports in Appendix B.

Multi-Photon Systems and Processes

Tasks 3, 4, 5 and 8 focused on how to use our current understanding of multi-photon phosphor processes to design new phosphor systems for application in fluorescent lamps.

The main drawbacks of the known multi-photon phosphor systems are as follows:

- weak absorption of exciting radiation by Gd^{3+} ions for excitation of the 7G manifold for initiating quantum splitting,
- emission from $^1\text{S}_0 \rightarrow ^1\text{I}_6$ transition of Pr^{3+} from the first cascading step near 400 nm,
- fluoride hosts for Gd^{3+} based phosphors,
- low quantum efficiency of Pr^{3+} activated oxide phosphors due to nonradiative relaxation from $^3\text{P}_0$ to $^1\text{D}_2$ manifold during the second cascading step.

Task teams 3, 4, 5 and 8 focused respectively on identifying new oxide hosts for Pr^{3+} , sensitizer ions for Gd^{3+} , oxide hosts for Gd^{3+} , and activator ions for Pr^{3+} for red shifting the blue emission from the first cascading step. A list of large gap oxides along with vibrational frequencies from complex anion groups was provided by Task 3 as candidate host materials for Pr^{3+} based multi-photon phosphor systems. Dy^{3+} , Tb^{3+} , Eu^{3+} , Er^{3+} , Ho^{3+} , Nd^{3+} , V^{2+} , V^{3+} , Mn^{2+} , Mn^{4+} , Cr^{2+} and Cr^{3+} were recommended for further study as activator ions in Pr^{3+} based phosphors to red-shift the ~400 nm radiation from Pr^{3+} . Among various schemes proposed for sensitizing Gd^{3+} ions (Task 4) in fluorides are charge transfer emission from Yb^{3+} , B-band emission from Pb^{2+} , and f→d transitions from Pr^{3+} , Er^{3+} , Nd^{3+} and Tm^{3+} . Difficulties associated with each sensitizing scheme were elaborated, and criteria for suitable host and ion combinations were described.

The main conclusion from these tasks is that the quickest way to developing multi-photon lamp phosphors lies in finding sensitizer ions for Gd^{3+} , and identifying activator ions to red shift the blue emission from Pr^{3+} due to the $^1\text{S}_0 \rightarrow ^1\text{I}_6$ transition associated with the first cascading step.

Chemistry and Material Issues

The most promising multi-photon phosphors are found in fluoride hosts. $\text{LiGdF}_4:\text{Eu}^{3+}$ shows a quantum efficiency of 1.95, and the quantum efficiency of $\text{YF}_3:\text{Pr}^{3+}$ approaches 1.4. Quantum efficiencies of Pr^{3+} activated oxides are far lower than unity. However, the fluoride phosphors are believed to be unstable in a discharge environment. Researchers from Philips recently demonstrated that the quantum efficiency of LiGdF_4 phosphor in the powder form is far lower than unity. This decrease in quantum efficiency in powder samples is attributed to an absorption band in the spectral regime from 150-200 nm. Additionally, the toxicity and cost of fluoride synthesis remain as major concerns. Information on the behavior of fluorides in coating suspension is limited. Tasks 1, 2 and 12 were designated to address the following issues:

- stability of fluorides in VUV environment
- stability of fluorides in discharge environment
- identification of the 150-200 nm absorption band in LiGdF_4 powder
- synthesis of fluoride phosphors
- behavior of fluorides in coating suspension.

Literature on defects in fluorides is rather sparse. The stability of fluorides under subband gap excitation was demonstrated for both crystalline and powder samples. Based on earlier data on fluorides, the 150 nm-200 nm band observed in powder samples of $\text{LiGdF}_4:\text{Eu}^{3+}$ appears to be associated with hole centers trapped at oxygen defects. Based on these findings, recommendations are made to focus on fluoride based phosphors activated by Gd^{3+} and Pr^{3+} while working for oxide alternatives.

Successful use of a multi-photon lamp phosphor will depend on its reliable performance in a discharge environment. It is therefore recommended to continue investigating the stability of fluoride based phosphors in actual lamp environments using experimental and theoretical methods, and to develop a better understanding of mechanisms of defect creation in fluorides.

Task 12 also showed alternative synthesis schemes for synthesis of fluorides by sol-gel, hydrothermal and chemical precipitation methods that do not use HF gas. The quality and cost of making phosphors by these approaches will remain a problem. These synthesis methods need to be optimized to reduce oxygen contamination.

Oxyfluorides are recommended as alternatives to fluorides and oxides. More work is needed to determine the suitability of oxyfluorides as hosts for designing multi-photon phosphor systems.

The most important recommendation from the feasibility study is to start working on fluorides to develop lamp phosphors while working on oxide and oxyfluoride alternatives.

Concepts and Models

Tasks 6, 7, 9, 10 and 11 focused on other plausible multi-photon schemes, and developing theoretical tools to predict germane spectroscopic properties for exploring new multi-photon phosphors. The feasibility study produced two new proposals which could be useful for designing novel multi-photon phosphor systems:

- activation by Tm^{3+} ions with energy transfer to Eu^{3+} or Tb^{3+} ,
- use of 4d and 5d- transition metal ions as sensitizers or activators.

Each of these proposals in principle has the potential for opening a new area of research in multi-photon luminescence.

Discussions during the workshop returned time and again to the theory of energy transfer and the Judd-Ofelt theory of intensity. Successful designing of a multi-photon phosphor based on cascading transitions of Gd^{3+} and Pr^{3+} depends critically on how the former can be sensitized and the latter can sensitize an activator ion. Sensitization depends on successful non-radiative energy transfer from one ion to the other non-radiatively. It is for this reason that Task 8 critically reviewed the process of energy transfer. One of the interesting conclusions from this study is the recommendation to use compounds stoichiometric either in the donor or the acceptor ions as a host. Another proposal is to explore transition schemes of 4d- and 5d-transition metal ions using both theoretical and experimental approaches concurrently. This could lead to identification of new activator ions for sensitization by the $^1\text{S}_0 \rightarrow ^1\text{I}_6$ transition of Pr^{3+} ions and sensitizers of Gd^{3+} ions.

Other predictive determinants of the multi-photon transitions are the energy level diagrams and the Judd-Ofelt parameters. There exist no reliable methods to predict either, and recommendations are made to approach these issues using reliable semi-empirical methods and/or first principles techniques.

Thanks to the sincere efforts by the participants in this project, and support from DOE, EPRI and OSRAM Sylvania, this project achieved the goals and objectives established at its beginning. It further demonstrated how resources at universities and national and industrial laboratories can be pulled together to work towards new technological developments.

A

FEASIBILITY RESEARCH PLANS

Task 1 Research Plan: Optical/Plasma Testing of Fluorides

SCOPE

Describe more completely the scope of the work to be accomplished PRIOR TO Workshop-II:

In spite of an effort to find photon cascade system based on oxide host lattices, the prospects for fluorides are more promising. If indeed a fluoride phosphor with a quantum efficiency close to 200 % is found, we are faced with potential problems related to an instability of fluorides under VUV radiation. The scope of this task is provide an initial understanding of these problems and possible solutions. A specific problem that has already been identified in the promising photon cascade material $\text{LiGdF}_4:\text{Eu}^{3+}$ is the presence of a defect absorption band between 170 and 200 nm which competes with VUV absorption by Gd^{3+} and is one of the reasons for the poor performance (without a sensitizer). Part of the task will be literature research on color center formation in fluorides (especially under VUV excitation), the influence of oxygen (or other impurities) and the influence of the type of fluoride lattice. In addition some simple experiments will be performed to test the stability of a variety of fluoride samples by measuring the intensity of lanthanide luminescence during prolonged exposure to VUV radiation or in a Xe or Hg discharge.

LONGER TERM SCOPE

Note other critical research that will be needed within the OVERALL scope of the task, but probably **cannot** be accomplished within the time and budget constraints prior to Workshop-II:

An important part of the research program will be the study of color center formation in fluorides under VUV radiation. It is expected that the information that is available in the literature is limited (not much research has been done using VUV radiation) and a thorough study is required to evaluate the stability of fluorides under VUV radiation. The research will involve the preparation of fluoride host lattices. Variables in the synthesis are the type of host lattice, the purity of the sample (e.g. oxygen or OH content), powder or single crystal, the presence of (lanthanide) activator ions etc. After the synthesis the samples need to be tested by subjecting the samples to VUV radiation (from a synchrotron, deuterium lamp or VUV laser) and in a Xe discharge. To study the formation and the nature of color centers various techniques need to be applied, e.g. luminescence spectroscopy, optical absorption, thermoluminescence, electron paramagnetic resonance and luminescence life time measurements. This research will provide insight in the stability of fluoride phosphors under VUV radiation. If indeed fluoride phosphors are potentially stable, the research will also provide insight in the specifications of stable fluoride phosphors. This will be of crucial importance for the synthesis conditions of commercial fluoride phosphors.

Subtasks <i>Develop and document some logical steps (e.g. 3 to 5 subtasks)</i>	Deliverables <i>Think through what outcomes will be expected along the way, and describe these outputs (deliverables) at the end of each subtask.</i>	Start/Finish Schedule
<p>Literature search on stability, color center formation and color center absorption characteristics in fluorides, especially under VUV excitation- From the field of VUV excimer lasers and VUV windows useful information may be available.</p>	<p>Overview of literature available. This will be the basis for further research.</p>	<p>Start: July Finish: December</p>
<p>Initial experiments on the VUV stability of various fluorides- From different sources (e.g. team members) fluoride samples will be obtained and the luminescence intensity will be measured as a function of VUV irradiation time. The change in intensity and color center formation will be related to the sample specifications. In view of the limited time available in this initial phase, only a few samples can be tested.</p>	<p>Basic understanding on the potential stability of fluorides under VUV radiation. (It is by no means possible to draw far reaching conclusions on the VUV stability of fluorides on the basis of these initial experiments.)</p>	<p>Start: July Finish: December</p>
<p>Simple test of fluoride crystals or fluoride powders in a Xe discharge - Before, during (if possible) and after the exposure to a Xenon discharge the luminescence properties will be evaluated. Also here experiments will be very limited in view of time. A simple test in a Hg discharge may also be useful to verify that indeed fluorides are not stable in a Hg discharge.</p>	<p>Basic understanding of the stability of fluorides during exposure to a Xe discharge.</p>	<p>Start: July Finish: December</p>

Final Task	Final Deliverable	Start/Finish
Combine the findings from the literature and the initial experiments to provide a good starting point for further research. Evaluate the chances for the possibility that a fluoride phosphor can be stable in a Xe discharge lamp (based on the limited knowledge available).	Report which forms the basis for a research plan to study color center formation in fluorides under VUV radiation and factors influencing the VUV stability of VUV phosphors.	Start: October Finish: December 15, 2001
From Other Task(s) To This Task (information needed to enable effective start or continuation of THIS TASK or subtasks) From Other Task #2 Input Required: There is some overlap between Tasks 1 and 2. Task 1 is more directed at initial experiments, Task 2 at a literature search. However, for the evaluation of the initial experiments a literature search is required. At the same time, the information obtained in Task 1 will be shared with members of the Task 2 team. From Other Task #:____; Input Required:		
To Other Task(s) From This Task (information needed to enable effect start or continuation of OTHER tasks or subtasks) To Other Task #: ; Input Required:		

Task 2 Research Plan: Bulk and Surface Defects

SCOPE Describe more completely the scope of the work to be accomplished PRIOR TO Workshop-II: A. Literature search on defect creation energies and mechanisms in fluorides. Discussions with scientists involved in the field. Comparison of the data with excitation energies in existing or candidate discharges. Conclusions. B. Literature search on surface states elimination and influence on luminescence efficiency. Discussions with scientists involved in the field. Conclusions. C. Understanding the effects of oxygen contaminants in fluoride lattices. Conclusions.		
LONGER TERM SCOPE Note other critical research that will be needed within the OVERALL scope of the task, but probably cannot be accomplished within the time and budget constraints prior to Workshop-II: Defect creation energies and mechanisms in other lattice types (oxides). Testing of fluoride (powder) samples of various quality.		
Subtasks <i>Develop and document some logical steps (e.g. 3 to 5 subtasks)</i>	Subtask Deliverables <i>Think through what outcomes will be expected along the way, and describe these outputs (deliverables) at the end of each subtask.</i>	Start/Finish Schedule
Literature search and discussions regarding defects in fluorides.	Compilation of defect creation energies in fluorides.	Start: July 2001 Finish: November 2001
Literature search and discussions regarding surface states.	Survey of present understanding.	Start: July 2001 Finish: November 2001
Literature search and discussions regarding surface states.	Survey of present understanding.	Start: July 2001 Finish: November 2001
Final Task	Final Deliverable	Start/Finish
Drawing conclusions on applicability of fluorides as host materials in discharges, on criticality of surface states influence and on oxygen contamination in fluoride lattices.	Conclusions.	Finish: November 2001
From Other Task(s) To This Task (information needed to enable effective start or continuation of THIS TASK or subtasks) From Other Task #: ; Input Required:		
To Other Task(s) From This Task (information needed to enable effect start or continuation of OTHER tasks or subtasks) To Other Task #: ; Input Required:		

Task 3 Research Plan: New Oxides for Pr³⁺ Cascading

SCOPE

Describe more completely the scope of the work to be accomplished PRIOR TO Workshop-II:

This task requires the identification of oxide systems with multi-photon cascading of Pr³⁺ with quantum efficiencies in excess of 100%. Most critical condition for cascading transition to occur is to have 5d –band to be energetically at higher energy compared to ¹S₀ state. For practical purposes of extracting the maximum lumen output, the ¹S₀ → ¹I₆ transition needs to be red shifted through an appropriate sensitization scheme (Task #8) and the ³P₀ → ¹D₂ non-radiative phonon relaxation should be minimized.

LONGER TERM SCOPE

Note other critical research that will be needed within the OVERALL scope of the task, but probably **cannot** be accomplished within the time and budget constraints prior to Workshop-II:

The systems identified in SCOPE above will have to be prepared, tested and optimized for actual visible quantum efficiencies.

Subtasks <i>Develop and document some logical steps (e.g. 3 to 5 subtasks)</i>	Deliverables <i>Think through what outcomes will be expected along the way, and describe these outputs (deliverables) at the end of each subtask.</i>	Start/Finish <i>Schedule (after completion of Steps 5 & 6)</i>
Identify systems where ¹ S ₀ lies below the lowest 4f5d state. Start with the tabulation of Dorenbos (J Lumin. 91, 155 (2000)). Emphasis should be placed on hosts with high coordination.	List of known and predicted materials where ¹ S ₀ lies below the lowest 4f5d.	Start: July Finish: October
Identify the general host characteristics and specific systems in which the ¹ S ₀ → ¹ I ₆ transition probability is maximized. This will require a survey of Judd-Ofelt parameters for Pr ³⁺ (done within the broader, more inclusive scope under Task#6). The results should be guidelines for the structure-bonding properties required for selecting the host for optimum cascading. The main requirement is that the Ω ₆ Judd-Ofelt term should dominate.	General guidelines for identifying systems and sites with maximized ¹ S ₀ → ¹ I ₆ transition probabilities. Specific systems in which this is likely to be maximized.	Start: July Finish: October

Identify the general host characteristics and specific systems for which the $^3P_0 \rightarrow ^1D_2$ non radiative phonon relaxation rate is minimized.	General guidelines for identifying sites (systems) with minimized $^3P_0 \rightarrow ^1D_2$ non radiative phonon relaxation rates. Compilation of vibrational modes facilitating nonradiative transitions. Specific systems in which this is likely to be minimized.	Start: July Finish: October
Other sources of quenching of the 3P_0 emission need to be examined.	Conclusions regarding other processes in the quenching of 3P_0 emission and the host characteristics that will minimize it.	Start: July Finish: October
Final Task	Final Deliverable	Start/Finish
Identify the general parameters and recommend specific systems for quantum efficiencies in excess of 100% for Pr^{3+} -doped oxides.	Since it is unlikely that any Pr^{3+} -doped system with simple cascade emission will give good lumen output because the first step has too short a wavelength, the main deliverable will be oxide systems that can be considered for Task #8 which will involve applications of energy transfer with some other activator.	Start: July Finish: December
From Other Task(s) To This Task (information needed to enable effective start or continuation of THIS TASK or subtasks) From Other Task #6 Input Required: Results on reduced matrix elements and Judd-Ofelt parameters from literature search on other systems and the organization of these results in a general form for identification of specific systems. From Other Task #: ____; Input Required:		
To Other Task(s) From This Task (information needed to enable effect start or continuation of OTHER tasks or subtasks) To Other Task #8 Input Required: Identification of systems with large $^1S_0 \rightarrow ^1I_6$ transition dipole moments as a necessary step to determining systems with likely prospects for efficient energy transfer by multipole-multipole interactions leaving the Pr^{3+} in the 3P_0 level for subsequent visible emission. To Other Task #: ; Input Required:		

Task 4 Research Plan: Sensitizer for Gd³⁺

SCOPE

Describe more completely the scope of the work to be accomplished PRIOR TO Workshop-II:

One of the promising routes to obtain an efficient quantum cutter is to use the high visible quantum efficiency that can be obtained with the Gd³⁺-Eu³⁺ couple or possibly Gd³⁺-other ion (topic for task 10) couples. The quantum efficiency of a VUV phosphor based on the Gd-Eu couple can be as high as 190%. The main problem to be solved is finding a sensitizer for the Gd³⁺ ion. In order to overcome the weak VUV absorption of Gd³⁺ it is essential to find a sensitizer which feeds the ⁶G level of Gd³⁺. It is the scope of this task to identify potential candidates for sensitization of the ⁶G level of Gd³⁺ which is situated around 205 nm. The main requirements of the sensitizer are an efficient VUV absorption in the wavelength region of approximately 145 to 190 nm and an emission in the region between approximately 190 and 205 nm. Sensitizers with these characteristics will be able to absorb the VUV radiation from a Xe discharge and transfer the energy to Gd³⁺. Subsequently, the Gd-Eu couple will take care of the emission of two visible photons. An additional requirement for the sensitizer is that possible lower energy levels of the sensitizer do not interfere with the two step energy transfer (downconversion) process of the Gd-Eu couple. Ideally, the sensitizer has no energy levels below 45 000 cm⁻¹. A logical choice for the sensitizers to be considered are classes of ions which show a strong absorption due to parity allowed transitions and are at present applied for UV absorption in oxide host lattices. In fluorides the energy levels may shift to the VUV. An initial search will involve charge transfer and fd transitions of lanthanide ions and the s²-sp transitions of s² ions.

LONGER TERM SCOPE

Note other critical research that will be needed within the OVERALL scope of the task, but probably **cannot** be accomplished within the time and budget constraints prior to Workshop-II:

After the identification of possible types of sensitizers, samples have to be synthesized and the (VUV) luminescence spectra of potential sensitizers have to be measured. In case of favorable luminescence characteristics, the sensitizer has to be combined in a system with the Gd-Eu couple to test if efficient sensitization does indeed occur. This research will require a considerable research effort. It will provide insight in the VUV luminescence properties of classes of potential sensitizers like charge transfer and fd transitions of lanthanides and s²-sp transitions of s² ions. Up until now the knowledge in the VUV region of these types of transitions is limited.

Subtasks <i>Develop and document some logical steps (e.g. 3 to 5 subtasks)</i>	Deliverables <i>Think through what outcomes will be expected along the way, and describe these outputs (deliverables) at the end of each subtask.</i>	Start/Finish <i>Schedule</i>
Investigate the possibilities for charge transfer transitions. The Yb ³⁺ ion is a possible candidate. The literature is limited. A recent publication from our group indicates that in oxides chances are minimal since the charge transfer transition is just at too low energy. Oxyfluorides or fluorides may be a possibility. Another class of charge transfer transitions to be investigated are highly charged transition metal ions (e.g. d ⁰) in fluorides.	Insight in the potential usefulness of charge transfer transitions for sensitization of the Gd ion.	Start: July Finish: November

Literature search on the VUV spectroscopy of s^2 ions in fluorides. There is some literature available. Literature research is expected to provide insight in the relation between the host lattice properties (nature of ligands and distance to ligands) and the positions of the sp excited states.	Insight that will help in deciding if research as described under LONGER TERM SCOPE above should be done on s^2 ions.	Start: July Finish: November
Literature research on fd transitions of lanthanides in the VUV. Identification of potential sensitizers is in this case complicated by the lower energy $4f^n$ levels. Some lanthanides may have good characteristics for the fd absorption and emission but the lower energy levels can hamper the Gd-Eu downconversion process. These problems should be identified as well.	Identification of lanthanide ions which may work as sensitizers and should be investigated as indicated under LONGER TERM SCOPE above.	Start: July Finish: November
Identify new classes of sensitizers. This will involve a literature study on VUV and UV spectroscopy in general.	New options for sensitization of the Gd ion not covered above.	Start: July Finish: November
Final Task	Final Deliverable	Start/Finish
Combine the information from the subtasks and weigh the potential of each class of the potential sensitizers. Compile the information from literature on the VUV spectroscopy of the various classes of ions.	An overview of the VUV spectroscopy which will serve as input for the research as defined under LONGER TERM SCOPE above. Based on the input provided, a research plan can be made which offers the highest chances for success and will address the most promising candidates first.	Start: July Finish: December
From Other Task(s) To This Task (information needed to enable effective start or continuation of THIS TASK or subtasks) From Other Task #10 Input Required: Other couples based on Gd^{3+} From Other Task #: ___1___; Input Required: Position of VUV absorption bands which may interfere with the sensitization process and compete with absorption by the sensitizer.		
To Other Task(s) From This Task (information needed to enable effect start or continuation of OTHER tasks or subtasks) To Other Task #: _____; Input Required:		

Task 5 Research Plan: Cascading from Gd^{3+} in Oxides

SCOPE

Describe more completely the scope of the work to be accomplished PRIOR TO Workshop-II:

To enumerate the requirements for a successful embodiment of this task

To set up a logic for choosing appropriate possibilities for such a successful embodiment

To select a list of such possibilities.

The results of the literature searches done here will not reveal a previously known but forgotten two photon emitting phosphor. It is highly unlikely that it will point to specific new phosphors guaranteed to perform well as two photon emitters. This present task should give guidance as to families of new phosphors to prepare.

LONGER TERM SCOPE

Note other critical research that will be needed within the OVERALL scope of the task, but probably **cannot** be accomplished within the time and budget constraints prior to Workshop-II:

Their preparation, their performance, and the understanding of the trends of their performance are for the next stage in this research grant. In the iteration of these three steps, if at all, will come the actual creation of useful two photon emitters. Without such an iterative effort, one is trusting to luck for eventual success.

Subtasks <i>Develop and document some logical steps (e.g. 3 to 5 subtasks)</i>	Deliverables <i>Think through what outcomes will be expected along the way, and describe these outputs (deliverables) at the end of each subtask.</i>	Start/Finish <i>Schedule</i>
Search for host materials with band gap greater than the Gd^{3+} ^6G excitation energy, i.e., below ~210 nm.	A literature search for the band gaps of various oxygen based phases.	Start: July 15 Finish: Sept 30
Determination of the position of the Eu^{3+} CTS band in such hosts	A literature search of Eu^{3+} luminescence, emphasizing the position of the CTS of Eu^{3+} .	Start: July 15 Finish: Sept 30
Evaluation of the efficiency of the sequential transfer of the Gd^{3+} ^6G to two Eu^{3+} ions.	This assessment depends strongly on our (limited) understanding of transfer rates and of nonradiative depopulation of the energy levels involved in transfer and in emission. The deliverable here may well be an assessment of the current status of luminescence theories of nonradiative rates and of energy transfer rates.	Start: July 15 Finish: December 1
A logic for choosing promising hosts must be formulated. The actual choices must be listed.	A statement of this logic. Some aspects may well be obvious, such as the proper band-gap, the proper position of the Eu^{3+} CTS. What governs these band gap and CTS energies are not obvious, and we will attempt to elucidate them. A list of the promising hosts will be delivered.	Start: July 15 Finish: December 1

<p>$Gd^{3+} \ ^6G \rightarrow$ ions other than Eu^{3+}.</p> <p>For the sequence of energy transfers leading to 2 photon emissions, the requirement is strict that the recipient of the Gd energy must have an energy level near 17000 cm^{-1}. Nd^{3+} and Pr^{3+} seem to meet this requirement. Of these Pr^{3+} seems preferable on the grounds that it has fewer energy levels near and below 17000 cm^{-1}. If there emerges some probability of success with Pr^{3+}, then we would also widen the scope of research to include Nd^{3+} as the second activator.</p>	<p>These restrictions then tie this subtask directly to Task 3. Any oxide hosts with wide enough band gap and which are identified there as giving significant Pr^{3+} emissions should be listed as worthy of investigation for $Gd^{3+} \ ^6G \rightarrow Pr^{3+}$ transfers.</p>	<p>Start: July 15 Finish: December 1</p>
Final Task	Final Deliverable	Start/Finish
The collection of the above		Start: Finish:
<p>From Other Task(s) To This Task (information needed to enable effective start or continuation of THIS TASK or subtasks) From Other Task #4 Input Required: Any promising sensitizer. From Other Task #3, 8, 9, 10 Input Required: Any promising output from each of these tasks will open up other approaches for accomplishing this task.</p>		
<p>To Other Task(s) From This Task (information needed to enable effect start or continuation of OTHER tasks or subtasks)</p>		

Task 6 Research Plan: Modeling

SCOPE

Describe more completely the scope of the work to be accomplished PRIOR TO Workshop-II:

The goal of this task is to develop an overall capability for modeling new multiphoton phosphors based on a combination of experimental data and theoretical predictions. Initial consideration will be given to lanthanide ions in crystalline hosts. Luminescence properties of interest include energy of excitation bands, ground and excited state absorption coefficients, radiative transition probabilities, Stokes shift of radiation, fluorescence branching ratios, nonradiative transition probabilities, probabilities for ion-ion energy transfer, and quantum efficiencies. The correlation of these properties with the ion and the host composition and structure will be investigated.

LONGER TERM SCOPE

Note other critical research that will be needed within the OVERALL scope of the task, but probably **cannot** be accomplished within the time and budget constraints prior to Workshop-II:

The procedures identified in this task need to be validated by first applying them to known lanthanide ion-host systems and multiphoton phosphors before applying them to new, unexplored materials. The development of modeling and predictive capabilities for transition metal ions being investigated in Task 7 may also be of interest

Subtasks <i>Develop and document some logical steps (e.g. 3 to 5 subtasks)</i>	Deliverables <i>Think through what outcomes will be expected along the way, and describe these outputs (deliverables) at the end of each subtask.</i>	Start/Finish <i>Schedule (after completion of Steps 5 & 6)</i>
Literature survey of Judd-Ofelt intensity parameters for lanthanide ions in crystals. Develop correlation of Judd-Ofelt parameters with host composition and structure.	Capability for estimating Judd-Ofelt parameters for lanthanide ions in crystalline hosts.	Start: July Finish: September 30
Literature survey of nonradiative multiphoton decay rates for lanthanide ions in crystals. Develop correlation of multiphoton decay rates with maximum phonon energies of host (from infrared spectra, Raman spectra, etc.) and the strength of ion-lattice coupling.	Capability for estimating nonradiative multiphoton decay rates for lanthanide ions in crystalline hosts.	Start: July Finish: Sept 30
Extend Dieke diagram for the higher ($> 40,000 \text{ cm}^{-1}$) excited states of the trivalent lanthanide ions. Tentative assignments will be validated by experimental studies in representative crystals.	More complete energy level diagram for the trivalent lanthanides. Identification of excitation bands, excited states for energy transfer, and cascade transitions of interest for multiphoton phosphors.	Start: July Finish: December 1

Calculation of reduced matrix elements for higher ($> 40,000 \text{ cm}^{-1}$) excited states of the trivalent lanthanide ions. Matrix elements from the ground state to all excited states are of interest for absorption; matrix elements for emission to all lower levels from those levels with a large energy gap to the next lower level are mainly of interest (any nearby levels with a significant thermal population should also be included).	Matrix elements needed for predictions of radiative decay rates, fluorescence branching ratios, excited state absorption, and electric dipole-dipole and electric dipole-quadrupole energy transfer using the Judd-Ofelt theory.	Start: July Finish: December 1
Survey of first-principles and semi-empirical approaches to the calculation of absorption and emission properties of lanthanide ions in crystals. Identify their usefulness for predicting the spectroscopic properties of multiphoton phosphors.	Recommendations for the best approaches to use for theoretical predictions of energy levels and transition probabilities relevant to the operation of multiphoton phosphors.	Start: July Finish: December 1
Final Task	Final Deliverable	Start/Finish
Integration of the above findings to develop selection rules and procedures for predicting the luminescence properties of lanthanide ions in crystals important for the operation of multiphoton phosphors.	Model for predicting the properties of multiphoton phosphors. This should serve as a tool for prescreening potential ion-host combinations before expending efforts to synthesize the materials.	Start: September Finish: December 1
From Other Task(s) To This Task (information needed to enable effective start or continuation of THIS TASK or subtasks) From Other Task #3 Input Required: Results from the investigation of maximizing radiative transition probabilities and minimizing nonradiative multiphoton processes for Pr^{3+} . This information will be useful in expanding the database needed to develop and validate the modeling capability.		
To Other Task(s) From This Task (information needed to enable effect start or continuation of OTHER tasks or subtasks) To Other Task 3, 4, 5, 8, 9, 10, and 11 Input Required: Modeling capabilities and predictions from this task, when validated, should be of helpful to several other tasks.		

Task 7 Research Plan: Sugano-Tanabe Diagram for Transition Metal Candidates

SCOPE

Describe more completely the scope of the work to be accomplished PRIOR TO Workshop-II:

The electronic structures of first-, second-, and third-row transition-metal (TM) ions in oxide local environments with octahedral and tetrahedral site symmetry will be determined as a basis for identifying activator ions which together with Pr^{3+} may lead to multi-photon emission via energy transfer. A first-principles method for calculating the multiplet structure (implicit in the Sugano-Tanabe diagrams) for d^N ions will be employed.

LONGER TERM SCOPE

Note other critical research that will be needed within the OVERALL scope of the task, but probably **cannot** be accomplished within the time and budget constraints prior to Workshop-II:

All possible oxides of practical lamp potential.

Subtasks

Develop and document some logical steps (e.g. 3 to 5 subtasks)

Deliverables

Think through what outcomes will be expected along the way, and describe these outputs (deliverables) at the end of each subtask.

Start/Finish

Schedule (after completion of Steps 5 & 6)

Determine electronic structures and Racah parameters of *first-row* TM ions in oxides.

Electronic structures and Racah parameters Sugano-Tanabe diagrams

Start: July, '01
Finish: Sept, '01

Determine electronic structures and Racah parameters of *second-row* TM ions in oxides.

Electronic structures and Racah parameters Sugano-Tanabe diagrams

Start: Sept, '01
Finish: Oct, '01

Determine electronic structures and Racah parameters of *third-row* TM ions in oxides.

Electronic structures and Racah parameters Sugano-Tanabe diagrams

Start: Oct, '01
Finish: Nov, '01

Analysis of calculated electronic structures for potential TM multiphoton activators.

Potential TM multiphoton activators

Start: Nov, '01
Finish: Dec, '01

From Other Task(s) To This Task

(information needed to enable effective start or continuation of THIS TASK or subtasks)

From Other Task #: ; Input Required:

To Other Task(s) From This Task

(information needed to enable effect start or continuation of OTHER tasks or subtasks)

To Other Task #: ; Input Required:

To Other Task #: 9,8 ; Input Required:

Task 8 Research Plan: Conversion of 407 nm to Red or Green

SCOPE

Describe more completely the scope of the work to be accomplished PRIOR TO Workshop-II:

Determine the required general properties and recommend specific sensitizer/activator combinations and hosts that should yield efficient energy transfer and conversion of Pr^{3+} in the $^1\text{S}_0$ state to the $^1\text{I}_6$ and the activator in an excited state such that it can emit green or red light with high efficiency. The ultimate goal is to achieve quantum efficiency in excess of 100% with visible photons with effective lumen output. The following characteristics are necessary:

- Energy match of activator absorption and the $^1\text{S}_0 \rightarrow ^1\text{I}_6$ transition of Pr^{3+} .
- Dominance of the Judd-Ofelt parameter Ω_6 .
- Favorable selection rules on the transition of Pr^{3+} and the activator (e.g. spin conservation).
- Minimal absorption of the activator in the 4f5d absorption band of Pr^{3+} (210-170 nm).

LONGER TERM SCOPE

Note other critical research that will be needed within the OVERALL scope of the task, but probably **cannot** be accomplished within the time and budget constraints prior to Workshop-II:

The systems identified in SCOPE above will have to be prepared, tested and optimized for actual visible quantum efficiencies. In addition, modeling of the system may be required.

Subtasks <i>Develop and document some logical steps (e.g. 3 to 5 subtasks)</i>	Deliverables <i>Think through what outcomes will be expected along the way, and describe these outputs (deliverables) at the end of each subtask.</i>	Start/Finish <i>Schedule</i>
Identify activator ions that have the appropriate transition energies which match the $^1\text{S}_0 \rightarrow ^1\text{I}_6$ transition of Pr^{3+} and that have appropriate selection rules to give large transition dipole moments. This will involve use of rare earth energy level diagrams and a literature search. Activators should not absorb strongly at other UV wavelengths corresponding to other $^1\text{S}_0$ emission energies.	Candidate activator ions and transfer schemes.	Start: July Finish: October

Estimate the energy transfer rates based on transition dipole rates calculated from Judd-Ofelt parameters, ion separations, and known rates in the literature for other similar systems. These need to be compared with radiative rates of 1S_0 of Pr^{3+} to predict if energy transfer will dominate the relaxation.	Plausible hosts, site symmetries and choices of activator.	Start: July Finish: October
Predict the resulting emission spectrum based on the sum of the emission of the Pr^{3+} and the added activator. Green emission will be especially important.	Expected emission spectrum.	Start: July Finish: October
Examine the application of transition metal (3d, 4d) ions as alternative activator candidates. Requires input from Task #7	A recommendation concerning the possibility of using transition metal ions as activator and, if so, specific candidates.	Start: July Finish: October
Final Task	Final Deliverable	Start/Finish
Examine the activator and host candidates, including transition metal ions, based on surveyed parameters from Tasks #6 and #7, to identify the most favorable systems for energy transfer yielding the maximized visible emission	A list of potential candidates for quantum efficiencies in excess of 100% including the identification of activators and hosts.	Start: Finish:
From Other Task(s) To This Task (information needed to enable effective start or continuation of THIS TASK or subtasks) From Other Task #3 Input Required: Identification of systems with large $^1S_0 \rightarrow ^1I_6$ transition dipole moments as a necessary step to determining systems with likely prospects for efficient energy transfer by multipole-multipole interactions leaving the Pr^{3+} in the 3P_0 level for subsequent visible emission. From Other Task #6 Input Required: Energy levels, reduced matrix elements, and Judd-Ofelt parameters for activator ions. From Other Task #7 Input Required: Results of literature search and calculations to help determine the possibility of using transition metal ions as activators.		
To Other Task(s) From This Task (information needed to enable effect start or continuation of OTHER tasks or subtasks) To Other Task #: ; Input Required: To Other Task #: ; Input Required:		

Task 9 Research Plan: New Green

SCOPE

Describe more completely the scope of the work to be accomplished PRIOR TO Workshop-II:

Known green emitting (both broad band and narrow line emitters) activators in oxide and fluoride lattices will be investigated. Attempts will be made to understand how site symmetry, coordination number and nature of ligands, and crystal structure affect their spectral properties. Their energy levels (based on their emission and absorption spectra and other relevant information from the literature) will be studied to determine if they would allow two-photon emission and/or if a suitable two-photon sensitizer can be found to induce emission in the green from these ions.

LONGER TERM SCOPE

Note other critical research that will be needed within the OVERALL scope of the task, but probably **cannot** be accomplished within the time and budget constraints prior to Workshop-II:

If literature search suggests a reasonable combination of impurity ion and host lattice that could provide a green emitting phosphor, synthesis and testing of such materials should be done.

Subtasks <i>Develop and document some logical steps (e.g. 3 to 5 subtasks)</i>	Deliverables <i>Think through what outcomes will be expected along the way, and describe these outputs (deliverables) at the end of each subtask.</i>	Start/Finish <i>Schedule (after completion of Steps 5 & 6)</i>
Investigate and compile a list of green emitting ions and corresponding hosts.	A list of green emitting ions and corresponding host systems and a comprehensive analysis of their emission and absorption spectra.	Start: September, 2001 Finish: December, 2001
Examine the electronic structure of these candidate ions to check if two photon emission is feasible	Compile a list of candidate ions.	Start: September, 2001 Finish: December, 2001
Compare its electronic structure with those of the known multi-photon emitters or emitters recommended by other Task Teams to identify candidate sensitizers and host lattices.	Recommend candidate sensitizer ions for further study.	Start: September, 2001 Finish: December, 2001

From Other Task(s) To This Task

(information needed to enable effective start or continuation of THIS TASK or subtasks)

From Other Task #8 Input Required: Recommended list of activators for sensitization by Pr^{3+}

From Other Task #7 Information on transition metal ions.

From Other Task #6 Information on rare-earth ions.

From Other Task #10 Information on new candidates for cascading ions

To Other Task(s) From This Task

(information needed to enable effect start or continuation of OTHER tasks or subtasks)

To Other Task #: ; Input Required:

Task 10 Research Plan: Search for New Cascading Ions

SCOPE

Describe more completely the scope of the work to be accomplished PRIOR TO Workshop-II:

1. To review patiently the systems that have been considered in the search for multiphoton-effect materials, including those summarily dismissed, to confirm the negative choices or to point to promising, even if elusive, possibilities.
2. To examine new materials and processes that may produce two visible photons following a one-photon excitation, including transition metal ions, and molecular systems.

LONGER TERM SCOPE

Note other critical research that will be needed within the OVERALL scope of the task, but probably **cannot** be accomplished within the time and budget constraints prior to Workshop-II:

Subtasks <i>Develop and document some logical steps (e.g. 3 to 5 subtasks)</i>	Deliverables <i>Think through what outcomes will be expected along the way, and describe these outputs (deliverables) at the end of each subtask.</i>	Start/Finish <i>Schedule</i>
<p>Identification of new systems that could exhibit the photon cascading similar to that observed in Pr:YF_3. That is, one UV photon in and two visible photons out from the single ion.</p> <ol style="list-style-type: none"> a. Rare Earth Ions. Look into energy levels in the VUV, i.e. the extended Dieke diagram. b. Transition Metals: What happens to metals such as V, Ti, and Mn when doped in insulators and when excited deep in the UV? c. Other Luminescent Systems: Molecular Systems (organic and inorganic) may exhibit the correct processes. Each of these requires a literature search. 	<p>List of candidate systems and processes for two photon emission.</p>	<p>Start: July Finish: December</p>

Investigation of the possibility of new cross-relaxation schemes involving two (like or unlike) ions in order to produce two visible photons. Thus, we extend the task to include two body processes.	List of candidate systems and processes for multi-photon emission.	Start: July Finish: December
From Other Task(s) To This Task (information needed to enable effective start or continuation of THIS TASK or subtasks) From Other Task #:__6,7__; Input Required:		
To Other Task(s) From This Task (information needed to enable effect start or continuation of OTHER tasks or subtasks) To Other Task #: ; Input Required:		

Task 11 Research Plan: Two Photon Emission from Hg 254 nm Excitation

SCOPE

Describe more completely the scope of the work to be accomplished PRIOR TO Workshop-II:

To evaluate the possibility of obtaining Two-Photon emission from Hg 254 nm excitation.

LONGER TERM SCOPE

Note other critical research that will be needed within the OVERALL scope of the task, but probably **cannot** be accomplished within the time and budget constraints prior to Workshop-II:

Our task now is to evaluate possibilities. If such possibilities seem promising, then future work to prepare phosphors, to measure their performance, and to evaluate these performances critically will be prudent. If they are deemed unpromising, we will recommend to eliminate this task.

Subtasks

Develop and document some logical steps (e.g. 3 to 5 subtasks)

Deliverables

Think through what outcomes will be expected along the way, and describe these outputs (deliverables) at the end of each subtask.

Start/Finish

Schedule (after completion of Steps 5 & 6)

The primary excitation is at 253.7 nm or 39416 cm^{-1} .

The emitters are either two red emissions at 17000 cm^{-1} with Eu^{3+} , with an outside chance that Pr^{3+} or Tm^{3+} might also provide a red photon or that Tb^{3+} might provide a green photon. The absorber would be ideally one which has energy levels only at 17000 cm^{-1} and at 39000 cm^{-1} . Pr^{3+} , Gd^{3+} , Er^{3+} and Tm^{3+} are shown with energy levels near 39000 cm^{-1} . The most promising one is Tm^{3+} . The others have a clutter of lines near (39000-17000=) 22000 cm^{-1} which would likely prevent emission of the second visible photon. The $\text{Tm}^{3+} {}^1\text{G}_4$ state, however, might itself emit in the red or it might transfer to the $\text{Eu}^{3+} {}^5\text{D}_1$ state with subsequent emission of a red photon. This seems the only reasonable lead to a 254 nm two-photon phosphor.

A literature search on Tm^{3+} luminescence.

The search for band gaps of oxygen-based hosts which is a deliverable of Task 5 will be useful here also.

An assessment of the possibility of accomplishing this task.

Start: July
Finish: Dec

From Other Task(s) To This Task

(information needed to enable effective start or continuation of THIS TASK or subtasks)

From Other Task #5 Input Required: list of band gaps of oxygen based hosts.

To Other Task(s) From This Task

(information needed to enable effect start or continuation of OTHER tasks or subtasks)

To Other Task #: ; Input Required:

Task 12 Research Plan: Synthesis and Chemical Stability of Fluorides

SCOPE

Describe more completely the scope of the work to be accomplished PRIOR TO Workshop-II:

This team is charged with examining the stability of fluoride hosts. Identifying synthesis techniques to fabricate high purity (oxygen reduced) materials is a priority. Synthesis techniques typically involve a metathesis (exchange) reaction with a fluoride-containing compound. New reactions that contain less toxic gases than HF will be the focus. Another important issue is addressing manufacturing compatibility (stability in aqueous solutions). The questions to be asked are: Do anions or cations leach out in the solution? Do hydroxyl groups present on the surface even after baking out at 600°C? If so, do they degrade luminescence properties? Are electrostatic forces created that agglomerate the powders? A comprehensive literature search will be undertaken to specifically target these areas. Some preliminary data on weight loss in aqueous solutions will be generated.

LONGER TERM SCOPE

Note other critical research that will be needed within the OVERALL scope of the task, but probably **cannot** be accomplished within the time and budget constraints prior to Workshop-II:

Experiments will be undertaken to fabricate the fluoride powders using different precursors. Evaluation of compatibility issues will be carried out in a manufacturing condition.

Subtasks <i>Develop and document some logical steps (e.g. 3 to 5 subtasks)</i>	Deliverables <i>Think through what outcomes will be expected along the way, and describe these outputs (deliverables) at the end of each subtask.</i>	Start/Finish <i>Schedule (after completion of Steps 5 & 6)</i>
Investigate fluoride-host phosphor synthesis via literature searching.	References and published data.	Start: 7/01/01 Finish: 9/30/01
Determine manufacturing pitfalls for using these phosphors.	Well-defined pitfalls will be identified with significant contribution from OSRAM personnel.	Start: 7/01/01 Finish: 9/30/01
Identify candidate materials for coating the fluoride-based phosphors as a hedge if surface stability remains the limiting factor.	Candidate systems that do not degrade under VUV not interfere with the luminescence behavior	Start: 7/01/01 Finish: 9/30/01
Determine weight loss of candidate (or model) phosphors in manufacturing solutions.	Data	Start: 7/01/01 Finish: 9/31/01

From Other Task(s) To This Task

(information needed to enable effective start or continuation of THIS TASK or subtasks)

From Other Task #1 Input Required: Why does blackening of fluorides occur in Hg-discharge?
Does it happen with Xe-discharge?

From Other Task# 2 Input Required: What is the effect of oxygen contamination? What does the
PTCOE say about surface losses as related to MPPs?

To Other Task(s) From This Task

(information needed to enable effect start or continuation of OTHER tasks or subtasks)

To Other Task #2; Input Required: What levels of oxygen contamination can be expected from bulk
powders in a real lamp.

To Other Task #: ; Input Required:

B

FINAL RESEARCH TASK REPORTS

Task 1: Optical/Plasma Testing of Fluorides

Task Leader: Andries Meijerink

Task Member: Barry DeBoer

Introduction

The search for new phosphors for vacuum ultraviolet (VUV) excitation aims at finding efficient visible two-photon emission [1]. A phosphor with a quantum efficiency well above 150% is required to make Xe discharge lamps more energy efficient than the presently used Hg based fluorescent tubes. Emission of two visible photons after excitation around 170 nm does not allow for large non-radiative losses (only some 33%). As a result high energy levels of lanthanides need to be involved as an initial level in the two-photon emission process. In fluorides high energy levels from which emission is observed are most easily found. Two concepts for two-photon emission are presently considered seriously: downconversion in $\text{Gd}^{3+}\text{-Eu}^{3+}$ couples and two-photon emission processes involving the $^1\text{S}_0$ state of Pr^{3+} . In both cases the initial level is situated just below $50\,000\text{ cm}^{-1}$ (^6G level in Gd^{3+} and $^1\text{S}_0$ level in Pr^{3+}). In oxides it more challenging to apply these concepts. For example, for Pr^{3+} the $4f5d$ state has to be situated above the $^1\text{S}_0$ level. In fluorides this is easily achieved and has been known for many years. Recent work of Srivastava et al. has shown that this is also possible in oxides [2, 3]. For the $\text{Gd}^{3+}\text{-Eu}^{3+}$ couple in an oxide the charge transfer band of Eu^{3+} is at relatively low energies (below $50\,000\text{ cm}^{-1}$) [4, 5]. As a result direct energy transfer from the ^6G state of Gd^{3+} to the CT state of Eu^{3+} (resulting in one photon emission) is expected to be more efficient than cross-relaxation involving the parity-forbidden $^7\text{F}\text{-}^5\text{D}$ transition on Eu^{3+} . Also for other concepts for two-photon emission which are presently considered, using oxides complicates the two-photon emission process by having opposite parity states and the band gap at relatively low energies. However, in view of the many advantages of using oxides (e.g. known coating technology and proven optical stability) oxides are strongly preferred over fluorides. It is for this reason that in Task#5 the important task of evaluating possibilities for two-photon generation in oxide matrices is undertaken. The present report on Task#1 is especially useful if it turns out that it is not possible to find an efficient oxide two-photon emitter, while an efficient fluoride system is found. If indeed fluorides are shown to be only type of host lattice where efficient two-photon emission is feasible, the stability of fluoride host lattices under high energy UV radiation is very important. If fluorides degrade at time scales of e.g. less than $10\,000\text{ h}$, the reduced life time of the fluorescent tubes is a serious drawback. Also the coating technology and other steps in the lamp manufacturing process may be complicated by having fluoride phosphors, e.g. due to sensitivity to water or oxygen. In this report some these issues are addressed and a few initial experiments are reported. The following questions will be addressed:

- Are fluorides intrinsically stable under VUV radiation? If defects are formed even in the most perfect fluoride crystals due to VUV irradiation, there is little hope for fluoride lamp phosphors.
- What is the influence of water, oxygen or other impurities on the defect formation? For powders the large surface area will make the material more sensitive to water or oxygen. The influence of water and oxygen will be important in the manufacturing and coating process.

Most of the report will be based on experiments on the stability of fluorides under VUV radiation reported in the literature. There is the fortunate circumstance that recently a vast amount of literature has appeared on this issue in relation to the development of VUV wafer steppers for chip manufacturing [6]. By using shorter wavelengths, smaller structures (and thus higher information densities) can be made in silicon, but in the present generation of 193 nm and the future generation of 157 nm wafer steppers, fluoride optics (e.g. MgF_2 and CaF_2) have to be used. The stability of the fluoride optics under VUV radiation is even more urgent in this field.

Defect Formation in Fluorides

Defect formation in fluoride crystals has been extensively studied in alkaline earth fluorides and lithium fluoride [7, 8, 9]. The general idea is that defect centres are formed after excitation over the band gap. After the creation of electron-hole pairs self trapped excitons (STE) are formed which may either decay radiative or non-radiative to the ground state or they may be converted into a pair consisting of a vacancy (an F center) and an interstitial (an H center). The formation of these color centres has been well studied. In a Xenon discharge the highest energy radiation is the Xe monomer emission line and is situated at 147 nm. The fluoride host lattices considered for the two-photon emission all have band gaps at shorter wavelengths (higher energies), e.g. $E_g = 127$ nm for LiGdF_4 and 120 nm for LiYF_4 [10, 11], so the Xe discharge emission will not result in excitation over the band gap. As a result, the formation of color centres via the usual STE mechanism is not expected to occur. For sub-bandgap excitation damage (color center formation) has been observed for extremely high laser powers and ascribed to two-photon events [9]. These non-linear effects are not expected for the low powers (compared to lasers) in a fluorescent tube. Thus, there is no reason why in a perfect, impurity free fluoride crystals color centres are formed due to the VUV radiation from the Xe discharge.

Literature confirming the stability of fluoride crystals under VUV radiation has emerged recently. In a large number of publications the long term stability of CaF_2 and MgF_2 optics (lenses and windows) for VUV lithography have been tested. Both 193 nm pulses from an ArF excimer laser and 157 nm pulses from a F_2 excimer laser have been used to study the formation of color centers and changes in the VUV transmission spectrum [14, 15]. As an example, it is interesting to look at the study reported in [15]. Changes in the transmission of CaF_2 optics are reported under VUV excitation with a F_2 laser operating at 157 nm. The stability of the optics is high enough to have changes of less than 0.002 cm^{-1} in the absorption coefficient after 100 billion pulses of $0.5 \text{ mJ/cm}^2/\text{pulse}$. The total dose after 10^{11} pulses corresponds to $5 \cdot 10^7 \text{ J/cm}^2$. This should be compared with the dose of 10^7 J/cm^2 experienced by a phosphor layer in a typical fluorescent tube (30 W, 300 cm^2) after 20 000 hours. Based on this comparison it can be concluded that the intrinsic stability of fluoride crystals is very high and can be good enough to allow for long life times of fluoride phosphors under VUV radiation. More studies

on the long term stability of fluoride optics under 157 nm and 193 VUV radiation can be found in the literature overview at the end of this section. Note that here the intrinsic stability of high quality single crystals is considered. For real phosphors the influence of defects, impurities and surface states on the color center formation is important. This will be discussed in the next section.

A second source of phosphor degradation may come from the impact of ions in the Xe discharge in the tube. A few studies have reported the formation of color centers in an Ar plasma [16, 17, 18]. Under the influence of an Ar discharge color center formation is found in a MgF_2 window [16]. In Reference [17] color center formation in LiF due to an Ar plasma is reported. Reference [18] discusses various origins of the reduced transmission of a MgF_2 window in contact with a pulsed Ar discharge. The influence of the rare gas plasma in combination with the high energy UV radiation may cause the formation of defect centers, even in high quality single crystals. Since the radiation of the Ar discharge extends to high energies (exceeding the fluoride band gaps) future studies should establish if the defect formation is related to the impact of plasma ions or band gap excitation.

In the table below an overview of additional literature related to optical testing and defect formation in pure fluoride crystals is given together with a short indication of the research topic and material studied. The table may serve as a reference source for future studies.

Table B-1
Literature Studies on Defect Formation and Optical Testing of Undoped Fluorides

Reference	Topic
G.P. Callahan and B.K. Flint, Proc. SPIE-Int. Soc. Opt. Eng. 3578 (1999) 45-53.	Stability of thin film coatings under 157 and 193 nm laser irradiation
Y.M. Aleksandrov, K.V. Glagolev, V.N. Makhov et al., Zh. Prikl. Spektrosk. 40 (1984) 244.	Synchrotron study using 5-25 eV radiation to study color center formation in LiF. Also the mobility of F centers at 300 K is discussed.
A. Engel, K. Knapp, L. Aschke et al, Proc. SPIE-Int. Soc. Opt. Eng. 4404 (2001) 298.	Development and investigations of high quality CaF_2 for 157 nm microlithography
P. Boher, P. Evrard, J.-P. Piel and J.-L. P. Stehle, Proc. SPIE-Int. Soc. Opt. Eng. 4404 (2001) 133.	Purged system (1 ppm O_2 or H_2O) for optical characterization of optical components for VUV applications.
J. Webb, Laser Focus World 36(9) (2000) 87.	Review on use of CaF_2 in lithography.
L.I. Shchepina, S.S. Kolesnikov et al., Opt. Spectrosc. 90 (2001) 552.	Study of color center formation in LiF.
I. Tale, M. Spingis, P. Kulis et al., Radiat. Meas. 29 (1998) 279.	The origin and absorption spectra of color centers in LiBaF_3 are discussed.
E. Stenzel, N. Bouchaala, S. Gogoll et al., Mater. Sci. Forum 239 (1997) 239.	Color center formation in CaF_2 under x-ray and electron irradiation.
V. Baryshnikov, L.I. Shchepina, S.V. Dorokhov et al., Opt. Spectrosc. 73 (1992) 499	Photothermal conversion of different color centers in MgF_2 .
S.P. Freidman, A.F. Golota, V.R. Galakhov et al. Zh. Strukt. Khim. 27 (1986) 70.	Electronic structure and spectral properties of color centers in MgF_2 . 5eV absorbing centers.
R.F. Blunt, M.I. Cohen, Phys. Rev. 153 (1967) 1031.	Color center formation in MgF_2 by x-rays and optical properties and assignment of centers.

Influence of Impurities and Surface

The intrinsic stability of high quality fluoride single crystals confirms that stable VUV fluoride phosphor may be possible. However, a polycrystalline powder will be more prone to defect formation than a single crystal. In this section research on the influence of imperfections on color center formation in fluorides will be discussed. Three types of imperfections are considered:

- oxygen impurities in the crystal
- surfaces and species adsorbed on the surface
- transition metal and lanthanide dopants

It will become clear that color center formation is enhanced by the imperfections. This is not unexpected. Based on the negative influence of impurities, the synthesis procedure and further processing of the lamp phosphors should be adapted to reduce the effects.

Oxygen and hydroxide are a common impurities in fluorides. Due to the very similar size and chemical properties, O^{2-} or OH^- can easily replace F^- . The presence of oxygen is known to strongly enhance color center formation. Of the various studies in this field, here we will discuss a beautiful illustration reported in Reference [19]. Two types of fluoride glasses were prepared: a pure fluoride glass ($35AlF_3-5YF_3-7MgF_2-26CaF_2-14SrF_2-9BaF_2$, mol%) and a similar fluoride glass intentionally doped with oxygen by adding 0.5, 1 or 3 mol% $PO_{2.5}$. The oxygen content in the pure fluoride glass was ~450 ppm. The formation of color centers under the influence of ArF excimer pulses (193 nm) was followed in time by optical absorption and EPR measurements. In the oxygen doped glass an oxygen related color center was formed (increase linear with laser dose) absorbing at 6.9 eV with an oscillator strength of 0.1. Based on the EPR measurements the color center was tentatively assigned to an oxygen associated hole trap defect. Significant changes in the absorption densities (0.8 cm^{-1}) were obtained after relatively low doses (1200 pulses of 75 mJ/cm^2). This study shows that oxygen enhances color center formation. VUV absorptions due to oxygen impurities have also been discussed in [20, 21, 22]. The position of the oxygen impurity related absorptions are in the same spectral region (200-150 nm) where absorption bands are observed in $LiGdF_4:Eu^{3+}$ and $GdF_3:Eu^{3+}$ [23]. The nature of these bands has been under discussion. Possibly they are related to oxygen contamination

The effect of the surface is especially important for polycrystalline powders where the surface area is much larger than for single crystals. To study the influence of surface absorption however single crystals are typically studied [24]. By measuring the luminescence properties of a crystal with a freshly cleaved surface and following the luminescence over time, information on changes at the surface are obtained. The influence of surface adsorption for CaF_2 has been reported in Reference [25]. Of the various effects studied in this paper, the most impressive picture is shown below (Figure B-1). For the freshly cleaved crystal (line 1 in Figure B-1a) the sub-band gap absorption is low. Due to various treatments or just aging (line 2 in Figure B-1c) sub-band gap absorption bands increase. The absorption bands have been associated with the presence of OH^- at the surface. The adsorbed species also enhance color centre formation during VUV irradiation. The sensitivity to water and oxygen is a clear disadvantage of fluorides in comparison with oxides. The results in Reference [25] suggest that during the synthesis and manufacturing process oxygen and water should be avoided.

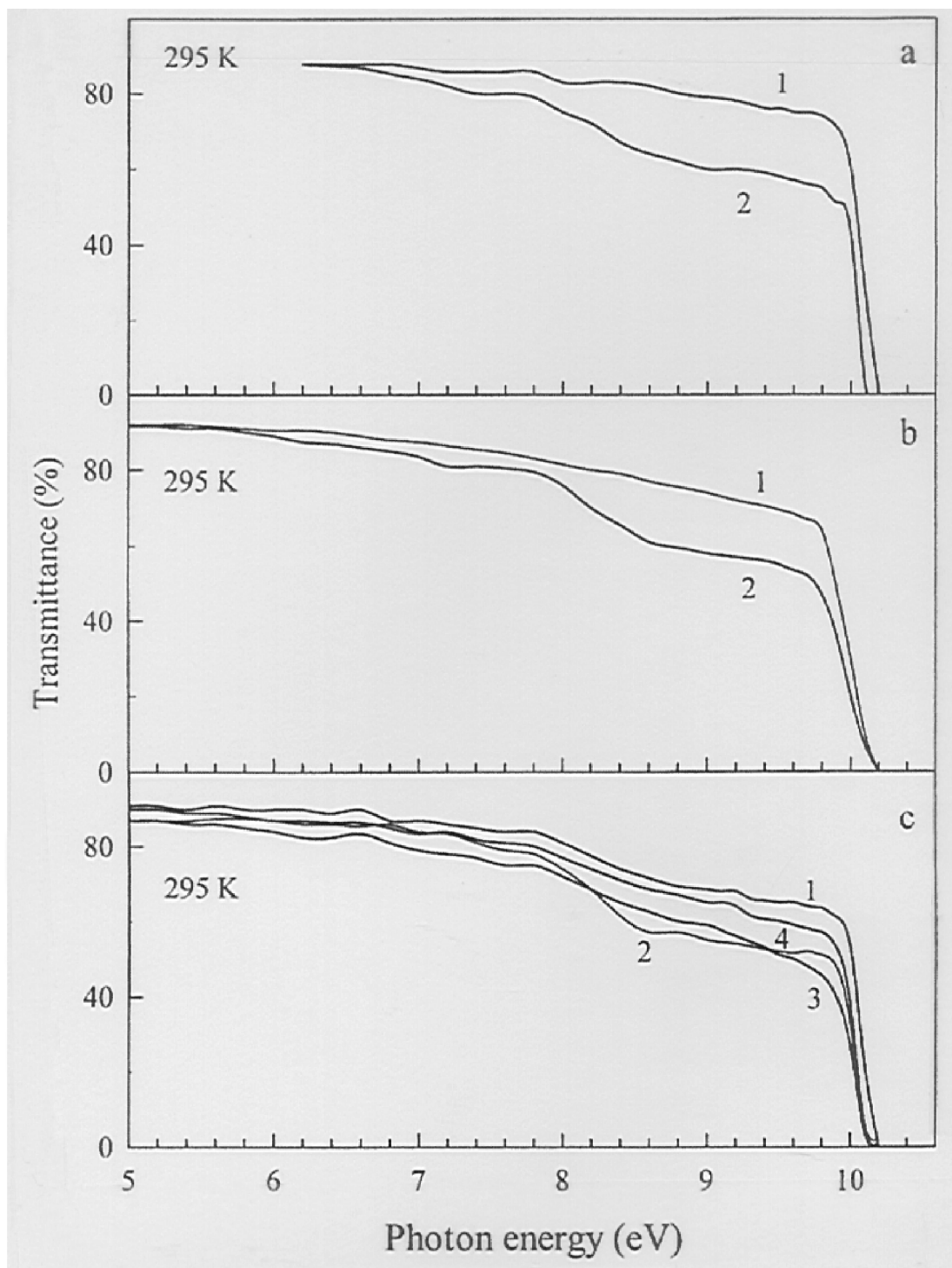


Figure B-1
Transmission Spectra of CaF_2 Crystals at 295 K. (a) Freshly Cleaved (1) and Polished (2) Samples. (b) Polished Samples before (2) and after (1) a Thermal Treatment. (c) Freshly Cleaved (1), Aged (2), Polished (3), Polished and Chemically Etched (4) Surface of Samples Cleaved from the Same CaF_2 Crystal. Reproduced from Reference [25].

Metal dopant ions have been reported to both stimulate color center formation and to reduce color center formation. In Reference [26] the reduction of radiation induced color center formation in BaF_2 is discussed. Reference [27] reports on suppression of VUV laser action in $\text{LaF}_3:\text{Nd}^{3+}$ by color center formation, while Reference [28] reports VUV laser action in the same material under 157 nm pumping. There is more consensus on the role of transition metal ions. Especially Fe^{2+} is frequently mentioned to have a strong absorption in the VUV. Additional literature (not discussed above) is included in Table B-2.

Table B-2
Literature Studies on Defect Formation and Optical Testing of Doped Fluoride Crystals

Reference	Topic
S. Fujino, M. Mueller, K. Morinaga, Proc. SPIE-Int. Soc. Opt. Eng. 4102 (2000) 324.	VUV transmission of fluoride glasses and the influence of Fe^{2+} .
I. Nuritdinov, M. Mussaeva, V.M. Reiterov, Opt. Spectrosc. 86 (1999) 262.	Radiation induced defects and luminescence of MgF_2 doped with Pr, Sm, Tb, Ho, Tm, Yb.
M. Mizuguchi, H. Hosono, H. Kawazoe, T. Ogawa, J. Opt. Soc. Am. B 16 (1999) 1153.	Study of color center formation in CaF_2 crystals doped with Ce^{3+} , Eu^{2+} , Tb^{3+} and Y^{3+} .
E.V. Zhukova, V.M. Zolotarev, L.P. Shishatskaya, Opt. Spectrosc. 81 (1995) 791.	Formation of F and M color centers in surface layer of MgF_2 under UV radiation.
G.J. Hollingworth, D.S. McClure, Phys. Rev. B 48 (1993) 13280.	Photoionization of Ce^{3+} in CaF_2 and defect migration. Diffusion leads to color centers.
P.V. Figura, A.I. Nepomnyashchikh et al. Opt. Spectrosc. 67 (1989) 1304.	Hole color centers (abs 6 eV) in $\text{CaF}_2:\text{Tm}^{3+}$ induced by x-rays.
G.A. Tavsshunskii, P.K. Khabibullaev, O.T. Khalikov, Zh. Tekh. Fiz. 53 (1983) 803.	UV/VIS absorption of radiation induced color centers in LiYF_4 doped with Er, Ho, Tm, Yb.
R. Rauch, R. Reinmann and G. Schwotzer, Physica Stat. Sol. A 23 (1974) 69.	Coloration of CaF_2 . Absorption band at 210 nm is assigned to O impurities.

Optical Testing

A few initial experiments were performed to test the stability of some fluoride samples under VUV radiation. Four samples were investigated: $\text{LiGdF}_4:\text{Eu}^{3+}$ 0.1% (polycrystalline powder), $\text{GdF}_3:\text{Eu}^{3+}$ (single crystal), $\text{LiYF}_4:\text{Er}^{3+}$ 2% (polycrystalline powder) and $\text{LiYF}_4:\text{Er}^{3+}$ 4% (single crystal). The polycrystalline samples were synthesized by mixing dry fluoride starting materials (LiF , GdF_3 , EuF_3 , YF_3 , ErF_3) in the correct molar ratio, using 5% excess of LiF . After mixing with NH_4F the samples were fired for 4 h at 550°C in a dry nitrogen atmosphere. The single crystals were grown by vertical Bridgman (see Reference [27]). After preparation, each

of the samples was irradiated with some 5 W/cm^2 VUV radiation of 160 nm (output from a 150 W deuterium lamp) for 24 h in a dry nitrogen flushed VUV spectrofluorometer. The luminescence spectra were recorded under identical conditions before and after irradiation. Also the time evolution of the luminescence intensity during irradiation was measured. The results are shown in Figures B-2 and B-3 for two of the samples. No changes in the emission spectra were observed for any of the samples. The luminescence intensity remains constant (apart from a periodic variation due a periodic change in the lamp intensity and an increase in the intensity for the $\text{LiGdF}_4:\text{Eu}^{3+}$ sample due to the slow removal of residual amounts of oxygen from the spectrofluorometer; oxygen absorbs the VUV radiation). Based on these initial experiments it can be concluded that there is no evidence for degradation of the phosphors due to VUV irradiation for the presently used irradiation time and dose. No evidence for defect formation is obtained (no broad defect related emission bands). Since the actual VUV doses during operation of a fluorescent tube will be at least 100 times larger, further experiments need to be done to properly address the issue of VUV induced degradation.

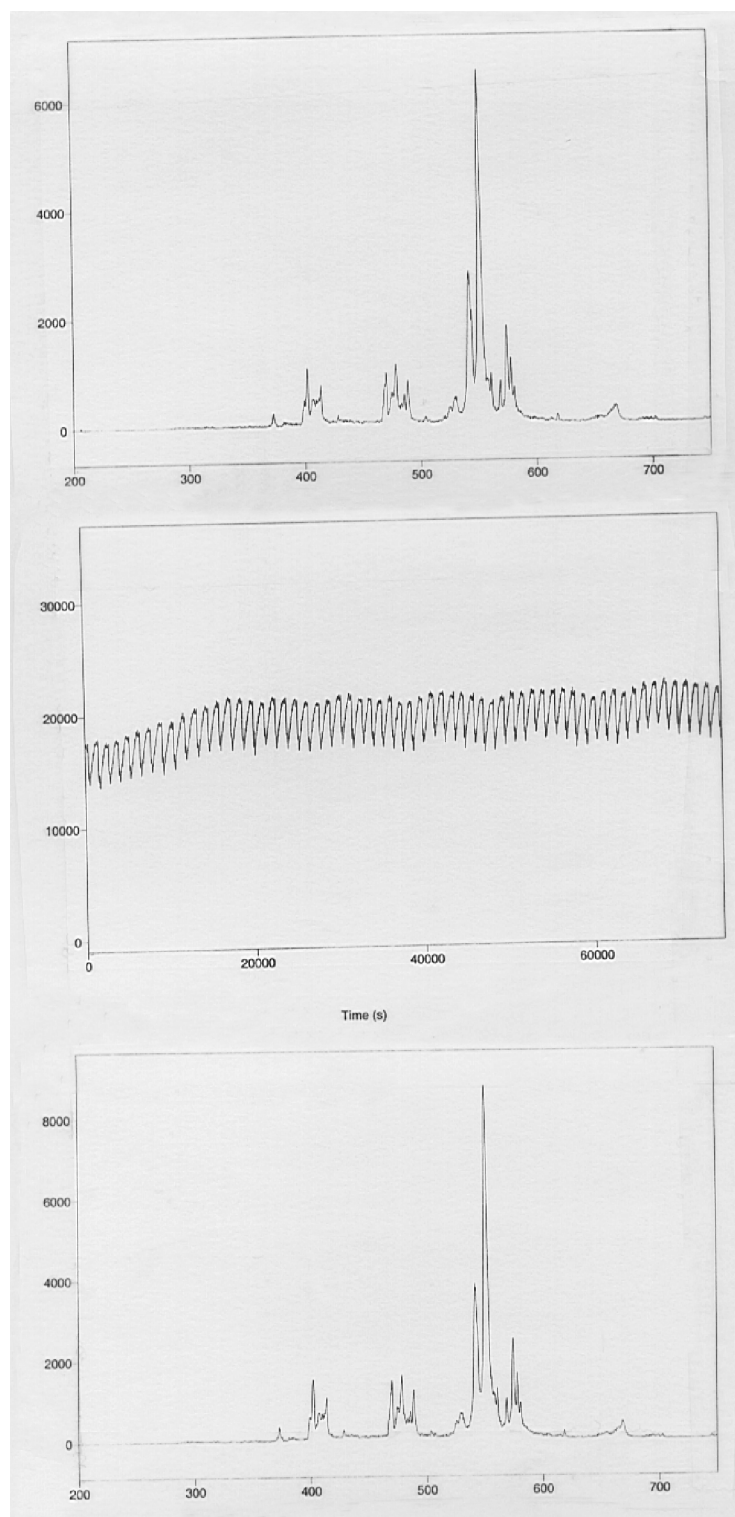


Figure B-2

(a) Emission Spectrum of a LiGdF₄:Eu³⁺ 0.1% Polycrystalline Sample before VUV Irradiation, (b) Time Evolution of the Emission Intensity During VUV Irradiation and (c) Emission Spectrum after Irradiation. The Gradual Increase in the Emission Intensity is due to the Slow Removal of Trace Amounts of Oxygen in the Spectrofluorometer. The Periodic Structure is due to Periodic Variations in the Lamp Intensity.

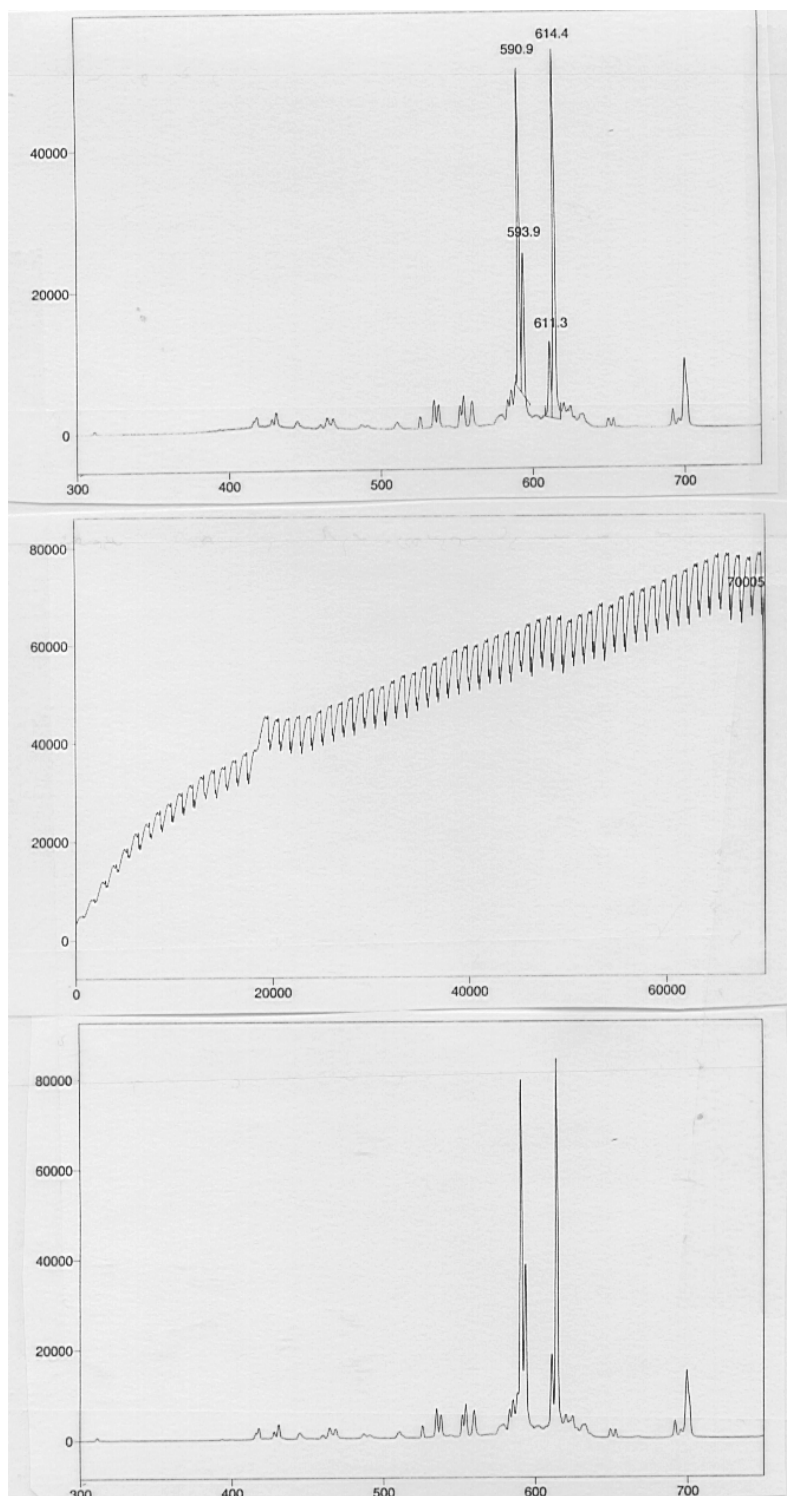


Figure B-3

(a) Emission Spectrum of LiYF₄:Er³⁺ 4% Single before VUV Irradiation, (b) Time Evolution of the Emission Intensity During VUV Irradiation and (c) Emission Spectrum after Irradiation. The Periodic Structure is due to Periodic Variations in the Lamp Intensity.

Conclusions and Recommendations

Research on optical testing of fluoride materials under vacuum ultraviolet excitation has provided a large number of useful publications from recent years due to the rapid development of new fluoride optics for VUV wafer steppers. One should benefit from experience in this field in the development of stable fluoride phosphors. Based on literature research and a few experiments the following conclusions can be formulated:

High Quality Fluoride Single Crystals

Optical testing of single crystals and theoretical models on defect formation in fluorides indicate that the intrinsic stability of fluoride crystals is very high under VUV (sub-band gap) excitation. VUV doses from lasers exceeding the estimated VUV dose for a Xe discharge phosphor during the life time of a fluorescent tube by a factor of five do not suffer from color center formation. Literature on the stability of fluoride crystals in contact with an Ar plasma indicate that a rare gas plasma promotes color center formation. This may be a problem.

Crystalline Fluoride Materials with Impurities

The presence of oxygen or hydroxide in or at the surface of fluoride crystals enhances color center formation under VUV irradiation. Oxygen color centers absorb in the (V)UV region and can cause a rapid decrease in the efficiency. This has important implications for the synthesis and tube manufacturing process. Other contaminations (e.g. Fe^{2+}) also cause strong VUV absorptions.

Optical Testing

Some simple initial tests on four samples did not provide evidence for a decrease in the luminescence efficiency after 24 h of 5 W/cm^2 160 nm radiation. No changes in the emission spectra have been observed. Since the actual dose during a realistic life time of a fluorescent tube is more than 100 times more, the initial tests are not very meaningful.

Recommendations

The research on the stability of fluoride phosphors in a Xenon discharge will become very important as soon as a two-photon emitting phosphor with a quantum efficiency close to 200% has been made. This is not the case yet. As long as this not the case research on optical testing and color center formation in fluoride phosphors should be aimed at doing well-planned initial experiments which will give an idea on the stability of non-optimized polycrystalline samples. In addition it should be investigated if color center formation occurs for high quality crystals in a xenon plasma. The initial research plan includes:

- testing of fluoride phosphors and high quality fluoride single crystals in a xenon discharge tube
- measuring the light output of fluoride phosphors under VUV laser (F_2 excimer at 157 nm) excitation as a function of time, using a high total VUV dose.

Based on these experiments an idea will be obtained on the stability of fluoride phosphors under VUV excitation and in combination with a VUV discharge. If the light output is relatively stable, further research can be started on optimizing the phosphor stability (reducing color center formation) as soon as an efficient multi-photon phosphor has been found (e.g. when a good sensitizer for the Gd-Eu couple has been found). Serious research on optimizing the stability will include careful studies on the defect formation under VUV excitation and requires help from additional techniques like Electron Paramagnetic Resonance and thermoluminescence to identify the nature and stability of color centers.

Task 2: Bulk and Surface Defects in Fluorides

–Final Report –

Task leader: Madis Raukas
Task members: Douglas Keszler
William White
Baldassare Di Bartolo

Goal

Understanding defect formation criteria and mechanisms, influence of surfaces and oxygen contamination on luminescence efficiency of future fluoride phosphors.

Part I (D. Keszler)

Recent observations of multiphoton emission in fluoride luminescent materials¹ have raised the possibility for their utilization in high-efficiency lamps. This use, however, is predicated on a suitable performance within the lamp discharge, i.e., the phosphor must exhibit both satisfactory light output and stability. In particular, the resistance of fluorides to degradation in the lamp manufacturing process and during lamp operation is vitally important for their successful use. While these aspects of fluoride-phosphor use have not been directly assessed, a literature review can provide considerable insight into some potential problems.

Degradation of phosphor performance in lamps has generally been associated with the lamp-manufacturing process, radiation-induced color-center formation, mercury adsorption, and ion-bombardment processes. It is anticipated that multiphoton fluoride phosphors will be used in conjunction with an inert-gas discharge, so mercury adsorption will not be considered here.

When irradiated with VUV radiation, many phosphors become slightly colored and their luminescence efficiency decreases.² The color is attributed to color-center formation. In Hg-lamp operation, these color centers lead to a decrease of luminescence efficiency through absorption of the 254-nm excitation light and subsequent relaxation by nonradiative processes. The effects of these color centers can be limited by their bleaching with the 254-nm light, high activator concentrations, and the addition of impurities that hinder formation. Such color centers and related defects could play major roles in determining the performance characteristics of multiphoton fluoride phosphors, possibly affecting absorption characteristics as well as important energy-transfer processes.

¹ R. T. Wegh, H. Donker, A. Meijerink, R. J. Laminmäki and J. Hölsä, Phys. Rev. B 56, 13841 (1997); R. T. Wegh, H. Donker, K. D. Oskam, and A. Meijerink, Science 283, 663 (1999); R. T. Wegh; E. V. D. van Loef, and A. Meijerink, J. Luminescence 90, 111 (2000).

² J. M. Flaherty, J. Electrochem. Soc. 128, 131 (1981).

An introduction to the creation, energetics, and mobilities of defects in wide band-gap solids is provided by the treatise of Crawford and Slifkin.³ Absorption of light and interaction with charged particles represent two important modes for the creation of defects in solids. Intrinsic light absorption in an undoped fluoride involves transfer of electron density from the valence band to the conduction band. This transferred electron can be trapped at a vacancy to produce a color center, and the resulting hole can be trapped on fluoride anions to produce a V_k center, F_2^- . To date, however, a stable V_k center has not been observed at room temperature in any fluoride. This result coupled with a light flux far below that required for dielectric breakdown⁴ indicates that fluorides should be intrinsically stable to the VUV radiation in a broad-band, inert-gas discharge such as Xe_2 . Incorporation of impurities, however, can considerably change this situation. In the case of fluorides, the impurities of most concern would appear to be metal species that can easily change oxidation states and oxygen. $CaF_2:Ce$ for example exhibits an absorption spectrum exhibiting normal Ce^{3+} features. Irradiation with light of energy greater than 2.8 eV, however, leads to new absorption features consistent with Ce^{2+} . Subsequent irradiation at 1–1.8 eV leads to the reformation of Ce^{3+} . Other fluorides such as $CaF_2:Sm^{2+}$, Eu^{3+} and $CaF_2:La$ are well-known photochromic systems.⁵ The effects associated with such photochromism could lead to deleterious consequences in VUV phosphors, although we are not aware of any specific studies on these types of photochromic effects induced by VUV radiations. To make predictions about the stability of various metal oxidation states requires specific information on the energies of the metal-centered levels relative to the valence and conduction bands of the host. These energies are generally extracted from photoemission measurements, but data for the lanthanides in insulating materials have only recently become available.⁶

In general, to achieve suitable charge compensation, substitution of O^{2-} for F leads to the formation of fluoride-vacancy defects, and these defects and their aggregates have been reported to produce absorption features in the VUV portion of the spectrum in the $KMgF_3$ ⁷ and the binary fluorides CaF_2 , SrF_2 , and BaF_2 .⁸ Numerous studies have been reported on O^{2-} substitution for F⁻ in the storage phosphor $Eu:BaFBr$.^{9,10} In this material, the substitution leads to an absorption band centered near 250 nm, and in the storage process the O^{2-} ions capture holes to form O^- centers. Each of these features could play a role in affecting the performance of a VUV fluoride phosphor. A theoretical treatment of the stability and optical properties of the O^- center in BaF_2 is available.¹¹ As an impurity, hydrogen could also play a role in affecting the optical properties

³ Point Defects in Solids, Vol. 1 General and Ionic Crystals, eds. J. H. Crawford and L. M. Slifkin, Plenum Press, New York, 1972.

⁴ See J. Reif, S. Petzoldt, A. P. Elg, and E. Matthias, Appl. Phys. A, 199 (1989) and references cited therein.

⁵ Z. J. Kiss, Phys. Today 23, 42 (1970).

⁶ C. W. Thiel, H. Crugal, H. Wu, Y. Sun, G. J. Lapeyre, R. L. Cone, R. W. Equall, and R. M. Macfarlane, Phys. Rev. B 64, 085167 (2001).

⁷ A. V. Gektin, V. K. Komar, N. V. Shiram, V. V. Dhlykhturov, N. P. Nesterenko, IEEE Trans. Nucl. Sci. 42, 311 (1995); A. V. Gektin, V. Komar, V. Shlyakhturov, N. Shiran, IEEE Trans. Nucl. Sci. 43, 1295 (1996).

⁸ E. Radzhabov, P. Figura, Phys. Stat. Sol. B, 136, K55 (1986); E. Radzhabov, P. Figura, Phys. Stat. Sol. B, 186, K37 (1994).

⁹ K. Takahashi, K. Kohda, J. Miyahara, Y. Kanemitsu, K. Amitani, S. Shionoya, J. Lumin. 31 & 32, 266 (1984); Y. Dong, M. Ren, C. Mu, J. Lin, M. Su, J. Lumin. 81, 231 (1999); F. K. Koschnick, Th. Hangleiter, K. S. Song, J.-M. Spaeth, J. Phys.: Condens. Matter 7, 6925 (1995); S. Schweizer, J.-M. Spaeth, J. Phys.: Condens. Matter 11, 1723 (1999).

¹⁰ For use of $BaFBr:Eu$ in detection of VUV, see: A. Ben-Kish, A. Fisher, E. Cheifetz, J. L. Schwab, Rev. Sci. Instrum. 71, 2651 (2000).

¹¹ J. M. Vail, E. Emberly, T. Lu, M. Gu, and R. Pandey, Phys. Rev. B 57, 764 (1998).

of fluoride phosphors. Hydride has been proposed to affect the storage properties of $\text{Eu}:\text{BaFBr}$,¹² and the presence of hydrogen has also been associated with the long afterglow of $\text{UO}_2^{2+}:\text{SrSO}_4$ ¹³ and electron trapping in $\text{Eu}^{2+}:\text{Ba}_3(\text{PO}_4)_2$.¹⁴ Some specific types of surface chemistry could also play a significant role in the creation of defects. For example, Eu^{2+} is often observed at the surface of phosphors, where the intention has been to dope them with Eu^{3+} .¹⁵

Most of the work on the creation of defects in ionic crystals with charged particles such as electrons, protons, and alpha particles has been done with irradiating energies on the order of MeV. This greatly exceeds the energies associated with an inert-gas discharge. The nature of the interactions between charged particles and phosphors at lamp energies has been summarized by Lehmann.¹⁶ Here, sufficient energy resulting from an acceleration of ions near the phosphor surface and their subsequent recombination with electrons at the surface produces sufficient energy to create and move defects in oxide phosphors. With a sufficient number of defects, the surface of the phosphor becomes amorphous. These defects can migrate deeper into the particle, degrading phosphor performance by producing a nonluminescent sheath that still absorbs excitation light. Considering the lower energies that are required for defect formation and migration in fluorides in comparison with oxides, this process could be a severe source of degradation for fluoride phosphors. Stable defects are reported to occur on exposure of clean CaF_2 surfaces to O_2 ,¹⁷ and many fluorides are known to hydrolyze at temperatures as low as 100°C . These features cause additional concern for the stability of fluorides in lamp operation, as lamp-manufacturing and phosphor-handling processes are likely to result in highly oxygenated phosphor surfaces. Such surface oxide could then be easily transferred deeper into the bulk of the phosphor during lamp operation via the energetic ion mechanism proposed by Lehmann.

Conclusions and Recommendations

Numerous impurities and defects could play major roles in affecting the performance characteristics of multiphoton fluoride phosphors. During phosphor development, it is likely that compositional variations and synthesis conditions will have to be carefully examined to minimize the effects of oxygen incorporation. Also any variable oxidation-state metal species having energy levels near the valence band can lead to the formation of color centers following photoexcitation. Considerable care will likely have to be undertaken in manufacturing and handling processes to minimize problems. Because incorporation of oxide through background gases (O_2 and H_2O) in the lamp may also lead to degradation, it is likely that the fluoride particles will require a protective oxide coating to realize their full potential. This oxide coating may also absorb the higher-energy portion of the inert-gas emission band, limiting color-center formation through photoionization processes. An additional approach is to examine mixed oxide fluorides, e.g., aluminate fluorides, borate fluorides, and silicate fluorides. Only a small number of such compounds are known, but new examples should consistently provide multiphoton emission from Pr^{3+} . For polyoxoanion-fluoride compounds, exceptionally low impurity and defect concentrations are possible.

¹² M. K. Crawford, L. H. Brixner, *J. Lumin.* 48-49, 37 (1991).

¹³ M. Kumar, A. G. Dalvi, M. D. Sastry, *J. Phys. C: Solid State Phys* 21, 5923 (1988).

¹⁴ W. J. Schipper, J. J. Hamelink, E. M. Langeveld, and G. Blasse, *J. Phys. D: Appl. Phys.* 26, 1487 (1993).

¹⁵ N. Mårtensson, B. Riehl, R. A. Pollack, F. Holtzberg, and G. Kindl, *Phys. Rev. B* 25, 6522 (1982).

¹⁶ W. Lehmann, *J. Electrochem. Soc.* 130, 426 (1983); see also O. Tada, K. Tominaga, T. Kondo, Y. Kondo, K. Ichinomiya, *J. Electrochem. Soc.* 131, 1365 (1984).

¹⁷ M. Reichling, C. Barth, *Phys. Rev. Lett.* 83, 768 (1999).

Part II (M. Raukas)

Introduction

The literature regarding point lattice defects and their electronic properties in compounds containing fluorine and other halides is extensive. However, halides of alkali metals and silver along with some semiconductors have been among the most favorite materials of the scientists working in this field [28-34]. A selection of oxides has also been studied quite thoroughly [35, 36]. All together it offers limited help towards understanding the stability of numerous other compounds (including fluorides) under ionizing radiation. Further, majority of the studies have utilized either high-energy particle (electrons, ions in MeV range) or radiation (x -, γ -ray) sources as means to create defects and focus thereafter on describing various properties of the appeared centers. Actual energy thresholds for forming the defects (sometimes in VUV range) have been studied much less. Cryogenic temperatures were often involved during either creating or observing the defects that leaves enough room for doubts about the existence of many of them at room temperature or higher. For example, V_k -centers (self-trapped holes) are typically not detected at higher than 200°K. From long term performance (lamp ‘maintenance’) point of view one should concentrate on defects and underlying mechanisms that persist up to about 100°C, i.e. temperatures that can be observed upon lamp operation.

Harmful effects of color centers and other defects appear in the competition for the exciting or emitted energy. This concerns also defects that are short-lived at a given temperature, contributing thus to the overall efficiency of the phosphor without being detected in ‘maintenance’ behavior. Defects typically manifest themselves in absorption that, depending on the defect, can be found in the spectral range from VUV to visible. One has the Mollwo-Ivey relation [37] describing correlation between peak color center absorption and average oxygen ion spacing in oxides of group II and III metals (the absorption energy increases as the distance decreases). It can be used to predict the deleteriousness of the specific defect with respect to the activator in terms of positioning of the absorption bands in various lattices. For fluorides we have not come across such generalized result. Some examples: In $LiYF_4$ [38], γ -irradiation resulted in at least four wide absorption bands at 272, 335, 450 and 650 nm. The bands were assigned to F-centers or their aggregates. In $NaMgF_3$ such bands appeared at 245, 290 and 345 nm [39] and in MgF_2 at 260, 370 and 400 nm (the latter due to M-centers) [40].

Phosphor Degradation in Lamps

Classification of underlying processes [41]:

1. Electronic class – no atomic/ionic defects are formed, just the electronic states of the *existing* lattice defects are changed as charge is moved around by photons inducing and bleaching color centers.
2. Photochemical class – new or additional atom or ionic defects are formed, typically by a series of reactions beginning with the photoexcited electron. There is usually not enough energy for “knock-on” events.

3. Diffusional class – new defects are formed under precipitation, aggregation or evaporation at extended defect locations or through external penetration of the phosphor by impurities.

Classes 2 and 3 contribute generally to long-term depreciation while phenomena in Class 1 can be short-lived.

Hypotheses and validated models regarding the reasons and mechanisms of phosphor degradation are the following [42-44]:

1. Bombardment by discharge ions and recombination of ions and electrons on the surface of phosphor; direct breaking of chemical bonds;
2. Structural changes in the phosphor material and/or formation of a nonluminescent amorphous layer; atoms are moved from their regular positions; in lamp phosphors takes place on the surfaces only due to low incident ion energies;
3. Photochemical processes – (V)UV-induced oxidation-reduction of host matrix and activator ions, particularly at shorter wavelengths than 254 nm; takes place via capturing or release of excited charge carriers at already *existing* defects that gives rise to various absorptions;
4. Formation of deep color centers that produce competitive absorption of the exciting and/or visible radiation, or alternatively stay in direct interaction with luminescence centers capturing and degrading the energy from activators;
5. Accompanying to (2) and/or (4) a release of anions (e.g. oxygen, chlorine, fluorine) from the phosphor material that leaves lattice vacancies behind;
6. Adsorption/absorption of Hg onto the surface of phosphors and/or forming mercury compounds;
7. Interaction with the glass envelope with e.g. sodium ion diffusion from glass onto the phosphor particles where they could act as seeds for Hg-absorption [45];
8. Material emission from and/or reactions due to electrodes;

First hypothesis is based on experiments with shielded (by MgF_2) phosphors in discharges. Estimated kinetic energy of ions cannot exceed about some 10-15 eV in Hg-discharge, imposed by sheath potential. Positive ions attracted by the sheath potential and electrons recombine at the surface, releasing for example 10.2 eV for Hg, 12.1 eV for Xe, 15.7 eV for Ar, etc. Possible combination of kinetic and recombination energies therefore amounts to some 20-25 eV in maximum. Ar ion recombination on silicon surface has been shown by an elegant experiment to release Na-ions bound to the surface [46]. Na-ions are found thereafter to diffuse into the bulk of the crystal. The structural damage in hypothesis (2) can be caused by the mechanisms indicated in (1), followed by diffusion of defects into lattice. This way useful energy transfer channels from the site where excitation is absorbed to the activator ions can be destroyed [45, 47]. Photochemical processes in (3) are caused by absorbing a photon of incident radiation and require significantly less energy than ion displacement in (2). Irradiation energies below the bandgap of the material are typically expected to cause only short-term degradation. Essentially,

(4) can be regarded as an extension of (3) with active vacancy creation. The formation of color centers and non-radiative or surface recombination centers (4) concentrates (at least initially) on the surface of the particles or on the topmost layer of the powder that is immediately adjacent to the discharge [20]. It is the result of a shallow absorption depth of the incident (V)UV-radiation and/or due to ions of relatively low energy striking the surface. In halophosphates, loss of surface fluorine has been shown to allow new vacancies to diffuse into the phosphor [44]. Some of the depreciation in phosphor luminance/efficiency (e.g. due to mechanisms in (2-5)) can be recovered by annealing. Hypotheses (6) and (7) are usually found to be of lower order than other effects. We found no comments in the literature on hypothesis (8) regarding fluoride materials.

Defect Formation

Stability Criteria and Defect Creation Energies

In general, the stability of a lattice against bombardment damage and heating is a function of binding energy between the atoms of the material. The kind of defect that will appear in the lattice depends on the amount of energy required for removal of an ion from the lattice site and its incorporation in the interstitial position. When this energy is considerably lower for a cation (anion) than for an anion (cation), the Frenkel (anti-Frenkel) type defects become dominant. (Frenkel defect is a cation situated in interstitial position and a vacancy in the cationic sublattice.) If the energies required for the formation of defects are comparable, the defects of the Schottky type appear [48]. (Schottky defect: one vacancy in both cationic and anionic sublattice with both ions diffused from their sites to the surface of the crystal.) However, it should be stressed that the same compound showing predominance of defects of one type in a given temperature range may show predominance of the other type in suitably changed thermodynamic conditions. In general, electrostatic binding energy in its basic form can be expressed as [41]

$$E_b = A(Ze)^2/r$$

where the ionic charges are $\pm Ze$, r is the nearest neighbor distance and A is the Madelung constant (about 1.6-1.8). E_b for alkali halides ($Z=1$) range from 6 to 10 eV whereas for the alkaline earth oxides ($Z=2$) the values are found to be around 30-40 eV. The energies of electronic excitations (excitons, in the broadest sense) in alkali halides have a range of 5-10 eV which is sufficient to create defects since the atomic binding energies are of the same order. In the alkaline earth halides the binding energies are higher and in alkaline earth oxides the excitons of a similar energy are not able to cause atomic displacements against 30-40 eV binding energies. The trend in interionic distance is well illustrated by calculations in [49] and also reflected in Table B-3 for CaF_2 , SrF_2 and BaF_2 .

The enthalpies (ΔH_s) and energies of formation for various defects can be calculated and in some cases have also been compared to experimental results (reliable values for the latter are hard to extract) [35, 36, 48, 50, 51]. Values presented in literature are with quite a wide spread and in some cases even confusing. Often the type of defect has not been described. This is reflected also in the values shown in Table B-3. However, one can note the trends in and between alkali halides, alkaline earth halides and oxides etc.

Table B-3
Approximate Energy Values of Defect Formation in Solids

Compound	ΔH_s (kcal/mole)	Energy (eV/defect)	Defect type
LiF	62	2.7	Schottky pair (singly charged)
LiCl	49	2.1	
LiBr	41.5	1.8	
LiI	31	1.4	
CaF ₂	65	2.8 (3.5*)	Frenkel pair $V_F^\bullet + F_i'$ $M_i^{**} + V_M''$
SrF ₂		1.8	
BaF ₂		2.0	
MgF ₂		3.6*	
Y ₂ O ₃	240	10.4	oxygen vacancy (doubly charged)
TiO ₂	105-115	4.6-5.0	
V ₂ O ₅	30	1.3	
Ta ₂ O ₅	150	6.5	
WO ₃	69	3.0	
MgO	90-150	4.0-6.5	Schottky pair
CaO, SrO, BaO	100	4.4	
Al ₂ O ₃	470	20.4	
MgO		>10 (12.7)	oxygen vacancy
SiO ₂		8.3	
ZnS	90-150	4.0-6.5	Frenkel pair

* - estimates based on the melting points.

Defects tend to form at points of the weakest local structure in lattice (in terms of bond strength) where ionic displacements can occur more easily. A typical mechanism for creating color centers is nonradiative recombination of a self-trapped exciton, demonstrated in alkali halides, or involves a self-trapped electron or hole that occur in many solids [52, 53]. The lattice structure in the region of trapping may be sufficiently weak to give in to the local distortions, resulting in a vacancy or/and interstitial creation. This can be also strongly influenced by the presence of local vibrations with higher than phonon frequencies or the existence of certain ion groups (e.g. silicates, tungstates, vanadates, see Table B-3).

At higher excitation energies than VUV radiation (x-rays, high-energy particles) the possibilities include either Varley mechanism with its multiple ionization events or, alternatively, a relaxation of core exciton, both followed by the ejection of the ion from the lattice site [29]. F-center production efficiency spectra for KBr at 77 K show the threshold at about 5 eV or lower, depending on the sample history [29], and in RbMgF_3 or NaMgF_3 at around 7.75 eV [39, 54]. In CaF_2 , the mechanism of decaying excitons is thought to be active [55]. The lowest-energy exciton prior to relaxation is formed at 11.2 eV, energy for creating a Frenkel pair has been calculated at around 6-8 eV [56] (or even lower according to the data in Table B-3). On the other hand, the direct displacement mechanism in CaF_2 [57] predicts the threshold to lie at around 20-30 eV, in accordance with the predictions from the bond strength. For comparison, discrete energy values or spectra of defect creation efficiency in quartz and other materials have been measured or calculated [31-33, 56, 58, 59].

Allen et al [60] have studied point defect formation in polished single crystals of LiF , CaF_2 and MgF_2 exposed to the outer space environment – mostly to solar UV-VUV spectrum of energies lower than 12 eV. With the exception of an inconclusive result regarding MgF_2 , all the samples exhibited degradation under solar radiation. Induced absorption is most likely due to F-centers and the aggregates. Another study tested the optical materials for space environment by exposing them to doses of 1-2 MeV electrons [61]. Apart from sapphire, MgF_2 and BaF_2 were pointed out as the most radiation resistant of the group including LiF , CaF_2 , fused SiO_2 and Al_2O_3 .

Effect of Ambient Temperature

As described previously, one expects alkaline earth fluorides to be more defect resistant than alkali halides. Indeed, MgF_2 and CaF_2 are used as materials for making single crystal optical elements suited for VUV range. Both of them are superior in radiation resistance to often used LiF . It has been stated that the efficiency of color center formation by x-rays is detectable only below 100°K in pure Ca or Sr fluorides and no evidence of it has been found at room temperature [62, 63]. For MgF_2 , the F- and H-center (here a F_2^- molecule at F site) production under high-energy electrons shows about 20% yield at room temperature but most of them are believed to decay within a few msec [55]. Yet, nominally pure MgF_2 in another study is described to have stable F-centers up to 300°C [40]. In the study involving exposure to space radiation [33], some of the samples that developed enhanced absorption were maintained at 60°C. Stable defects were observed in LiYF_4 at room temperature after x-ray irradiation [38]. It is known that annealing at elevated temperatures (hundreds of °C or more) is used to eliminate many lattice defects by forced mutual recombination or by utilizing ambient atmosphere in the diffusion process (e.g. removal of oxygen vacancies). One may conclude that there exist color centers or other point defects in fluorine containing materials that persist at room temperature or higher and are responsible for the absorption features observed.

Effect of Impurities in the Material

Although majority of studies focus on pure materials, the influence of impurities cannot be overlooked [30, 40]. Regarding Class 1 phenomena, host impurities and intrinsic defects are intimately connected (the presence of one often requires the presence of the other). Pre-existing defects are influenced by growth conditions, stoichiometry and charge compensation mechanisms. Unintentional or intentional doping (“activating”) increases the efficiency of creating defect absorption bands compared to the pure materials [64], as it is observed in $\text{MgF}_2\text{:Co}$ [40]. Impurities or dopants that require charge compensation of some sort

(e.g. Gd^{3+} in KBr, [30]) give rise to clearly more intense defect absorption upon irradiation in VUV range. The impurity cations that easily change their valence states (e.g. Ce, Tb, Eu or transition metals) afford a higher probability of bringing about a variety of defects. Also, one would expect undesired oxygen for F⁻ ion substitution to create anion vacancies (and therefore color centers) in fluorides. On the other hand, no VUV or x-ray induced absorption was detected in Pb-doped RbMgF_3 [54] whereas pure material developed clear evidence of F^\cdot , F_2^\cdot and V_k -centers. The exact mechanism of this is not understood although Pb-ions could suppress the coloration by absorbing the energy otherwise used to create defects. In conclusion, the presence of other than constituting elements in the host lattice typically raises the chances for defect formation under irradiation.

Effect of Sample Morphology. Surface Defects

The degree of defect creation in polycrystalline materials under high-energy irradiation is many times higher than in single crystals as demonstrated by the example of coloring LiF single crystals and thin films [64]. It can be understood in relatively simple terms when considering the orders of magnitude larger surface area and enhanced scattering power of a powder compared to a single crystal. Enhanced scattering in nominally pure polycrystalline material creates orders of magnitude higher chances for the incident photons to get absorbed even if its energy falls low of the bandgap. Weak absorption due to band tailing or impurities/defects of low concentration is amplified by multiple reflection and transmission events that significantly increase the effective path length in bulk. Therefore, comparing the radiation resistance results obtained on single crystal materials (effectively one pass for each photon per thickness of the sample) and powders can be misleading.

At surface, the periodical structure of the lattice has been disrupted for each point where the bulk meets a surrounding atmosphere. The interface is thought to be irregular, containing random vacancies and/or adsorbed ions. Such situation would lower significantly the energies for defect creation as has been shown in case of MgO [36]. Formation energies of a neutral oxygen vacancy V_o^\cdot (F-center) in the bulk and on the surface have been calculated to be >10 eV (11.9 eV) and 5.6-8.5 eV, respectively. Because of that the surface defects are expected to be thermodynamically more stable than bulk defects [65]. At temperatures $T > 0$, such a defect can diffuse into the bulk thus “vacating” a spot for the next event. The sequence of formation energies for e.g. oxygen vacancies in MgO depends directly on the number of surrounding ions [65] (see Table B-4), as in $E(\text{bulk}) > E(\text{surface}) > E(\text{step=edge}) > E(\text{corner})$.

Table B-4
Formation Energies of a Neutral Oxygen Vacancy in MgO [65]

Site	Coordination	Formation Energy (eV)
sub-surface (bulk)	6	9.7
sub-surface (bulk) [36]	6	>10
surface	5	8.1
surface	5	7.8
surface	5	8.5
step (edge)	4	6.85
corner	3	5.6

It is also a known fact that milling or any other disruptive mechanical treatment of a freshly synthesized polycrystalline material can introduce lattice distortions that result or assist in the generation of defects [66-68]. For the case of halophosphate, the brightness of luminescence decreases up to 20% (depending on the duration of grinding) with the dislocation density increasing from 10^8 to 10^{10} cm^{-2} [69]. The reasons for this can be multiple, starting from adding sites for ion-electron (or electron-hole) recombination to gaining higher surface area that has a lowered threshold for radiation damage. Faster non-radiative surface recombination rate for electrons and holes competes with the radiative relaxation at activator ions.

It has been shown that understanding the role of a surface in photo- and cathodoluminescence phenomena requires studying the nature of the surface states, local electric fields due to trapped charges and the band structure at surfaces [70-72]. For example, luminescence intensity in $\text{Y}_2\text{O}_3:\text{Eu}$ and $\text{Y}_2\text{SiO}_5:\text{Tb}$ (under low-voltage CR excitation) can to an extent be controlled by impressed external electric fields over phosphor layer [73]. According to the classical picture of non-radiative loss mechanism at defect sites, the sequential trapping of electrons and holes is involved. The rate of it is governed by the smaller capture cross-section of the two processes. Controlling the capture and/or mobility of electrons or holes permits the control over losses of excitation. External electric field can slow down or accelerate charge carriers towards the surface, therefore changing the balance of electrons and holes at the surface.

Conclusions

Most of the considerations presented in Sections 1-3 make use of energetics criteria for defect formation, particularly concerning the values presented in Table B-3 for displacing a lattice ion. In this context we should recall the difference between the Class 1 and Class 2 type of processes. In the latter, it is unlikely that the kinetic energies of the ions in discharge alone were enough for direct displacement of the lattice ions in fluorides of divalent and trivalent metals (the most likely hosts for multiphoton phosphors). However, this does not rule out the possibility of influencing the surface of such materials through combined kinetic+recombination energy (given that ionization has occurred in discharge species). The fact that most of the values presented in Table B-3 would decrease for processes at the surface needs also attention. More likely to occur in the energy range available in the discharges is the mechanism in Class 2 type of processes where the energy is converted first into some electronic excitation that in the course of its decay releases it into ion displacement. The probabilities of defect formation may need to be revised for mixed-cation materials like $\text{Li}^{+1}\text{Y}^{+3}\text{F}_4^{-1}$. Yet more likely are the processes of Class 1 where ion displacement step is not required and only redistribution of the charge occurs between host lattice, impurity or activator ions and already *existing (in-grown)* defect centers. Such transitions can occur at significantly lower energies than Class 2 processes.

From the practical point of view – whether or not a fluorine-containing compound is good as a host for phosphors in discharges, one should weigh the following aspects.

- What is the bandgap value of the material, in comparison with the energy of incident radiation?
- What is (if any) in this respect the energy released upon recombination of the emitting ionic species in the discharge?

- Does the material exhibit absorption in the particular spectral range for depositing the energy of the incident photon in the lattice?
- Is the absorption due to strong or weak bandgap transitions (band-tailing), impurities, pre-existing defects or activator ions?
- Is any absorption induced by the move from single crystal to polycrystalline material?
- What would be an efficient electronic mechanism that converts the deposited energy to defects rather than phonons (photons) emitted upon nonradiative (radiative) relaxation?

With the present understanding of the defect formation processes occurring in fluorides it is in principle possible yet hard to predict the length of the period such materials would last without major changes under VUV radiation. We can make note of some trends, rather. High-bandgap fluorides of divalent and trivalent metals have higher likelihood to withstand the effects of irradiation than single- or mixed-valency compounds (one of the cations is monovalent). Studies on an undoped single crystal of a material do not necessarily tell much about the behavior of it when in “activated” (doped) powder form. Higher temperature during lamp operation may have a positive influence by “erasing” the damage created under irradiation. Compounds of higher stoichiometry in both cation and anion sublattices are expected to exhibit better radiation resistance.

Recommendations

Understanding the defect formation processes and radiation resistance properties of phosphor fluoride materials is at its early stages. At this moment, the fastest progress can be made through acquiring significantly more experimental data on materials of interest and in “real-life” conditions. Exposure of activated polycrystalline fluoride or fluorine-containing phosphor materials of interest to the irradiation of appropriate energy and “live” discharges would prove or disprove the suitability of these compounds for lamp applications in each case. These studies could be complemented by calculations using *ab initio* quantum computational methods in analogy to [36, 65].

Part III (W. White)

Surface states, defects, and impact of electrons, ions, and high energy photons play an important role in the aging and degradation of all phosphor materials. Defect-induced degradation is particularly important for fluoride based systems. Most investigations using the best of surface characterization tools, however, have been directed toward sulfide based phosphors because these are useful in low voltage cathodoluminescence, electroluminescence, and field-emission cathodoluminescence devices. Further, most of the investigations have dealt with electron beam effects rather than high energy photon effects. The Phosphor Technology Center of Excellence (PTCOE) was particularly active in this research. Some of the findings on sulfides may be of relevance to fluorides.

The group headed by P.H. Holloway at the University of Florida has invested more than five years in a study of the degradation of a limited set of sulfide phosphors under electron beam excitation using Auger electron spectroscopy as their primary characterization tool. Both powder phosphors and thin film phosphors were investigated. The phosphors investigated are:

ZnS:Cu,Al,Au

ZnS:Cu,Cl

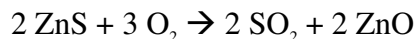
ZnS:Mn²⁺

SrS:Ce³⁺

Y₂O₂S:Eu³⁺

In each case, the phosphor was aged in an electron beam for varying periods of time in a vacuum typically 10⁻⁶ torr with a controlled bleed of H₂, O₂, H₂O CO or CO₂. Over time the luminescence brightness decreased, concurrent with a loss of S and a buildup of O on the surface. Carbon was also lost from the surface for all gases except CO which resulted in a carbon buildup.

The proposed mechanism was an electron stimulated surface chemical reaction between the phosphor and other species adsorbed on the surface from the ambient gas phase. A typical reaction would be



The volatile products are swept off through the vacuum system and the solid products accumulate to form a dead layer on the phosphor surface. ZnO and ZnSO₄ were proposed as the products on the ZnS based phosphors. Ion milling depth profiling with the Auger spectrometer suggested dead layer thicknesses of 70 – 85 nm.

The interpretation of the loss of luminescence intensity throughout the extensive series of papers listed below was in terms of dead layer buildup. Although color center formation could not be ruled out, no specific evidence for color center formation was offered.

The mechanisms uncovered for sulfide phosphors show why oxide phosphors are generally more stable in electron beam environments because the phosphor surface is already a completely oxidized layer. Do any aspects of this mechanism apply to fluoride phosphors in a hard ultraviolet rather than electron beam environment? Quite possibly, even in the absence of direct experimental evidence. The degradation of the sulfide phosphors was by electron-stimulated reaction with trace gases in the vacuum chamber. Hard UV photophosphors will be operating at much higher gas pressures allowing a greater concentration of trace impurities from the xenon or xenon/neon primary gas. Photon energies in the range of 7.5 to 8.5 eV are sufficient to drive chemical reactions. Bombardment by energetic ions will add to the stimulus.

Task 3: New Oxides for Pr³⁺ Cascading

Task Leader: Richard Meltzer
Task Members: Marvin Weber
R.S. Rana
Andries Meijerink

Subtask A: New Oxide Systems for Pr³⁺ (Low-lying ¹S₀)

Photon cascade emission (PCE) of Pr³⁺, initially demonstrated in fluoride hosts, has also been observed in several oxide crystals (LaBaB₉O₁₆, YBaB₉O₁₆, LaB₃O₆, LaMgB₅O₁₀, SrAl₁₂O₁₉, CaAl₁₂O₁₉, SrB₄O₇, Sr_{0.7}La_{0.3}Al_{11.7}Mg_{0.3}O₁₉) [80-85]. Emission involves transitions from the ¹S₀ and the ³P₀ and/or ¹D₂ levels. Although oxide hosts are desirable from the point of view of current fluorescence lamp technology, the number of oxide hosts suitable for Pr³⁺ photon cascade emission is limited by several requirements:

1. Wide bandgap: greater than or ~6 eV (~200 nm).
2. ¹S₀ level below the 4f5d level.
3. Low lattice vibrational frequencies and/or weak Pr³⁺ lattice coupling.
4. Small Judd-Ofelt parameter ratios Ω_2/Ω_6 and Ω_4/Ω_6 to maximize the ¹S₀–¹I₆ intensity.
5. Absence of competing host absorption unless it efficiently transfers energy to Pr³⁺ 4f5d or ¹S₀.

The position of the lowest level in Pr³⁺, i.e. 4f5d vs. 4f², ¹S₀, depends on both the baricenter and the extent of the splitting of the 4f5d band. Whereas in fluoride hosts the crystal-field splittings and baricenter centroid shifts of the lanthanides are usually small so that the 5d levels remain above the ¹S₀ level, oxide hosts are more covalent and, as a result, these splittings and shifts are generally larger. However, in the above-mentioned oxide lattices reported to exhibit cascade transitions, the crystal field splitting is small due to the high coordination number of the lanthanide ion. Thus a high coordination number can be used as one criterion for selecting Pr³⁺ hosts for PCE. The near-neighbor coordination shell distances and geometries at a given lattice site can be derived using data from crystal structure databases such as the Inorganic Crystal Structure Database [86] and computer programs such as SEXIE [87]. Many programs also exist for visualizing the crystal structure and are frequently included in quantum chemistry codes.

In Dorenbos' survey of 38 oxide hosts containing Pr³⁺ only six are predicted to have the ¹S₀ level below the lowest 5d level [88]. It has since been shown that there are a number of other materials that have their ¹S₀ below that of 4f5d. These 10 hosts are included in Table B-5 (a number of them have already been exploited for PCE).

Table B-5
Properties of Demonstrated Oxide Pr³⁺ Phosphors with Low-lying ¹S₀

Host	Crystal System	Oxygen Coordination	Ref	Comments
SrAl ₁₂ O ₁₉	hexagonal	12-fold, AlO _n	4	Pr ³⁺ substituted at Sr ²⁺ sites charge compensated by Mg ²⁺ substituted at Al ³⁺ sites. Al has tetrahedral, octahedral and pentagonal bipyramidal coordination
CaAl ₁₂ O ₁₉			5	6 at.% Mg at Al sites
Sr _{0.7} La _{0.3} Al _{11.7} Mg _{0.3} O ₁₉			6	Avg. Sr-O distance=0.279nm
LaB ₃ O ₆	monoclinic	10-fold, BO ₃ and BO ₄	2	
LaMgB ₅ O ₁₀	monoclinic	10-fold, BO ₄	3	distorted LaO ₁₀ polyhedra; mean La-O distance: 0.262 nm
LaBaB ₉ O ₁₆	rhombohedral	12-fold, BO ₃	1	acentric sites
YBaB ₉ O ₁₆	rhombohedral	12-fold, BO ₃	1	centrosymmetric sites
LaPO ₄ *	orthorhombic	PO ₄	7	pentagonal interpenetrating tetrahedral polyhedron
SrSO ₄ , BaSO ₄	orthorhombic	12-fold SO ₄ coordination	17	very distorted SrO ₁₂ polyhedra
LaP ₃ O ₉	orthorhombic	8-fold, PO ₄	7	distorted PO ₄ polyhedra
SrB ₄ O ₇	orthorhombic	10-fold, BO ₄	6, 9	site for charge compensation?

* Based on the location of the Pr³⁺ 4f5d level from Dorenbos [88] and a ¹S₀ level at ~46,500 cm⁻¹.

Dorenbos has demonstrated that the systematics in the energy levels of trivalent rare earth ions allow one to predict the lowest 4fⁿ → 4fⁿ⁻¹5d transition energy according to the relationship

$$E(\text{Ln}, \text{A}) = 49,340 - D(\text{A}) + \Delta E^{\text{Ln}, \text{Ce}}$$

where D(A) is the crystal field depression energy which depends on the host, A, and $\Delta E^{\text{Ln}, \text{Ce}}$ is the difference in the lowest 5d level in Ln³⁺ and that of Ce³⁺.¹⁰ For Pr³⁺, $\Delta E^{\text{Pr}, \text{Ce}} = 12,240 \pm 750 \text{ cm}^{-1}$. Assuming that the ¹S₀ level of Pr³⁺ is $46,500 \pm 1000 \text{ cm}^{-1}$, then it can be expected that hosts in which $D(\text{A}) < 15,800 \text{ cm}^{-1}$ can be expected to have ¹S₀ below the lowest 4f5d level. Given the range of both the ¹S₀ energy and the value of $\Delta E^{\text{Pr}, \text{Ce}}$ one must consider that hosts for which $D < 16,800 \text{ cm}^{-1}$ have the potential for producing a low-lying ¹S₀ level. However a near degeneracy will not be acceptable since even a small thermal population of the 4f5d level (>10%) will limit radiation from ¹S₀. Since any real phosphor will operate at room temperature, it must be required that the splitting should be below about 2kT. As a result, one should only consider systems for which $D < 16,400 \text{ cm}^{-1}$.

Taking advantage of the information collated by Dorenbos for the values of $D(A)$ in a large number of hosts, it is possible to compile a list of oxide systems which should be examined as potential candidates for a low-lying 1S_0 situation. All of the oxide systems for which $D(A) < 16,400 \text{ cm}^{-1}$, including those hosts appearing in Table B-5, are listed in Table B-6 in order of increasing values of $D(A)$. Oxides containing waters of hydration or carbonates have been omitted since they would not be suitable for lamp phosphor applications. Included in the table are the peak absorption wavelengths of Ce^{3+} and Pr^{3+} (if known). Clearly, the potential exists for discovering a number of new systems doped with Pr^{3+} where the 1S_0 level lies below that of the lowest 4f5d level. Note, however, there must be lattice sites appropriate for the substitution of Pr^{3+} . In cases such as alkaline earth sites, charge compensating ions such as Mg^{2+} for Al^{3+} in the aluminates or Na^+ in Sr^{2+} sites for SrSO_4 are needed. This may eliminate some of the compounds in Table B-6.

Subtask B Maximize Radiative $^1S_0 \rightarrow ^1I_6$ Transition

For the $^1S_0 \rightarrow ^1I_6$ transition to be dominant, the Judd-Ofelt intensity parameters should be $\Omega_6 \gg \Omega_2, \Omega_4$. Reported ratios Ω_2/Ω_6 and Ω_4/Ω_6 for several oxide and fluoride crystals are given below. Note the small values for the successful PCE phosphors $\text{SrAl}_{12}\text{O}_{19}$ and YF_3 . It is however important to note that Ω_6 does not necessarily have to be very large; even if the $^1S_0 \rightarrow ^1I_6$ transition does not have the highest dipole moment, there may still be very efficient energy transfer to a second ion if the resonance conditions are favorable, or if the second ion has a large dipole moment (see report of Task #8). Of course this is all subject to the requirement that the energy transfer must still dominate over radiative processes. Although valid criteria for predicting the relative values of the Judd-Ofelt parameters for Pr^{3+} other hosts based on the local structure and bonding remain to be established there are a few general properties that have been noted by several researchers.

Jorgensen and Reisfeld [98] point out that Ω_2 is strongly enhanced by covalent bonding which is consistent with the fact that Ω_2/Ω_6 is smaller for the fluorides than for the oxides. A number of proposals for the physical origin of this effect have been discussed including dynamic polarization of the ligands by the quadrupole moment of the transition [99, 100]. In contrast, it has been suggested that Ω_6 is related to the rigidity of the medium and is smallest in crystalline mixed oxides and increases in the order glasses, viscous solutions, hydrated ions, halide vapors and complexes of organic ligands [101]. However, the ratio of Ω_2/Ω_6 does not necessarily get smaller in this series since Ω_2 and Ω_4 also tend to increase as Ω_6 increases.

Table B-6

Demonstrated and Potential Oxide Hosts with Low-lying 1S_0 Level and some of their Optical Properties. (Bold Indicates Observation of Low-lying 1S_0 .)

Host	λ_{ABS} (Ce ³⁺)	λ_{ABS} (Pr ³⁺)	D* cm ⁻¹	Comments
SrAl ₁₂ O ₁₉	261	197	11050	
CaAl ₁₂ O ₁₉	265		11604	
Sr _{0.7} La _{0.3} Al _{11.7} Mg _{0.3} O ₁₉	260	197 (218)		Type I Pr ³⁺ (type II) Pr ³⁺
SrSO ₄	267	199		
BaSO ₄	266	199		
LaB ₃ O ₆	270	204	12286	
LaMgAl ₁₁ O ₁₉	270		12303	
La ₂ (SO ₄) ₃	270		12303	
YMgB ₅ O ₁₀	271		12440	
GdB ₃ O ₆	270		12526	
LaMgB ₅ O ₁₀	272		12568	
CaMgAl _{11.33} O ₁₉	272		12575	
CaLaB ₇ O ₁₃	273		12710	Ca site?
LaPO ₄	272		12778	
LiLaP ₄ O ₁₂	278		13369	
CePO ₄			13387	
SrB ₄ O ₇	280	210	14080	
La _{9.33} (SiO ₄) ₆ O ₂	285		14252	4f site
BaAl ₁₂ O ₁₉			(14665)	
Gd _{9.33} (SiO ₄) ₆ O ₂	289		14738	4f site
SrB ₆ O ₁₀	289		14738	
LaP ₃ O ₉	290	212	14808	
Ce ₂ (SO ₄) ₃			(14984)	
Mg ₂ P ₂ O ₇			15092	
LaP ₅ O ₁₄	293		15210	
CeP ₅ O ₁₄	296		15556	
TbBaB ₉ O ₁₆	297		15602	
LaBaB ₉ O ₁₆				
YBaB ₉ O ₁₆				
Sr ₃ (PO ₄) ₂			15687	
PrP ₅ O ₁₄	298		15783	
KAl ₁₁ O ₁₇			15841	
GdP ₃ O ₉	300		16007	
KBaPO ₄			16137	
La _{0.86} Al _{11.9} O _{19.4}	303		16337	
Ce _{0.92} MgAl _{11.13} O _{19.08}	303		16337	
GdAlO ₃	307		16356	

* Based on the location of the 4f5d level of Ce³⁺ from Dorenbos [89].

Table B-7
Experimental Judd-Ofelt Parameters for Pr³⁺

Host	Crystal System	Ω_2/Ω_6	Ω_4/Ω_6	Ref.
Oxides				
SrAl ₁₂ O ₁₉	hexagonal	0.23	0.59	14
PrP ₅ O ₁₄	monoclinic	0.22	0.20	15
LiPrP ₄ O ₁₂	monoclinic	0.28	0.43	15
KPrP ₄ O ₁₂	monoclinic	0.19	2.40	18
YAlO ₃	orthorhombic	0.29	0.86	15
Y ₃ Al ₅ O ₁₂	cubic	0	1.37	15
Y ₂ O ₃	cubic	3.52	4.06	18
Li ₃ Ga ₅ SiO ₁₄		1.10	0.44	18
Fluorides				
YF ₃	orthorhombic	0.013	0.07	16
LaF ₃	trigonal	0.025	0.37	15
		0.013	0.07	15
		0.24	0.44	15
BaYb ₂ F ₈	monoclinic	0.25	1.47	15
LiYF ₄	tetragonal	0	1.1	15
ZBLAN glass		0	0.38	18

Subtask C Minimize Nonradiative ³P₀-to-¹D₂ Transitions

The rate of nonradiative multiphonon emission also affects the cascade process and is host dependent. Nonradiative decay rates between lanthanide energy levels is determined predominately by the energy gap and the particular host medium. This is expressed by the simple energy gap law for nonradiative decay

$$W_{nr} = A \exp(-a \Delta E / h \nu_{max}),$$

where A and a are empirically fitted parameters, $h\nu_{max}$ is related to the highest phonon frequency of the host medium, and ΔE is the energy gap between the excited lanthanide state and the next lower lying energy level. $\Delta E/h\nu_{max}$ represents the number of phonons required to bridge the energy gap.

Van Dijk and Schuurmans [90, 91] developed a modified energy gap law for nonradiative decay where only a few phonons participate in the transition of the form

$$W_{nr} = \beta_{el} \exp[-\alpha(\Delta E - 2h\nu_{max})].$$

The parameter β_{el} was found to vary by only a factor of 10 in a whole series of compounds. (The energy gap law has also been explored in the regime of picosecond nonradiative processes [92].)

In LaB_3O_6 and $\text{LaMgB}_5\text{O}_{10}$ radiative emission from the $^3\text{P}_0$ level was weak because of rapid competing nonradiative decay arising from the large vibrational frequencies of the coordinating BO_3 groups in these borates. In contrast, Pr^{3+} in $\text{LaBaB}_9\text{O}_{16}$ and $\text{YBaB}_9\text{O}_{16}$ is coordinated by BO_4 groups (BO_3 groups are present but their oxygens are not coordinated with the RE) which have significantly smaller vibrational frequencies and hence reduced probability for nonradiative decay by multiphonon emission. Similarly, the Sr site in $\text{SrAl}_{12}\text{O}_{19}$ is coordinated by AlO_6 octahedra with vibrational frequencies $\sim 700 \text{ cm}^{-1}$. Other examples of crystals containing Al-anion octahedra include MgAl_2O_4 and LiCaAlF_6 . Table B-7 lists the maximum vibrational frequencies of a number of compounds and crystals. (Note the low frequencies of the fluorides.) Based on the above results, promising hosts for efficient radiative emission from the $^3\text{P}_0$ level appear to be borates having Pr^{3+} coordinated by BO_4 tetrahedra and aluminates having Pr^{3+} coordinated by AlO_6 octahedra. Germanates and tellurites might be other possibilities, provided they have sufficiently large bandgaps, but this is questionable.

One must also consider other possible non-radiative mechanisms. A number of these have been considered for Pr^{3+} . The first of these is cross-relaxation which will increase with Pr^{3+} concentration and for lattices where pairs are likely to form. Host lattices where the Pr^{3+} substitutes for a divalent ion are more likely to form pairs as the ions assume positions that provide charge compensation. For example, two Pr^{3+} ions can substitute for three Sr^{2+} ions with a vacancy located at the third Sr^{3+} site. This mechanism can be tested by adding La^{3+} to a host while maintaining a constant Pr^{3+} concentration, thereby decreasing the likelihood that a Pr^{3+} - Pr^{3+} pair will occur. A second mechanism involves an intersystem crossing through a low-lying 4f5d state as proposed by Arai et al. [102] and by de Mello Donega et al. [103]. This will be most likely in systems with low-lying 4f5d levels. For Pr^{3+} systems with $^1\text{S}_0$ low, this will not be important, but for systems where the 4f5d state is low, a possible scenario for energy transfer to another activator (see report Task 3), this should be considered. Finally an intersystem crossing via tunneling through a low-lying Pr-to-metal charge-transfer state (virtual charge exchange) has been proposed by Reut and Ryskin²⁵ for Pr^{3+} in scheelite and fergusonite type crystals. Furthermore, both covalency and a short Pr^{3+} - O^{2-} distance will increase the electron-phonon coupling, an important factor in controlling any phonon-induced relaxation rate.

Table B-8
Approximate Frequencies of the Highest Energy Phonons in Oxide and Fluoride Hosts

Host	Maximum Vibrational Frequency (cm ⁻¹)
<i>Compounds</i>	
Borates, BO ₃	~1300-1400
Borates, BO ₄	~900-1100
Borate, B ₃ O ₆ ring	~1500
Phosphates, PO ₄	~1100
Sulfates, SO ₄	~1100
Silicates, SiO ₄	~1050
Germanates, GeO ₄	~900
Tellurites, TeO ₆	~800
Aluminates	~900
<i>Crystals</i>	
Al ₂ O ₃	750
SrAl ₁₂ O ₁₉	~700
Y ₃ Al ₅ O ₁₂	850
SrF ₂	370
LaF ₃	450
LiYF ₄	490

There are many borate and aluminate compounds to explore. The Inorganic Crystal Structure Database [86] contains structural data for 190 boron-oxygen ternary compounds, 514 boron-oxygen quaternary compounds, 546 aluminum-oxygen ternary compounds, and 1054 aluminum-oxygen quaternary compounds (these numbers include multiple data sets for some compounds). The number of potential candidates is quickly reduced by limiting it to those that have either (1) a trivalent ion site suitable for substitution of Pr or (2) a divalent ion site suitable for substitution of Pr together with another site suitable for substitution of a charge compensating ion. For those that survive this test, the coordination is the next test.

Mineralogy databases were also consulted. The www.webmineral.com database lists compounds by element. There are 217 minerals containing boron and 929 containing aluminum. Another reference is mineral.galleries.com where minerals are organized by classes (elements, oxides, halides, silicates, phosphates, carbonates, sulfates, sulfides, and organics); 109 boron-containing minerals are listed. Many of the above minerals can be eliminated, however, because they contain hydroxides or are hydrated; others can be eliminated because they contain halides and chalcogenides.

Conclusions and Recommendations

Although photon cascade emission of Pr^{3+} can produce quantum efficiencies much greater than 100%, even approaching 200%, it is incapable, alone, of generating a useful phosphor since one of the photons will occur in the deep blue or UV where it will not contribute useful visible emission. None the less, combining Pr^{3+} with other ions to which it can transfer a portion of its energy, may circumvent this limitation (see report Task #8). As a result, there are a number of subtasks described in this report that should undergo further study since they are relevant to the development of systems which can undergo energy transfer. The following are some recommendations that can contribute to further advancement:

1. Prepare and examine the spectra of Pr^{3+} in LaPO_4 (and perhaps YPO_4) since according to Table B-5 it should have a low-lying $^1\text{S}_0$ level.
2. Prepare and examine the spectra of Pr^{3+} in the hosts listed in Table B-6 in order to identify other hosts where the $^1\text{S}_0$ level of Pr^{3+} lies below that of $4f5d$.
3. Develop methods to predict Judd-Ofelt parameters based on crystal structure.

Task 4: Sensitizer for Gd³⁺

Task Leader: Andries Meijerink
 Task Members: Charles Struck
 Marvin Weber

Introduction

The finding of multi-photon emission through downconversion has provided new excitement in the search for phosphors with quantum efficiencies exceeding unity [105, 106, 107]. The couple Gd³⁺-Eu³⁺ offers the possibility to obtain efficiencies near 200%. Via a two-step energy transfer process (shown in Figure B-4) one Gd³⁺ ion excited into the ⁶G_J level will relax via a two-step energy transfer process yielding ⁵D_J emission from two Eu³⁺ ions. Also for Gd-Ho a similar two-photon emission process has been observed starting from the ⁶G level of Gd³⁺ [108].

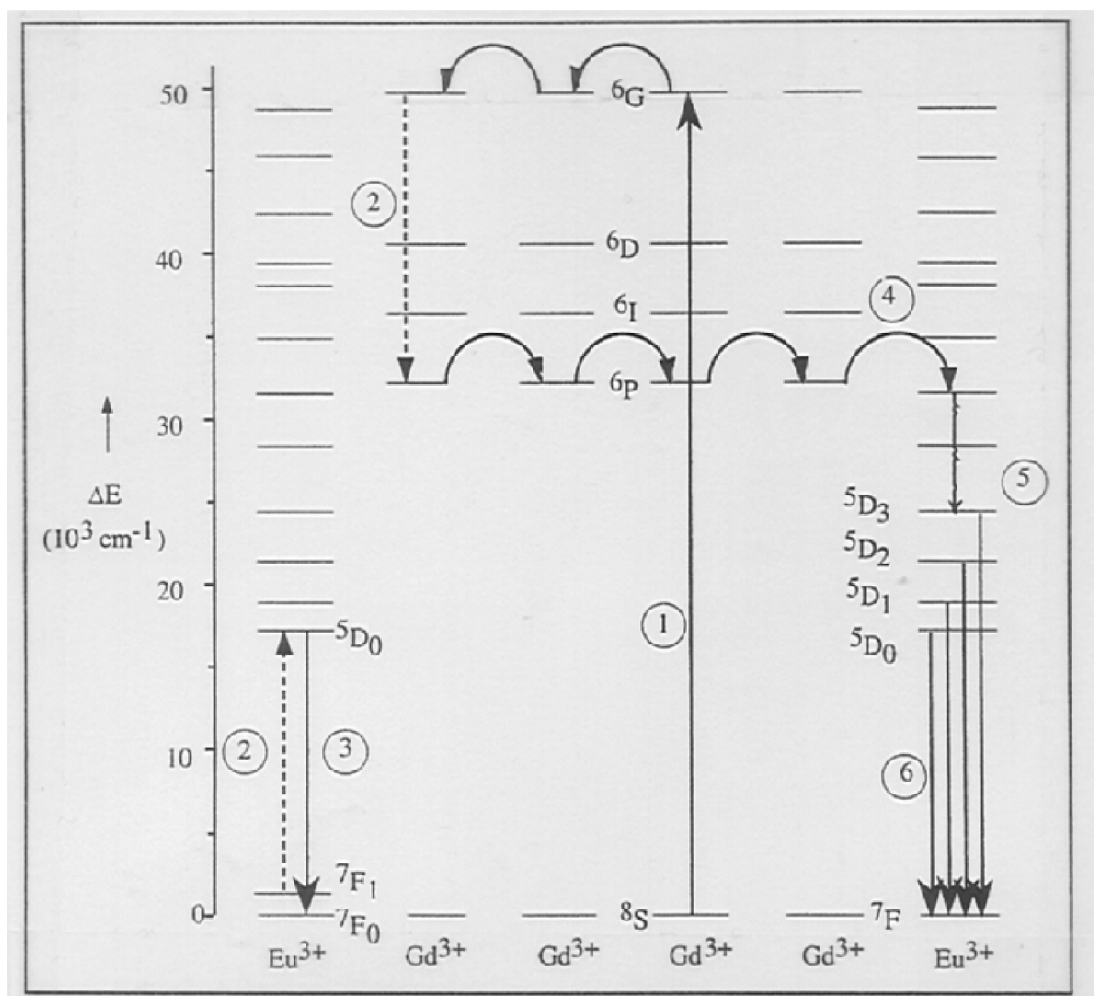


Figure B-4
 Quantum Cutting through Downconversion for the Gd-Eu Couple in LiGdF₄:Eu³⁺

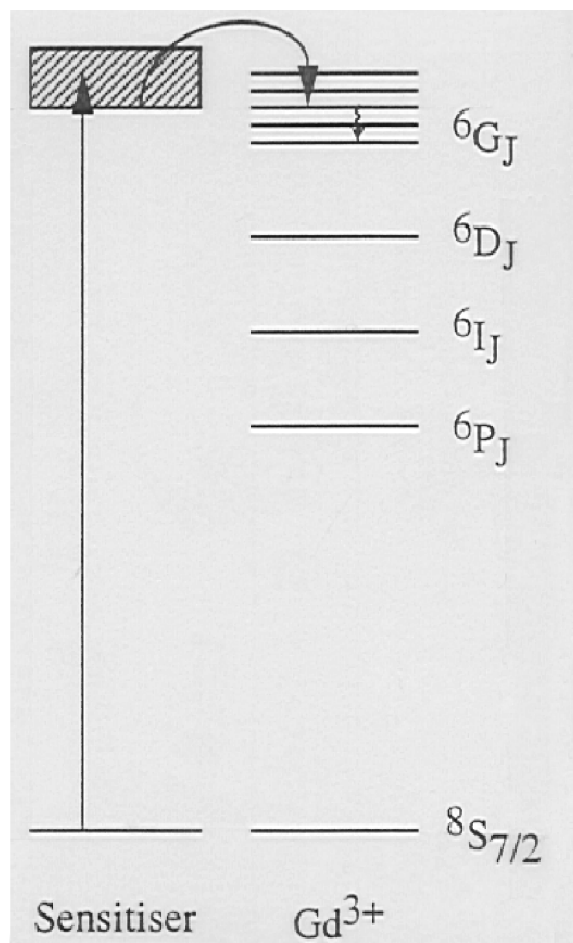
In spite of the high potential efficiencies, the actual efficiency of the $\text{LiGdF}_4:\text{Eu}^{3+}$ and the $\text{GdF}_3:\text{Eu}^{3+}$ phosphors is low [109]. The reason is obvious: the absorption strength for excitation in the forbidden f-f transitions of Gd^{3+} is low and thus the VUV radiation is only partly absorbed by Gd^{3+} . In order to make an efficient lamp phosphor the absorption of the exciting radiation has to be strong. Thus, a sensitizer is required which can absorb the vacuum ultraviolet (VUV) radiation generated in the xenon discharge. The sensitizer should transfer the energy to VUV levels of Gd^{3+} resulting in Gd^{3+} in the excited ^6G state. As soon as this state is reached efficient two-step energy transfer to Eu^{3+} can occur and a phosphor with a visible quantum efficiency close to 200 % can be obtained.

The requirements of an ideal sensitizer for the ^6G level of Gd^{3+} are:

1. Strong absorption in the VUV range between 145 and 190 nm to absorb the VUV output of the Xe-discharge in this energy range.
2. Emission between 190 and 210 nm to have a good spectral overlap with the ^6G absorption lines of Gd^{3+} .
3. No levels at lower energies which may interfere with the Eu^{3+} or Gd^{3+} excited states which are populated during the downconversion process (i.e. no quenching by back transfer to the sensitizer).

In Figure B-5 the situation is schematically shown.

In order to find a good sensitizer the VUV absorption and emission properties of potential sensitizer ions have to be studied. Up until now, the research on the VUV luminescence properties of luminescent ions has been rather limited. In this report various classes of potential sensitizers will be discussed: (1) charge transfer transitions, mainly focussed on Yb^{3+} , (2) s^2 ions, mainly focussed on Pb^{2+} , (3) fd transitions of lanthanide ions and (4) host lattice excitation. Since the research of the luminescence properties of ions in VUV part of the spectrum is scarce, the number of references is limited, although in recent years there is a clear increase in luminescence research using VUV radiation. The overview presented here includes also recent (unpublished) results. Based on these results research plans are outlined which may result in finding a good sensitizer.

**Figure B-5**

Schematic Picture of Energy Transfer from an Ideal Sensitizer to the 6G Level of Gd^{3+}

Charge Transfer

Charge transfer (CT) transitions are often situated at relatively high energies [110]. Typically, ligand-to-metal charge transfer transitions are situated in the ultraviolet or even vacuum ultraviolet region of the electromagnetic spectrum. In view of the high energy position and allowed character (parity allowed) of charge transfer transitions, they are worth considering as sensitizers for the 6G level of Gd^{3+} . Charge transfer transitions have been studied for transition metal ions (3d, 4d and 5d) in the visible and UV part of the spectrum, especially for d^0 complexes [110, 111, 112]. For the lanthanide ions the charge transfer absorption transitions are well studied for Eu^{3+} and Yb^{3+} [113, 114, 115]. For Eu^{3+} the efficient CT absorption of the UV output of the Hg discharge is essential for the red phosphor in fluorescent tubes. Relaxation from the CT state to the lower energy $4f^6$ states is fast and has been well studied. In view of the fast relaxation to the $4f^6$ states, it is highly unlikely that energy transfer from the CT state to e.g. Gd^{3+} can compete with the fast non-radiative relaxation to lower f^6 levels for Eu^{3+} . In the case of Yb^{3+} CT emission can be observed [116, 117]. For most other lanthanide ions the lowest energy parity allowed transition is to $4f^{n-1}5d$ state and charge transfer absorption will not result in CT emission. The possibility of using fd luminescence to sensitize the Gd-Eu couple will be discussed in

section 4. In this section we will focus on the possibility of using the CT state of Yb^{3+} to sensitize the Gd-Eu couple. The charge transfer luminescence of the 3d, 4d and 5d transition metal ions is not considered at present since little is known on charge transfer transitions of these ions in the VUV. A study of the VUV spectroscopy of these transition metal ions in fluorides will be worthwhile in future research on multi-photon VUV phosphors. Possibly, some information will be provided in the task#7 report.

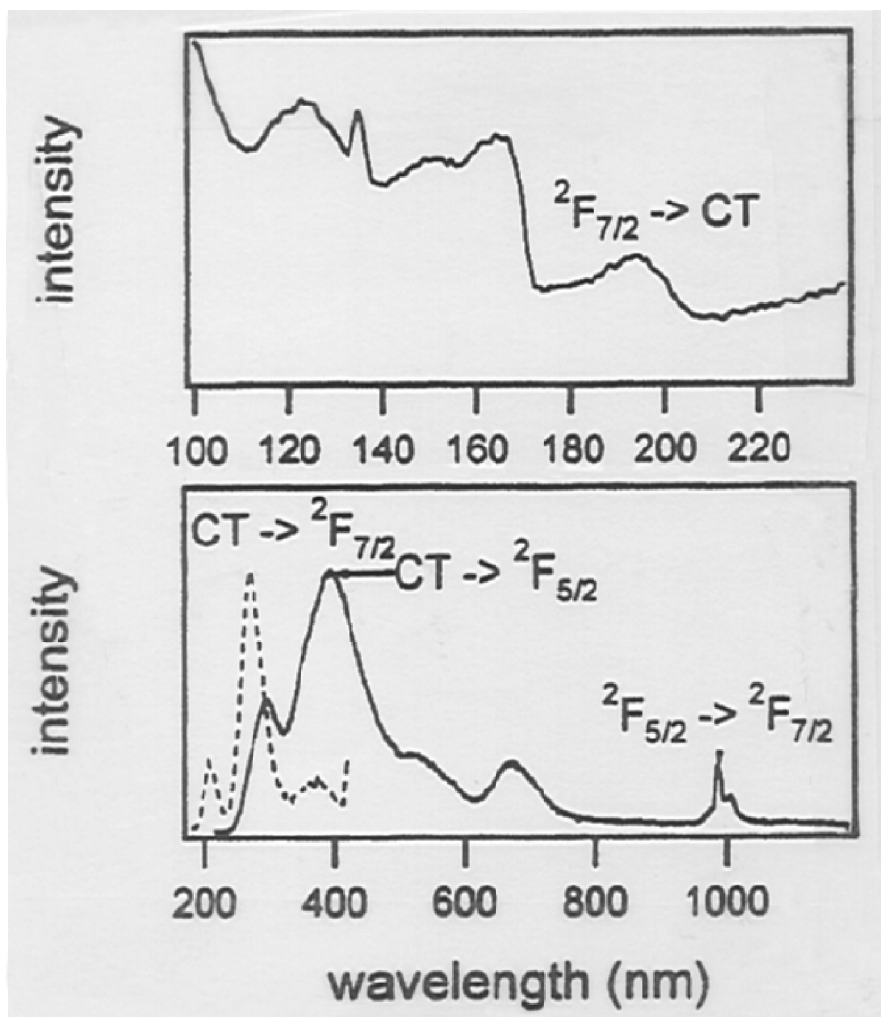


Figure B-6

Emission (exc=140 nm) and Excitation (em=270 nm) Spectra of Yb^{3+} in ScPO_4 at 10 K. In the Emission Spectrum the Broken and Drawn line are Emission Spectra Recorded with Different Detection Set-up (VUV/UV Broken Line, UV/VIS Drawn).

Charge transfer luminescence of Yb^{3+} has been reported in 1978 by Nakazawa for Yb^{3+} in oxysulphides and orthophosphates [116, 117]. The energy level scheme of Yb^{3+} is relative simple. The $4f^{13}$ state is split by spin-orbit coupling in a $^2F_{7/2}$ ground state and a $^2F_{5/2}$ excited state some 10 000 cm^{-1} higher in energy. At much higher energies the charge transfer state situated. In view of the large energy gap between the CT state and the highest energy 4f state, charge transfer luminescence can be observed. If the charge transfer state is situated at high enough energies

(above 50 000 cm⁻¹), the Yb³⁺ energy level scheme resembles the energy level scheme of an ideal sensitizer (see Figure B-5), apart from the presence of the ²F_{5/2} level between the ground state and the CT excited state.

Until three years, only a few publications reported the CT luminescence of Yb³⁺. In a recent publication the CT luminescence in a large number of host lattices has been reported [118, 119, 120]. In this overview the charge transfer absorption in various oxides and fluorides was presented. A typical excitation and emission spectrum are shown in Figure B-6.

The results of the charge transfer luminescence studied for Yb³⁺ in 18 different host lattices are compiled in Table B-9. The results show that in oxide host lattices the charge transfer absorption is situated between 200 and 300 nm. The emission is shifted to lower energies (large Stokes shift). In none of the oxide host lattices the CT state is situated at high enough energies to have the CT emission resonant with the Gd³⁺ absorption lines around 205 nm. In ScPO₄:Yb³⁺ the CT emission is at the highest energy (270 nm) of all oxides. For efficient energy transfer to Gd³⁺ the emission should be at shorter wavelengths. Based on these results it seems not likely that Yb³⁺ can serve as an efficient sensitizer for the Gd-Eu couple in an oxide host lattice.

In a fluoride host lattice the charge transfer absorption is shifted to considerably higher energies. The CT absorption is around 160 nm. In LiYF₄ weak CT emission is observed around 182 nm. These optical properties are promising for using Yb³⁺ as a sensitizer for Gd³⁺ in fluorides. There are several problems which need to be addressed however:

- The quenching temperature of the CT emission is low in LiYF₄. An efficient sensitizer should have a high quenching temperature of the luminescence. Possibly the quenching temperature of the Yb³⁺ luminescence is higher in other fluorides. This needs to be investigated
- The 10 000 cm⁻¹ gap between the two 2F states of Yb can provide an alternative cross-relaxation channel for Gd³⁺ (Gd: 6GJ-6DJ, Yb: 2F7/2-2F5/2). This may interfere with the desired cross-relaxation of Gd (6G) with Eu. Since a high Yb concentration is required to have efficient absorption of the VUV radiation this problem may be a serious one and needs to be studied.

Based on the considerations discussed above, the prospect for Yb³⁺ as a sensitizer for the Gd-Eu couple is not very hopeful but worthwhile investigating in fluoride host lattices. In oxide host lattices the charge transfer emission is too low in energy. Based on the study of the CT luminescence of Yb³⁺ in a large number of oxide host lattices, it does not seem useful to pursue the idea using Yb³⁺ as a sensitizer around 200 nm in oxides. In a mixed oxygen/fluoride coordination, the CT state may be situated at energies in between those for oxides and fluorides. Research of the Yb³⁺ luminescence in oxyfluorides should be done to see if indeed the CT emission of Yb³⁺ in this type of compounds can be used as a sensitizer for Gd³⁺ (⁶G). Charge transfer luminescence of transition metal ions (e.g. 3d⁰, 4d⁰ and 5d⁰ complexes) may be situated at high enough energies in fluorides. No information has been found on the VUV spectroscopy of these complexes in fluorides. Future research in this area within the present framework is recommended.

Table B-9
Charge Transfer Luminescence Properties for Yb³⁺ in Various Host Lattices [118]

Host lattice	Absorption Max. (nm)	Emission (nm)	Stokes shift (cm ⁻¹)	τ (ns)	T _q (K)
ScPO ₄	195	270, 370	14 500	163	225
LuPO ₄	210	290, 340	15 000	175	250
YPO ₄	210	304, 445	15 000	120	290
LaPO ₄	228	-	-	-	<10
NaScO ₂	208	322, 431	15 000	130	225
NaLaO ₂	262	-	-	-	<10
LiScO ₂	206	312, 448	16 000	190	180
LiYO ₂	214	355, 495	16 500	55	125
LiLaO ₂	252	-	-	-	<10
Sc ₂ O ₃	225	367, 485	14 000	13	<30
Y ₂ O ₃	227	368, 533	15 500	72	130
YAG	210	334, 493	17 500	28	<80
YAlO ₃	235	360, 533	14 000	100	100
LaAlO ₃	244	-	-	-	<10
Y ₂ O ₂ S	309	390, 612	6 000	250	140
La ₂ O ₂ S	317	439, 759	8 500	223	150
ScBO ₃	-	-	-	-	<10
YBO ₃	216	-	-	-	<10
LaBO ₃	-	-	-	-	<10
REOX [*]	-	-	-	-	<10
LiYF ₄	160	182, 228	8 000	13	<30

* RE=Sc, Y, La ; X=F, Cl, Br

s^2 Ions

The energy level scheme of s^2 ions is well understood [121, 122, 123]. From the s^2 ground state transitions to several sp excited states are possible. In Figure B-7 the energy levels in the sp excited states are indicated by the free ion symbols. Transitions to the lower energy triplet excited states ($^3P_{0,1,2}$) are spin forbidden, but due to spin-orbit coupling the transitions to the 3P_1 and 3P_2 are relatively intense, especially for the heavier ($6s^2$) ions like Pb^{2+} . The transition to the 1P_1 state is fully allowed. The transitions to the 3P_1 , 3P_2 and 1P_1 states are labelled A, B and C bands (in order of increasing energy) in the absorption spectrum. A fourth state is labelled D and is assigned to a charge transfer type transition [124]. The emission usually occurs from the $^3P_{0,1}$ state (A-band emission) but in few cases also 3P_2 (B-band) emission has been observed at low temperatures [125]. The positions of the absorption and emission bands and also the Stokes shift and quenching temperature of the emission vary strongly as a function of host lattice. The highest energy sp excited states are found in ionic host lattices like fluorides. If the 3P_0 excited state can be shifted to sufficiently high energies ($E > 50\,000\text{ cm}^{-1}$, $\lambda < 200\text{ nm}$) the s^2 ion will be an ideal sensitizer for the $Gd^{3+} \text{ } ^6G$ level. Pb^{2+} has the sp excited state at the highest energies in comparison to other s^2 ions. In the remainder of this section we will focus on the optical properties of Pb^{2+} in fluoride host lattices. Only in fluoride host lattices there is a possibility to shift the sp excited states to sufficiently high energies to sensitize the 6G of Gd^{3+} . Based on the existing literature, it can be ruled out that the sensitisation will work in oxides (including aluminates, sulphates, borates, phosphates), chlorides, bromides, sulphides or other more covalent (compared to F) host lattices [121, 122, 123, 126].

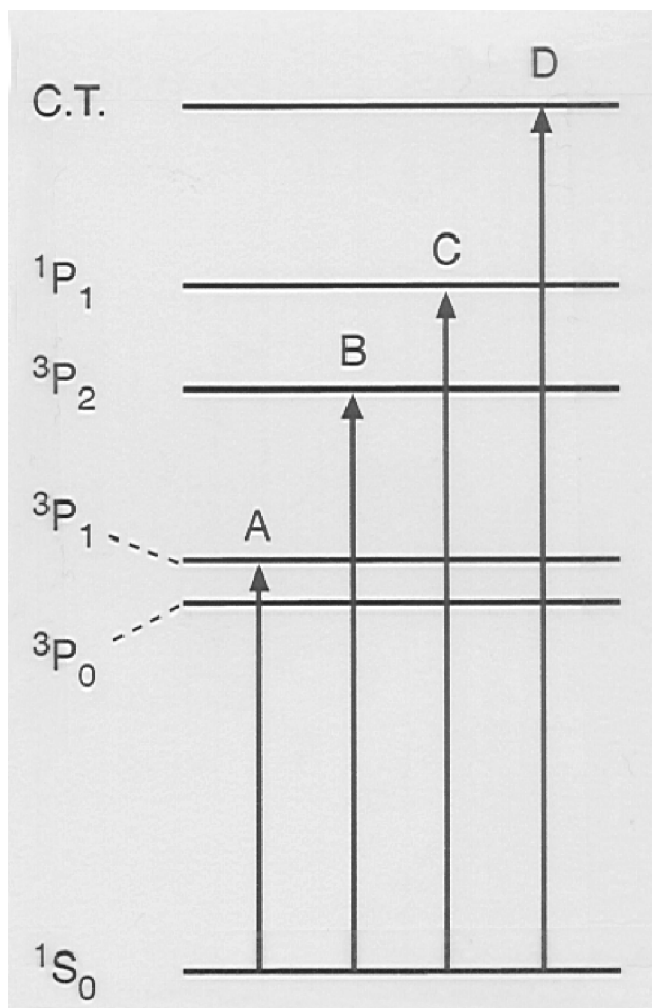
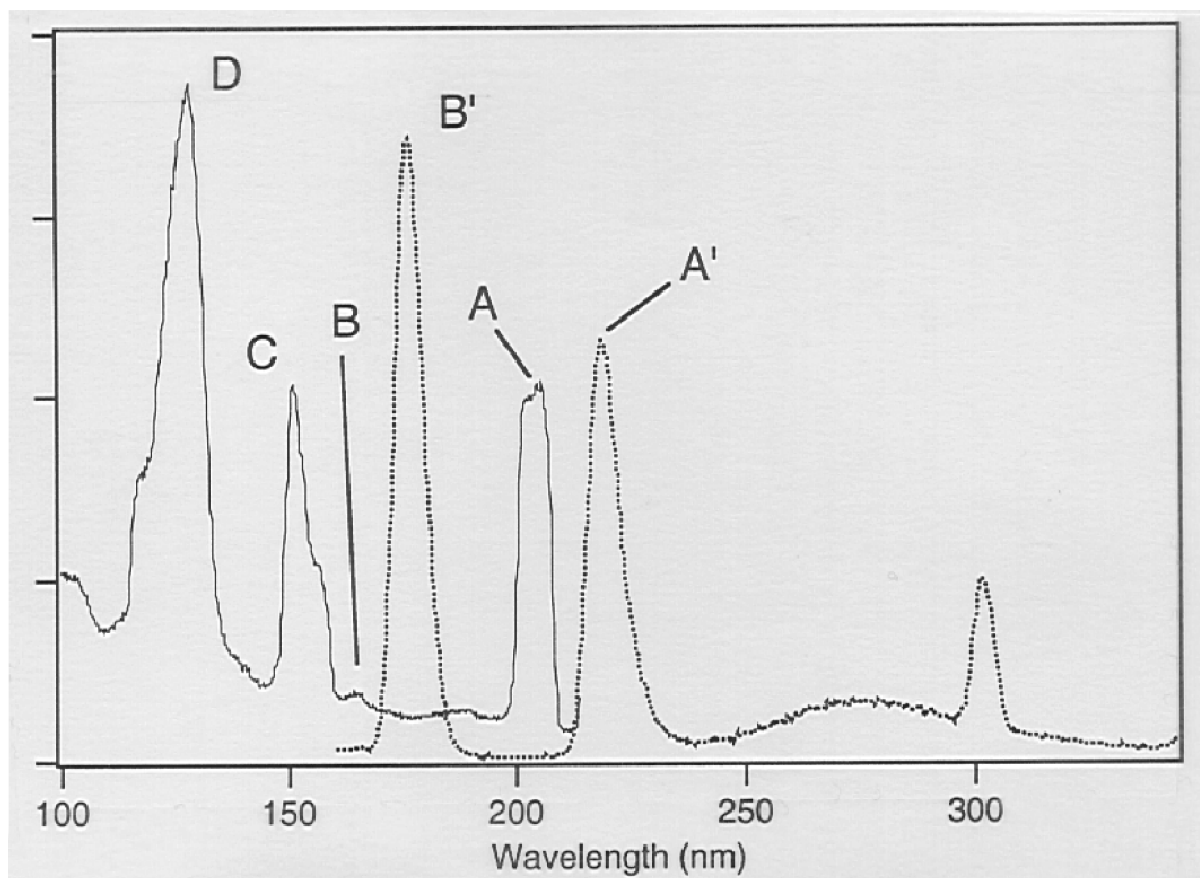


Figure B-7
Energy Level Diagram for s^2 Ions

In the past only a few studies have investigated the VUV luminescence of Pb^{2+} . The luminescence spectra of Pb^{2+} in MF_2 ($M=Ca^{2+}$, Sr^{2+} or Ba^{2+}) were investigated under VUV excitation by Oboth et al. [125]. Typical luminescence spectra are shown in Figure B-8. In addition to the commonly observed A-band emission, also strong B-emission is observed around 175 nm. The A-band emission for Pb^{2+} is at too low energies for sensitisation of the Gd^{3+} ion in the 6G levels around 205 nm. The B-band emission is resonant with high energy 6G levels. Unfortunately, at room temperature the B-band emission is quenched which limits the use as a sensitizer in a lamp operating at room temperature. In order to investigate the potential of Pb^{2+} as a sensitizer, the luminescence properties of Pb^{2+} in a large number of fluoride host lattices was studied. Two possibilities were considered:

- Shifting the A-band to high enough energies so that the A-band emission is resonant with the 6G excitation lines around 200 nm.
- Finding a host lattice in which the B-band (VUV) emission is not quenched at room temperature.

**Figure B-8**

Excitation Spectrum (Solid) of $\text{CaF}_2:\text{Pb}^{2+}$ for the A-band Emission at 220 nm and Emission Spectrum (Dotted) upon Excitation in the C-band at 152 nm ($T=10$ K)

In Table B-10 the results of the Pb^{2+} emission in various fluorides is summarized. The results show that indeed B-band emission can be observed at energies which are resonant with excitation lines of Gd^{3+} in the VUV, for example in $\text{BaY}_2\text{F}_8:\text{Pb}^{2+}$. In this host lattice the B-band emission is not quenched at room temperature. Energy transfer from the B-band to Gd^{3+} has been observed and is able to sensitize the Gd-Eu couple resulting in quantum cutting [127]. Complications arise due to back transfer from Gd^{3+} (${}^6\text{G}$) to the A-band of Pb^{2+} , which subsequently transfers the energy to a lower energy excited state of Gd^{3+} . This ‘ping-pong’ ($\text{Pb} \rightarrow \text{Gd} \rightarrow \text{Pb} \rightarrow \text{Gd}$) behavior lowers the efficiency of the B-band sensitisation. This problem may be absent in systems where the A absorption band does not overlap with the ${}^6\text{G}$ emission lines around 205 nm. This will require further investigation of the Pb^{2+} luminescence in other fluoride systems.

Table B-10
Position of Absorption and Emission Bands of Pb^{2+} in Various Fluoride Host Lattices.
Most Data are from Unpublished Results of Oskam et al.

Host Lattice	A-band (nm)	B-band (nm)	C-band (nm)	Em. A band (nm)	Em. B-band (nm)
CaF_2	205	165	151	219	176
SrF_2	204	165	155	223	177
BaF_2	203	165	156	260	189
YF_3	210	170	162	288	-
GdF_3	206	195	170	-	-
LaF_3	200	193	159	280	-
BaY_2F_8 site I	187	156	148	228	175
site II	200	172	167	289	200
LiBaF_3	191	158	154	247	185
KMgF_3	185	154	138	217	169

The sp excited states of Pb^{2+} shift to higher energies if the coordination number of Pb^{2+} increases and the cation site becomes larger (see also Table B-10). For high coordination numbers and large cation sites the highest energy ^3P states is expected. In KMgF_3 the Pb^{2+} will substitute for K^+ on a large 12-coordinated site [128]. The luminescence spectra of Pb^{2+} in KMgF_3 are shown in Figure B-9. The A-band emission does overlap with the Gd^{3+} excitation lines around 205 nm. The A band in the absorption (excitation) spectrum is situated at much too high energies to allow for back transfer. Thus, in KMgF_3 the energy level scheme of Pb^{2+} resembles that of the ideal sensitizer shown in Figure B-5. This shows that Pb^{2+} is a promising candidate. Obviously, in the KMgF_3 host lattice it is not possible to incorporate large amount of Gd^{3+} and Eu^{3+} . In the search for a successful Pb-Gd-Eu system, one should investigate host lattices which offer a large 12-coordinated site for Pb^{2+} (similar to the situation in KMgF_3) in combination with trivalent lanthanide sites (for quantum cutting by Gd and Eu). The search for such a material is not easy, since the KMgF_3 lattice is quite extreme. Also the $4f^{n-1}5d$ state of divalent and trivalent lanthanides ions is at higher energies than in any other host lattice (see e.g. References [129, 130]) and it may not be easy to find a similar coordination for Pb^{2+} in another host lattice.

Research on s^2 ions may result in finding a good sensitizer for the $\text{Gd}^{3+} {}^6\text{G}$ level. It has been shown that for the Pb^{2+} ion the energy level scheme resembles that of the ideal sensitizer as shown in Figure B-5 for Pb^{2+} in KMgF_3 . Research should be focussed at finding a similar coordination for Pb^{2+} in a host lattice with trivalent lanthanide sites. Also the B-band emission of Pb^{2+} may be used (and has been shown to work) to sensitize the VUV levels of Gd^{3+} . Due to back transfer processes the efficiency of the quantum cutting process is reduced. In order to use the B-band emission for sensitization research should be aimed at a proper tuning of the A-band (no absorption around 205 nm) in a host lattice where B-band emission is observed.

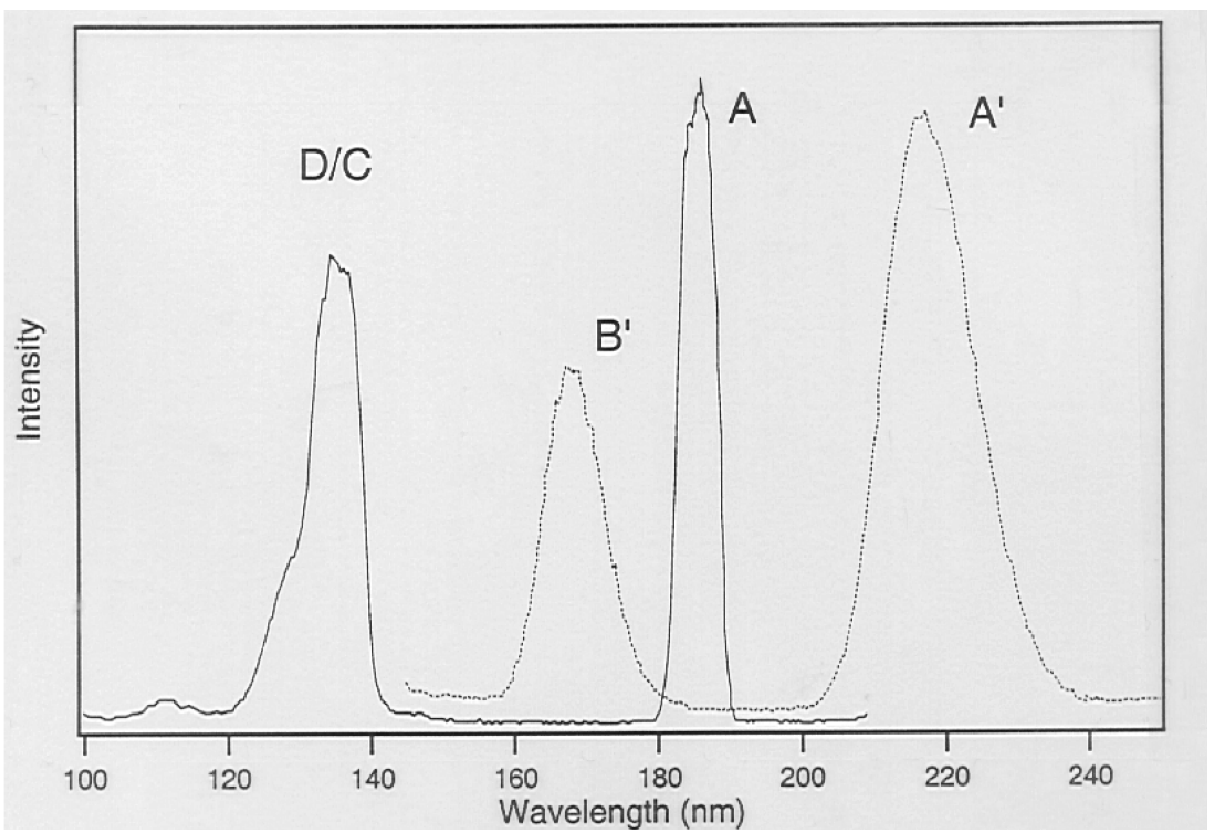


Figure B-9
Excitation Spectrum of the A-band Emission at 217 nm (Drawn Line) and Emission Spectrum for 135 nm Excitation (Broken Line) for $\text{KMgF}_3\text{:Pb}^{2+}$ at 10 K

The prospects for finding a good system here are low, since B-band emission is not often observed, especially at room temperature, so the number of host lattices will be limited. Finally, also other s^2 ions ($4s^2$, $5s^2$ and other $6s^2$) may be investigated. Even though the ^3P states are in general located at lower energies than for Pb^{2+} it may be possible to find a good candidate. The VUV spectroscopy of most s^2 ions has hardly been studied and is worthwhile investigating in the context of the EPRI/DOE program. Finally it should be mentioned that Pb^{2+} and also other s^2 ions (e.g. Sb^{3+}) are well known as efficient sensitizers in mercury discharge phosphors.

fd Transitions

In addition to weak (parity forbidden) intraconfigurational $4f^n-4f^n$ transitions, lanthanide ions show intense (parity allowed) $4f^n-4f^{n-1}5d$ (fd) transitions [131, 132]. These transitions are situated at high energies, often in the vacuum ultraviolet part of the spectrum [133-140]. In recent years the VUV spectroscopy of these transitions has been extensively studied and the increase in the understanding of the position of fd excited states has also greatly benefited from the thorough literature search by Dorenbos. As a result, we can now understand and predict the fd luminescence for a lanthanide ion in a host lattice as soon as the properties for the fd luminescence from Ce^{3+} have been measured. In addition, the reviews by Dorenbos contain a very useful collection of references to the fd luminescence of lanthanide ions in many different host lattices [141-143].

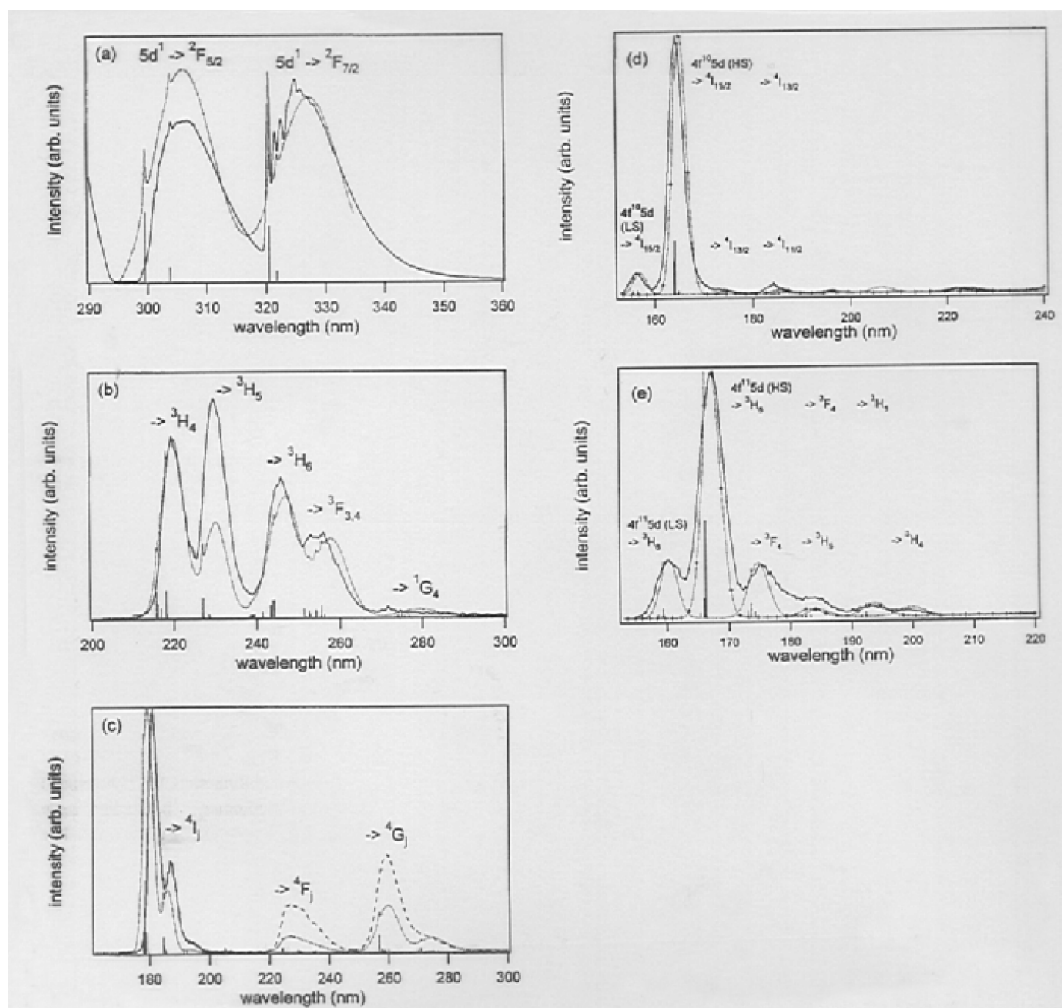
A strong absorption of VUV radiation from a xenon discharge is possible by using fd transitions of lanthanides. In this section it will be discussed which lanthanides may be useful to sensitize the 6G level of Gd^{3+} .

The energy level scheme of lanthanides has one important drawback for acting as a sensitizer. Between the ground state and the strongly absorbing fd state there are many $4f^n$ levels. These $4f^n$ excited states complicate the efficiency of the desired process (efficient fd absorption, followed by efficient energy transfer to Gd and subsequently two photon emission) in several ways:

1. Often fast relaxation from the fd state to lower energy $4f^n$ states occurs [144]. If this is the case, energy transfer to Gd^{3+} may not occur. Only for ions for which fd emission is observed one can expect that energy transfer can compete with fast non-radiative relaxation within the sensitizer.
2. After energy transfer from the sensitizer fd state to the 6G state of Gd^{3+} the lower energy $4f^n$ levels may serve as acceptors for the excitation energy from Gd^{3+} or Eu^{3+} . This will quench the desired luminescence.
3. In addition to the fd transition to the ground state, also transitions to higher $4f^n$ states occurs. These transitions are at lower energies and will result in energy transfer to a lower energy level of Gd^{3+} . This will in general not result in visible two-photon emission.

Based on the first criterion only lanthanide ions for which VUV fd emission has been observed are potential sensitizers. If we go through the series of lanthanide ions, this leaves only Pr^{3+} ($4f^2$), Nd^{3+} ($4f^3$), Er^{3+} ($4f^{11}$) and Tm^{3+} ($4f^{12}$) [145]. The ions in the middle of the series (Sm^{3+} ($4f^5$), Eu^{3+} ($4f^6$), Tb^{3+} ($4f^8$), Dy^{3+} ($4f^9$) and Ho^{3+} ($4f^{10}$)) have a dense energy level structure and also many levels close to the lowest energy $4f^{n-1}5d$ state. As a result, fast non-radiative relaxation to lower energy $4f$ levels occurs. The energy level scheme of Ce^{3+} ($4f^1$) is very simple and Ce^{3+} shows very efficient fd emission, but the emitting d state is at too low energies (it will never be in the VUV) [146].

Of the four remaining ions (Pr, Nd, Er and Tm) all four ions are in principle useful [145]. For Pr^{3+} the fd level is often located at too low energies and lattices will have to be chosen in which the emitting fd states is at the highest possible energies [147]. For Er and Tm the fd emission is at rather high energies and for most fluorides the excitation energies will be at too high energies, which will result in only a partial absorption of the VUV output of the xenon discharge [148]. The energy transfer from the Er^{3+} and Tm^{3+} fd states to Gd^{3+} has been shown to be very efficient [149]. The most promising ion is Nd^{3+} where with the proper choice of host lattice the fd absorption and emission can easily be tuned to positions that match the xenon discharge (fd absorption) and the Gd^{3+} excitation lines (fd emission) [145, 147]. In Figure B-10 the fd emission spectra of all five lanthanide ions which are known to show fd emission in $LiYF_4$ are shown to illustrate the arguments presented above.

**Figure B-10**

Emission Spectra of (a) Ce³⁺ (1%), (b) Pr³⁺ (2%), (c) Nd³⁺ (5%), (d) Er³⁺ (1%) and (e) Tm³⁺ (1%) Incorporated in LiYF₄, Recorded upon Excitation the 4fⁿ-5d Levels

The problems mentioned under (2) and (3) may be solved and this will require extensive research in the framework of the EPRI/DOE program. For example, Nd³⁺ has some energy levels in close resonance to the ⁶P and ⁶D excited states of Gd³⁺. Energy transfer from the ⁶P state of Gd³⁺ to Nd³⁺ instead of Eu³⁺ will result in a lower the Eu³⁺ emission intensity. Since the energy transfer from Gd³⁺ (⁶P) to Eu³⁺ is extremely efficient, a proper choice of the Eu³⁺ concentration and fd sensitizer concentration (as low as possible for complete absorption of the VUV radiation) may minimize this problem.

The point mentioned under (3) is evident from the emission spectra shown in Figure B-10. Lower energy emission bands are observed which are resonant with lower energy Gd³⁺ excited states. For example, the fd transition on Nd³⁺ ending in the ⁴G₁ states of Nd³⁺ is resonant with the ⁶D excitation lines on Gd³⁺. Energy transfer to these lower lying Gd³⁺ will result in one-photon emission. Fortunately, the highest energy fd emissions are strongest since the transition probabilities are proportional to E³ (where E is the photon energy). This will favor the energy transfer to the highest energy Gd³⁺ levels (assuming dipole-dipole interaction).

In the present task report it is not possible to discuss in detail all problems that are expected for all different ions and possible solutions. The situation is complex. Finding the proper fd sensitizer will require extensive research where in addition to varying the host lattice also the concentrations of the sensitizer and Eu^{3+} ion need to be varied to obtain the most efficient quantum cutting. Careful analysis and interpretation of the experimental results will require a good study of all possible energy transfer processes. Recent studies on the VUV spectroscopy of fd luminescence of lanthanide ions [145, 147, 148, 151, 152, 153] and of energy transfer processes [149] will provide a good background for this research. In spite of the complexity, the research is promising since energy transfer from the fd states of lanthanides to the VUV levels of Gd^{3+} has been observed to be efficient. In addition to optimizing the energy transfer in a specific host lattice, the research should aim at preventing or minimizing the problems of back transfer to the lower energy $4f^n$ levels of the sensitizer.

Host Lattice Excitation

Excitation in the host lattice is a convenient method to obtain efficient absorption of VUV radiation. Host lattice absorption is strong and if energy transfer to the emitting state is efficient, host lattice excitation is a relatively simple method for sensitization [154, 155]. Energy transfer from the host lattice usually occurs at energies where host lattice emission is observed. The exact nature of the emitting center in an undoped host lattice is often not known and described as ‘self trapped exciton’ (STE). For sensitization of the ^6G level of Gd^{3+} via host lattice excitation two problems are expected:

1. STE emission is commonly found at energies considerably below the band edge. Due to this, the emission will usually be at too low energies for energy transfer to the ^6G level of Gd^{3+} . Instead energy transfer to the ^6I or ^6P levels is expected.
2. By creating free electrons and holes non-radiative losses due to trapping of the free charge carriers by defects or impurities are enhanced. This will reduce the quantum efficiency.

In Reference [52] data on host lattice bandgaps are compiled. In Table B-11 some data on the absorption onset and host lattice emission are tabulated [118, 157]. The table shows that mostly the host lattice emission is at substantially longer wavelengths than 200 nm. Thus energy transfer to Gd^{3+} (^6G) is not expected, except for a few cases. For example, in ScPO_4 also an emission peak is present around 211 nm, close to Gd^{3+} ^6G absorption lines (see also Figure B-6). Still, host lattice excitation does not seem to be a promising route. Even if the non-radiative losses as mentioned under (2) can be prevented by making a perfect (defect free) phosphor the energy transfer will be mainly to lower energy $4f^n$ states. In spite of the pessimistic expectations for sensitization via host lattice excitation, it will be interesting to study the energy transfer process to luminescing lanthanides under host lattice excitation. Up until now the energy transfer process from the host lattice to emitting centers is not well understood. An increased understanding is important for a more general understanding of luminescence processes after high energy excitation (VUV, x-ray, electron beam).

Table B-11
Data on Host Lattice Luminescence in some Oxides and Fluorides
(Data from References [118, 157])

Host Lattice	Absorption Edge (nm)	Host Lattice Emission Bands (nm)
ScPO ₄	168	211, 350, 470
LuPO ₄	140	not measured
YPO ₄	144	233, 440
LaPO ₄	153	262, 328
NaScO ₂	189	400 (very broad)
NaLaO ₂	242	Not measured
LiScO ₂	188	250, 350-450
LiLaO ₂	229	400
Sc ₂ O ₃	196	not measured
Y ₂ O ₃	208	370
Y ₃ Al ₅ O ₁₂	178	260, 460
YAlO ₃	158	not measured
LaAlO ₃	211	280, 600
Y ₂ O ₂ S	262	318, 590
La ₂ O ₂ S	276	377, 560
CaF ₂	105	279
SrF ₂	117	300
BaF ₂	123	310

Conclusions

In this report an overview of luminescence properties for four possible classes of VUV sensitizers has been given. The discussion has been focussed on finding a good sensitizer for the Gd³⁺ ⁶G level (around 205 nm) because of the immediate need for a good sensitizer for the Gd-Eu couple. However, the report is also valid for sensitization of 4fⁿ VUV levels of other lanthanides. The discussion, based on existing literature and recent unpublished research, leads to the following recommendations for each class of sensitizer.

Charge Transfer Transitions

The discussion has been focussed on the charge transfer (CT) luminescence of Yb^{3+} . In oxides the charge transfer state of Yb^{3+} is at too low energies. Research on charge transfer luminescence of Yb^{3+} in fluorides and possibly oxyfluorides may result in finding an efficient VUV sensitizer. Problems that will be encountered are thermal quenching of the CT luminescence and cross-relaxation processes involving the $^2F_{7/2} \rightarrow ^2F_{5/2}$ transition of Yb^{3+} . Charge transfer luminescence of 3d, 4d and 5d transition metal ions (e.g. d^1 ions) may also be situated in the VUV in fluoride host lattices. The VUV spectroscopy of charge transfer luminescence of transition metal ions is a new area of research. Interesting scientific results are expected, but it is not easy to indicate if there is a reasonable chance to find a good VUV sensitizer.

s^2 Ions

The class of s^2 ions is well known to provide efficient sensitizers for the mercury discharge oxidic lamp phosphors. In order to find a VUV sensitizers it is clear that this can only be achieved in fluoride host lattices. Even in a fluoride it is a challenge to shift the lowest sp excited state to sufficiently high energies (above $50\,000\text{ cm}^{-1}$). Recent work has shown that it is possible (for Pb^{2+} in KMgF_3). Future research should be aimed at finding systems where also Gd^{3+} and Eu^{3+} can be included and where the lowest sp excited state (A-band) of Pb^{2+} is at similar high energies as in KMgF_3 . This may not be easy, but it is very promising in view of the energy level scheme of Pb^{2+} (no energy levels between the ground state and the 3P_0 excited state). Alternatively, B-band emission may be used to sensitize the VUV levels of Gd^{3+} . Future research should aim at finding systems where VUV sensitisation occurs, but not back transfer from Gd to the A-band. Finally, also the VUV luminescence other s^2 ions may be studied in fluoride host lattices.

$4f^{n-1}5d$ Luminescence

The parity allowed $4f^n \rightarrow 4f^{n-1}5d$ (fd) transitions of lanthanides are often situated in the VUV part of the spectrum. fd emission can be observed for Ce^{3+} , Pr^{3+} , Nd^{3+} , Er^{3+} and Tm^{3+} . Apart from Ce^{3+} all these ions may be used as a VUV sensitizer. On the basis of the presently known positions of the fd states, the Nd^{3+} ion is the most promising candidate. The main problems envisaged for using the fd luminescence of lanthanide ions are energy transfer and cross-relaxation to the lower energy f^n states of the sensitizer. This lowers the efficiency of the desired two-step energy transfer from $\text{Gd}(^6G)$ to Eu^{3+} or it may quench the Eu^{3+} emission. Also in this area more research is recommended and expected to yield useful information which may lead to finding a useful VUV sensitizer.

Host Lattice

Host lattice luminescence absorption and emission bands have been tabulated for a number of different host lattice. The results show that the host lattice emission (usually called Self Trapped Exciton (STE) emission) is at too low energies to allow for energy transfer to the VUV states of lanthanide ions. Research in this area is not recommended if the priority is finding a good sensitizer. Fundamental insight in the relaxation from highly excited e-h pairs to the emitting states of dopant ions is however poorly understood and may be unravelled by studying the host lattice emission under VUV excitation.

Task 5: $\text{Gd}^{3+} {}^6\text{G}_{7/2}$ Based 2 Photon Generation in Oxide Solids

Task Leader: Charles Struck
Task Members: Douglas Keszler
Andries Meijerink
Norman Barnes

Introduction

The goal of this task is to assess whether in an oxide host the high energy $\text{Gd}^{3+} {}^6\text{G}_{7/2}$ state can be efficiently populated and can be expected, by the sequential energy transfers of energy to two emitting ions, to have quantum yields approaching 2. If and only if the excitation can be efficiently produced, if it is strongly absorbed, and if the quantum yield approaches 2 will such an excitation plus a two-photon per excitation phosphor become a candidate to replace the current fluorescent lamp based on the Hg discharge and a set of phosphors tuned to the Hg 254 nm emission.

Possible Oxide Hosts for $\text{Gd}^{3+} {}^6\text{G}_{7/2}$ Sensitized Phosphors

To have the $\text{Gd}^{3+} {}^6\text{G}_{7/2}$ state efficiently populated, one needs to place Gd^{3+} into a high band-gap material with some allowed transition such as an $f^n \rightarrow f^{n-1}d$ transition at an energy such that it efficiently feeds this $\text{Gd}^{3+} {}^6\text{G}_{7/2}$ state. Explicitly, the $\text{Gd}^{3+} {}^6\text{G}_{7/2}$ state is at $\sim 49000 \text{ cm}^{-1} = 204 \text{ nm} = 6.0 \text{ eV}$. The allowed transition which feeds this $\text{Gd}^{3+} {}^6\text{G}_{7/2}$ state must be at $\sim 57000 \text{ cm}^{-1} = 175 \text{ nm} = 7.1 \text{ eV}$. The excess $\sim 8000 \text{ cm}^{-1}$ will be lost, half to reach the minimum of the offset $f^{n-1}d$ state and half to reach from this crossover energy to the minimum of the ${}^6\text{G}_{7/2}$ state. For a Gd impurity band to be placed at 57000 cm^{-1} , the bandgap must be above $\sim 7.1 \text{ eV} = 175 \text{ nm}$, and at least by several kT, e.g., at $\sim 7.15 \text{ eV} = 173 \text{ nm}$.

The relationship of the feeding state to the $\text{Gd}^{3+} {}^6\text{G}_{7/2}$ state is illustrated in Figure B-11.

The total Stokes shift of 8000 cm^{-1} is a typical value for charge transfer states we have studied. One can expect such offsets for any strong transition in a solid, because strong transitions imply significant changes in the occupied electronic orbitals, and the environment around the ion will adjust to such orbital changes. We believe that this value of 8000 cm^{-1} will underestimate the demands on the host, i.e., will lead to considering hosts which will in fact fail rather than cause overlooking one which would have been adequate.

The indications are that only some borates, some phosphates, possibly some oxyfluorides, and possibly some Be compounds, might have band gaps above 7 eV. There are no counter-indications that such a high bandgap is impossible for all complex oxides. The expectation seems to be confirmed in this list of choices that to have a high band gap one must have oxygens tightly bound to some small positive ion so that they will be as weakly negatively charged as possible.

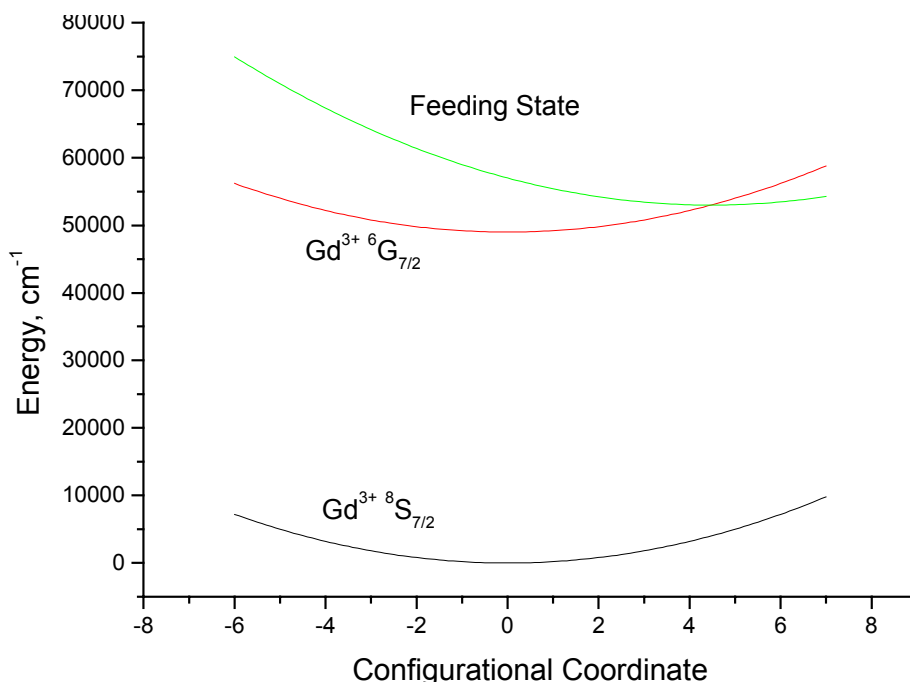
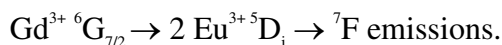


Figure B-11
Gd f^8 States and Offset Feeding State

The Activator for Visible Emissions

Eu³⁺

Our first choice for the activator emitting the visible photons is Eu³⁺ because of its ideal emission spectrum. The Eu³⁺ spectrum is the basis of both the fluorescent lamp red emitter and the color television red emitter. Thus we are aimed at the scheme



The difficulty in this Task 5 is that one must avoid the Eu³⁺ $f \rightarrow d$ bands and charge transfer bands. If any Eu³⁺ strong absorption bands are near the $^6\text{G}_{7/2}$ state at $49000 \text{ cm}^{-1} = 204 \text{ nm} = 6.0 \text{ eV}$ then the Eu³⁺ energy levels responsible for these bands will allow efficient losses down the ladder of Eu³⁺ energy levels to the ^5D states and thereby afford only one emitted red photon. At this point, avoiding Eu³⁺ energy levels near 49000 cm^{-1} and still providing a broad band at $57000 \text{ cm}^{-1} = 175 \text{ nm} = 7.1 \text{ eV}$ to absorb the UV photons seems a daunting task. Dorenbos [158], in Table 4 of his first paper, shows that if Gd has fd bands at 57000 cm^{-1} , then one can expect Eu fd bands at $47100 \text{ cm}^{-1} = 212 \text{ nm} = 5.8 \text{ eV}$. Such an fd band placement would imply strong interference with the desired Gd³⁺ $^6\text{G}_{7/2}$ state at $\sim 49000 \text{ cm}^{-1} = 204 \text{ nm} = 6.0 \text{ eV}$.

The only hope is that there is a host in which the lowest broad band of Eu³⁺ is at $57000 \text{ cm}^{-1} = 175 \text{ nm} = 7.1 \text{ eV}$. By some good luck one might find that absorbing into this state leads to populating Eu³⁺ energy levels near 49000 cm^{-1} and that these levels efficiently transfer their energy to the Gd³⁺ $^6\text{G}_{7/2}$ state. In Figure B-12, the ladder of f^6 electronic states of b Eu³⁺ in the $30000\text{--}50000 \text{ cm}^{-1}$ is only schematic. The actual set of these levels is shown in Figure B-13.

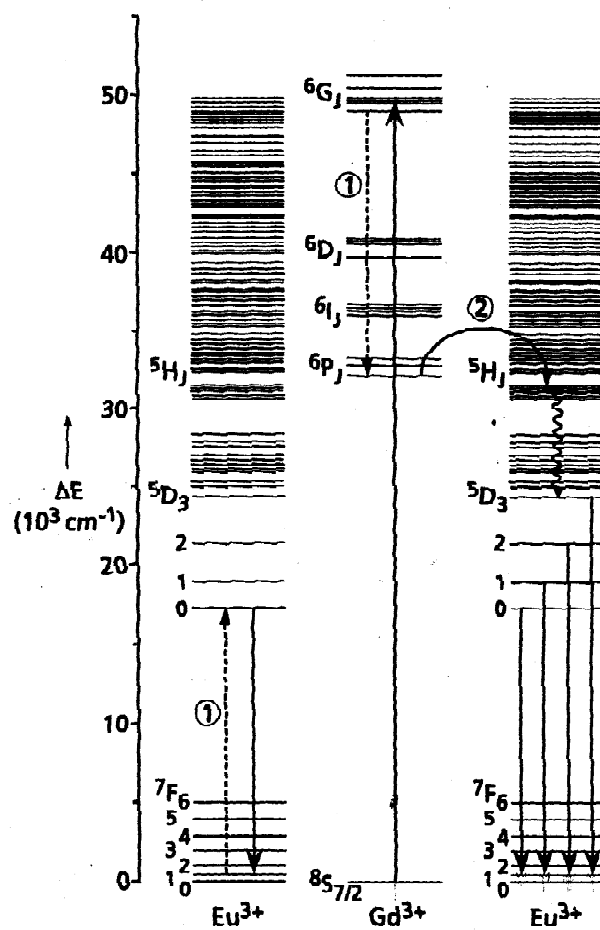
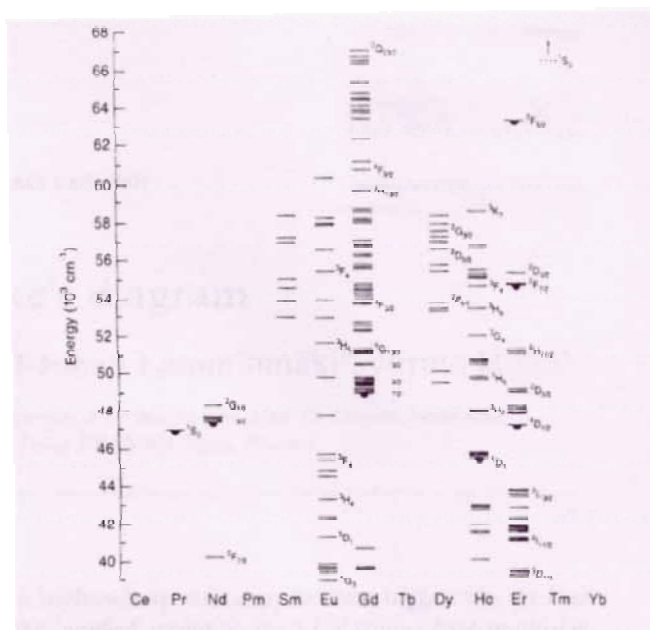
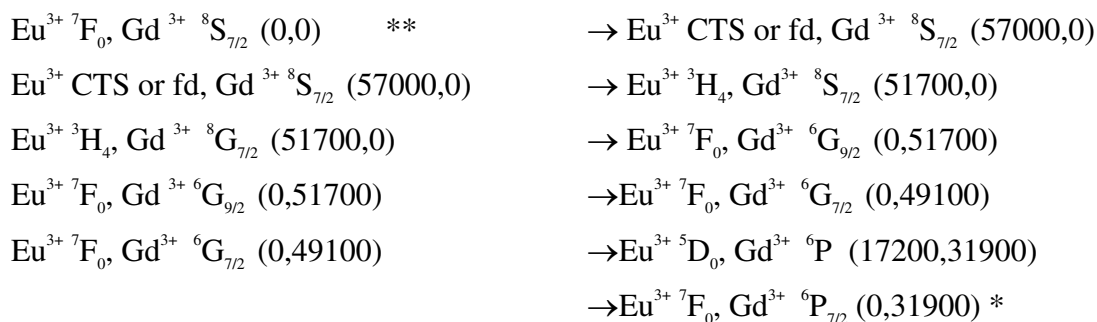


Figure B-12
Diagram from Meijerink Showing the Sequence of Energy Transfers from Gd to Two Eu Ions

**Figure B-13**

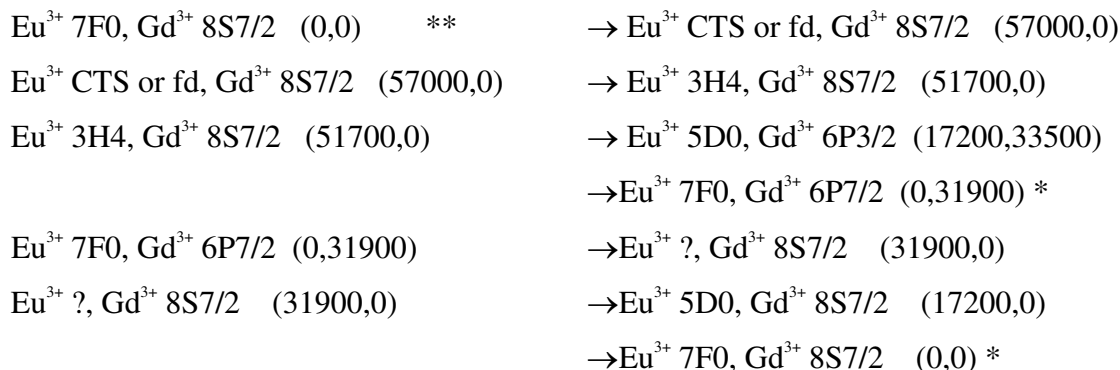
Extension of the Dicke Diagram in the VUV Region. For the Ions in the Middle of the Series (Sm through Dy) Only the Strongest Experimentally Observed Lines are Included. Assignments for Sm and Dy are Lacking Since Energy Level Calculations have not been Performed Yet.

Figure B-13 is a photograph of a figure from Meijerink showing the extension of the Dicke energy level chart of trivalent rare earths energy levels beyond 40000 cm^{-1} . It shows only 15 levels between 40000 and 57000 cm^{-1} . There seems to be 2000 cm^{-1} gaps between levels around 50000 cm^{-1} . Such gaps are not always bridged quickly by nonradiative processes. For example, one can see at low Eu concentrations and at low temperatures emissions from the upper ^5D levels, which have similar spacings in energy. Nevertheless, it would be in the category of very good luck if in some host Eu^{3+} has a charge transfer band in the neighborhood of 57000 cm^{-1} , if populating that band led directly to populating Eu^{3+} levels near 51000 cm^{-1} , if the Eu concentration were low enough such that the dominant depopulation of this 51000 cm^{-1} level is by energy transfer to one of the $\text{Gd}^{3+} {}^6\text{G}$ levels but ending in $\text{Gd}^{3+} {}^6\text{G}_{7/2}$, and, finally, if the concentration of Eu were simultaneously high enough that the desired sequence of energy transfers from $\text{Gd}^{3+} {}^6\text{G}_{7/2}$ back to the emitting $\text{Eu}^{3+} {}^5\text{D}$ states dominates. Explicitly, the sequence of states pictured here would be:





An alternative sequence is



The double** indicates absorption of a UV photon, and the single * emission of a visible photon. The second emission might be at higher energy from a higher ${}^5\text{D}_j$ state, and it may not end in ${}^7\text{F}_0$. In both sequences, it would seem that the competing transfers, which we could label $\text{Eu}(\text{E}1)\text{Eu}(0) \rightarrow \text{Eu}(\text{E}1-x)\text{Eu}(x)$ summed over all possible states x , would have to be slow in comparison. This consideration points to high Gd concentrations, approaching a gadolinium compound, and low Eu concentrations, below perhaps 1%.

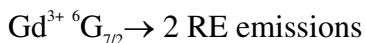
The search for a host showing either sequence of events is worth pursuing, even though the quantum deficit efficiency will be near $(17200 \times 2 / 57000)$ or, 6. Thus efficiency might be a little higher because some Eu emissions might be from ${}^5\text{D}_2$ or ${}^5\text{D}_1$ rather than ${}^5\text{D}_0$. The overall efficiency will also be multiplied also by the efficiency of converting the electric power into radiation at 57000 cm^{-1} . and will likely be in the neighborhood of .0.35, marginally higher than the efficiency of the current fluorescent lamp.

The probability for success in uncovering such a host is very small but not rigorously zero, and even in failure it will provide at least an understanding of how the charge transfer bands and the $f \rightarrow d$ bands of Eu^{3+} vary with the band-gap of the host. This is important background information to have. Thus our recommendation is to conduct a survey of various Gd^{3+} and Eu^{3+} co-doped complex borate and oxyborate hosts with 12-coordinated trivalent sites, with attention given to the positions of the f^5d states and of the charge transfer states and to any signs of the desired energy transfers. The limit to high coordination number is to due to a desire for small crystal field splittings of the f^5d states. The Gd content might be so high that the host will be a Gd compound.

Marvin Weber has informed me of one reference [159] of importance here which offers some hope for success. Andreas Meijerink has informed me of a reference to the work of van Pieterse [160] which lists the band gaps and the position of the Eu and the Yb CTS and fd bands in various hosts. The highest energy Eu CTS was at 205 nm in ScPO_4 . Meijerink suggests oxyfluorides as the best hope for an oxygen containing host which might have the Eu CTS high enough in energy to allow strong feeding of the $\text{Gd} {}^6\text{G}_{7/2}$ state.

Other Activators than Eu^{3+}

If in fact no useful phosphor is found based on $\text{Gd}^{3+} {}^6\text{G}_{7/2} \rightarrow 2 \text{Eu}^{3+} {}^5\text{D}_j \rightarrow {}^7\text{F}$ emissions, then one might think of studying other activators for the possibility that some rare earth may provide this sequence of energy transfers from $\text{Gd}^{3+} {}^6\text{G}_{7/2}$.



For the sequence of energy transfers leading to 2 photon emissions, the requirement is strict that the recipient of the Gd energy must have an energy level in the $17000 - 20000 \text{ cm}^{-1}$ range.. Nd^{3+} , Pr^{3+} and Ho^{3+} seem to meet this requirement. Of these Pr^{3+} seems preferable on the grounds that it has fewer energy levels near and below 17000 cm^{-1} .

However, all these ions have $f \rightarrow d$ bands at considerably lower energy than either Gd^{3+} or Eu^{3+} . Table 4 of Dorenbos's first paper would predict Nd^{3+} fd bands 17000 cm^{-1} lower than Eu^{3+} and Pr^{3+} fd bands 27000 cm^{-1} lower than Eu^{3+} . Even Ho^{3+} would be expected 4000 cm^{-1} lower. These ions would not in our opinion be any more favorable than Eu^{3+} itself. We therefore offer no suggestions for further work in this area.

Recommendations

To repeat, our recommendation is to conduct a survey of various Gd^{3+} and Eu^{3+} doped complex borate, oxyborate, and oxyfluoride hosts with as high a coordination number as possible around the trivalent sites, with attention given to the positions of the f^5d states and of the charge transfer states and to any signs of preferring one of the desired energy transfers. The probability of finding a useful phosphor by this search is small but not zero. The possibility of understanding the nature of these states and of the variation of their energies from host to host is great.

Bibliography

Band Gaps Compilations

1. Rodnyi, P. A., Sov. Phys. Solid State 34(1992)1053-1066.
2. Bakcerzyk, M., Gontarz, Z., Moszynski, M., and Kapusta, M., J. Luminescence 78-89 (2000)963-966.
3. Strehlow, W. H. and Cook, E.L., J. Phys. Chem. Ref. Data 2(1973)163-192.

fd Transitions

1. Dorenbos, P. J. Luminescence 91(2000) 91-106, and 155-176.
2. Meijerink, A. and Wegh, R. T., Proceedings of IREC'98, Freemantle, Australia, "VUV Spectroscopy of Lanthanides: Extending the Horizons."

3. Hamilton, D.S., DOE/ER/45056-10 DE93 002133, Final Report for the period June 1, 1984 to May 31, 1992, "Energy Transfer and Non-linear Optical Properties at Near Ultraviolet Wavelengths: Rare Earth 4f→5d Transitions in Crystals and Glasses."

Crystal Field Analysis

1. Holsa, J., *Annales Academiae Scientiarum Fennicae*, Helsinki University of Technology, Department of Chemistry, Thesis March 1, 1983.

Band Gap Calculations

1. Mishra, K. C., DeBoer, B. G., Schmidt, P. C., Osterloh, L., Stephan, M., Eyert, V., and Johnson, K. H., *Ber. Bunsenges Phys. Chem* 102 (1998) 1772-1782.
2. Mishra, K. C., Osterloh, L., Anton, H., Hannebauer, B., Schmidt, P. C., and Johnson, K. H., *J. Luminescence* 72-74 (1997) 144-145.
3. Mishra, K. C., Osterloh, L., Anton, H., Hannebauer, B., Schmidt, P. C., and Johnson, K. H., *J. Mater. Research* 12 (1997) 2183-2190.

Appendix

Barnes 5-30-01

A first cut at assessing task 5 appears below. It appears to me that there are actually 2 tasks here, first determine if there is a suitable oxide host for Eu sensitization of Gd and second determine if there is a favorable multiphoton emission scheme associated with the excitation of Gd. A suggested scope of the project and approach for each task appears below.

As presently understood, the first objective is to absorb ultraviolet radiation using a 4f to 5d transition, probably in Eu, and transfer the excitation to Gd. The 4f to 5d transition is sought because a large absorption coefficient is needed. The 4f to 5d transition, being parity allowed, can be strong. To obtain a 2:1 quantum efficiency in the visible, it is desired to excite some 6G_J manifold. For this to happen, the following are required:

1. Oxide materials where the 4f to 5d absorption band is higher than the 6G_J manifold should be identified.
2. The dependence of the efficiency of the process on the energy difference between the Eu 4f to 5d absorption band and the 6G_J manifold should be characterized. If the Eu 4f to 5d band is too high, little transfer occurs. If the band is too low, too much excitation will remain with the Eu.
3. The multiphonon decay rate of the 6G_J manifold should be determined for the potential oxide materials. A low multiphonon decay rate will enhance the probability of energy transfer by minimizing the nonradiative losses.

4. The transition probability of the 6G_J to ${}^8S_{7/2}$ manifold should be determined for the oxide materials. This transition probability influences both the energy transfer rate from Eu to Gd and the fluorescent loss of the 6G_J manifold.
5. The transition probability for the 6G_J to 6P_J manifolds should be determined for the potential oxide materials. A large transition probability enhances the rate of energy transfer or fluorescence.

Given these parameters, some relative comparisons can be made from the available oxide laser materials. However, the energy transfer rates from Eu to Gd need to be measured to lend much credence to the efficacy of a particular oxide material.

To obtain some information on each of the topics listed above, the following may be tried.

1. The data of Dorenbos can be utilized to estimate the position of the 4f to 5d absorption band. Essentially, the position of the Ce 4f to 5d absorption band has been measured for many materials. Furthermore, given the position of the Ce absorption feature, the position of the 4f to 5d absorption band, the position of the 4f to 5d absorption features can be estimated $\pm 600 \text{ cm}^{-1}$. Although the variety of materials is not extensive, it will provide some guidance for a variety of some common materials.
2. A relative estimate of the relative energy transfer rates can be obtained by performing an overlap integral of the Eu emission feature and the Gd absorption feature. Presumably the latter is known. The former may be estimated by knowing the position of the Eu absorption feature. It may be possible to estimate the relative populations of the Eu and the Gd using the same overlap integral. An absolute estimate of these quantities will require more labor.
3. The multiphonon decay rate can be estimated from the energy gap law. This requires a knowledge of the maximum phonon energy for the material and the energy gap of Gd. To first order, it may be sufficient to assume a constant energy gap.
4. The manifold to manifold transition probabilities of Gd can be obtained using a Judd-Ofelt analysis. However, the Ω_λ parameters of the materials and the reduced matrix elements of the transitions need to be known. Some of this information may be available in the literature. However, because the manifolds are so energetic, the possibility of obtaining this information becomes more problematic. The Judd-Ofelt parameters and the reduced matrix elements should become available when task 7 is completed.
5. This transition probability can be determined in the same manner if the requisite parameters are available.

It should be emphasized that the above analysis will only yield a relative comparison of the materials for which the requisite parameters can be found. It should be a useful exercise to indicate the direction of further experimental research. What is really needed is a measurement of the relevant parameters in the materials under consideration.

Obtaining a 2:1 quantum efficiency, given that a Gd atom has been excited to the 6G_J manifold can be subdivided into 2 parts, transitions yielding the first photon and transitions yielding the

second photon. There are several possibilities for obtaining each of these photons. For the first photon, among the possibilities are:

1. Fluorescence from the Gd 6G_J to 6P_J manifold with no intermediate energy transfer process.
2. Energy transfer from the Gd 6G_J to the Eu 6P_J manifold with subsequent fluorescence from the Eu 6P_J manifold to the 7F_J manifold.
3. Energy transfer from the Gd 6G_J to the Pr 1D_2 manifold with subsequent fluorescence from the Pr 1D_2 manifold to the 3H_J manifold.
4. For the second photon, among the possibilities are:
5. Energy transfer from the Gd ${}^6P_{7/2}$ manifold to Eu with subsequent nonradiative relaxation to the Eu 1D_0 . From there, fluorescence from the 1D_0 to the 7F_J .
6. Energy transfer from the Gd ${}^6P_{7/2}$ manifold to Tb with subsequent nonradiative relaxation to the Tb 5D_3 . From there, fluorescence from the 5D_3 to the 7F_J .
7. Energy transfer from the Gd ${}^6P_{7/2}$ manifold to Dy with subsequent nonradiative relaxation to the Dy ${}^4F_{9/2}$. From there, fluorescence from the ${}^4F_{9/2}$ to the 6H_J .
8. Energy transfer from the Gd ${}^6P_{7/2}$ manifold to Er with subsequent nonradiative relaxation to the Er ${}^2P_{3/2}$. From there, fluorescence from the ${}^2P_{3/2}$ to the 4I_J .

Having identified possible transitions for a 2:1 quantum efficiency, the choice of host material and concentration of both the sensitizer and active atom can be optimized. To do this, the rate equation approach can be used with the pertinent manifolds. Obtaining the parameters needed to describe the rate equations can be accomplished in at least 2 ways. One way uses spectroscopic methods. Both emission spectrum of the sensitizer and absorption spectrum of the active atom are needed for the forward transfer process. In addition, the emission spectrum of the active atom and the absorption spectrum of the sensitizer are needed for the backward transfer process. Also radiative transition rates between the various manifolds must be measured and the branching ratios computed. A second way is the direct measurement of the energy transfer rates. These rates can be inferred through a measurement of the rate of rise and decay of the manifolds involved. Because the dynamics of the situation is complicated involving excited manifolds and may be subject to other effects, such as nonradiative decay, this method can be difficult. Any experimental program along these lines will not be completed in 10 days.

Nonradiative decay rates must be taken into account. Many glasses have relatively high phonon energies which promotes nonradiative losses. Obviously, nonradiative losses can degrade the probability of the 2:1 quantum efficiency. If the positions of the energy levels are known, the nonradiative decay rate can be estimated using the maximum phonon energy and the energy gap. A more sophisticated approach will also take into account the transition probabilities between the interacting manifolds. To obtain information on the position of the manifolds as well as the maximum phonon energy, spectroscopic methods can be employed again.

Besides measuring the rates of the favorable processes, the rates of competing energy transfer processes must be measured as well. Competing processes can represent losses. When these

processes become too probable, a loss in efficiency will be the result. Measurement of the competing rates can be accomplished in the same manner as the measurement of the favorable rates. To limit the number of measurements, some judicious approximations may have to be made.

Because there are a multitude of possible host materials, the probability of finding an efficient phosphor becomes more probable. However, with the multitude of host materials, each with a variety of sensitizer and active atom concentrations the task could become quite time consuming. But, it is felt that with an understanding of the germane physical processes, enough insight will be gained so that favorable host materials and concentrations will become predictable.

Task 6: Modeling

Task leader: M. Weber
Task members: K. Johnson
A. Meijerink
R. Rana
W. White

Objective

This task is to develop an overall capability for modeling new multiphoton phosphors based on a combination of experimental data and theoretical predictions. Modeling should serve as a tool for prescreening potential ion-host combinations for multiphoton phosphors before expending efforts to synthesize the materials. Initial consideration is given to lanthanide ions in crystalline hosts. Luminescence properties of interest include energy of excitation bands, ground and excited state absorption coefficients, radiative transition probabilities and fluorescence branching ratios, nonradiative transition probabilities, probabilities for ion-ion energy transfer, and overall quantum efficiencies.

Subtask A

Literature survey of Judd-Ofelt intensity parameters for lanthanide ions in crystals.
Develop correlation of Judd-Ofelt parameters with host composition and structure.

Conclusions

Many and varied attempts have been made to relate Judd-Ofelt intensity parameters with the chemical nature of the lanthanide-ligand bond, with the properties of the ligand itself, or with the structure of the complex. Thus far no well-validated methodology has emerged to predict the relative magnitude of Judd-Ofelt parameters for different host crystals.

Recommendations

Although the Judd-Ofelt theory has several approximations that limit its accuracy, it can provide useful predictions of absorption and emission probabilities. Therefore a further comprehensive study and critical evaluation of available literature is warranted to obtain a better understanding of the physical origin of the Judd-Ofelt parameters in various materials and to develop a capability for estimating Judd-Ofelt parameters for lanthanide ions in crystalline hosts. In some cases, modifications of the assumptions in the Judd-Ofelt theory may be necessary to obtain meaningful results.

In place of the Judd-Ofelt treatment that relies on empirical parameters, first-principles calculations of the probabilities of radiative electric-dipole transitions of lanthanide ions should also be explored.

Subtask B

Literature survey of nonradiative multiphonon decay rates for lanthanide ions in crystals. Develop capability for estimating nonradiative multiphonon decay rates for lanthanide ions in crystalline hosts.

Conclusions

Multiphonon decay rates from excited states of lanthanide ions in crystals depend upon the phonon density of states and maximum phonon energies of host and the strength of the ion-lattice coupling. The influence of the reduced matrix elements of electronic transitions and selection rules are known. Predictions of multiphonon decay rates can therefore be made, albeit without high accuracy, given experimental or theoretical information about the phonon spectrum and the strength of the ion-lattice coupling of comparable materials. Meaningful first-principles calculations are lengthy and can be applied to a particular material but are not useful for survey of many materials.

Recommendations

Sufficient experimental data and guidance exists for initial estimates of multiphonon decay rates from excited J states of lanthanide ions, thus further research is not needed at present.

Subtask C

Extend Dieke diagram to include the higher ($> 40,000 \text{ cm}^{-1}$) excited states of the trivalent lanthanide ions.

Conclusions

Although several higher-lying excited states of the lanthanide ions have been determined, additional measurements are needed to complete the energy level diagrams. In a number of cases, tentative level assignments require further validation; more detailed and higher resolution work is needed to establish their identity unequivocally. Calculation of the energy levels, using the parametric approach for the $4f^n$ configuration, have been refined successfully for identifying the lower levels of the ground $4f^n$ configuration empirically. Whether this program and these parameters can be used to predict upper levels that are close to or overlap levels of excited configurations may require extension of the theoretical programs used for the lower levels of the ground $4f^n$ configuration.

Recommendations

The location and identification of higher-lying excited states of interest for energy transfer and cascade transitions should be determined experimentally for selected lanthanide ions considered to be candidates for multiphoton phosphors. Measurements can be made using upconversion techniques or synchrotron radiation. Wide bandgap halide hosts are suitable for such studies. LaCl_3 crystals containing most of the Ln^{3+} ions are available and could be used (R.Rana).

Subtask D

Calculation of reduced matrix elements for higher ($> 40,000 \text{ cm}^{-1}$) excited states of the trivalent lanthanide ions.

Conclusions

Matrix elements involving higher excited states are needed for predictions of radiative and nonradiative decay rates, fluorescence branching ratios, excited state absorption, and electric dipole-dipole and electric dipole-quadrupole energy transfer using the Judd-Ofelt theory. Matrix elements for absorption from the ground state to all excited states are of interest; matrix elements for emission or energy transfer from those levels with a large energy gap to the next lower level to all lower levels are of main interest. Although the calculations are not too complicated, they can be extensive. A prerequisite for these calculations is the correct identification and assignment of the energy levels in subtask c.

Recommendations

Reduced matrix elements required in the Judd-Ofelt treatment of electric-dipole transitions should be calculated for selected lanthanide ions considered to be candidates for multiphoton phosphors. The groups of M.Reid and A. Meijerink should be encouraged to undertake this project.

Subtask E

Survey of first-principles and semi-empirical approaches for theoretical predictions of energy levels and transition probabilities of lanthanide ions in crystals. Recommendations for the best approaches to be used to calculate absorption and emission properties relevant to the operation of multiphoton phosphors.

Conclusions

The Self-Consistent-Field Xalpha (Density-Functional) Scattered-Wave (SCF-X α -SW) Cluster Molecular-Orbital (MO) Method has been used successfully at Sylvania for many years (see, also, Task 7). It is the fastest (it runs fast on any PC) practical DF method to calculate reliably, from first principles, the electronic energy levels and wave functions of both the ground and excited states of molecules and clusters, including the heaviest elements in the Periodic Table. Experience and expertise in applying this method are well established at M.I.T and Osram-Sylvania.

Recommendations

The SCF-X α -SW method should be used for calculations of ground and excited states to evaluate the potential of ions of interest for multiphoton phosphors.

Final Task

Integration of the above findings to develop selection rules and procedures for predicting the luminescence properties of lanthanide ions in crystals.

Conclusions

This is a continuing and involving process. It makes use of results of all of the subtasks described above, several of which will require extensive, long-term investigations.

Recommendations

Refinement and integration of the results of the above subtasks for lanthanide series ions should continue. If there is interest in exploring transition metal and post-transition group ions for multiphoton phosphors, developing selection rules and procedures for predicting the luminescence properties of these ions in crystals should be pursued.

Background and Elaboration

Judd-Ofelt Parameters

The theoretical expressions for the Judd-Ofelt intensity parameters involve products of (1) odd-parity terms of the crystal field and (2) terms including the energy difference between the $4f^n$ configuration and the admixed $4f^{n-1}nl^1$ configuration and $4f-5d$ radial integrals.

The parameter Ω_6 is affected more by a change of the radial integrals than are Ω_2 and Ω_4 and, accordingly, is more sensitive to changes of electron density of the $4f$ and $5d$ orbitals.

On contrast, Ω_2 is more sensitive to the asymmetry of the crystal field than are Ω_4 and Ω_6 . A not too useful generalization is that all Judd-Ofelt parameters depend in some degree on covalency.

There are several approximations made in the Judd-Ofelt treatment of electric-dipole transitions, in particular the use of a single value for the energy of each perturbing configuration. Thus the energy denominator is the same for all states of a given configuration. This is a poor approximation, for example, for the 1S_0 state of Pr^{3+} because it is frequently only a few thousand cm^{-1} from the wide $4f5d$ band. Small admixing of the 1S_0 state of $4f^2$ with the 1F_3 and 1H_5 states of $4f^15d$ can affect calculated transition probabilities. This can be treated by modifications of the Judd-Ofelt theory.

For the $^1S_0-^1I_6$ transition of Pr^{3+} to be dominant, the Judd-Ofelt intensity parameters should be such that $\Omega_6 \gg \Omega_2, \Omega_4$. Reported ratios Ω_2/Ω_6 and Ω_4/Ω_6 for several oxide and fluoride crystals are reported in Task 3 where small ratios for the successful PCE phosphors SrAl_2O_9 and YF_3 are noted. The experimental errors associated with reported Judd-Ofelt parameters are usually relatively large ($\sim 5-20\%$). In addition, parameter sets determined by different authors may be substantially different, due on part to the number of transitions chosen for the fitting procedure. Valid criteria for predicting the relative values of the Judd-Ofelt parameters for Pr^{3+} in other hosts based on the local structure and bonding remain to be established.

In a 163-page survey article by Görller-Walrand and Binnemans [161] devoted to the spectral intensities of f - f transitions of lanthanide ions in crystals, glasses, and liquids, only three and one-half pages address the compositional dependence of the intensity parameters. The authors note that various researchers have related these parameters with the rigidity of the medium, covalency, overlap integral of the $4f$ and $5d$ orbitals, distortion of the ligand field in the vicinity of the lanthanide ion, local basicity, cationic strength of the network-forming ions (in glasses), the dielectric constant of the solvent (liquids), and symmetry and number of alcohol molecules in the first coordination sphere in different alcohols. The section concludes with “The last word about the meaning of the intensity parameters has not been said yet, and further research is necessary.” Hallelujah!

Multiphonon Relaxation

The rate of nonradiative multiphonon emission affects cascade processes within the energy level schemes of the lanthanide and the overall quantum efficiency. Nonradiative decay rates between lanthanide ion energy levels is determined predominately by the energy gap and the particular host medium. This is expressed by the simple energy gap law for nonradiative decay

$$W_{nr} = A \exp(-a \Delta E / h \nu_{max}),$$

where A and a are empirically fitted parameters, $h \nu_{max}$ is related to the highest phonon frequency of the host medium, and ΔE is the energy gap between the excited lanthanide state and the next lower lying energy level. $\Delta E / h \nu_{max}$ represents the number of phonons required to bridge the energy gap. This simple model of the crystal lattice vibrations also predicts the temperature dependence of the multiphonon decay rates rather well [162].

Van Dijk and Schuurmans [163, 164] developed a modified energy gap law for nonradiative decay where only a few phonons participate in the transition of the form

$$W_{nr} = \beta_{el} \exp[-\alpha(\Delta E - 2h\nu_{max})].$$

The parameter β_{el} was found to vary by only a factor of 10 in a whole series of compounds. The energy gap law has also been extended to the region of small energy gaps where only a few phonons are required to conserve energy and multiphonon decay rates are in the picosecond regime [165].

Given that $h \nu_{max}$ of the host medium can be determined, for example, from infrared or Raman spectra, and the energy gap ΔE between the excited lanthanide J states of interest and the next-lower-lying J state vary by only a small amount in different hosts, reasonable order-of-magnitude estimates can be made of the multiphonon decay rates.

Computing Electronic-Structure-Properties of Potential Activators

In addition to the SCF- $X\alpha$ -SW method, recently developed DF-MO-LACO methods are, in principle, applicable, but require orders of magnitude more computer time for many-electron

systems such as the second- and third-row transition metals, not to mention lanthanide ions. They simply haven't been applied much beyond the first two rows of the Periodic Table. Pseudopotential simplifications won't help much for the heavier elements. Also, the practitioners of the Kohn-Shan-type DF theory typically limit themselves to ground state properties, although Slater's transition-state method for calculation the excited states (which Johnson and Mishra have been routinely using in the SCF- $X\alpha$ -SW method) is valid for any DF method.

Hartree-Fock (HF) –MO-LCAO methods are also, in principle, applicable to the systems we are interested in, but suffer from the demand of even more computer time and the failure of HF theory to yield excited states (beyond Koopman's theorem), unless one resorts to even more extensive GW methods. One must use HF methodology only as a starting point for configuration interactions (CI), or equivalent many-body-theory computations to calculate spectra. This is rarely, if ever, done for systems of the complexity we are interested in.

Semi-empirical MO-LCAO methods—even the ZNDO method and especially the extended Huckel method—are unreliable beyond the first and second rows of the Periodic Table.

Task 7: Sugano-Tanabe Diagram for Transition Metal Candidates

Task Leader: Keith Johnson
 Task Members: Charles Struck
 Kailash Mishra
 William White

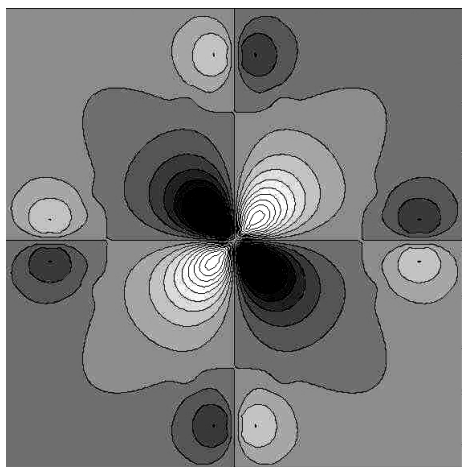
Conclusions

We have completed Self-Consistent-Field Xalpha Scattered-Wave (SCF-X α -SW) cluster molecular-orbital calculations for the *second-row* transition-metal ions, Zr²⁺, Nb³⁺, and Mo⁴⁺, having the t_{2g}(d²) orbital configuration, in octahedrally-symmetric oxide environments representative of potential multiphoton phosphors.

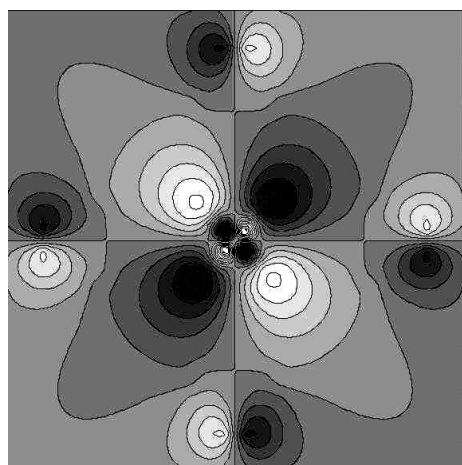
The resulting electronic structures have been compared to those obtained earlier for *first-row* transition-metal ions, such as Ti²⁺, at Osram-Sylvania by Mishra *et al.* They have been used as the basis for calculating the crystal-field splitting parameter, Dq, and the Racah parameters, B and C, as was done previously by Mishra *et al* for the *first-row* transition-metal ions and summarized in the table.

ion	N	Dq (cm ⁻¹)	B (cm ⁻¹)	C (cm ⁻¹)
Ti ²⁺	2	1871.2	370.4	1550.7
V ³⁺	2	2184.2 (1860)	622.8 (642)	2756.3
Cr ⁴⁺	2	2377.0	681.6	3104.2
V ²⁺	3	1728.5	495.6	2135.9
Cr ³⁺	3	2059.9 (1720)	678.9 (765)	3056.8
Mn ⁴⁺	3	2155.2	733.7	3390.8
Cr ²⁺	4	1236.4 (1390)	603.8 (810)	2449.0
Mn ³⁺	4	1572.0 (2100)	676.8	2958.4
Mn ²⁺	5	994.5 (1230)	739.4 (860)	2850.8

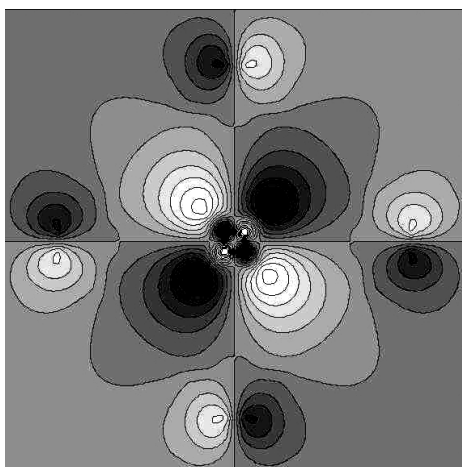
The principal difference between the electronic structures of the first-row and second-row transition-metal ions is the greater metal-oxide covalency in the latter case. This is revealed, for example, in the following t_{2g}(d²) cluster molecular-orbital wavefunction contour maps resulting from the SCF-X -SW computations.



$TiO_6\ t_{2g}(d^2)$



$ZrO_6\ t_{2g}(d^2)$



$MoO_6\ t_{2g}(d^2)$

The wavefunctions are plotted in a plane centered on the transition-metal ion and four of the surrounding octahedrally symmetric oxygen ions. In classical crystal-field theory, the central metal-ion d-orbitals are split ($10Dq$) into the t_{2g} (d_{xy}, d_{yz}, d_{xz}) and e_g ($d_{x^2-y^2}, d_{z^2}$) orbitals by the electrostatic field of the surrounding oxygen ions. However, we see in the above diagrams that even in the case of TiO_6 , there is significant *antibonding* oxygen p-orbital character. This covalency increases measurably for the second-row transition-metal ions, Zr^{2+} , Nb^{3+} , and Mo^{4+} , due to the greater spatial delocalization of the metal d-orbitals arising from “inner-shell screening.”

A principal conclusion of this study is that the larger covalency of the second-row transition-metal ions in phosphor-relevant oxides will have a profound effect on the determination of the multiplet structure and Racah parameters of activators. These systems should be investigated further, both theoretically and experimentally, to determine their suitability as activator ions in a multiphoton phosphor design.

We have, first of all, determined the *free-Ion* Racah Parameters for the second-row transition metal ions in the d^2 configuration. The possible multiplet electronic states are: $^3P, ^3F, ^1S, ^1D, ^1G$. The spectroscopically observed states are:

Ion	Observed States
Zr^{2+}	$^3P, ^3F, ^1S, ^1D, ^1G$
Nb^{3+}	$^3P, ^3F, ^1D, ^1G$
Mo^{4+}	$^3F, ^3P$

The *free-Ion* Racah Parameters (in cm^{-1}) for Zr^{2+} , where all the possible multiplets are observed, are:

Parameter	HF (Froese-Fischer)	HF (Cowan)	HF (Cowan)	Expt.
Charge State	0	0	+2	
B	616.2	605.7	659.5	$604.9^a, 552.2^b$
C	2409.4	2360.1	2609.4	$629.7^a, 2062.1^b$
γ	3.90	3.90	3.96	$1.04^a, 3.73^b$

^a All levels were used.

^b $^3F, ^3P$ and 1G were used.

The Racah Parameters from theory (Neutral Atoms, Froese-Fischer) are:

Ion	B (cm-1)	C(cm-1)	γ
Zr	616.2	2409.4	3.90
Nb	683.9	2692.2	3.93
Mo	744.2	2942.5	3.95
Ru	846.4	3360.0	3.97
Rh	893.0	3548.2	3.97
Pd	939.5	3736.5	3.98
Ag	985.5	393.5	3.98

The SCF-X α -SW molecular-orbital calculation for an octahedral (MoO₆)⁻⁸ cluster with the “Sambe” occupation of the 2t_g and 3e_g orbitals yields the energy levels (in Rydbergs) and the charge and angular momentum decomposition (note the Mo and O charges in the 2t_g and 3e_g orbitals):

level	occup	energy	charge	%s	%p	%d	%f	charge	%s	%p	%d	%f
3eg	.90	-.330	69% Mo	0	0	100	0	26% o1	8	92	0	0
2%int	***	***	3%out	0	0	76	0					
3alg	.00	-.460	1% Mo	100	0	0	0	17% o1	51	49	0	0
58%int	***	***	25%out	93	0	0	0					
2t2g	1.10	-.631	73% Mo	0	0	100	0	18% o1	0	100	0	0
8%int	***	***	2%out	0	0	48	0					
3t1u	6.00	-.899	12% Mo	0	100	0	0	69% o1	0	100	0	0
12%int	***	***	7%out	0	49	0	17					
1t1g	6.00	-.951	0% Mo	0	0	0	0	66% o1	0	100	0	0
30%int	***	***	4%out	0	0	0	0					
1t2u	6.00	-1.001	0% Mo	0	0	0	0	60% o1	0	100	0	0
36%int	***	***	4%out	0	0	0	80					
2alg	2.00	-1.045	30% Mo	100	0	0	0	55% o1	7	93	0	0
8%int	***	***	7%out	21	0	0	0					
2eg	4.00	-1.058	43% Mo	0	0	100	0	51% o1	4	96	0	0
0%int	***	***	6%out	0	0	61	0					
2t1u	6.00	-1.074	10% Mo	0	100	0	0	51% o1	2	98	0	0
34%int	***	***	5%out	0	12	0	80					
1t2g	6.00	-1.163	26% Mo	0	0	100	0	39% o1	0	100	0	0
32%int	***	***	4%out	0	0	85	0					
1t1u	6.00	-2.062	11% Mo	0	100	0	0	70% o1	100	0	0	0
16%int	***	***	3%out	0	50	0	36					

leg	4.00	-2.087	18% Mo	0	0	100	0	70% o1	100	0	0	0
9%int	***	***	***	***	3%out	0	0	77	0			
1alg	2.00	-2.115	16% Mo	100	0	0	0	66% o1	100	0	0	0
15%int	***	***	***	***	3%out	61	0	0	0			
3Mop	6.00	-3.254	100% Mo	0	100	0	0	0% o1	0	0	0	0
0%int	***	***	***	***	0%out	0	0	0	0			
4Mos	2.00	-4.941	100% Mo	100	0	0	0	0% o1	0	0	0	0
0%int	***	***	***	***	0%out	0	0	0	0			
1Mod	10.00	-17.066	100% Mo	0	0	100	0	0% o1	0	0	0	0
0%int	***	***	***	***	0%out	0	0	0	0			
2Mop	6.00	-27.988	100% Mo	0	100	0	0	0% o1	0	0	0	0
0%int	***	***	***	***	0%out	0	0	0	0			
3Mos	2.00	-33.921	100% Mo	100	0	0	0	0% o1	0	0	0	0
0%int	***	***	***	***	0%out	0	0	0	0			
1Os	12.00	-37.705	0% Mo	0	0	0	0	100% o1	100	0	0	0
0%int	***	***	***	***	0%out	0	0	0	0			
1Mop	6.00	-182.408	100% Mo	0	100	0	0	0% o1	0	0	0	0
0%int	***	***	***	***	0%out	0	0	0	0			
2Mos	2.00	-197.803	100% Mo	100	0	0	0	0% o1	0	0	0	0
0%int	***	***	***	***	0%out	0	0	0	0			
1Mos	2.00	-1420.186	100% Mo	100	0	0	0	0% o1	0	0	0	0
0%int	***	***	***	***	0%out	0	0	0	0			

The SCF-X α -SW molecular-orbital calculation for an octahedral (NbO $_6$)⁻⁹ cluster with the “Sambe” occupation of the 2t_{2g} and 3e_g orbitals yields the energy levels (in Rydbergs) and the charge and angular momentum decomposition (note the Nb and O charges in the 2t_{2g} and 3e_g orbitals):

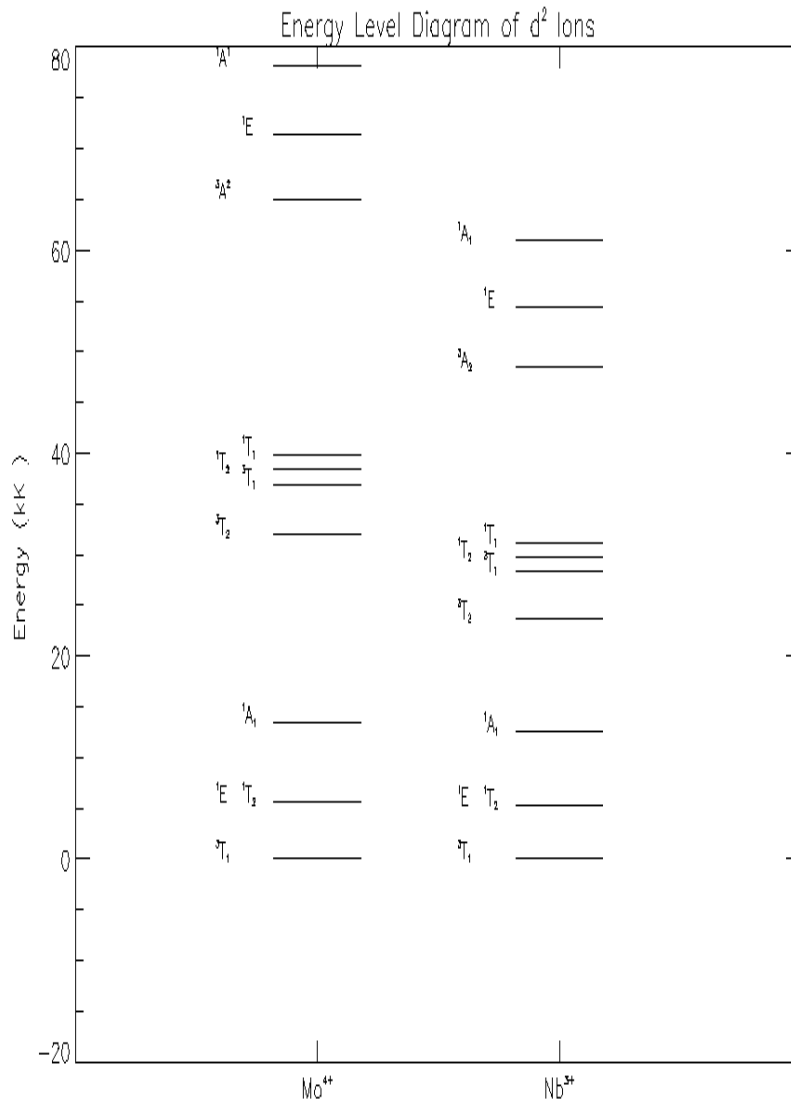
level	occup	energy	charge	%s	%p	%d	%f	charge	%s	%p	%d	%f
4tlu	.00	-.083	2% Nb	0	100	0	0	10% o1	23	77	0	0
			26%int	***	***	***	***	61%out	0	95	0	3
3eg	.90	-.148	74% Nb	0	0	100	0	20% o1	10	90	0	0
			2%int	***	***	***	***	4%out	0	0	86	0
3alg	.00	-.174	3% Nb	100	0	0	0	10% o1	59	41	0	0
			35%int	***	***	***	***	52%out	97	0	0	0
2t2g	1.10	-.373	70% Nb	0	0	100	0	21% o1	0	100	0	0
			7%int	***	***	***	***	2%out	0	0	45	0
1t1g	6.00	-.617	0% Nb	0	0	0	0	71% o1	0	100	0	0
			26%int	***	***	***	***	4%out	0	0	0	0
3tlu	6.00	-.628	2% Nb	0	100	0	0	69% o1	0	100	0	0
			23%int	***	***	***	***	7%out	0	63	0	0

1t2u	6.00	-.639	0% Nb 28%int	0 ***	0 ***	0 ***	0 ***	68% o1 4%out	0 100 0 0	0 0 0 76	0 0
2t1u	6.00	-.746	20% Nb 15%int	0 ***	100 ***	0 ***	0 ***	59% o1 6%out	2 98 0 4	0 0 0 83	0 0
1t2g	6.00	-.780	28% Nb 25%int	0 ***	0 ***	100 ***	0 ***	43% o1 4%out	0 100 0 0	0 0 80 0	0 0
2alg	2.00	-.812	30% Nb 7%int	100 ***	0 ***	0 ***	0 ***	56% o1 7%out	6 94 26 0	0 0 0 0	0 0
2eg	4.00	-.821	35% Nb 1%int	0 ***	0 ***	100 ***	0 ***	56% o1 8%out	5 95 0 0	0 0 60 0	0 0
1t1u	6.00	-1.750	10% Nb 14%int	0 ***	100 ***	0 ***	0 ***	73% o1 3%out	100 0 0 45	0 0 0 38	0 0
1alg	2.00	-1.793	14% Nb 13%int	100 ***	0 ***	0 ***	0 ***	70% o1 3%out	99 1 53 0	0 0 0 0	0 0
1eg	4.00	-1.800	17% Nb 8%int	0 ***	0 ***	100 ***	0 ***	73% o1 3%out	99 1 0 0	0 0 72 0	0 0
3Nbp	6.00	-2.606	100% Nb 0%int	0 ***	100 ***	0 ***	0 ***	0% o1 0%out	0 0 0 0	0 0 0 0	0 0
4Nbs	2.00	-4.313	100% Nb 0%int	100 ***	0 ***	0 ***	0 ***	0% o1 0%out	0 0 0 0	0 0 0 0	0 0
1Nbd	10.00	-14.992	100% Nb 0%int	0 ***	0 ***	100 ***	0 ***	0% o1 0%out	0 0 0 0	0 0 0 0	0 0
2Nbp	6.00	-25.427	100% Nb 0%int	0 ***	100 ***	0 ***	0 ***	0% o1 0%out	0 0 0 0	0 0 0 0	0 0
3Nbs	2.00	-31.110	100% Nb 0%int	100 ***	0 ***	0 ***	0 ***	0% o1 0%out	0 0 0 0	0 0 0 0	0 0
10s	12.00	-37.892	0% Nb 0%int	0 ***	0 ***	0 ***	0 ***	100% o1 0%out	100 0 0 0	0 0 0 0	0 0
1Nbp	6.00	-171.132	100% Nb 0%int	0 ***	100 ***	0 ***	0 ***	0% o1 0%out	0 0 0 0	0 0 0 0	0 0
2Nbs	2.00	-186.039	100% Nb 0%int	100 ***	0 ***	0 ***	0 ***	0% o1 0%out	0 0 0 0	0 0 0 0	0 0
1Nbs	2.00	-1349.023	100% Nb 0%int	100 ***	0 ***	0 ***	0 ***	0% o1 0%out	0 0 0 0	0 0 0 0	0 0

The resulting crystal field Racah parameters according to theory for Mo^{4+} and Nb^{3+} (Zr^{2+} doesn't exist) are:

Ion	Dq (cm^{-1})	B (cm^{-1})	C (cm^{-1})	γ	Dq/B
Mo^{4+}	3301.8	396.6	1568.1	3.95	8.3
Nb^{3+}	2468.1	374.5	1474.2	3.93	6.59

The resulting energy-level diagram is:



Comparing the above results for Mo^{4+} and Nb^{3+} with those for the first-row transition-metal ions on Page 1, we conclude that for the d^2 configuration:

1. Dq is significantly larger for the second-row transition-metal ions
2. Dq increases toward the right of the Periodic Table second row transition series
3. B and C are smaller
4. Dq/B is very large – corresponding to the “high-field” region of the Tanabe-Sugano Diagram
5. $\gamma = C/B$ is close to Slater’s value of 4.0
6. The above energy-level diagram suggests that the second-row transition-metal ions in the d^2 configuration are not good candidates for multiphoton phosphors because emission will occur between the lowest, closely spaced multiplet levels.

Given these results, what about the possibility that oxygen(p)-to-metal(d) “charge transfer” (CT) transitions might be potentially useful for multiphoton phosphors? In general, these transitions are broadband, and they usually lead to large Stokes shift in emission. It is not very promising to use these ions as activators in a situation where one of the photons by the primary cascading ion is being used to sensitize them. However, we decided to examine their charge-transfer bands theoretically to determine their spectral position and their suitability for energy transfer from cascading Pr^{3+} ions.

To help answer this question, SCF-X α -SW “transition-state” calculations have been performed for the Mo^{4+} and Nb^{3+} systems - removing one half an electron from the oxygen(p) $3t_{1u}$ orbital defining the top of the oxygen “valence band” and adding half an electron to the $2t_{2g}$, predominantly metal, d-orbital. This transition is allowed by molecular-orbital selection rules, whereas transitions from the somewhat higher oxygen “non-bonding” $1t_{1g}$ level to the $2t_{2g}$ level are not orbitally allowed. The resulting molecular-orbital energy-level difference between the converged, repopulated $3t_{1u}$ and $2t_{2g}$ levels is a good approximation to the CT transition energy.

The resulting SCF-X α -SW *transition-state* calculation for an octahedral $(\text{MoO}_6)^{-8}$ cluster yields the following energy levels (in Rydbergs), charge and angular momentum decomposition:

level	occup	energy	charge	%s	%p	%d	%f	charge	%s	%p	%d	%f
3a _{1g}	.00	-.082	1% Mo 24%int	100 ***	0 ***	0 ***	0 ***	5% o ₁ 69%out	87 97	13 0	0 0	0 0
2t _{2g}	2.50	-.239	71% Mo 7%int	0 ***	0 ***	100 ***	0 ***	20% o ₁ 2%out	0 0	100 0	0 58	0 0
1t _{1g}	6.00	-.544	0% Mo 24%int	0 ***	0 ***	0 ***	0 ***	72% o ₁ 4%out	0 0	100 0	0 0	0 0
3t _{1u}	5.50	-.562	2% Mo 22%int	0 ***	100 ***	0 ***	0 ***	69% o ₁ 7%out	0 0	100 68	0 0	0 0
1t _{2u}	6.00	-.571	0% Mo 27%int	0 ***	0 ***	0 ***	0 ***	69% o ₁ 4%out	0 0	100 0	0 0	0 78
2t _{1u}	6.00	-.708	20% Mo 11%int	0 ***	100 ***	0 ***	0 ***	61% o ₁ 7%out	3 0	97 7	0 0	0 81
1t _{2g}	6.00	-.748	28% Mo 24%int	0 ***	0 ***	100 ***	0 ***	44% o ₁ 4%out	0 0	100 0	0 82	0 0
2a _{1g}	2.00	-.777	27% Mo 5%int	100 ***	0 ***	0 ***	0 ***	60% o ₁ 8%out	7 33	93 0	0 0	0 0

2eg	4.00	-.803	32% Mo	0	0	100	0	59% o1	6	94	0	0
			0%int	***	***	***	***	8%out	0	0	64	0
1tlu	6.00	-1.706	13% Mo	0	100	0	0	72% o1	100	0	0	0
			12%int	***	***	***	***	3%out	0	48	0	37
1alg	2.00	-1.775	19% Mo	100	0	0	0	69% o1	99	1	0	0
			10%int	***	***	***	***	2%out	58	0	0	0
1eg	4.00	-1.787	23% Mo	0	0	100	0	73% o1	98	2	0	0
			3%int	***	***	***	***	2%out	0	0	75	0
3Mop	6.00	-2.878	100% Mo	0	100	0	0	0% o1	0	0	0	0
			0%int	***	***	***	***	0%out	0	0	0	0
4Mos	2.00	-4.483	100% Mo	100	0	0	0	0% o1	0	0	0	0
			0%int	***	***	***	***	0%out	0	0	0	0
1Mod	10.00	-16.592	100% Mo	0	0	100	0	0% o1	0	0	0	0
			0%int	***	***	***	***	0%out	0	0	0	0
2Mop	6.00	-27.515	100% Mo	0	100	0	0	0% o1	0	0	0	0
			0%int	***	***	***	***	0%out	0	0	0	0
3Mos	2.00	-33.449	100% Mo	100	0	0	0	0% o1	0	0	0	0
			0%int	***	***	***	***	0%out	0	0	0	0
10s	12.00	-37.862	0% Mo	0	0	0	0	100% o1	100	0	0	0
			0%int	***	***	***	***	0%out	0	0	0	0
1Mop	6.00	-181.940	100% Mo	0	100	0	0	0% o1	0	0	0	0
			0%int	***	***	***	***	0%out	0	0	0	0
2Mos	2.00	-197.332	100% Mo	100	0	0	0	0% o1	0	0	0	0
			0%int	***	***	***	***	0%out	0	0	0	0
1Mos	2.00	-1419.749	100% Mo	100	0	0	0	0% o1	0	0	0	0
			0%int	***	***	***	***	0%out	0	0	0	0

The resulting SCF-X α -SW *transition-state* calculation for an octahedral (NbO₆)⁻⁹ cluster yields the following energy levels (in Rydbergs), charge and angular momentum decomposition:

=====												
level	occup	energy	charge	%s	%p	%d	%f	charge	%s	%p	%d	%f

4t1u	.00	-.083	2% Nb	0	100	0	0	10% o1	23	77	0	0
			26%int	***	***	***	***	61%out	0	95	0	3

3eg	.00	-.146	74% Nb	0	0	100	0	20% o1	10	90	0	0
			2%int	***	***	***	***	4%out	0	0	87	0

3alg	.00	-.173	3% Nb	100	0	0	0	10% o1	59	41	0	0
			35%int	***	***	***	***	52%out	97	0	0	0

2t2g	2.50	-.371	71% Nb	0	0	100	0	21% o1	0	100	0	0
			7%int	***	***	***	***	2%out	0	0	45	0

1t1g	6.00	-.617	0% Nb	0	0	0	0	71% o1	0	100	0	0
			26%int	***	***	***	***	4%out	0	0	0	0

3t1u	5.50	-.628	2% Nb	0	100	0	0	69% o1	0	100	0	0
			23%int	***	***	***	***	7%out	0	63	0	0

1t2u	6.00	-.639	0% Nb	0	0	0	0	68% o1	0	100	0	0
			28%int	***	***	***	***	4%out	0	0	0	76

2t1u	6.00	-.746	20% Nb	0	100	0	0	59% o1	2	98	0	0
			15%int	***	***	***	***	6%out	0	4	0	83

1t2g	6.00	-.779	28% Nb	0	0	100	0	43% o1	0	100	0	0
			25%int	***	***	***	***	4%out	0	0	80	0

2alg	2.00	-.811	30% Nb	100	0	0	0	56% o1	6	94	0	0
			7%int	***	***	***	***	7%out	26	0	0	0

2eg	4.00	-.820	35% Nb	0	0	100	0	56% o1	4	96	0	0
			1%int	***	***	***	***	8%out	0	0	60	0

1t1u	6.00	-1.750	10% Nb	0	100	0	0	73% o1	100	0	0	0
			14%int	***	***	***	***	3%out	0	45	0	38

1alg	2.00	-1.793	14% Nb	100	0	0	0	70% o1	99	1	0	0	
			13%int	***	***	***	***	3%out	53	0	0	0	

1eg	4.00	-1.800	17% Nb	0	0	100	0	73% o1	99	1	0	0	
			8%int	***	***	***	***	3%out	0	0	72	0	

3Nbp	6.00	-2.604	100% Nb	0	100	0	0	0% o1	0	0	0	0	
			0%int	***	***	***	***	0%out	0	0	0	0	

4Nbs	2.00	-4.308	100% Nb	100	0	0	0	0% o1	0	0	0	0	
			0%int	***	***	***	***	0%out	0	0	0	0	

1Nbd	10.00	-14.987	100% Nb	0	0	100	0	0% o1	0	0	0	0	
			0%int	***	***	***	***	0%out	0	0	0	0	

2Nbp	6.00	-25.422	100% Nb	0	100	0	0	0% o1	0	0	0	0	
			0%int	***	***	***	***	0%out	0	0	0	0	

3Nbs	2.00	-31.105	100% Nb	100	0	0	0	0% o1	0	0	0	0	
			0%int	***	***	***	***	0%out	0	0	0	0	

10s	12.00	-37.893	0% Nb	0	0	0	0	100% o1	100	0	0	0	
			0%int	***	***	***	***	0%out	0	0	0	0	

1Nbp	6.00	-171.127	100% Nb	0	100	0	0	0% o1	0	0	0	0	
			0%int	***	***	***	***	0%out	0	0	0	0	

2Nbs	2.00	-186.033	100% Nb	100	0	0	0	0% o1	0	0	0	0	
			0%int	***	***	***	***	0%out	0	0	0	0	

1Nbs	2.00	-1349.017	100% Nb	100	0	0	0	0% o1	0	0	0	0	
			0%int	***	***	***	***	0%out	0	0	0	0	

Converting from Rydbergs to electron volts ($1\text{Ry} = 13.6\text{eV}$), the resulting CT energies are 4.4eV and 3.5eV for $(\text{MoO}_6)^{8-}$ and $(\text{NbO}_6)^{9-}$, respectively. These values, especially the former, are in reasonable agreement with available experimental data.

To aid in understanding the possible relevance of CT transitions to multiphoton phosphor activation by second- (and third-) row transition-metal ions, we summarize the known experimental emission properties of the activators in a variety of host materials. The emission colors in all the examples are believed to be due to CT transitions.

Emission from Third and Fourth Row Transition Metal Ions.

Activator Ion	Host	Color	Oxidation State
Ag Oxidation state: +1 Configuration: $4d^{10} 5s^1$	ZnBorate	yellowish-white (s)	
	Cd Borate	yellow(s)	
	ZnS	blue (s)	1
	Ca Phosphate	yellowish-white	
Au Oxidation state: +1, +3 Configuration: $5d^{10}, 6s^1$	CdWO ₄	orange	
Mo Oxidation state: +2,+3,+4,+5,+6 Configuration: $4d^5, 5s^1$	Al ₂ O ₃	blue	
	CaMoO ₄	yellowish green	+6
	Ca(PO ₃) ₂	green	
	CaWO ₄	yellow	
	CdMoO ₄		
	PbMoO ₄	green	
	SrMoO ₄	blue-violet, yellow-green	
	Zn ₂ SiO ₄	green	
Nb Oxidation state: +5, +3 Configuration: $4d^4, 5s^1$	ZnF ₂	greenish-blue	
	CaNb ₂ O ₆	blue-green	+5
	ScTaO ₄ , Mg ₄ Ta ₂ O ₉ , Li ₃ TaO ₄ , CaTaO ₄ (?)	transparent	+5
Pt Oxidation state: +4, +2 Configuartion: $5d^9, 6s^1$	Al ₂ O ₃	green	
	Y, Er, Yb platincyanides	blue, green, orange	
Re Oxidation state: +7, +6, +4, +2, -1	Zn ₂ SiO ₄	violet	
	Re ₂ O ₇	pink	+7
	Alkaline-earth silicates	violet	
Rh Oxidation state: +3, +2, +4 Configuratio: $4d^8, 5s^1$	Al ₂ O ₃	red	+3(?)
	RhF ₃	purple	+3
	Rh ₄ (P ₂ O ₇) ₃	blue	+3
	Rh(NO ₃) ₂	pink	
W Oxidation state: +6, +5, +4, +3, +2 Configuration: $5d^4, 6s^2$	Al ₂ O ₃	orange	
	BaWO ₄	blue	+6
	CaWO ₄	blue	+6
	Ba ₂ W ₂ O ₅	green	+3
	βMgWO ₄	blue-green	+6
	SrWO ₄	blue	+6
Zr	Zn ₂ SiO ₄	blue	
Oxidation state: +4	ZrO ₂	blue-green	
Configuration: $4d^2, 5s^2$	ZrSiO ₄	blue-green-yellow	

Recommendations for Future Research

1. It is evident in the above Table that many of the second- and third-row transition-metal ions have a relatively large number of valence (oxidation) states. For example, $\text{Mo}^{+2,+3,+4,+6}$ and $\text{W}^{+2,+3,+4,+5,+6}$, versus the first-row element, $\text{Cr}^{+2,+3,+6}$. *Yet, the lower valence states of the second- and third-row transition-metal activators have not been observed! We recommend that this is a possibly fruitful area for experimental investigation for incorporating these ions in lower valence states into suitable hosts and studying their spectral characteristics due to transitions within the d-manifold. This could potentially open a new class of luminescent materials.*
2. We have concluded above that the second-row transition-metal ions in the d^2 configuration are not good candidates for multiphoton phosphors. Although we have determined the Racah parameters for the d^2 configuration of second-row transition-metal ions and shown them to be very different from those for the first row, we do not know yet what the trends will be for higher d^n configurations. *Therefore, a theoretical investigation of higher d^n configurations for the second-row transition-metal ions is recommended.*
3. *Finally, it is recommended that both theoretical and experimental work of the type completed thus far be extended to third-row transition-metal ions as possible activators in developing new multiphoton phosphors.*

Report on Cascade Phosphors

William B. White

The optical absorption spectra and luminescence spectra of first row (3d) transition metal ions in ionic hosts such as oxides and fluorides can be interpreted by crystal field theory in terms of empirically derived parameters: the Racah parameters B and C describing interelectron repulsion and the crystal field strength parameter, Dq. The crystal field interaction can be described by a single parameter only for sites with near-cubic symmetry, either tetrahedral, octahedral, or cubic or small distortions from these. Large distortions from regular symmetry require multiple parameters. The sensitivity of the crystal field energy levels to deviations from cubic symmetry varies with electron configurations. Configurations d^1 , d^4 , d^6 , and d^9 are much more sensitive to local symmetry than d^2 , d^3 , d^5 , d^7 , and d^8 .

Free Ion Parameters

Racah parameters for free ions can be calculated from atomic emission spectra. Values presented below were taken from the compilation by Sugano et al. (1970).

Table B-12
Racah Parameters for Free Ions of the First Transition Series

M^{2+}	B (cm^{-1})	C (cm^{-1})	M^{3+}	B (cm^{-1})	C (cm^{-1})
Ti ²⁺	695	2910	Ti ³⁺	---	---
V ²⁺	755	3257	V ³⁺	862	3815
Cr ²⁺	810	3565	Cr ³⁺	918	4133
Mn ²⁺	860	3850	Mn ³⁺	965	4450
Fe ²⁺	917	4040	Fe ³⁺	1015	4800
Co ²⁺	971	4497	Co ³⁺	1065	5120
Ni ²⁺	1030	4850	Ni ³⁺	1115	5450

Tetravalent ions occur for the lower atomic number members of the transition metal series. Racah parameters were calculated for the more chemically stable ions using the atomic spectra data from Moore (1952).

Table B-13
Racah Parameters for M^{4+} Ions

Ion	Configuration	B (cm^{-1})	C (cm^{-1})
Ti ⁴⁺	d ⁰	---	---
V ⁴⁺	d ¹	---	---
Cr ⁴⁺	d ²	1013	3791
Mn ⁴⁺	d ³	1069	4618
Fe ⁴⁺	d ⁴	980	5195

Tanabe-Sugano Diagrams

The Racah parameters decrease somewhat when transition metal ions are inserted into crystals because of the delocalization of the d-orbitals due to covalent bonding. A full description of the energy levels for transition metal ions in octahedral field is given by diagonalization of the Tanabe-Sugano matrices. A typical set of diagrams is attached. These were generated by setting the Racah B and C parameters to selected values and then diagonalizing the matrices for a range of values of Dq. In effect, this method of presentation generates a Tanabe-Sugano diagram tailored for any experimentally determined set of Racah parameters. The diagrams attached are illustrative rather than generalized. It should be noted that many of the diagrams that appear in books on crystal field theory are abbreviated. These are complete.

Data for Crystal Field Parameters

The tables that follow give values for Dq and the Racah parameters for a selection of host crystals. These were limited to oxides, silicates, phosphates and a few other compounds that would be of potential interest as phosphor hosts. Many of these data were extracted from an extensive compilation by Burns (1993) along with additional data and some calculations in a few cases. Only Dq is needed for the d^1 and d^9 configurations. Racah parameters are rarely calculated for the d^4 and d^6 configurations because both B and C parameters must be extracted from weak spin-forbidden transition which may not appear in the spectra. Racah B can be easily extracted from spin-allowed transitions for the d^2 , d^3 , d^7 , and d^8 configurations but here also Racah C must be extracted from spin-forbidden transitions.

The data given in the tables are illustrative rather than comprehensive. Likewise, the values are less precise than the numerical data would indicate. Agreement between different authors is not very good even when published spectra are very similar.

The host compounds are given but not the location of the transition metal ion, mostly because the ion distributions are rarely given in the original sources. In most cases, the location can be interpreted. The coordination number (c.n.) of the site occupied by the transition metal ion is given.

Table B-14
Crystal Field Parameters for Ti^{3+} .

Host Compound	c.n.	Dq (cm^{-1})
$Ti(H_2O)_6^{3+}$	6	1895
MgO	6	1130
Al_2O_3	6	1910

Table B-15
Crystal Field Parameters for V^{3+} .

Host Compound	c.n.	Dq (cm^{-1})	B (cm^{-1})
$V(H_2O)_6^{3+}$	6	1910	614
Al_2O_3	6	1873	594
Al_2MgO_4	6	1920	595
Al_2BeO_4	6	1776	589
$Mg_3Al_2Si_3O_{12}$	6	1843	396
$Ca_3Al_2Si_3O_{12}$	6	1768	545
Al_2SiO_5 (kyanite)	6	1856	599
$LiAlSi_2O_6$	6	1726	578

Table B-16
Crystal Field Parameters for Cr³⁺

Host Compound	c.n.	Dq (cm ⁻¹)	B (cm ⁻¹)	C (cm ⁻¹)
Cr(H ₂ O) ₆ ³⁺	6	1740	729	
MgO	6	1620	651	
Al ₂ O ₃	6	1815	636	3300
Cr ₂ O ₃	6	1667	475	
Al ₂ MgO ₄	6	1852	612	
YCrO ₃	6	1645	542	
Cr ₂ MgO ₄	6	1770	431	
Al ₂ BeO ₄	6	1770	556	
Mg ₃ Al ₂ Si ₃ O ₁₂	6	1779	617	
Ca ₃ Cr ₂ Si ₃ O ₁₂	6	1667	589	
Mg ₂ SiO ₄	6	1690	655	
Al ₂ SiO ₅ (ky)	6	1650	790	
LiAlSi ₂ O ₆	6	1625	758	
Be ₃ Al ₂ Si ₆ O ₁₈	6	1613	783	2960
Y ₃ Al ₅ O ₁₂	6	1640	650	3250
Y ₃ Ga ₅ O ₁₂	6	1650	570	3400

Table B-17
Crystal Field Parameters for Cr²⁺

Host Compound	c.n.	Dq (cm ⁻¹)
Cr(H ₂ O) ₆ ²⁺	6	1390
CaMgSi ₂ O ₆	6	900
Al ₂ MgO ₄	4	646

Table B-18
Crystal Field Parameters for Mn³⁺

Host Compound	c.n.	Dq (cm ⁻¹)
Al ₂ O ₃	6	1937
Ca ₃ Al ₂ Si ₃ O ₁₂	6	1815

Table B-19
Crystal Field Parameters for Mn²⁺

Host Compound	c.n.	Dq (cm ⁻¹)	B (cm ⁻¹)	C (cm ⁻¹)
Mn(H ₂ O) ₆ ²⁺	6	848	621	3781
MnO	6	979	786	3210
MnF ₂	6	780	721	3594
LiMnPO ₄	6	680	673	3628
HZnBO ₃	6	874	646	3634
MnCO ₃	6	750	636	3678
Mn ₂ SiO ₄	6	875	577	3772
MnS	6	730	583	3125
NaMnF ₃	6		661	3776
ZnS	4		585	3129

Table B-20
Crystal Field Parameters for Fe³⁺

Host Compound	c.n.	Dq (cm ⁻¹)	B (cm ⁻¹)	C (cm ⁻¹)
Fe(H ₂ O) ₆ ³⁺	6	1370		
MgO	6	1340	861	2571
Al ₂ O ₃	6	1527	643	3154
Fe ₂ O ₃	6	1590	414	3931
γ-LiAlO ₂ -	4	835	571	3177
Ca ₃ Al ₂ Si ₃ O ₁₂	6	1280	596	3380

Table B-21
Crystal Field Parameters for Fe²⁺

Host Compound	c.n.	Dq (cm ⁻¹)
MgO	6	1080
Al ₂ O ₃	6	1150
Al ₂ MgO ₄	4	483
Fe ₃ Al ₂ Si ₃ O ₁₂	8	550
Mg ₂ SiO ₄	6	976
MgF ₂	6	812
ZnO	4	450
ZnSe	4	320

Table B-22
Crystal Field Parameters for Co^{2+}

Host Compound	c.n.	Dq (cm^{-1})	B (cm^{-1})
$\text{Co}(\text{H}_2\text{O})_6^{2+}$	6	905	589
MgO	6	927	845
Co_2SiO_4	6	721	451
ZnO	4	390	700
Al_2MgO_4	4	410	830

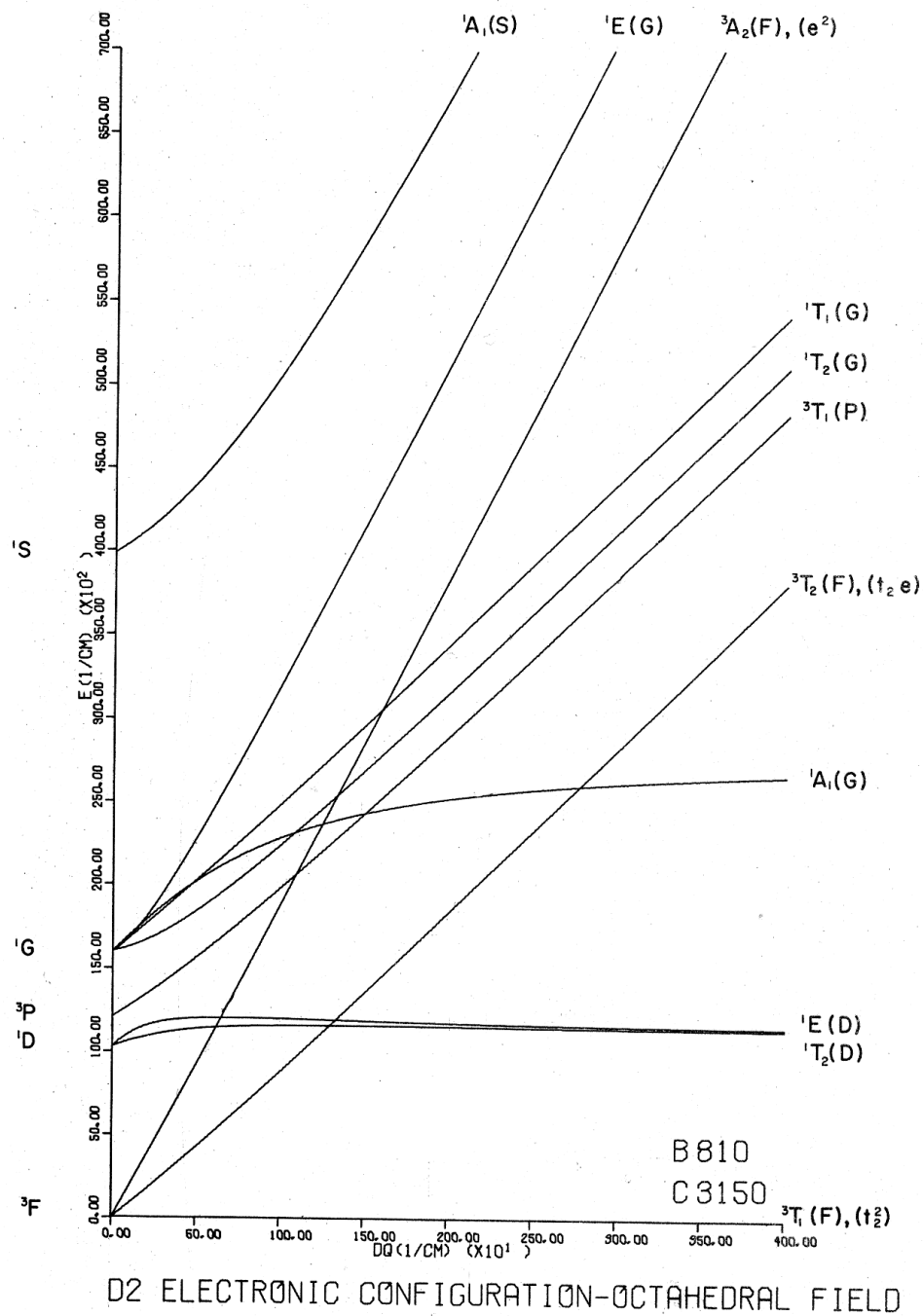
Table B-23
Crystal Field Parameters for Ni^{2+}

Host Compound	c.n.	Dq (cm^{-1})	B (cm^{-1})
$\text{Ni}(\text{H}_2\text{O})_6^{2+}$	6	851	930
MgO	6	860	971
NiO	6	876	808
Al_2MgO_4	6	980	907
$\text{CaNiSi}_2\text{O}_6$	6	840	881
ZnO	4	405	795

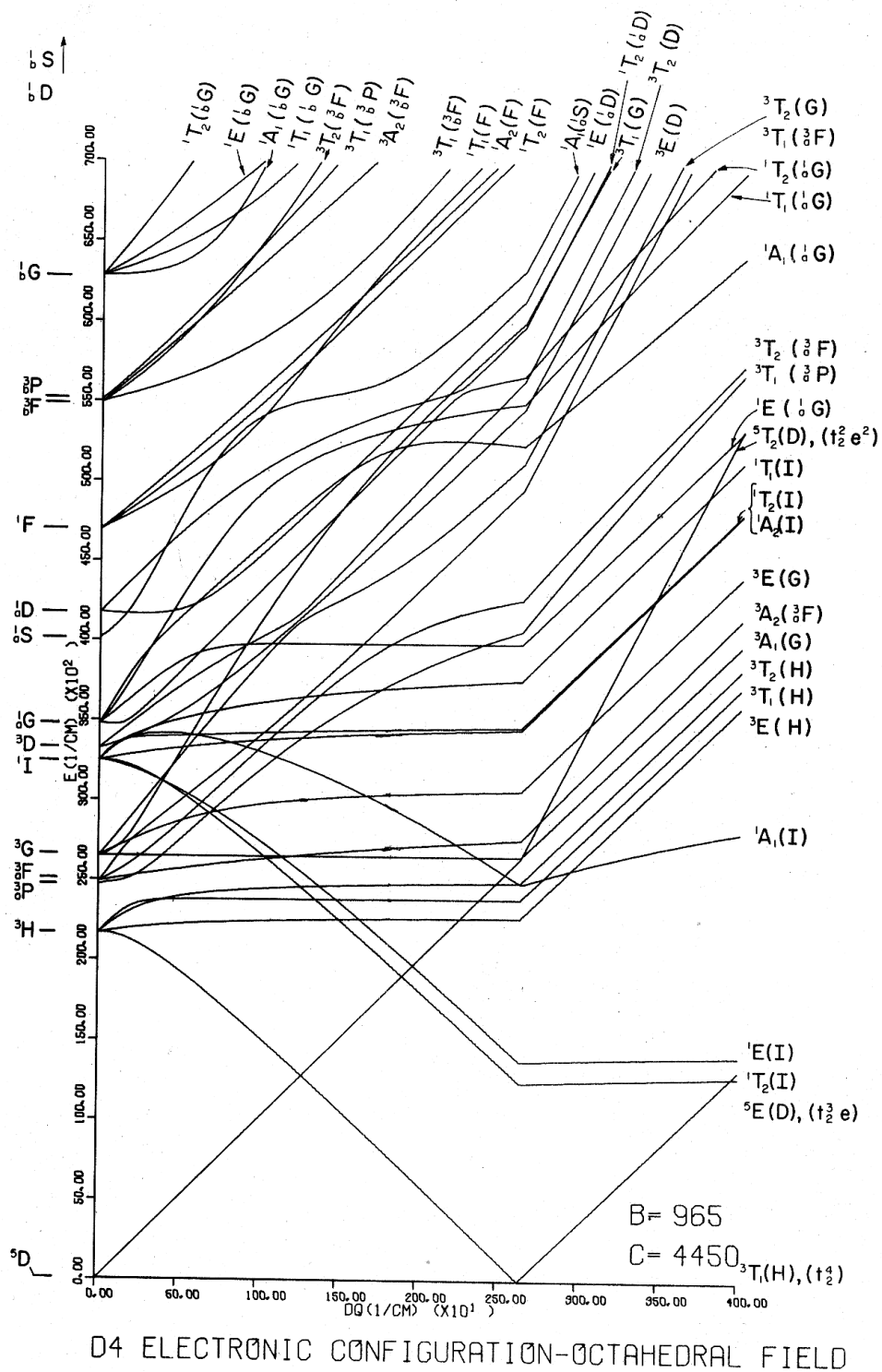
Interpretation and Conclusions

The crystal field parameters for any given ion vary with host structure but rarely by more than a factor of 2. Visible luminescence is observed from the lowest crystal field states of V^{3+} , Cr^{3+} , Mn^{2+} , Mn^{4+} and Fe^{3+} and infrared luminescence from Co^{2+} and Ni^{2+} . The luminescence is described, after taking account of the Stokes shift, by the crystal field energy level diagrams. Excitation transfer of the form lanthanide \rightarrow transition metal might be possible under extremely limited conditions, given the wide variety of non-radiative pathways available.

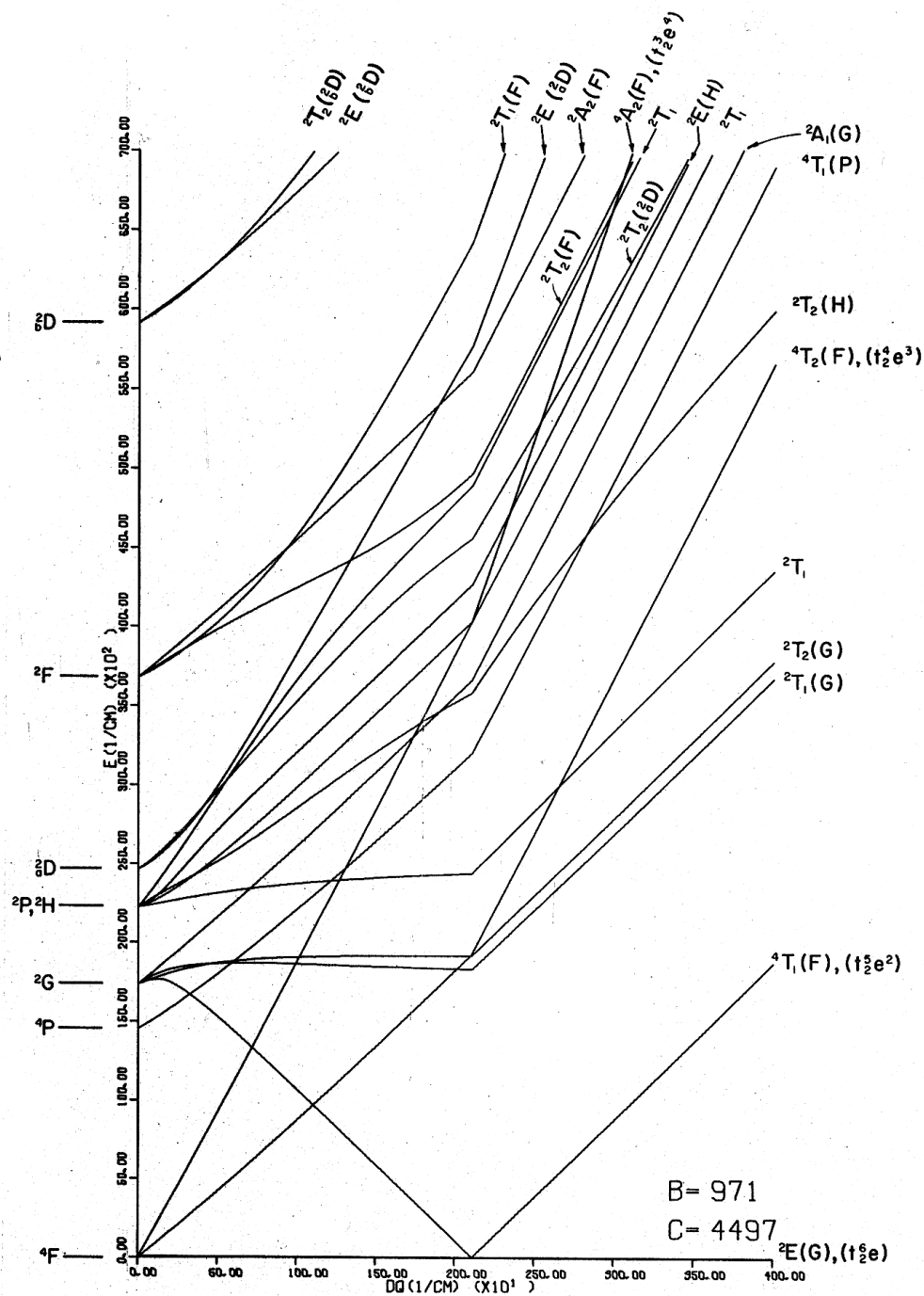
This file contains Tanabe-Sugano Diagrams.



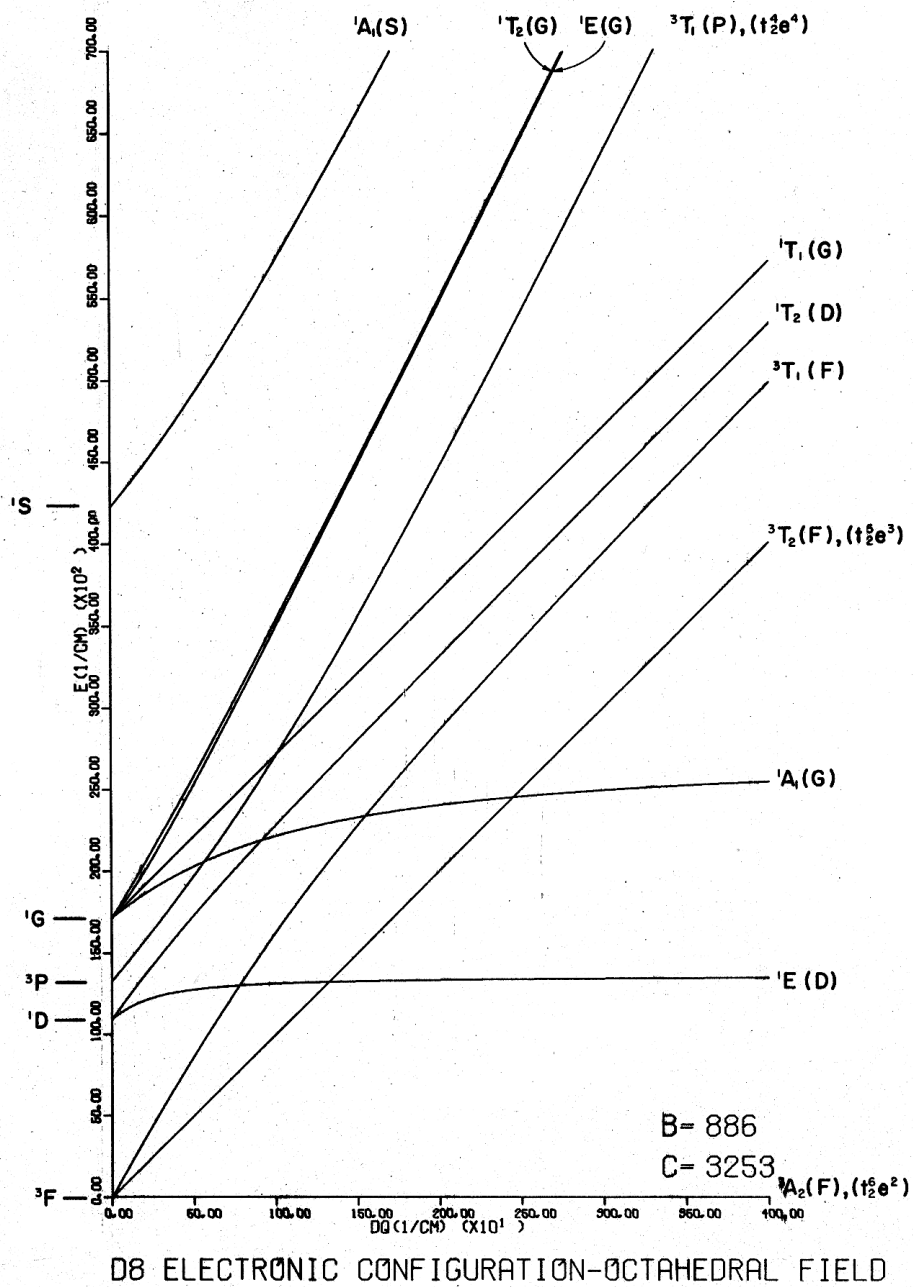








D7 ELECTRONIC CONFIGURATION-OCTAHEDRAL FIELD



Task 8: Conversion of 407 nm to Red or Green

Task Leader: Richard Meltzer
 Task Members: Kailash Mishra
 Andries Meijerink

Introduction

Although photon cascade emission (PCE) using Pr^{3+} has been demonstrated with quantum efficiencies in excess of 100%, the first photon is emitted predominantly in the deep blue or near UV portion of the spectrum and therefore does not lead to useful lumen output. The likelihood of circumventing this fundamental limitation is small due to the energy level structure of Pr^{3+} . The initially excited $^1\text{S}_0$ state at about $46,500\text{ cm}^{-1}$ radiates most strongly to other singlets such as $^1\text{I}_6$, $^1\text{D}_2$ or $^1\text{G}_4$ in the deep blue or UV. As a result, this first emitted photon is not very useful as a phosphor in conventional lighting applications. If non-radiative processes are weak, the second photon will occur in the visible where it does contribute to useful lumen output, but total visible quantum efficiencies in excess of 100% are not possible.

An alternative to simple PCE on Pr^{3+} that can avoid the first deep blue or UV photon is to transfer a portion of the $^1\text{S}_0$ energy of Pr^{3+} to another ion which in turn emits a visible photon. This requires a cross relaxation energy transfer in which the Pr^{3+} ion undergoes a transition to $^1\text{I}_6$ and another ion simultaneously undergoes a transition to an excited state. This leaves both the Pr^{3+} and other ion in their excited states from which visible emission can occur. Since energy must be conserved in the process, it is straight forward to identify suitable ions from the rare earth energy level diagrams. While the concept is easy to understand, a number of requirements must be met if this concept is to be practical:

1. The host must have a wide-bandgap, greater than $\sim 6\text{ eV}$ ($<200\text{ nm}$).
2. Host absorption must either be absent at the 4f5d excitation wavelength or the host must efficiently transfer its energy to the $^1\text{S}_0$ level of Pr^{3+} .
3. The $^1\text{S}_0$ level of Pr^{3+} should lie below the 4f5d level (or energy transfer directly from the 4f5d state should occur).
4. The downward Pr^{3+} transition energy must be closely matched to the upward transition energy of the other ion (activator).
5. The activator ion should not have significant absorption from its ground state at the same transition energy as the excitation of $^1\text{S}_0$.
6. The Judd-Ofelt parameters Ω_2 and Ω_4 should be small relative to Ω_6 to favor the downward transition of Pr^{3+} to $^1\text{I}_6$.
7. The energy transfer rate must compete effectively with the $^1\text{S}_0$ radiative rate such that the cross relaxation dominates.
8. The host should have relatively low vibrational frequencies or weak Pr^{3+} lattice coupling to minimize non-radiative relaxation from $^3\text{P}_0$.

Subtask A: Potential Rare Earth Candidates for Energy Transfer

For phosphor applications, cross-relaxation of Pr^{3+} should leave the Pr^{3+} in the $^1\text{I}_6$ or $^3\text{P}_0$ levels from which a second visible photon will be emitted. The $^1\text{S}_0 \rightarrow ^1\text{I}_6$, $^3\text{P}_0$ transition releases an energy $\sim 24,500\text{--}25,500\text{ cm}^{-1}$. One then finds the following RE^{3+} ions, listed in Table B-24 along with the appropriate transitions and their transition energies which could be excited from their ground state Stark components to suitable excited states (in some cases, transitions need to be phonon assisted).

For oxides, where the phonon frequencies are relatively large, multiphonon relaxation will leave the first five of these ions in the metastable levels, $^4\text{F}_{3/2}$ (Nd^{3+}), $^4\text{G}_{5/2}$ (Sm^{3+}), $^3\text{D}_{J=0,1,2,3}$ (Eu^{3+}), $^5\text{D}_3$ (Tb^{3+}) and $^4\text{F}_{9/2}$ (Dy^{3+}), respectively. For Nd^{3+} visible emission is not expected to occur and therefore it should be excluded. For two of these, Sm^{3+} and Dy^{3+} , the many levels to which emission can occur span a large energy range above the ground state so that much of the resulting emission will occur in the deep red or infrared, thereby limiting the luminous output from the second step. For Tb^{3+} , much of the emission would still occur in the deep blue. Cross relaxation could circumvent this problem by producing relaxation to $^5\text{D}_4$. From this point of view the most favorable system could be $\text{Pr}^{3+} - \text{Eu}^{3+}$. Formation of a $\text{Pr}^{4+} - \text{Eu}^{2+}$ charge transfer state is a potential problem as discussed below.

Table B-24

Candidate Rare Earth Ions for Energy Transfer from Pr^{3+} Corresponding to the $^1\text{S}_0 \rightarrow ^1\text{I}_6$ Transition. In Order to Obtain some Typical Numerical Energies, Values are taken from the Example of Rare Earths in LaF_3 where the Energy Levels are Well-known.

Ion	Ground State	Excited State	Energy Range(cm^{-1})	$ \Delta J $
Nd^{3+}	$^4\text{I}_{9/2}$	$^2\text{P}_{3/2}$	26378-26426	3
Sm^{3+}	$^6\text{H}_{5/2}$	$^6\text{F}_{7/2}$, $^6\text{P}_{3/2}$, $^4\text{G}_{11/2}$, $^4\text{M}_{15/2}$, $^4\text{H}_{11/2}$	24900-25900	1,1,3,5,3
Eu^{3+}	$^7\text{F}_0$	$^5\text{L}_6$	25067-25098	6
Tb^{3+}	$^7\text{F}_6$	$^5\text{D}_3$	26263-26344	3
Dy^{3+}	$^6\text{H}_{15/2}$	$^4\text{M}_{21/2}$ (also $^4\text{I}_{13/2}$, $^4\text{K}_{17/2}$)	24984-25990	3,1,1
Ho^{3+}	$^5\text{I}_8$	$^3\text{K}_7$, $^5\text{G}_4$	26266-26328	1,4
Er^{3+}	$^4\text{I}_{15/2}$	$^2\text{G}_{9/2}$, $^4\text{G}_{11/2}$	24600-24862, 26526-26707	3,2

Additional candidates are the $\text{Pr}^{3+} - \text{Er}^{3+}$ and $\text{Pr}^{3+} - \text{Ho}^{3+}$ systems. Although the excitation energy of Er^{3+} from the ground state to the $^2\text{H}_{9/2}$ or $^4\text{G}_{11/2}$ excited states are not energy-conserving for cross-relaxation with Pr^{3+} , phonon-assisted energy transfer involving emission or absorption of phonons, respectively, might make this system viable. Indeed energy transfer for the $\text{Pr}^{3+} - \text{Er}^{3+}$ pair has been investigated in $\text{CaAl}_{12}\text{O}_{19}:\text{Pr}^{3+}$ (1%), Er^{3+} (5%) by Wang et al. [169] where they find a 25% energy transfer efficiency for the conversion of $^1\text{S}_0$ to Er^{3+} . However, this does not all occur

through cross-relaxation as there are many possible channels for the energy transfer. For example, direct resonant transfer to the $^4D_{1/2}$ state of Er^{3+} can occur, followed by multi-phonon relaxation within Er^{3+} , a process that saps much of the energy to phonons. Another channel involves radiative transitions to 1I_6 , leading to a deep blue photon with little lumen efficacy. This is followed by phonon relaxation to 3P_0 and then energy transfer to Er^{3+} , but this just provides an alternative radiative channel to Pr^{3+} 3P_0 emission and does not lead to an additional visible quantum. Nonetheless, the potential of this system should be considered. Pr^{3+} - Ho^{3+} cross relaxation energy transfer should also be investigated, although the energy mismatch is worse than for Er^{3+} and would require even more phonon assistance. The need for extensive phonon assistance also applies to Tb^{3+} since the energy mismatches with Pr^{3+} are nearly identical for Ho^{3+} and Tb^{3+} (see Table B-24).

The selection rules for energy transfer between two one-electron ions was originally derived by Dexter [170]. Later, Kushida [171] investigated the energy transfer process between two rare earth ions assuming that the wavefunctions for the initial and final states of the coupled system could be expressed as a product of respective multi-electron states of these ions. For example, if the initial states of the sensitizer ion, A and the activator ion, B are Ψ_{Ai} and Ψ_{Bi} respectively, the ground state of the coupled system can be written as $\Psi_{Ai}\Psi_{Bi}$. The final state of the coupled system can be chosen similarly. Using a multipole expansion of the interaction Hamiltonian due to the electron-electron interaction between the two ions, the selection rules for energy transfer from A to B can be shown to be combinations of those for electric dipole, electric quadrupole, and magnetic dipole transitions resulting in absorption or emission of radiation from rare earth ions. Although the magnetic dipole-dipole interaction was considered negligible by Dexter, it could be comparable to the forced electric dipole-dipole interaction in the case of rare-earth ions. The selection rules are listed in the following Table B-25.

Table B-25
Selection Rules for Energy Transfer Between Two Rare Earth Ions Involving States within the f-manifold

Nature of Multipole at A	Nature of Multipole at B	Selection Rule for A		Selection Rule for B	
		J=0	$J_{if} \neq 0$	J=0	$J_{if} \neq 0$
electric dipole	electric dipole	$ \Delta J = 2, 4, 6$	$ \Delta J \leq 6$	$ \Delta J = 2, 4, 6$	$ \Delta J \leq 6$
electric dipole	electric quadrupole	$ \Delta J = 2, 4, 6$	$ \Delta J \leq 6$	$ \Delta J = 2$	$ \Delta J \leq 2$
electric quadrupole	electric dipole	$ \Delta J = 2$	$ \Delta J \leq 2$	$ \Delta J = 2, 4, 6$	$ \Delta J \leq 6$
magnetic dipole	magnetic dipole	$ \Delta J = 1$	$ \Delta J \leq 1$	$ \Delta J = 1$	$ \Delta J \leq 1$

The subscript “if” implies both initial and final state. The “J=0” condition implies that the J quantum number of either the initial or the final state is zero. When both the quantum numbers are zero, any transition is strictly forbidden. Based on the selection rules listed in Table B-25, it is obvious that the energy transfer involving $\Delta J \leq 1$ will be stronger than that for other transitions. The selection rules for the orbital and spin angular momenta have not been listed since both L^2

and S^2 are not good quantum numbers in the intermediate coupling scheme. The pseudo quadrupolar transitions corresponding to hypersensitive transitions are covered by the selection rules for quadrupolar transitions. We have also not listed selection rules for phonon assisted energy transfer. They need to be explored in the next phase.

These selection rules do not include the case when the energy transfer is mediated by the exchange interaction. Dexter [170] approached the problem with two one-electron systems with the coupled state being described by a 2x2 Slater determinant. With the choice of Kushida's functions [171], the selection rules for exchange mediated energy transfer cannot be obtained unless the product wave function is written in the following determinantal form:

$$\begin{vmatrix} \Psi_A(1...n) & \Psi_B(1,n) \\ \Psi_A(n+1...n+m) & \Psi_B(n+1..n+m) \end{vmatrix}$$

when there are n and m electrons in the f-shell of ions A and B respectively. One can use this wavefunction to calculate the energy transfer probability resulting from the exchange interaction due to electrons of A and B. The other alternative is to express this exchange interaction by the interaction (Heisenberg) Hamiltonian

$$H_I = \sum_{i,j} JS_{ai} \cdot S_{bj}$$

and then to evaluate the transition matrix element using the product wavefunctions by Kushida [171]. Without carrying out the analysis completely, one can speculate that the selection rules would be

$$\Delta S_A = 0 \quad \Delta S_B = 0 \quad \Delta S = 0$$

Subtask B: Energy Transfer Rates

The cross-relaxation between Pr^{3+} and another activator RE^{3+} needs to be fast since it must compete effectively with the 1S_0 radiative emission. This is typically sub-microsecond through spin –allowed transitions to 1I_6 , 1G_4 and to a lesser degree to 1D_2 .

Cross relaxation energy transfer can occur by multipole-multipole interactions or by exchange interactions. At nearest neighbor distances, exchange will usually dominate. At more dilute concentrations, typical of phosphors, the short range exchange interaction-mediated transfer rate will rapidly fall leaving the dipole-dipole interaction which falls as R^{-6} to dominate, even over the other terms in the multipole-multipole interactions which fall as R^{-8} or R^{-10} for dipole-quadrupole or quadrupole-quadrupole interactions, respectively. The dipole-dipole transfer rate can be written in terms of the oscillator strengths of the optical transition connecting the initial and final states of the cross relaxation [171]. This is expressed as

$$P_{AB}^{dd} = (2/3)(2\pi/\hbar)(e^2/R^3)^2(3\hbar/2m_e)^2(1/\omega)^2 f_A f_B S$$

where ω is the transition frequency on each ion involved in the cross relaxation, f_A and f_B are the oscillator strengths of the transitions occurring on the two ions, and S is the overlap of the these two transitions. Putting in values for the constants and expressing the transition energy, $\Delta E = \hbar\omega$, in eV, the overlap integral in $1/\text{cm}^{-1}$, and the ion-ion separation in Angstroms, the transition rate can be calculated as

$$P_{AB}^{dd} = (1.4 \times 10^{24} f_A f_B S) / (\Delta E^2 R^6).$$

For typical f-f oscillator strengths of 10^{-6} a transition energy of 3 eV and a perfect overlap of transitions whose widths at room temperature are 10 cm^{-1} wavenumbers, this yields, for ions separated by a typical nearest neighbor distance of 3.5 Angstroms, a rate of $8 \times 10^6 \text{ s}^{-1}$. This corresponds to the situation of resonant energy transfer in a stoichiometric rare earth systems. For a 5% concentration of ions, this rate will drop by more than two orders of magnitude to $\sim 10^5 \text{ s}^{-1}$. While this is still appreciable, it would not effectively compete with the 1S_0 radiative rate ($\sim 2 \times 10^6 \text{ s}^{-1}$). In the presence of significant energy mismatch in transition energies or even lower concentrations, the cross relaxation will almost surely not be sufficient to prevent cascade emission on a single Pr^{3+} ion, except perhaps in highly concentrated systems. Thus while it is possible for cross relaxation energy transfer to convert the 1S_0 deep blue emission to visible emission, it will require an ideal energy match and a fairly high level of dopant concentrations that may generate other unwanted non-radiative processes.

We can perhaps take as an example the well studied cross-relaxation between Gd^{3+} and Eu^{3+} in LiGdF_4 and GdF_3 [172]. In this case, cross-relaxation between $\text{Gd}^{3+} (^6G_J \rightarrow ^6P_J)$ and $\text{Eu}^{3+} (^7F_1 \rightarrow ^5D_0)$ is 90% efficient – a very impressive result. In the above example, the Eu^{3+} concentration was 0.5% and therefore rapid energy migration among the Gd^{3+} ions must occur so that a Gd^{3+} nearby a Eu^{3+} can be found to allow effective cross-relaxation. The cross-relaxation must compete effectively with radiative transitions from 6G_J . The energy migration within the Gd^{3+} lattice ensures that the excitation energy will spend at least a fraction of its time near the Eu^{3+} activator. This would not occur in a non-stoichiometric system with concentrations at the 1% level.

As another benchmark for a non-stoichiometric system consider the $\text{Pr}^{3+} \rightarrow \text{Er}^{3+}$ energy transfer in $\text{CaAl}_{12}\text{O}_{19}$, containing 1% and 5% of Pr^{3+} and Er^{3+} , respectively; the energy transfer rate was estimated as $4.9 \times 10^4 \text{ s}^{-1}$ [169]. However, given that several channels exist for the transfer in addition to cross-relaxation, the cross-relaxation rate must be even smaller. Such a slow rate would not compete effectively with the 1S_0 radiative processes where in this example the two ions are not likely to be nearest neighbors. Therefore, it will be necessary to use more highly concentrated systems, perhaps even those that are stoichiometric in one of the two ions. For oxides, this means that the host may have to contain a lanthanide in the intrinsic structure. Fortunately there are a number of such examples (see Task 3 report).

A rare earth system studied extensively by Wegh [173], is the case of energy transfer from the 4f5d states of Er^{3+} or Tm^{3+} to $\text{Gd}^{3+} 4f^7$ levels. For the low-spin 4f5d state, the rate is $\sim 10^9 \text{ s}^{-1}$ at concentrations of $\sim 1\%$. Such a process would dominate the radiative rate of 1S_0 provided that the energy transfer rates from the 1S_0 state were as large. However the $4f5d \rightarrow 4f^2$ oscillator strength is about 10^3 larger than that for transitions within the $4f^2$ configuration so the rates for the Pr^{3+} systems being considered for multiphoton phosphors will be somewhat lower (perhaps 10^6 s^{-1} in the most favorable situations. Wegh has concluded that exchange interactions also contribute in this system [173].

If one chooses materials in which the rare earth is stoichiometric as one of the host constituents, then in addition to multipole-multipole interactions, exchange interactions may also contribute to the energy transfer rates. These can be very fast. For example, in GdCl_3 or $\text{Gd}(\text{OH})_3$ the observed exciton dispersions of a few cm^{-1} imply transfer rates of $\sim 10^{10} \text{ s}^{-1}$ for exchange-induced resonant energy transfer [174]. For exchange interactions, the weak oscillator strengths of the Gd^{3+} transition involved in the energy transfer are not relevant in determining the energy transfer rates.

As an example of a system that should be examined, consider a concentrated rare earth systems containing Eu and Pr. Oxides for which it has been demonstrated that $^1\text{S}_0$ is low (see report Task 3) and which contain a rare earth as one of the host cations include $\text{LaBaB}_9\text{O}_{16}$, [175] $\text{LaMgB}_5\text{O}_{10}$ [176], and LaB_3O_6 [177]. One can consider systems in which the La is substituted with Pr containing Eu as the dopant, or ones in which Eu substitutes for La as the host cation with Pr as the dopant. In both cases, one can anticipate rapid migration within the host cation system providing access to the region where there are Pr-Eu nearest neighbors pairs. Under this circumstance, exchange can play an important role as a mechanism for the cross-relaxation. Since it is unlikely that a perfect energy resonance will occur for the Pr^{3+} and Eu^{3+} transitions, the cross-relaxation will require some phonon assistance making it quite variable from one system to the next. Energy transfer back and forth between the Pr^{3+} and Eu^{3+} can be a potential problem particularly if the energy ends up in the $^1\text{D}_2$ level of Pr^{3+} from which much of the emission is in the infrared. Since $^5\text{D}_0$ of Eu^{3+} lies above $^1\text{D}_2$ of Pr^{3+} this may tend to limit the Eu^{3+} emission. On the other hand, transfer to $^3\text{P}_0$ of Pr^{3+} is not so serious if non-radiative relaxation to $^1\text{D}_2$ is not too rapid.

One potential problem for this system is the possibility of the Pr-Eu pair forming a $\text{Eu}^{2+} - \text{Pr}^{4+}$ charge transfer state. If such a state were created upon exciting the Pr^{3+} , then multi-photon emission would be impossible. This problem would need investigation. However, it may not be a problem in all or even most oxide systems.

The use of Er^{3+} instead of Eu^{3+} should also be examined for a Pr-Er cross-relaxation process as described previously [169]. If Er^{3+} is used as the host cation, rapid migration within the Er^{3+} should occur until the energy finds an Er-Pr pair where exchange can produce the cross-relaxation. In this system transfer back and forth between the Pr^{3+} and Er^{3+} should not limit the visible quantum efficiency since both ions will radiate visible photons as long as non-radiative relaxation from $^3\text{P}_0$ to $^1\text{D}_2$ does not deplete the $^3\text{P}_0$ population before emission. Cross relaxation within the Er^{3+} system is a likely problem and would probably quench the emission in a system with 100% Er^{3+} .

Subtask C: Spectral Output of the Systems

The $^3\text{P}_0 - ^3\text{H}_4$, $^3\text{F}_2$ ratio will dominate the green/red ratio from Pr^{3+} and can be determined from the Judd-Ofelt parameters. The emission from potential activators (see subtask A) can also be determined/predicted. It should be checked if conditions for mainly green emission ($^3\text{P}_0 - ^3\text{H}_4$ from Pr^{3+}) does not conflict with mainly green emission from the activators (based on the J-O parameters). For the spectral output of transition metal activators, see Subtask D, below.

Subtask D: Transition Metal Activators for Energy Transfer

The transition metal ion series has been examined in order to identify new Pr^{3+} activated phosphors for which the unusable near-UV photon ($25,200\text{ cm}^{-1}$) from the $^1\text{S}_0$ to $^1\text{I}_6$ transition can be converted to visible emission through energy transfer. The transition metal ions offer the advantage that the expected delocalization of the d-orbitals can increase the overlap of the localized f-orbitals of Pr^{3+} with the transition metal. Such an increase in the overlap among the orbitals involved in energy transfer will enhance the transfer probability and will suppress the channel of radiative relaxation.

For this process to occur efficiently the following conditions need to be satisfied:

1. The absorption spectrum for the transition metal ion should not overlap the excitation spectrum for the $^1\text{S}_0$ state. If there are no multiplet states originating from the d-manifold of the transition metal ion near $47,000\text{ cm}^{-1}$, there would be no overlap in energy of its absorption spectrum with that of Pr^{3+} . Only under such a condition will the transition metal not be excited directly by the photons used to excite the $^1\text{S}_0$ state of Pr^{3+} . In addition, the position of the charge transfer band of the transition metal ion should not overlap the Pr^{3+} excitation spectrum.
2. In order to suppress the radiative transition from $^1\text{S}_0$ to $^1\text{I}_6$, and transfer this energy directly to the activator ion, the absorption spectrum of the activator ion must overlap the emission spectrum associated with this Pr^{3+} transition near 405 nm. If there are several term levels associated with the d-manifold in this energy region, the probability of energy transfer from the rare earth ion to the transition metal could be appreciable.
3. Subsequent to the sensitization, the activator ion must emit in a desirable region of the visible spectrum.
4. As in all energy transfer schemes, the 5d band of Pr^{3+} should lie above $^1\text{S}_0$, since this level is connected to the ground state by a high transition moment and provides the pathway to $^1\text{S}_0$ through a nonradiative transition.

Sensitization of $3d^n$ Transition Metal Ions

The electronic structure of a number of ions have been calculated and the corresponding multiplet energy levels generated to identify transition metal ions which may fluoresce subsequent to the energy transfer from a Pr^{3+} ion [178]. The multiplet states were generated from one-electron states within a density functional theory. This circumvents the use of the time consuming, sometimes unreliable, configuration interaction formalism.

The Hartree Fock equations (HHF), originally proposed by Slater [179], were solved in order to generate a one-electron picture which corresponds to the average of all the multiplet configurations associated with a partially filled electronic shell. The multiplet configurations can then be generated from the one-electron energies of the HHF equations and the associated Coulomb and exchange integrals, by assuming that these parameters do not change even if the occupancies of various levels change for the various Slater determinants used in the expansion of the multiplet states. This assumption establishes a correspondence between, on the one hand, the

crystal field parameters, i.e., $10 Dq$ and the Racah parameters B and C [180] and, on the other hand, the one-electron energy levels and the Coulomb and exchange integrals from the HHF method [181]. $10 Dq$ is very sensitive to the metal-ligand separations; these were obtained from the literature [182, 183]. In most cases, they correspond to average d_{M-O} values in different crystal structures in six-fold coordination with oxygen atoms but it would be best to obtain these values for specific cases obtained either from experiment or from molecular modeling.

A number of transition metal ions, that may yield an efficient multi-photon phosphor in combination with Pr^{3+} , have been identified on the basis of their energy level diagrams and anticipated absorption characteristics. They include V^{2+} , V^{3+} , Mn^{2+} , Mn^{4+} , Cr^{2+} and Cr^{3+} as described below for the various d^n configurations.

d^1 Ions

It may be worthwhile considering Ti^{3+} in the d^1 ion series. Two criteria that must be satisfied are (1) the charge transfer transition must be sufficiently high in energy and (2) the energy of the metastable emitting level must be great enough to produce visible emission. Since Ti^{3+} has only one excited level, it has the advantage that it will not compete with the Pr^{3+} 4f5d absorption. Hosts with large crystal fields will be required to push the Ti^{3+} emission into useful visible wavelengths.

d^2 Ions

The d^2 transition metal ions Ti^{2+} , V^{3+} and Cr^{4+} in an ideal octahedral coordination with six oxygen atoms were examined. In octahedral symmetry (O_h), a five-fold d-like orbital splits into two degenerate molecular orbitals: t_{2g} and e_g , the former being lower in energy. These orbitals were found to be considerably delocalized with significant admixture of the oxygen-like orbitals. For V^{3+} and Cr^{4+} , the contributions from the metal ions to the molecular charge is approximately 85%, which justifies the calculation of B and C from the contribution of the metal ion. However, the t_{2g} molecular orbital for Ti^{2+} is found have only 73% of total charge localized at the titanium site, suggesting substantial covalency between the metal and ligand ions. Because of this delocalization, values of B and C estimated from the contributions by the titanium ion are significantly smaller, and are probably underestimated.

3T_1 is the ground state for the d^2 ions; the other triplet excited states are 3T_2 , 3T_1 and 3A_2 in order of increasing energy. The oscillator strengths for spin allowed intrasystem transitions among these levels are expected to be orders of magnitude higher than those for the intersystem transitions from the ground state to the states with different spin multiplicity. However, the 3A_2 state is a pure state within the d-manifold corresponding to the configuration e_g^2 . Any transition to this state is therefore forbidden since it would entail simultaneous excitation of two electrons. Therefore, the spectral region above the 3T_1 state will have no dominant absorption peaks above the excitation energy of 1S_0 ($46,500\text{ cm}^{-1}$); so that for the d^2 ions absorption at the Pr^{3+} excitation energy will not occur satisfying condition (1) for MPCE for all these ions. Near $25,200\text{ cm}^{-1}$, there are several excited states to which these ions can be excited. The most likely excitations will be to the 3T_1 or 3T_2 states, which suggests that there is a reasonable expectation that condition (2) can be fulfilled for these ions. However, the probability of visible emission is not great since the transition metal ions tend to emit from the first excited state irrespective of the state to which they are excited. If that happens, emission will involve either the 1T_2 or 1E levels which for V^{3+} and Cr^{4+} places the emission at about 1000 nm. For Ti^{2+} , this emission will definitely occur in the

infrared region. If the site symmetry is reduced from octahedral, the emission frequency will definitely shift to the infrared region. Thus, condition (3) rules out any possibility of a MPCE phosphor from these ions in oxide lattice. In a fluoride lattice, if Dq were to increase or if the Racah parameters were to become larger, this might shift the emission up into the red for these ions. Thus, one would expect that most likely phosphor material would be a fluoride doped with Pr^{3+} and V^{3+} or Cr^{4+} , depending on which one gives emission in the visible part of the spectrum.

d^3 Ions

V^{2+} , Cr^{3+} and Mn^{4+} with three d electrons are likely candidates for MPCE. The t_{2g} molecular orbitals associated with these ions have ~80% charge localized at the metal site. The values of B, C and Dq increase monotonically from V to Mn and are in good agreement with those for Cr^{3+} from Reference [17]. The ground state for d^3 ions is 4A_2 , arising from a high spin configuration, t_{2g}^3 and is a pure state within the d-manifold. The next quartet level 4T_2 , another pure state, is associated with the excitation of an electron from the t_{2g} to the e_g orbital. The other quartet states, both 4T_1 levels, originate from the configuration $t_{2g}^2 e_g^2$ and the other from $t_{2g} e_g^3$. The latter configuration is expected to be higher in energy, possibly resonant with the excitation of the 4f5d bands of Pr^{3+} . However any transition from 4A_2 to 4T_1 associated with this configuration should be forbidden because it requires a two electron excitation. Although these two quartet states mix leading to a small but non vanishing dipole transition probability from the ground state to this level, the transitions should be relatively weak.

To determine whether condition (1) can be satisfied, consider as a typical case, the absorption spectrum for Cr^{3+} in alumina. Three major peaks centered at $\sim 18,000 \text{ cm}^{-1}$, $\sim 25,000 \text{ cm}^{-1}$ and $\sim 40,000 \text{ cm}^{-1}$, are respectively assigned to the intrasystem transitions from 4A_2 to the 4T_2 , 4T_1 and 4T_1 states. These are broad band transitions with widths $\sim 3,000 \text{ cm}^{-1}$. Other transitions are mostly intersystem transitions with weak oscillator strengths. A gap in the absorption occurs between $30,000$ and $35,000 \text{ cm}^{-1}$, with very low absorption. Similar gaps in the absorption spectrum can be used to satisfy condition (1) for MPCE when the excitation energy of the Pr^{3+} ion ($>46,500 \text{ cm}^{-1}$) occurs in this gap. If one of the other two peaks is in resonance with the blue radiation ($25,200 \text{ cm}^{-1}$), the system would be an ideal case for MPCE transition provided the transition metal ion emits in the visible. All the three ions studied in the present case are known activator ions; so the search for a MPCE phosphor reduces to identifying a transition metal ion and its environment that meet the first two conditions. Considering the similarities in eigenfunctions t_{2g} and e_g for all the three ions, it is reasonable to assume that the absorption spectra associated with these ions would be similar to that of Cr^{3+} in alumina. A simulation of the absorption spectrum of these d^3 ions using a half width of $1,600 \text{ cm}^{-1}$ and a Gaussian profile for the dominant intrasystem transitions obtained from the term energies yields an absorption spectrum very similar to that observed except for a band near $45,000 \text{ cm}^{-1}$ that is probably due to a charge transfer transition. In going to Mn^{4+} , the gap between the peaks moves to lower energy, but unfortunately the peak is at $46,000 \text{ cm}^{-1}$. For V^{2+} , all the three peaks are at energy lower than $46,000 \text{ cm}^{-1}$. Thus if V^{2+} does not introduce any charge transfer band as in Cr^{3+} , this may be a potential ion in an oxide lattice. However, for all three ions, the 2E emission will be too far in the red to provide optimal lumen output. Mn^{4+} would offer the highest energy 2E emission and could produce useful visible output. In a fluoride, its charge transfer transition might be sufficiently high in energy.

In summary, these three ions hold some promise for a MPCE phosphor which, for oxides, points to V^{2+} . However, of the three ions, the emission of V^{2+} would be the furthest to the red and might be too far in the red to provide much visible useful output.

d^4 Ions

For the d^4 ions Cr^{2+} and Mn^{3+} the crystal field parameters tend to increase with the atomic number. The t_{2g} molecular orbitals show ~88% charge at the metal site. The calculated value of Dq agrees very well with that for Cr^{2+} ; however, the experimental value for B for Cr^{2+} implies 100% localization which is implausible. The ground state for d^4 ions is 5E for both the ions. The other quintet state is 5T_2 . Both quintet states are pure and differ from each other by the excitation of an electron from a t_{2g} to an e_g orbital. One would expect the transition from 5E to 5T_2 to be strong and broad. This transition leads to peaks in the visible at $12,000\text{ cm}^{-1}$ and $15,000\text{ cm}^{-1}$ for Cr^{2+} and Mn^{3+} respectively, which is one major drawback. Below 5T_2 , there is one 3T_1 state for Cr^{3+} and two triplet states 3T_1 and 3E for Mn^{4+} . These states would be the emitting states following the excitation to 3T_2 state; and the emission would be in the infrared. It is very unlikely that these ions would lead to designing an efficient MPCE lamp phosphor.

d^5 Ions

Mn^{2+} is studied as an example of a d^5 ion. Divalent manganese is one of the most popular activator ions in lamp phosphors. The calculated crystal field parameters are in good agreement with experiment. The ground state for Mn^{2+} is 6A_1 and there are no excited sextet states since both t_{2g} and e_g levels are occupied by five up-spin states. Therefore, all the excitations are weak intersystem transitions to quartet states mediated through spin orbit interactions. Since there are no such states available beyond $45,000\text{ cm}^{-1}$, the Mn^{2+} ion will not compete with Pr^{3+} ions in the primary excitation process to the 1S_0 state. However, there are many triplet states available between $\sim 15,000\text{ cm}^{-1}$ and $\sim 43,000\text{ cm}^{-1}$. Although this is favorable to transfer radiation from Pr^{3+} to Mn^{2+} , it may lead to transfer of the entire quantum of energy to Mn^{2+} before splitting the energy into two quanta. However, we feel that this is a good candidate for MPCE and should be studied further.

Sensitization of $4d^n$ and $5d^n$ Transition Metal Ions

An extension of a similar approach to that used for the $3d^n$ ions was attempted for the transition metal ions in the next two rows. The literature on luminescence from transition metal ions from these rows is rather limited and our search resulted in only few cases listed in Table B-26.

It is obvious from Table B-26 that

1. in most cases, these metal ions exist in more valence states than those in the first row;
2. there is no evidence for the existence of absorption or emission within the d-manifold of these ions;
3. emission appears to result from charge transfer transitions associated with the d^0 or d^{10} configurations.

Utilizing a charge transfer band for energy transfer does not appear promising because of the large band width and associated Stoke's shift in emission. It is not at all obvious why spectral characteristics of these ions in the d^n configuration have not been investigated in appropriate lattices where these ions can be accommodated.

The next question is then whether their absorption spectra in various hosts could be predicted using the available methods of electronic structure calculations. The procedure developed by Sambe and Felton [177] within the framework of the hyper Hartree-Fock theory to calculate the multiplet structure of the d^n -manifold within the framework of the MS-X α procedure was extended to the second and third row transition metal ions. However the following difficulties were identified

1. Complete free ion spectra for most of these ions are not available in the literature. In the case of d^2 ions, only Zr has the complete spectrum (Table B-27).
2. We observed that it is not possible to fit the d^2 -spectra of free ions using the Racah parameters only. This suggests significant inter-configuration mixing due to the proximity of the state arising from higher energy configurations (Table B-28).
3. It is possible to calculate the B and C parameters using first principle methods, but calculations in an oxygen environment using the MS-X α method indicates significant covalency with the ligand orbitals. This strongly suggests that a modification of this approach is needed in order to apply this approach to these ions. This probably can be done using a renormalization procedure within the d^n manifold.
4. In general, we observed significantly larger values of the crystal field splitting, Dq , for Zr^{2+} , Nb^{3+} and Mo^{4+} (Table B-29). This would suggest that in most cases one should observe a multiplet splitting characteristic of a high crystalline field.

Table B-26
Emission from Third and Fourth Row Transition Metal Ions

Activator Ion	Host	Color	Oxidation State
Ag Oxidation state: +1 Configuration: $4d^{10} 5s^1$	ZnBorate	yellowish-white (s)	
	Cd Borate	yellow(s)	
	ZnS	blue (s)	1
	Ca Phosphate	yellowish-white	
Au Oxidation state: +1, +3 Configuration: $5d^{10}, 6s^1$	CdWO ₄	orange	
Mo Oxidation state: +2,+3,+4,+5,+6 Configuration: $4d^5, 5s^1$	Al ₂ O ₃	blue	
	CaMoO ₄	yellowish green	+6
	Ca(PO ₃) ₂	green	
	CaWO ₄	yellow	
	CdMoO ₄		
	PbMoO ₄	green	
	SrMoO ₄	blue-violet, yellow-green	
	Zn ₂ SiO ₄	green	
Nb Oxidation state: +5,+3 Configuration: $4d^4, 5s^1$	ZnF ₂	greenish-blue	
	CaNb ₂ O ₆	blue-green	+5
	ScTaO ₄		
Pt Oxidation state: +4,+2 Configuartion: $5d^9, 6s^1$	Al ₂ O ₃	green	
Re Oxidation state: +7,+6,+4,+2,-1	Zn ₂ SiO ₄	violet	
	Re ₂ O ₇	pink	+7
Rh Oxidation state: +3,+2,+4 Configuratio: $4d^8, 5s^1$	Al ₂ O ₃	red	+3(?)
	RhF ₃	purple	+3
	Rh ₄ (P ₂ O ₇) ₃	blue	+3
	Rh(NO ₃) ₂	pink	
W Oxidation state: +6, +5,+4,+3,+2 Configuration: $5d^4, 6s^2$	Al ₂ O ₃	orange	
	BaWO ₄	blue	+6
	CaWO ₄	blue	+6
	Ba ₂ W ₂ O ₅	green	+3
	βMgWO ₄	blue-green	+6
	SrWO ₄	blue	+6
Zr	Zn ₂ SiO ₄	blue	
Oxidation state: +4	ZrO ₂	blue-green	
Configuration: $4d^2, 5s^2$	ZrSiO ₄	blue-green-yellow	

Table B-27
Experimentally Observed Terms of Zr^{2+} , Nb^{3+} and Mo^{4+}

Ion	Observed States
Zr^{2+}	3P , 3F , 1S , 1D , 1G
Nb^{3+}	3P , 3F , 1D , 1G
Mo^{4+}	3F , 3P

Table B-28
Racah Parameters (cm^{-1}) of Zr^{2+} , Nb^{3+} and Mo^{4+}

Parameter	HF (Froese-Fischer)	HF (Cowan)	HF (Cowan)	Expt.
Charge State	0	0	+2	
B	616.2	605.7	659.5	604.9 ^a , 552.2 ^b
C	2409.4	2360.1	2609.4	629.7 ^a , 2062.1 ^b
γ	3.90	3.90	3.96	1.04 ^a , 3.73 ^b

Table B-29
Crystal Field Parameters (Theory) for Mo^{4+} and Nb^{3+}

Ion	Dq (cm^{-1})	B (cm^{-1})	C (cm^{-1})	γ	Dq/B
Mo^{4+}	3301.8	396.6	1568.1	3.95	8.3
Nb^{3+}	2468.1	374.5	1474.2	3.93	6.59

Conclusions and Recommendations

Conclusions: Subtasks A-C

It will be difficult to find a system, especially oxides, whereby energy transfer cross relaxation will successfully compete with radiative emission to convert the 1S_0 deep blue emission of Pr^{3+} to visible output in the green or red, providing quantum efficiencies in excess of 100%. This will require a nearly perfect resonance energy match between the Pr^{3+} ion and the other rare earth activator. The system will also have to have fairly high concentrations of both Pr^{3+} and rare earth activator or it should be stoichiometric in the activator. The activator oscillator strength for electric dipole radiation should be high and the activator must radiate with high efficiency in the visible. The system should be such as to minimize non-radiative relaxation on Pr^{3+} from 3P_0 to 1D_2 . The most likely activator candidates are Eu^{3+} , Er^{3+} or Ho^{3+} .

Recommendations: Subtasks A-C

1. Energy transfer from Pr^{3+} to Dy^{3+} , Tb^{3+} , Eu^{3+} , Er^{3+} , Ho^{3+} and Nd^{3+} should be investigated in various hosts.
2. Selection rules for phonon assisted energy transfer need to be investigated for more general cases of energy transfer.
3. Systems containing Pr^{3+} and either, Eu^{3+} , Er^{3+} or Ho^{3+} at relatively high (or even stoichiometric) concentrations should be studied for efficient cross relaxation and high quantum efficiencies.

Conclusions: Subtask D

Unfortunately, we do not find a $3d^n$ ion that satisfies all the conditions for a MPCE process. However, there are certain ions which show some promise: V^{3+} and Cr^{4+} (d^2 ions), V^{2+} , Cr^{3+} and Mn^{4+} (d^3 ions), and Mn^{2+} (d^4). In every group, there are certain difficulties to overcome. Among the d^2 ions, the emission may occur in the infrared. The V^{2+} ion and Mn^{2+} ion may function in oxide lattice, but V^{2+} ion may introduce charge transfer or other bands near $45,000\text{ cm}^{-1}$. In the case of Mn^{2+} , the energy transfer may involve all of the absorbed quantum of energy because of the presence of several quartet states spanning the range from $15,000\text{ cm}^{-1}$ to $45,000\text{ cm}^{-1}$. There is also the additional problem of the ordering of $5d$ bands and $^1\text{S}_0$ state of Pr^{3+} . It appears that Mn^{4+} would be an ideal candidate in a fluoride host. For Mn^{4+} , the gap in the absorption band should be centered at $45,000\text{ cm}^{-1}$. This may happen in a fluoride lattice where Dq is expected to be higher.

The following systems should be studied for the MPCE process: 1) V^{3+} , Cr^{4+} , Cr^{3+} or Mn^{4+} codoped with Pr^{3+} in a cubic fluoride crystal and 2) V^{2+} and Mn^{2+} in high gap oxides. It is suggested that the oxide crystals should be ones composed of functional groups like PO_4 , SiO_4 or aluminate groups where the band gap is expected to be high and the crystal is expected to be highly ionic. In the case of PO_4 , the large phosphate vibrational frequency (1100 cm^{-1}) may cause rapid $^3\text{P}_0 \rightarrow ^1\text{D}_2$ nonradiative relaxation. An appropriate host system can be found from a database on inorganic crystal structures such as the ICSD system currently being used at Towanda for similar studies. First, the phosphors doped with one kind of ion should be synthesized and spectroscopically studied to determine if the four conditions outlined earlier are actually satisfied. Only then one should form the codoped systems to identify the appropriate ion combinations. In the meantime, it would be worthwhile to investigate the multiplet splitting of ions in a cubic fluoride environment.

The spectroscopy of the d^n ions in the second and third row transition metal ions should be pursued both experimentally and theoretically. In addition, a reliable theoretical method needs to be developed for predicting energy levels of the $4d$ and $5d$ transition metal ions. This method should handle explicitly any covalency effects.

Recommendations – Subtask D

1. Spectroscopy of d^n ions for the 3d, 4d and 5d transition metal ions should be pursued both experimentally and theoretically and this should include the VUV spectral region.
2. A reliable theoretical method needs to be developed for predicting energy levels of a transition metal ions. This method should handle explicitly any covalency effects.

Task 9: New Green

Task Leader: K. C. Mishra
Task Members: M. Raukas
M. Zachau
A. Meijerink
R. Rana
A. Ellens

Recommendations

1. Designing a green phosphor using a multi-photon transition scheme is a difficult task in view of the strict excitation and emission criteria to match one green emitting ion with another cascading ion, and color requirements for lamp blending. The promising candidate coactivators are Mn^{2+} , Tb^{3+} , Ce^{3+} , Eu^{2+} , Ho^{3+} , Er^{3+} , Nd^{3+} , Dy^{3+} , Sm^{3+} and Tm^{3+} .
2. Phosphors based on s^2 -ions should be considered further as activator ions for sensitization by a cascading ion. The excitation and emission spectra of Ag in KCl is almost an ideal match for sensitization by Pr^{3+} by $^1\text{S}_0 \rightarrow ^1\text{I}_6$ transition. Unfortunately neither the host nor the activator ion is appropriate. Although the s^2 -ions do not appear to be very promising as green emitters, this example of Ag illustrates the need for further investigation of luminescence from s^2 -ions in the context of multiphoton phosphors.
3. It may be hard to achieve a green emitting phosphor with a cascading, sensitizer ion that would match the current requirements of triblend phosphors for white light. The blend composition needs to be revisited to utilize high quantum efficiency of such phosphors.

Summary of Investigation

Introduction

The main objective of this task was to study known green emitting phosphors for identifying candidate activator ions and hosts for designing multi-photon phosphors for lamp application. This study can be pursued in the context of the following three multi-photon transition scenarios:

1. a cascading transition at a single ion leading to two green photons;
2. a cascading ion emitting a green photon during one of the cascading transitions;
3. a cascading ion sensitizing a green emitting activator ion.

The first case is almost an impossibility. The second case is technically possible. The $^3\text{P}_0 \rightarrow ^3\text{H}_4$ transition of Pr^{3+} comes very close to bluish-green region of the visible spectrum. This case needs to be addressed within the framework of new cascading schemes or ions.

In the present investigation, we focus on the third case. This involves activator ions which emit in the green region and which can be sensitized by a cascading ion. These ions are expected to split the incident UV photons. The selection criteria for new green activators involve the following issues:

1. overlap of the excitation spectrum of the activator ion and the emission spectrum of the cascading ion from a specific cascading step;
2. no overlap of the excitation spectrum of the activator ion and that of the sensitizer ion which leads to its multiphoton transition;
3. efficient emission in the green part of the visible spectrum by the activator ion following the nonradiative energy transfer from the sensitizer ion during a dominant cascading step.

Spectral Requirements of a Green Emitting Activator Ion

We have made an attempt to identify activator ions which emit in the green region of the spectrum, and which can be excited by energy transfer from another cascading ions such as Gd^{3+} , Er^{3+} or Pr^{3+} . One such system based on energy transfer from Er^{3+} to Tb^{3+} has already been discovered by Meijerink. Even if this task is not limited by any specific cascading ion, one of the primary goals of this multi-photon project is to utilize energy from the first cascading step of Pr^{3+} ion involving $^1\text{S}_0 \rightarrow ^1\text{I}_6$ transition to excite a green emitting activator ion by a nonradiative energy transfer process. The luminescence characteristics of such an activator ion must satisfy the following conditions to be a good partner in a multi-photon scheme:

1. It should not compete with the cascading ion in absorbing the exciting ultraviolet (UV) radiation.
2. Its excitation spectrum should overlap with the emission spectrum corresponding to the transition of the cascading ion which is being converted to a green photon.
3. In the context of sensitization by the $^1\text{S}_0 \rightarrow ^1\text{I}_6$ transition of Pr^{3+} , the associated Stokes shift should not exceed ~ 0.9 eV, otherwise it will shift the emission to orange or orange red region.

These conditions are very restrictive in choosing a green emitting activator ion. Additionally, the requirements of a tri-phosphor blend for generating white light with high efficacy (>100 LPW) and color rendering index (CRI >80) impose further restrictions.

Lamp Requirements for Generating White Light

Visible radiation from ~ 480 nm to ~ 575 nm has a green component in visually evaluated light. Green with a minimal blue or yellow component falls in the range from ~ 500 nm to ~ 530 nm. Thus any phosphor with its principal emission in a range even greater than ~ 500 nm to ~ 530 nm can be considered as a candidate for a green emitting phosphor. However, for a triblend phosphor system composed of green, red, and blue emitting phosphors, a green phosphor with the emission peak at longer wavelengths in this region is preferred because of the efficacy

requirement. A photon at 555 nm is most efficacious and contributes 683 LPW. It is for this reason that a green phosphor activated by Tb^{3+} with the emission peak around ~ 545 nm is preferred over one activated by Dy^{3+} with emission peaks around ~ 470 nm and ~ 570 nm. The phosphor blending requirements to generate white light efficaciously (and with acceptable quality properties evaluated by metrics such as *Color Rendering Index*) need to be remembered in our search for a green emitting phosphor. However, if a multi-photon phosphor is found that emits in the spectral regime almost out to ~ 480 nm to ~ 575 nm, it may be possible to use this phosphor to generate white light by adding an additional phosphor component provided that the gain from increased quantum efficiency compensates for any loss in LPW.

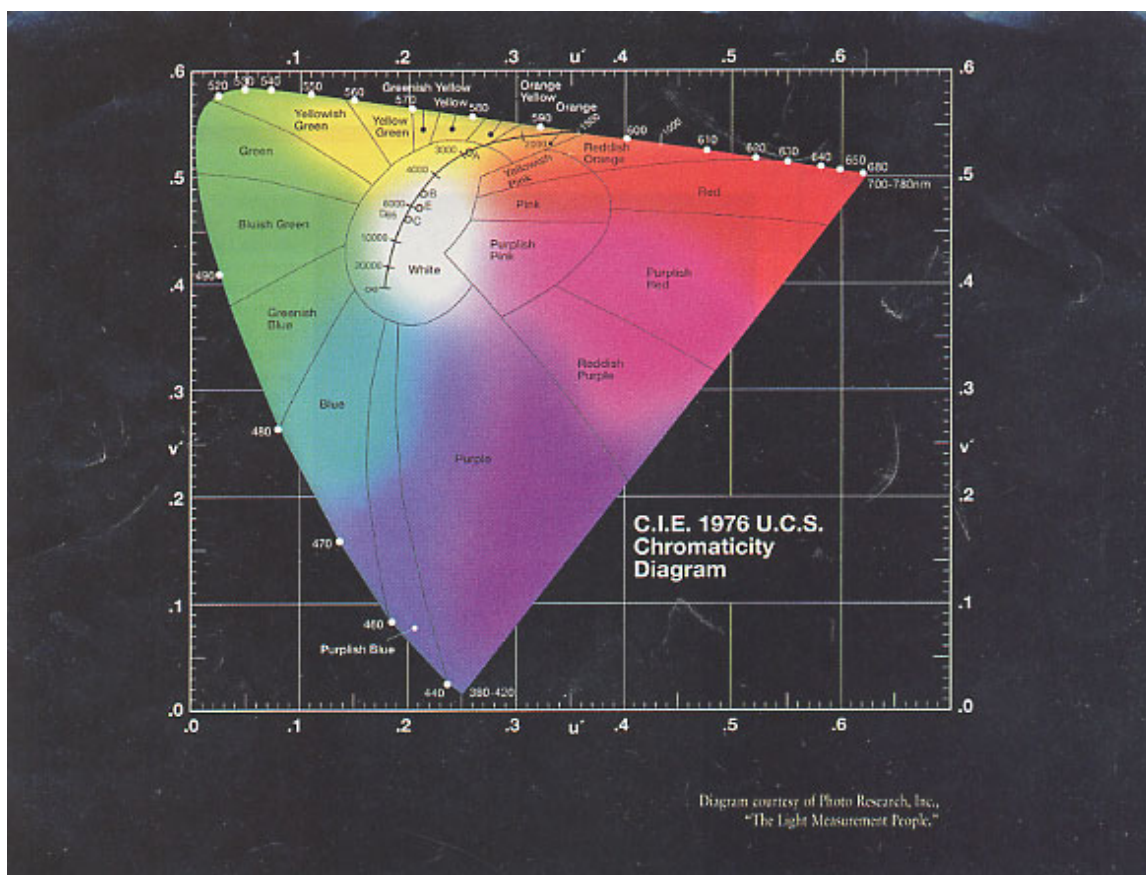


Figure B-14
Defining Color: CIE Chromaticity Diagram

Review of Green Emitting Phosphors

We will limit our discussion to inorganic, green emitting phosphors. We classify these phosphors according to their fluorescence schemes based on the nature of the electrons undergoing excitation.

s^2 Group

The electronic configuration of these activator ions outside the closed shell is ns^2 . In the literature, the excitation process is formally described as excitation of an electron from the s-like state to a p-like state. The ground state is 1S_0 , and the three excited states are 3P_j and 1P_1 . The correlation scheme in O_h symmetry is as follows: $^1S_0 \rightarrow ^1A_{1g}$, $^3P_0 \rightarrow ^3A_{1u}$, $^3P_1 \rightarrow ^3T_{1u}$, $^3P_2 \rightarrow ^3E_u + ^3T_{2u}$ and $^1P_1 \rightarrow ^1T_{1u}$. The characteristic absorption bands, A, B and C refer to excitation from 1S_0 to 3P_1 , 3P_2 and 1P_1 states. These excitations usually result in emissions from the lowest 3P_1 state and consist of two bands, A_l and A_x . The higher energy A_l band results due to spin-orbit interaction between $^1T_{1u}$ and $^3T_{1u}$ levels and is often described as a (pseudo) Jahn-Teller distortion of the excited state.

Due to the diffuse nature of s and p levels, both the excitation and emission spectra are rather broad and depend strongly on the host lattice. The Stokes shift can be very large. Although the above description gives the false impression about the nature of the ground state being a pure s- and p-like states, there is always strong hybridization of the s- and p-like states. These transitions occur within the strongly hybridized “sp” manifold.

The following s^2 -ions are known to emit in the green region of the spectrum in the listed host lattices:

1. $\text{Sn}^{2+}(5s^2)$: CaI_2 , Cd-phosphate, KBr, K-borate, KCl, KI, La-borate, LiI, Li-phosphate, Na-borate, NaI, Na-phosphate, RbBr, RbCl, RbI, Sn-Phosphate, Zn-phosphate;
2. $\text{Sb}^{3+}(5s^2)$: CaO, MgS, SrO, $\text{Ca}_3(\text{PO}_4)_3\text{F}$ (480 nm)
3. $\text{Ga}^+(4s^2)$: KBr (553nm), KCl(527nm), NaCl(506 nm)
4. $\text{In}^+(5s^2)$: KI (563 nm)
5. $\text{Bi}^{3+}(6s^2)$: $\text{Bi}_4\text{Ge}_3\text{O}_{12}$ (550 nm), BaCO_3 , (Ca,Sr) S, SrS, SrSe
6. $\text{Pb}^{2+}(6s^2)$: BaSiO_3 , BaS, CaSe, CsBr, PbI_2 , SrS, ZnS
7. $\text{Ge}^{2+}(4s^2)$: MgO

This is in no way an exhaustive list. Except where it is indicated, we do not have a complete picture of their excitation and luminescence spectra. In most cases, the associated charge compensation scheme plays a very important role in the luminescence process. Due to large Stokes shift, most of these ions may not be suitable as an activator ion. However, an examination of their excitation spectra may reveal situations in which these ions can be coupled to a cascading ions. For example, consider the luminescence spectra of Ag^- in KCl (Figure B-15). This material is described to emit white light; its absorption spectrum appears to be ideal for excitation by the $^1S_0 \rightarrow ^1I_6$ transition from Pr^{3+} . Of course potassium chloride cannot be used in a fluorescent lamp. This absorption spectrum may change drastically in another host.

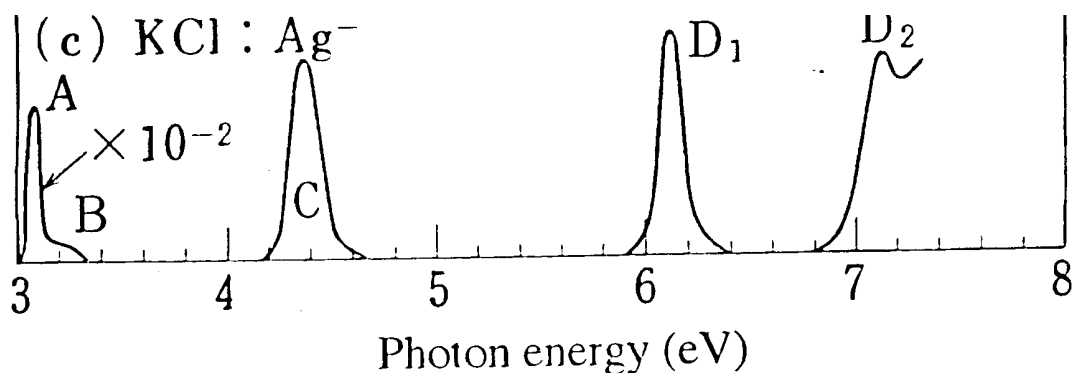


Figure B-15
Absorption Spectrum of Ag^+ at 77 K in KCL

The key to using a s^2 -ion as an activator ion lies in the tunability of its excitation/absorption spectra to match with the emission pattern of the sensitizer ion relaxing from an excited state in the cascading mode.

d^N -Ions

The 3d transition metal ions generate highly structured excitation and emission spectra. Cr^{3+} and Mn^{4+} ions with d^3 configuration and Mn^{2+} and Fe^{3+} with d^5 configuration are utilized in making several commercial phosphors. The absorption and emission spectra of transition metal ions depend strongly on the host lattice. Both broad band and narrow band emission are observed due to transitions within the d^N manifold, intra-configuration-level transitions leading to the former and inter-configuration-level transitions to the latter. When higher energy levels within the d^N manifold are excited, emission is only observed from the lowest energy level. This is an important difference from the emission spectra of f^N ions to be discussed later.

Mn^{2+} ion in tetrahedral coordination is extensively used for green emission. The emission spectrum usually consists of a structureless band with a half width of 0.1 to 0.2 eV with the peak wavelength varying between 490 to 750 nm. The transitions are usually characterized by weak crystal field of $Dq/B \cong 1$ and the luminescence corresponds to the ${}^4T_1 \rightarrow {}^6A_1$ transition in a cubic field.

This ion fluoresces in more than 500 inorganic crystals. In an earlier internal report, this ion was recommended as an activator ion for sensitization by the ${}^1S_0 \rightarrow {}^1I_6$ transition from Pr^{3+} based on results from a theoretical calculation using hyper Hartree-Fock approach for both octahedral and tetrahedral coordination. Since the ground state is a sextet state and all the excited states are either spin quartet or doublet states, transitions from the ground state are usually weak. We did not find any absorption due to transitions within d-manifold above 5.6 eV for octahedral coordination. However, around this excitation energy, transitions outside d^N manifold will be observed which could be very strong, and may compete effectively with the absorption of the Pr^{3+} ion. Measurements on two phosphors $\text{SrAl}_{12}\text{O}_{19}:\text{Pr, Mn}$ and $\text{LaMgB}_5\text{O}_{10}:\text{Pr, Mn}$ showed that at 170 nm excitation, direct absorption by Mn^{2+} competes strongly with the absorption by the Pr^{3+} ion.

In Figure B-16, we show luminescence and excitation spectra for Mn^{2+} in $\text{LaAl}_{11}\text{O}_{18}$. Excitation between 200 nm and 400 nm is rather very weak. This together with the fact that the absorption peaks are very sensitive to crystalline environment (Table B-30) could be used to identify suitable lattice to develop a green emitting multiphoton phosphor system based on this ion.

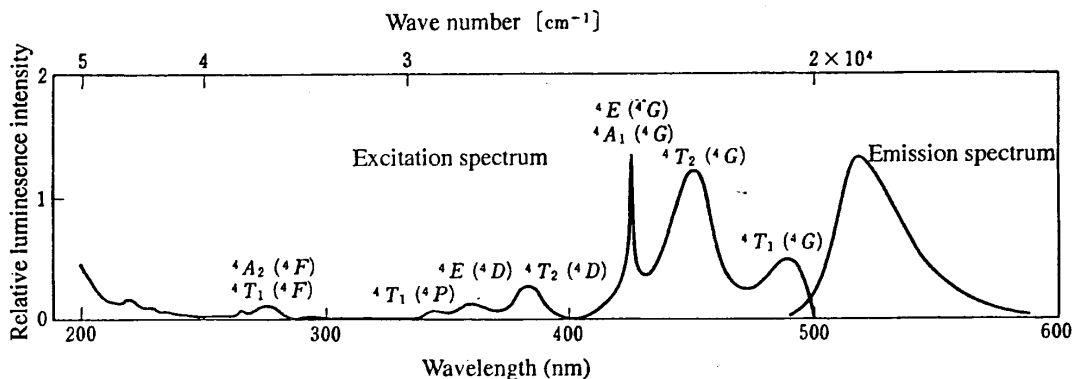


Figure B-16
Excitation and Emission Spectra of Mn^{2+} in $\text{LaAl}_{11}\text{O}_{18}$

Table B-30
 Mn^{2+} Sites and Luminescence Properties

Host	Site Symmetry	Coordination Number	Inversion Symmetry	Emission Wavelength (nm)
CaF_2	O_h	8	g	495
ZnGa_2O_4		4	u	506
ZnAl_2O_4		4	u	513
Zn_2SiO_4	C_{3i}	4	u	525
Zn_2GeO_4	C_{3i}	4	u	537
$\text{Ca}_5(\text{PO}_4)_3\text{F}$	C_{6h}	6	u	570
$\text{CaSiO}_3(\text{mono})$	C_2	6	u	588

f^N Ions

Transitions within the f^N Manifold

Most of the efficient lamp phosphor utilize rare earth ions as activators. Transitions within the f-manifold lead to narrow emission lines and are insensitive to host lattice. Commercially popular green emitting phosphors use Tb^{3+} as the activator ion. Its dominant emission around 545 nm results from the $^5\text{D}_4 \rightarrow ^7\text{F}_5$ transition. One can use this transition as a guide to choose other rare earth ions from Dieke's energy level diagram (Figure B-17) as candidates for green emission.

This diagram is generated analyzing transitions associated with rare earth ions in LaCl_3 . Unlike d-like states, the 4f-states do not mix with the host lattice. Therefore, the associated energy levels do not vary from one crystalline lattice to other that significantly. However, when the energy levels are very close together, the designation of energy levels is not unambiguous and might differ from that for LaCl_3 . This is not a serious problem.

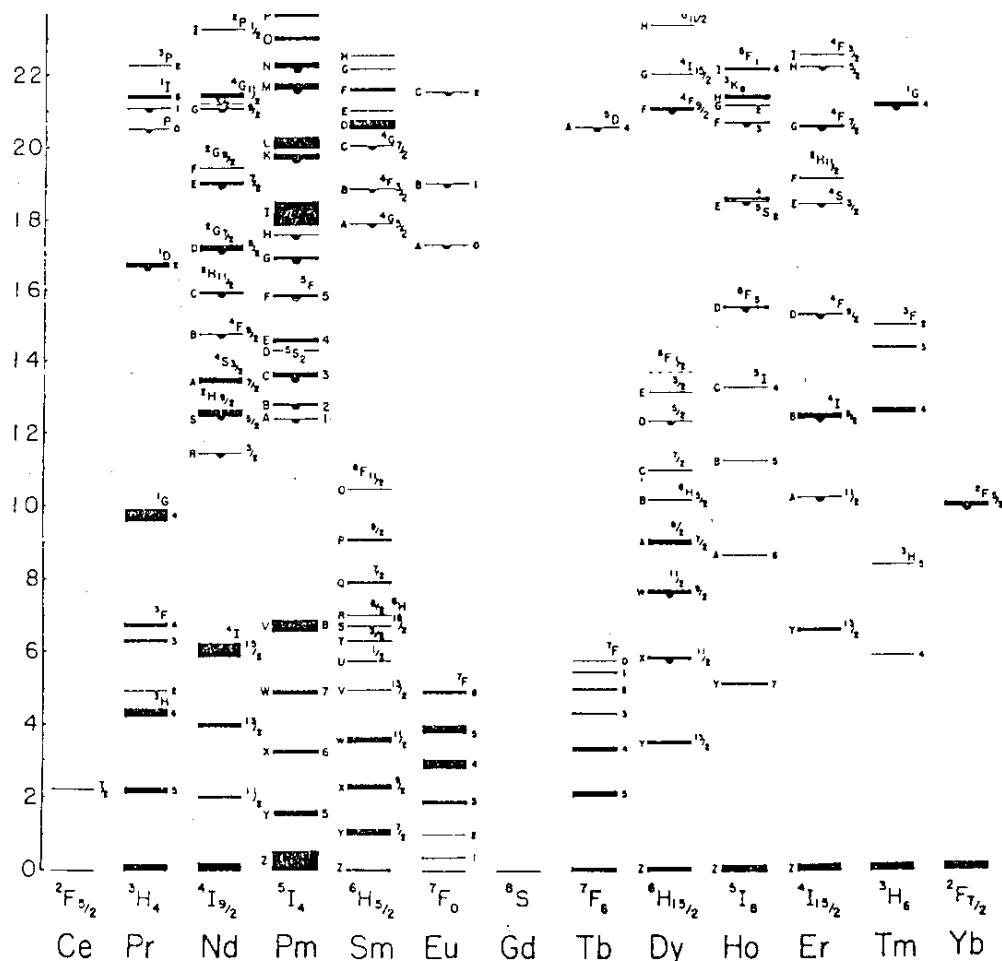


Figure B-17

Energy Level Diagram for Ln^{3+} in LaCl_3 . Transitions up to Energies Slightly Higher than that of $^5\text{D}_4$ State of Tb^{3+} are Indicated.

Light emitting levels are shown in Figure B-17 by semicircle. Comparing the $^5\text{D}_4$ level of Tb^{3+} with that of other rare earth ions, it is easily seen most of the ions have a luminescent energy level close to this state except for Gd^{3+} , Ce^{3+} , and Yb^{3+} . In the case of Eu^{3+} , emission from $^5\text{D}_2$ and $^5\text{D}_1$ is usually quenched at higher concentration of Eu^{3+} . One cannot also use Pm^{3+} because of its radioactivity. Thus, we have Pr, Nd, Sm, Dy, Er, Ho and Tm which could emit in the green region of the spectrum. However, unlike transition metal ions, emission from the rare earth ions from higher excited states also occur. These transitions usually reduce the efficacy of the phosphor, and bring additional problems for generating white light as discussed earlier.

Table B-31
Transitions from Candidate Green Emitting Rare Earth Ions

Ion	Final State	Excited State	Emission (nm)
Tb ³⁺	⁷ F ₆	⁵ D ₄	488
	⁷ F ₅		542
	⁷ F ₄		581
	⁷ F ₃		619
	⁷ F ₂		645
	⁷ F ₁		665
	⁷ F ₀		677
Pr ³⁺	³ H ₄	³ P ₀	481
		¹ D ₂	594
		³ P ₁	471
Nd ³⁺	⁴ I _{9/2}	⁴ G _{7/2}	526
		² G _{9/2}	514
		² H _{11/2}	628
		⁴ F _{9/2}	680
Sm ³⁺	⁶ H _{5/2}	⁴ G _{7/2}	475
		⁴ F _{3/2}	560
		⁴ G _{5/2}	560
Dy ³⁺	⁶ H _{15/2}	⁴ F _{9/2}	477
	⁶ H _{13/2}	⁴ F _{9/2}	571
	⁶ H _{15/2}	⁶ F _{5/2}	812
Ho ³⁺	⁵ I ₈	³ K ₈	469
	⁴ I _{15/2}	⁵ F ₃	485
	³ H ₆	⁵ S ₂	542
		⁵ F ₅	696
Er ³⁺	⁴ I _{15/2}	⁴ F _{9/2}	488
		⁴ S _{3/2}	543
		⁴ I _{9/2}	807
Tm ³⁺	³ H ₆	¹ G ₄	475
		³ F ₂	664
		³ F ₃	694

Using energy levels from LaCl_3 , we have computed approximate emission frequencies for transitions when these ions are excited in the green region of the spectrum (Table B-31). Multiple line emissions that could occur are indicated in the last column. Unless the branching ratio for the transitions leading to green emission is high, phosphors using these ions will not be efficient green emitters.

5d→4f Transitions

Ce^{3+} and Eu^{2+} are known to emit in the green due to 5d→4f transition. Because of the diffuse nature of the 5d states, its absorption and emission bands change depending on the host lattice. Both emission and absorption bands are rather broad. Recent works of Dorenbos would be very helpful in identify suitable host systems. Several examples of phosphors containing these ions which emit in the green are listed below:

1. Ce^{3+} : $\text{Y}_3\text{Al}_5\text{O}_{12}$ – Emission spectrum extends from 550 nm to 700 with the emission peak near 560 nm, and two prominent excitation peaks are near 250 nm and 350 nm.
2. Eu^{2+} : SrGa_2S_4 – Emission peak at 535 nm; $\text{Ba}_{0.75}\text{Al}_{11}\text{O}_{17.25}$ - Emission peak at ~500 nm.
3. Complex Ions

There are many complex ions or functional groups that are known to emit in the green. Some example are listed below:

1. Molybdate groups in Al_2O_3 , $\text{Ca}(\text{PO}_3)_2$, PbMoO_4 , SrMoO_4 , Zn_2SiO_4 , Nb in ZnF_2 ,
2. tungstate groups in ZnWO_4 an PbWO_4 ;
3. uranyl groups in $\text{Cs}_2\text{UO}_2\text{Cl}_4$, AlBO_3 , $\text{KAl}(\text{SO}_4)_2$, Li_3PO_4 , Na_3BO_3 , $\text{NaPO}_3\text{Na}_3\text{PO}_4$, $\text{Sr}_2\text{W}_2\text{O}_5$
4. Cu in MgSiO_3 , Mg_2SiO_4 , SrO , SrSe , ZnS and CaO

Absorption and emission from these groups are associated with transitions between the highest occupied molecular orbital and the lowest unoccupied molecular orbital of the corresponding functional groups. Emission efficiency is usually highly temperature dependent and the Stokes shifts are large. In the case of uranyl group excitation involves charge transfer transition from oxygen to 5f orbital due to U. The emission spectrum is characterized by many sharp lines from 500 nm to 588 nm. Being a radioactive ion, it is very unlikely to be considered as a serious candidate for designing a lamp phosphor.

Copper does not belong to this group but we have included it because excitation of this ion both in its divalent or mono-valent state involves the host lattice. $\text{ZnS}:\text{Cu}$ is a commercial electro-luminescent phosphor.

Task 10: New Cascading Ions

Task Leader: Baldassare Di Bartolo
Task Members: Norman P. Barnes
John M. Collins

Purpose of Task 10

1. To review, patiently, the systems that have been considered in search of multiphoton-effect materials, including those summarily dismissed, to confirm the negative choices or point to promising, even if elusive possibilities.
2. To examine new materials and processes that may produce two visible photons following a one-photon excitation, including transition metal ions and molecular systems.

Subtask A

Identification of new systems that could exhibit the photon cascading similar to that observed in Pr:YF₃. That is, one UV photon in and two visible photons out.

Subtask B

Investigation of the possibility of new cross-relaxation schemes involving two like (or unlike) ions in order to produce two visible photons. Thus we extend the task to include two-body processes.

Subtask A

Identification of new systems that could exhibit the photon cascading similar to that observed in Pr:YF₃. That is, one UV photon in and two visible photons out.

Conclusions

The search for organic molecules that could exhibit photon cascading focused on aromatic molecules, which absorb strongly throughout the UV and occasionally exhibit high quantum yields. UV absorption leads to excited singlet and triplet states of the pi-bonding electrons. Absorption and emission bands are broad and Stokes shifts are large (several thousand cm⁻¹), indicating strong coupling to the vibrations of the molecule and the local environment. Though most emit in the near UV, some systems (e.g. 1-amino anthracene, pyrene, and 1, 6 diphenylhexatriene) show broad emission in the blue, centered at about 470 nm. We found however, no evidence of two-photon emission. Apparently, excitation in the UV leads to an excited singlet state, from which it undergoes a rapid nonradiative decay to a lower excited singlet state, and/or intersystem crossing to a triplet state. Emission is from one of these states to the ground state [192, 193, 194].

Recommendations

The organic systems investigated, mostly aromatic molecules, show no evidence of two-photon emission, and can be dismissed.

Transition metal ions show no likelihood of two-photon emission, and should not be considered as part of a strategy for yielding quantum efficiencies greater than one.

Subtask B

Investigation of the possibility of new cross-relaxation schemes involving two like (or unlike) ions in order to produce two visible photons. Thus we extend the task to include two-body processes.

Conclusions

There are many possible combinations of lanthanide series atoms that could produce a 2:1 quantum efficiency. Pr and Gd appear to be the most promising lanthanide series atoms. The efficiency with which the 2:1 process will occur depends critically on the host material. Choice of the host material will affect the dynamics of the situation because the various rates, such as the energy transfer rate and the nonradiative decay rate, vary an order of magnitude or more depending on the host material. Fortunately, there is a plethora of host materials from which to choose. It is probable that a favorable host can be found.

In addition to the data taken from the literature, computer calculations can be used to predict the likelihood of efficient transfer. These calculations can identify various energy transfer schemes among rare-earth ions that could (a) convert the 400 nm photon of Pr^{3+} into the visible, or (b) use the first Gd photon to excite a center more efficient in visible emission. A computer program can find combinations of ions and energy levels that lead to energetically feasible transfer paths.

Recommendations

The search has been divided into 2 parts: systems that can be excited by a Hg discharge and systems that can be excited by Xe discharges. Lanthanide series ions have been categorized into sensitizers, ions which absorb the excitation radiation, and active ions, ions which receive part of the absorbed energy from the sensitizer and subsequently emit a photon.

1. Pr and Gd should be considered the most promising sensitizers. The potential sensitizers Nd, Er, and Tm are not as attractive as Pr and Gd. Pr, Sm, Eu, Tb, Dy, and Tm are possible active atoms. Specific combinations of sensitizers and active atoms have been identified for both types of discharge.

2. Germane spectroscopic parameters should be determined for Pr and Gd in promising host materials. These parameters can be approximated using the quantum mechanical approach outlined in Appendix B or measured using standard spectroscopic techniques. A dual approach will probably produce the best results. Specifically, the quantum mechanical model can be used to identify potential host materials and detailed spectroscopic measurements can verify and refine the predictions for selected host materials.
3. Investigations should be conducted with the purpose of verifying the most convenient schemes that would allow the shift of the energetic photon absorbed by the Pr and Gd ions into 2 photons in the visible region. In particular the following endeavors are recommended:
4. Investigation of the shifting the first Pr photon into the visible via energy transfer to Eu, Dy, Sm, Tb, and possibly Er. No other RE ions show promise as both an efficient activator for Pr and as an efficient emitter in the visible.
5. Investigation of the shifting of the first Gd photon into the visible via energy transfer to Pr, Eu and Tb. Though other RE ions show the possibility of being efficient activators none will lead to efficient emission in the visible.

Appendices

This Report has three Appendices:

- A. N. P. Barnes, Potential Lanthanide Series Atoms for a 2:1 Quantum Efficiency
- B. N. P. Barnes, Quantum Efficiency Lighting - Quantum Efficiency Greater than Unity Prospects
- C. J. M. Collins, A Computer Program to Calculate Energy Mismatches

Appendix 10A: Potential Lanthanide Series Atoms for a 2:1 Quantum Efficiency

Norman P. Barnes, Task 10 Member

Introduction

There are several potential candidates for a 2:1 quantum efficiency among the lanthanide series atoms, including Pr and Gd. Potential 2:1 candidates are described below. The efficacy of the potential candidates depends critically on the choice of the host material. Choice of the best host material could be made using measurements of the germane spectroscopic parameters. However, this would require obtaining and measuring a plethora of materials if the information is not available in the open literature. Fortunately, the needed spectroscopic parameters, including the energy transfer rates, can also be approximated through calculations. The physics and calculation procedures of the 2:1 quantum efficiency are outlined in the appendix. The candidates depend on the excitation wavelength. The discussion below is separated into the candidates that can be excited utilizing a Hg discharge and the candidates that require a shorter excitation wavelength.

Technical Discussion

A few simple observations concerning the nature of the spectra of lanthanide series atoms can be used to simplify the search. First, the lanthanide series atoms that are represented as a single 4f electron or the equivalent of a single 4f hole, specifically Ce and Yb respectively, can be eliminated because they lack the needed intermediate manifolds. Conversely, lanthanide atoms with too many 4f electrons or the equivalent 4f holes have too many manifolds. Numerous manifolds abet nonradiative decay and therefore detract from the quantum efficiency. Therefore, Pm, Sm, Eu, Tb, Dy, and Ho do not have a high probability of having a metastable manifold that promotes a 2:1 quantum efficiency. Pm also has no stable isotopes and is therefore eliminated from consideration. This leaves Pr, Nd, Gd, Er, and Tm as likely candidates.

There are many common situations where 1 atom absorbs the exciting radiation and subsequently transfers all or part of the absorbed energy to another atom. In these cases, the atom that absorbs the exciting radiation is referred to as the sensitizer. On the other hand, the atom, which receives all, or part of the absorbed energy from the sensitizer is referred to as the active atom. This nomenclature is utilized in describing lasers.

Lanthanide series atoms that can be excited by 0.254 μm radiation include Nd, Gd, and Er. To promote the 2:1 quantum efficiency, a metastable manifold should exist at or slightly below the manifold used for excitation. Nd could possibly meet this requirement because the gap between the $^2F_{5/2}$ manifold and the next lowest manifold, the $^2H_{11/2}$ manifold, is about 4000 cm^{-1} . Unfortunately, the gap in Gd and Er is less than 3000 cm^{-1} . This detracts from a high potential quantum efficiency because the excited manifold has an increased nonradiative decay rate.

If a Nd atom is excited to the $^2F_{3/2}$ manifold and relaxes to the $^2F_{5/2}$ manifold, there is a reasonable probability that it can successfully transfer part of its energy to another lanthanide series atom. However, after sharing part of its energy with a second lanthanide series atom, the Nd atom is likely to relax by nonradiative transitions to the $^4F_{3/2}$ manifold. This manifold is too low to produce a visible photon. Thus the prospects of Nd being an useful 2:1 quantum efficiency under Hg excitation are not bright.

Gd, when excited by a 0.254 μm photon, will probably relax to the $^6P_{7/2}$ manifold. As there are no intermediate manifolds between this manifold and the ground manifold, beneficial energy sharing is not likely.

Er, when excited by a 0.254 μm photon, is likely to relax to the $^2P_{3/2}$ manifold. This manifold may be metastable in a host material with low phonon energies. The $^4S_{3/2}$ manifold is lower in energy than the $^2P_{3/2}$ and the most likely to be metastable. The energy gap between the $^2P_{3/2}$ and the $^4S_{3/2}$ manifold is too small to produce an useful photon. Another possibility for a metastable manifold is the $^4F_{9/2}$ manifold. This manifold could self quench the $^2P_{3/2}$ manifold and produce 2 red photons if nonradiative transitions do not relax the manifolds too quickly. Thus, Er remains a possibility if a low phonon energy host material can be used.

If a more energetic photon is used to excite the lanthanide series atom, more possibilities exist. To avoid the problems associated with nonradiative relaxation processes, Pr, Gd, and Tm are considered. Pr is attractive if the 1S_0 manifold can be excited. Direct excitation of this manifold would be difficult unless the source were narrow and coincided with the absorption features of the 1S_0 manifold. Unfortunately, this absorption feature is approximately at 47000 cm^{-1} ,

somewhat too long for a Xe resonance excitation. Fortunately, there are $4f^n$ to $4f^{n-1}5d$ transitions somewhat above 50000 cm^{-1} . If absorption occurred on this transition, it may well relax to the 1S_0 manifold. From this manifold, a 2:1 quantum efficiency is possible. Gd can possibly be excited in the 6G_i or 6F_j manifolds. Unfortunately, the nearby $^2G_{7/2}$ manifold does not correspond closely to the Xe resonance line. However, if properly excited, the Gd will quite likely relax to the $^6G_{3/2}$ manifold, a manifold that is likely to be metastable. From here, it is likely that an useful energy transfer process can occur. Like Pr, Tm also has a 1S_0 manifold but it is much higher than the similar manifold in Pr, somewhat too high to be excited utilizing the Xe resonance line. Consequently, it is not likely that Tm atom can be excited via a $4f^n$ to $4f^n$ transition. However, it may still be possible that a $4f^n$ to $4f^{n-1}5d$ transition can occur and yet retain a beneficial energy transfer process, possibly in Pr or Gd. As a result, the likely initial lanthanide series atoms are Pr and Gd.

Having tentatively identified candidate initial lanthanide series atoms, or sensitizers, another lanthanide series atoms to participate in the energy transfer process, or active atoms can be identified. These atoms should have a metastable manifold with an energy such that useful visible photons can be produced. A table listing potential active atoms appears below. Energy levels depend on the particular host material and are therefore approximate.

Atom	Metastable Manifold	Energy cm^{-1}	Possible Wavelengths
Pr	3P_0	20500	0.49 to 0.65
Pr	1D_2	16700	0.61 to 0.69
Sm	$^4G_{5/2}$	17900	0.56 to 0.70
Eu	5D_0	17300	0.58 to 0.70
Tb	5D_4	20700	0.48 to 0.68
Dy	$^4F_{9/2}$	21200	0.48 to 0.66
Tm	1G_4	21400	0.47 to 0.66

An approximate energy resonance is a requirement for a lanthanide series sensitizer to efficiently transfer energy to an active atom. Using this as a criterion, it is possible that a Gd atom in the $^6G_{7/2}$ manifold can participate in an efficient energy transfer with Pr 1D_2 and the Eu 5D_0 . The energy remaining with Gd can then be transferred to another lanthanide series atom. Among possible atoms are Eu, Tb, or Dy. In these cases, energy transfer may not be directly to the metastable manifold but to a higher energy manifold. From the higher manifolds, a nonradiative decay would likely bring the lanthanide series atom to the metastable manifold. Eu is an attractive choice as it would simplify the phosphor. The other possibilities tend to require too much energy. Conversely, it is likely that Pr 1S_0 can support an efficient energy transfer to produce an excited Sm, Eu, Tb, Dy, or possibly Pr.

Several possible colors can be produced from many of the lanthanide series atoms. Which transition will dominate the fluorescent decay from a metastable manifold is described by the manifold to manifold branching ratio. Although these branching ratios tend to follow a similar pattern for different host materials it does depend on the specific host material. Thus, some amount of wavelength selection is probable.

At this point, it appears that there are at least 2 good possibilities for achieving a 2:1 quantum. In 1 case, a Pr atom absorbs Xe excitation, possibly using $4f^n$ to $4f^{n-1}5d$ transition. From here, it relaxes to the 1S_0 manifold. From this metastable manifold, it could fluoresce to the 3P_1 or 1I_6 manifolds or it could transfer energy to the Eu 5D_1 manifold that in turn would produce visible photons. From the 3P_0 manifold, the Pr could fluoresce to the 3H_1 manifolds or could transfer energy to the Tb 5D_4 manifolds that in turn would produce visible photons. In another case, Gd would absorb the Xe excitation. Because the Gd absorption is weak, perhaps another lanthanide series atom would absorb and transfer the energy to Gd. The Gd would relax to the $^6G_{7/2}$ manifold from which it could fluoresce to the 6P_1 manifold or it could transfer to either Pr or Eu that, in turn, would produce visible photons. From the 6P_1 manifold, the energy could be transferred to either Eu or Tb. The Eu would relax to the 5D_3 or 5D_0 manifold which would then produce the visible photons. The Tb would relax to either the 5D_3 or 5D_4 manifold which would then produce the visible photons.

The wavelengths produced by the lanthanide series atoms depends on the particular host material. Methods of analyzing the potential of the various host materials have been outlined in the interim report. Also, the radiative and nonradiative lifetimes as well as the energy transfer rates are dependent on the host material. For example, order of magnitude differences in the energy transfer parameters were predicted and observed in different laser materials. Thus, the recommended next step is the calculation of the germane parameters for the potential candidates for various host materials. Once promising host materials have been identified, spectroscopic measurements can confirm and refine the calculations.

We can make the following conclusions:

There are many possible combinations of lanthanide series atoms that could produce a 2:1 quantum efficiency. From the first order analysis outlined below, Pr and Gd appear to be the most promising lanthanide series atoms. The efficiency with which the 2:1 process will occur depends critically on the host material. Choice of the host material will affect the dynamics of the situation because the various rates, such as the energy transfer rate and the nonradiative decay rate, vary an order of magnitude or more depending on the host material. Fortunately, there is a plethora of host materials from which to choose. It is probable that a favorable host can be found.

The following recommendations are in order:

Germane spectroscopic parameters should be determined for Pr and Gd in promising host materials. These parameters can be approximated using the quantum mechanical approach outlined in the appendix or measured using standard spectroscopic techniques. A dual approach will probably produce the best results. Specifically, the quantum mechanical model can be used to identify potential host materials and detailed spectroscopic measurements can verify and refine the predictions for selected host materials.

Appendix 10B: High Efficiency Lighting Quantum Efficiency Greater than Unity Prospects

Norman Barnes, Task 10 Member

Technical concerns associated with high quantum efficiency lighting are considered. Present fluorescent lamps are limited in efficiency by the large quantum defect between ultraviolet photon that excites the phosphor and the visible photon that is emitted by the phosphor. An appealing method of improving the efficiency of the lighting is to employ a phosphor that emits 2 visible photons for each ultraviolet photon absorbed. This is energetically possible, at least to a degree, with the present Hg discharge fluorescent lamps. Discharges with more energetic ultraviolet photons may be more favorable to this possibility. The technical issues associated with implementing a high quantum efficiency are explored.

There exists a plethora of possible fluorescent schemes and material combinations that may produce 2 visible photons for a single absorbed ultraviolet photon. With so many possibilities the probability of finding a suitable candidate appears good. However, there are too many to analyze in the time available. Within the available time interval, the physics issues that need to be considered can be identified, the basic formalism germane to the evaluation of the quantum efficiency can be approximated, and some possible contenders for a high quantum efficiency phosphor can be identified.

It is likely that a phosphor having a quantum efficiency greater than 1 can be achieved but it will likely require the use of 2 lanthanide series atoms. A likely scenario would have 1 lanthanide atom absorb the ultraviolet photon. It would then transfer part of the energy to another lanthanide series atom. The remaining energy would produce a visible photon. The second lanthanide series atom would produce the second visible photon. Each atom has a certain probability of undergoing the processes that produce any useful visible photon. The entire process can be characterized by a single parameter that is related to the probability that these processes occur and is referred to as the quantum efficiency. If 2 visible photons are produced upon the absorption of an ultraviolet photon, the quantum efficiency is 2. If no visible photons are produced, the quantum efficiency is 0.

To determine the quantum efficiency, several parameters must be known. For example, if the 2 lanthanide series atoms transfer energy, this process is characterized by an energy transfer parameter. The efficiency of this energy transfer process is dependent on the spectra of the lanthanide series atoms, their concentrations and the properties of the host material. Data, such as the energy transfer parameters may be either calculated or found in the literature.

Data needed to determine the quantum efficiency is host dependent and is not commonly available in the open literature but can be calculated. Among the needed data are the emission and absorption spectra, the radiative lifetime of the manifolds involved, the branching ratios, the nonradiative lifetime, and the operative energy transfer parameters. These parameters are both host material and concentration dependent. For example, the energy transfer is a resonant process and the transition frequencies are dependent on the host material. Thus, a huge number of possibilities for a high quantum efficiency phosphor exist. In addition, parameters such as energy transfer rates are difficult to measure and have not been widely researched and published.

Furthermore, several parameters must be known for a reasonable evaluation, not just 1 or 2 of the parameters. The required parameters could possibly be available in the open literature or could be calculated. In either case, it is imperative to understand the physics issues and to predict which combination of lanthanide series atoms, which concentrations of these atoms, and what host materials are fruitful areas for further investigation.

Potential Discharges

Hg is used in the presently available fluorescent lamps and may support a higher quantum efficiency. If Hg is used, strong emission exists at 0.254 μm . These ultraviolet photons are then absorbed by phosphors that are located on the lateral surfaces of the fluorescent tube. These phosphors emit in the visible region of the spectrum, the center of which is about 0.555 μm . Because of the quantum defect, the efficiency of fluorescent lamps is limited to 0.46. It is highly appealing to consider a system that produces 2 fluorescent photons after absorbing a single ultraviolet photon. This is energetically possible and could double the efficiency of fluorescent lamps.

Although the average visible photon wavelength is about 0.555 μm ; to create white light red, green, and blue photons are required. Required approximate wavelengths are 0.450, 0.555, 0.610 μm , respectively although there is a degree of tolerance in the exact wavelengths. While 2 green photons can be produced by a single 0.254 μm ultraviolet photon, it is not energetically possible to produce 2 blue photons after absorbing a single ultraviolet photon. To be able to produce blue photons in the proper ratio, an ultraviolet wavelength that is sufficiently energetic to generate 2 blue photons may be sought. It also may be desirable to avoid the use of Hg in the fluorescent lamp to avoid environmental concerns. From this point of view, noble gasses, except for radon, are appealing.

When considering other possible discharges, other material properties in addition to the emission wavelength need to be considered. An important material property to consider is the vapor pressure. Specifically, a gaseous discharge is preferred to produce a resonant line emission spectrum. Besides Hg, other discharges that can produce ultraviolet photons are listed in the table below.

Table B-32
Emission Spectra in Electric Discharges

Atom	Resonant line	Continuum
H	0.1026, 0.1216	0.160-0.500
He	0.0537, 0.0584	0.058-0.110
Ne	0.0736, 0.0744	0.070-0.100
Ar	0.1048, 0.1067	0.105-0.155
Kr	0.1164, 0.1235	0.124-0.180
Xe	0.1295, 0.1470	0.147-0.200

As a zeroth order approximation, the resonant wavelength should be longer than half of the Hg resonant line wavelength. Suppose that the Hg discharge efficiency and the discharge listed above are approximately equal. Given that, and the fact that the Hg discharge produces 1 visible photon, a discharge with a resonant line with half the wavelength must produce 2 visible photons to achieve the same efficiency. This quickly focuses the possible discharges on Xe. Fortunately, Xe discharges have been used for years to pump solid state lasers and have proven to be quite efficient.

The discharge must be designed to enhance the production of the ultraviolet photons. Continuous Xe discharges used to pump solid state lasers are usually near atmospheric pressure devices that produce line dominated spectra mainly in the near infrared. The pressure and the electric field of the Xe discharge must be designed to favor the production of ultraviolet photons. Such a design is beyond the scope of this investigation.

Other discharge considerations must be taken into account for a practical lighting system. Continuous Xe discharges used for pumping solid state lasers need to be initiated with a high voltage transient to create a few ions. These ions are needed to initiate the discharge. A second discharge is usually used, in essence, to warm up the lamp to a point where the primary discharge can be sustained at its operating point. This is similar to the fluorescent lamps with a starter circuit.

Phosphors

The prime candidates for phosphors with narrow emission features are the lanthanide series atoms. In these atoms the emission features result from transitions of the 4f electrons. Because the 4f electrons are shielded from the electric field of the crystal lattice by the 5s and 5p electrons, the emission features can be narrow and lifetimes can be long. The long lifetimes allow time for efficient energy transfers to occur between the lanthanide series atoms.

Other possible atoms for phosphors include the transition metal atoms and actinide series atoms. Transition metal atom emission features result from transitions of the 3d electrons. Because these 3d electrons are not shielded from the crystal field, they are strongly affected by the electric field of the crystal lattice. Consequently, the transition metal emission features are affected by lattice vibrations and tend to be wide. Lattice vibrations promote nonradiative decay via multiphonon processes that, in turn, decrease the quantum efficiency. On the other hand, the emission features of the actinide series atoms are produced by transitions of the 5f electrons. Even though the 5f electrons are shielded from the crystal field, they are radioactive, severely limiting their potential use in commercial or residential lighting applications. Considering the limitations of these atoms, the focus of this investigation will be on the lanthanide series atoms.

To achieve a high quantum efficiency, the following steps may occur. Where 2 or more possibilities exist, they are listed with different letters. The steps that are necessary are noted in the following:

1. The first step is the absorption of an ultraviolet pump photon. It is preferable that a lanthanide series atom is the absorbing atom. However, it may be possible to have the host material absorb the pump radiation and transfer the energy to the lanthanide series atom.

2. Once the lanthanide series atom is excited, it may relax by a nonradiative transition to a metastable manifold. A small energy decrement between the excited manifold and the metastable manifold is needed. If the energy decrement is too large, a quantum efficiency of 2 will not be possible. Because a strong absorption feature is needed to minimize the amount of phosphor material required, the lifetime of the absorbing manifold is apt to be short. If there is no relaxation to a metastable manifold the excited manifold is apt to fluoresce emitting the recently absorbed ultraviolet photon.
3. A visible photon may be generated through a transition from this metastable manifold to some lower manifold. For a high quantum efficiency, this transition can use only about half of the energy of the ultraviolet photon. However, there may also be an energy transfer to second lanthanide series atom.
4. Energy transfer from the initially excited lanthanide series atom to a second lanthanide series atom that in turn will produce a visible photon. As before, only about half of the energy of the ultraviolet photon is transferred in the process. The energy transfer to this second atom may be followed by a nonradiative transition to a metastable manifold. From the second metastable manifold, a visible photon can be produced.
5. After a visible photon is produced by either 3 or 4 above, another nonradiative transition to another metastable manifold is probably needed. Again, the energy decrement should be small so that 2 visible photons can be produced from a single pump photon.
6. A second visible photon can be produced by the initial lanthanide series atom through a transition from the second metastable manifold to a lower manifold. After emitting the second photon, the lanthanide series atom relaxes to the ground manifold probably via a nonradiative transition. At this point, a single lanthanide series atoms produces 2 visible photons.
7. An energy transfer process can occur from the second metastable manifold of the first lanthanide series atom to a second lanthanide series atom. After the energy transfer, the first lanthanide series atom relaxes to the ground manifold.
8. Another nonradiative relaxation process can occur in the second lanthanide series atom to a metastable manifold. As before, the energy decrement should be small to preserve the efficiency.
9. A second visible photon can be produced by the second lanthanide series atom. After producing the second visible photon, the second lanthanide series atom can relax to the ground manifold, probably by nonradiative transitions.

Other more complicated schemes to produce 2 visible photons from a single absorbed ultraviolet photon are possible. However, the probability that these more complicated schemes would be more efficient than those outlined above is diminished. A diminution is a result of the probability that more nonradiative processes will deplete the energy of the absorbed ultraviolet photon.

Properties of the host material can abet the high quantum efficiency process. Desirable properties include ultraviolet transmission, low phonon energy spectrum, and a trivalent site. For a Hg ultraviolet source, the transmission should extend to 0.254 μm . For a Xe source,

the transmission should extend to 0.130 μm . The transmission requirement eliminates many potential materials. Possible host materials are listed in Table B-33.

Table B-33
Properties of Host Materials

Material	UV Cutoff	Phonon Peak	Site Valence
SiO_2	0.12	1100 cm^{-1}	4+
Al_2O_3	0.15	920 cm^{-1}	3+
LiF	0.10	310 cm^{-1}	1+
CaF_2	0.13	cm^{-1}	2+

Several materials can serve as a host materials If a Hg source is used. However, if a Xe source is used, the ultraviolet transmission is more of a problem.

Quantum Efficiency Physics

The quantum efficiency can be approximated if sufficient spectroscopic information is available. This is approximated using a product of efficiencies approach.

Given the ultraviolet excitation wavelength, the first step is the absorption this photon. Absorption can be characterized by an absorption coefficient, β_a . If d is the average particle diameter, the photon absorption efficiency, η_{PA} , is approximately

$$\eta_{\text{PA}} = 1 - \exp(-\beta_a d).$$

Once the ultraviolet photon is absorbed, the excited atom will probably relax to a metastable manifold. This may occur by a single radiative transition to the metastable manifold or in several steps via nonradiative transitions. If the metastable manifold is immediately below the pumped manifold, the lifetime of the pumped manifold, τ_p , is

$$1/\tau_p = 1/\tau_{\text{NR}} + \sum_j \beta_{pj}/\tau_R$$

where τ_{NR} is the nonradiative lifetime, β_{pj} is the manifold to manifold branching ratio and τ_R is the radiative lifetime. Assuming that the metastable manifold is immediately below the pumped manifold, the fraction of the excited atoms that come to reside in the metastable manifold is approximately

$$\eta_Q = [1/\tau_{\text{NR}} + \beta_{\text{PQ}}/\tau_R]\tau_p.$$

Similar expressions can be derived if the metastable manifold is not immediately below the pumped manifold.

In general, manifolds with a long nonradiative lifetime are preferred. A long nonradiative lifetime necessitates having a large energy gap to the next lowest manifold and a host material with a low phonon energy. The nonradiative lifetime can be described by

$$1/\tau_{NR} = C[\exp(-h\nu_p/kT)/(\exp(-h\nu_p/kT) + 1)]^n \exp(-\alpha\Delta E_g)$$

where C and α are constants that are material dependent, ν_p is the maximum phonon frequency, T is the temperature, ΔE_g is the energy gap, and

$$n = \Delta E_g/h\nu_p.$$

Thus, metastable levels with a large energy gap and materials with a low maximum phonon energy are sought. Maximum phonon energies for candidate host materials are listed in Table B-33.

If the lanthanide series atom is in a metastable manifold, it can emit a photon. Given that the manifold is metastable, it is implied that the nonradiative lifetime is long. If this is true, the nonradiative decay rate can be ignored. However, there can be several radiative transitions. If only 1 of these transitions is useful, the probability that the useful transition occurs is β_{Q1} .

Manifold to manifold branching ratios describe the fraction of the fluorescence that is associated with the transitions from a specific manifold to all lower manifolds. In principle, there can be transitions between the given manifold and all of the manifolds below it. In actuality, selection rules make some of the transitions rather improbable. Nevertheless, lower lying metastable manifolds are preferred for this application because there are fewer manifolds to which radiative transitions can occur. Thus, with fewer manifolds to which the transition can occur, the probability of the desired transition occurring is increased. Some branching ratios have been measured for the lower lying manifolds of a few materials such as Nd:YAG [195], Ho:YLF [196], and Tm:YLF [196]. In general, the branching ratios are not known for most materials.

If an energy transfer process is needed, the probability that it occurs depends both on the lifetime of the manifold and the energy transfer rate. If the lifetime of the manifold is τ_p , the differential equation describing the energy transfer process can be approximated as

$$\frac{dN_i}{dt} = -\frac{N_i}{\tau_i} + P_{ij}N_iN_j$$

where P_{ij} is the energy transfer coefficient, N_i is the density of atoms in the upper manifold, and N_j is the density of atoms in the lower manifold. In this expression, τ_i is a combination of the radiative and nonradiative decay rates. To maximize the energy transfer rate, the density of atoms in the lower manifold should be as high as practical, faster than the fluorescent decay rate, τ_i . This implies that the lower manifold should be the ground manifold so that N_j is large. Restricting the lower manifold to the ground manifold significantly simplifies the search for prospective schemes. Under this approximation, the efficiency of the energy transfer process can be approximated as

$$\eta_T = P_{ij}N_j\tau_i/(1 + P_{ij}N_j\tau_i).$$

The energy transfer parameters depend on the properties of the host material. Although not commonly done, energy transfer parameters can be calculated using [197]

$$P_{ij} = (9\pi(h/2\pi)^7 c^6 / 8n^6 R^6) (E/\epsilon_r^{1/2} E_c)^2 \sum_{ij} \sum_{\alpha\beta} \int dE (Z_{is} Z_{ia} / Z_s Z_a) \\ g(E - E_{ifs}) g(E - E_{ifa}) / (\tau_{ifa} \alpha \tau_{ifs} \beta E_{ifa} E_{ifs}) \\ [(2+\alpha+\beta)!(2-\alpha-\beta)!/(1+\alpha)!(1-\alpha)!(1+\beta)!(1-\beta)!] C_{2,\alpha+\beta}(R)$$

for a dipole dipole interaction where $\tau_{ifa}\alpha$ and $\tau_{ifs}\beta$ is the level to level lifetimes for the transition from the i to j manifold and R is the distance between the interacting atoms. In cases where a dipole quadrupole or quadrupole quadrupole interaction is effective, the power of R is 8 or 10, respectively. Because of the energy resonant denominator, the largest contributions to the summation come from the level where resonance is achieved. In turn, the energy levels responsible for the resonance are dependent on the host material. Therefore, the energy transfer rate is highly dependent on the host material.

The above approximation works well for low concentrations of atoms. At higher concentrations, diffusion can promote even faster energy transfer rates. The simple exponential decay as described above becomes faster than a single exponential. This faster decay results from the quantum of excitation being able to diffuse or migrate among the lanthanide series atoms of the same type. The process of diffusion permits the quantum of excitation to migrate to lanthanide series atoms that are more favorably situated for the energy transfer processes. Although the diffusion problem has been addressed in the literature, there is not universal acceptance of a single energy diffusion and energy transfer description.

Both modeling and supportive experimental work have been performed on describing the energy transfer process [197]. This work concentrated on lower lying manifolds associated with the Ho:Tm laser. However, there is no reason to believe that the same approach would not work with the higher lying manifolds associated with the visible portion of the spectrum.

With the above definitions, the quantum efficiency, η_{QT} , is approximated as

$$\eta_{QT} = 2\eta_A \eta_{Q1} \beta_{Q1} \eta_T \eta_{Q2} \beta_{Q2}$$

This expression uses manifold to manifold branching ratios rather than level to level quantum efficiencies. The factor of 2 arises because there are 2 visible photons created. Quantum efficiency is the quantity that should be optimized. Several approximate, closed form expression to evaluate the individual factors are given above.

Thus, given enough spectroscopic information about a host material, the quantum efficiency of that candidate can be approximated. The problem is obtaining good spectroscopic data.

Appendix 10C: A Computer Program to Calculate Energy Mismatches

Task 10 Member: John M. Collins

The fundamental objective of this computer program is to calculate energy mismatches for all possible energy transfer paths. Naturally, the only viable paths are those in which the energy mismatch is small. Specifically, the program does the following:

1. Reads from an Excel file the energy levels of any two rare earth ions; one is labeled as sensitizer and the other as activator. Our energy levels include all manifolds and Stark levels of trivalent rare earth ions in LaCl_3 as recorded in Dieke's text [198].
2. Finds the differences in energy among all pairs of energy levels within each ion.
3. Calculates the energy difference between each pair of levels of the sensitizer and each pair of levels of the activator. That is, we calculate the energy mismatches of transfers between all combinations of pairs of levels.

The results of the calculations and the details of the analysis can be summarized as follows:

With 13 trivalent RE ions, the RE to RE energy transfer involving two ions has $13^2 = 169$ possible ion pairs. Excluding Yb and Ce (which have no levels that emit in the visible) and Pm (radioactive), this limits the number to 100 possible combinations. Thus far, Pr and Gd have shown demonstrated the most promising likelihood of a single UV absorption leading to the emission of two visible photons. Dismissing systems in which Gd and Pr act as both sensitizer and activator, we have concentrated on these two ions in the role of the sensitizer, and examined 18 ion pairs: Pr to REI and Gd to REI.

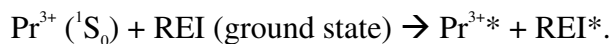
The most likely candidates for shifting the first photon of Pr are Eu and Er, which show 15 and 9 viable transfer paths, respectively. Tb, an efficient emitter, shows only two viable transfer paths, and in addition has the problem of the 4f-5d band lying below the 1S_0 level of Pr, meaning it would compete with Pr in absorption. Thus it is less worthy of serious consideration. Other ions also show possible paths (e.g. Sm has 9 possible paths for transfer from the 1S_0 level of Pr), but most result in the second Pr photon being in the infrared and/or the activator does not emit efficiently in the visible.

We note that each of the recommended activators has drawbacks. Eu has a charge transfer state at low energies in many hosts. Er emits in the infrared as well as the visible, and so even if the transfer is 100% efficient, quantum yield in the visible for that energy will be less than unity. Because these drawbacks are host-dependent, they may be relevant considerations in the search for a suitable host.

The most likely candidates for shifting the first photon of Gd are Eu and Pr. Though the Gd to Eu transfer leads to visible emission by only one path, that transfer path is not in competition with any other. If transfer occurs, Eu will emit with a quantum efficiency of near unity. The transfer has been observed [199], and so additional studies of this transfer are warranted. One potential problem, as noted elsewhere, is the charge-transfer state of Eu competing for the UV absorption with Gd. With Pr as an activator, the Gd to Pr transfer has three viable transfer paths. Two of those paths lead to Pr in the 1D_2 level, which can emit in the visible or in the infrared. Since the 1D_2 to 3H_4 emission at $16,800\text{ cm}^{-1}$ has been found to dominate emission from the 1D_2 [200], further study of Pr as an activator for Gd is warranted. The low lying 4f-5d band of Pr presents a problem for this scheme, so care must be taken in the selection of a host material.

Pr to REI Energy Transfer

We present the results of calculations of energy mismatches of the following transfer:



The final states of Pr and the REI can be any of a variety of $^{2S+1}L_J$ manifolds. The goal is to find a REI such that both ions emit in the visible once the above transfer has occurred. Listed in this appendix are the transfer paths for which the energy mismatch is between 2000 cm^{-1} and -1000 cm^{-1} . A negative energy mismatch means that energy must be absorbed from the lattice in order to conserve energy. The energy levels used are of REI in LaCl_3 taken from Dieke's text, *Spectra and Energy Levels of Rare Earth Ions in Crystals*. (The Tm^{3+} energy levels are from the YCl_3 host.) Only the lowest level of each manifold was considered in these calculations. We show wide range of energy mismatches recognizing that the energy levels shift from host to host, are split by the crystal field, and that energy transfer can be efficient even if it is phonon-assisted. Somewhat arbitrarily, we term as 'viable' those transitions with an energy mismatch between 1200 cm^{-1} and -500 cm^{-1} .

Pr to Nd

Table B-34
Pr to Nd Transfer Paths

Pr (Initial)	Pr (Final)	Nd (Initial)	Nd (Final)	Energy Mismatch (cm-1)
1S0	1I6	4I9/2	2P1/2	1986
1S0	1D2	4I9/2	4D3/2	1896
1S0	1D2	4I9/2	4D5/2	1764
1S0	3P1	4I9/2	2D5/2	1674
1S0	1D2	4I9/2	2I11/2	1659
1S0	1I6	4I9/2	2D5/2	1441
1S0	1D2	4I9/2	4D1/2	1354
1S0	3P2	4I9/2	2P1/2	1078
1S0	3P2	4I9/2	2L15/2	651
1S0	3P2	4I9/2	2D5/2	533
1S0	3P0	4I9/2	2P3/2	-110
1S0	1D2	4I9/2	4D7/2	-174
1S0	1D2	4I9/2	2I13/2	-242
1S0	3P1	4I9/2	2P3/2	-701
1S0	1I6	4I9/2	2P3/2	-934

There are 6 viable transfer paths. Of these 6 paths, two have the Pr final state as the 1D_2 manifold, which emits both in the visible and the infrared. The other four lead to emission from the 3P_0 level. Several of the Nd final states lead to visible emission, but the close spacing (\leq about 3000 cm^{-1}) of the Nd levels makes high efficiency in the visible unlikely. Still, there are several possible transfer channels, and if the proper host is found, there is an outside chance Nd could be a useful activator.

Pr to Sm

There are 9 viable transfer paths, all of which lead to Pr emitting from the 3P_0 level. The excited Sm ions will all decay nonradiatively to the $^4G_{5/2}$ level ($17,850\text{ cm}^{-1}$), from which they will then emit efficiently, since the next lowest manifold is separated by over 7000 cm^{-1} . The actual amount of emission from Sm in the visible will be host-dependent, but the sheer number of possible transfer paths, that the Pr emission exclusively from the 3P_0 state, and that the Sm state will emit radiatively with a very high efficiency makes Sm a good candidate for study. One potential problem is the tendency for Sm to substitute in its divalent state in some hosts.

Table B-35
Pr to Sm Transfer Paths

Pr (Initial)	Pr (Final)	Sm (Initial)	Sm (Final)	Energy Mismatch (cm-1)
1S0	1I6	6H5/2	4K11/2	1981
1S0	3P2	6H5/2	4F9/2	1768
1S0	3P0	6H5/2	4K11/2	1697
1S0	3P1	6H5/2	N1	1434
1S0	1I6	6H5/2	N1	1201
1S0	3P1	6H5/2	4K11/2	1106
1S0	3P2	6H5/2	4K11/2	1073
1S0	3P0	6H5/2	O'1	1040
1S0	1I6	6H5/2	4K11/2	873
1S0	3P1	6H5/2	O'1	449
1S0	3P2	6H5/2	N1	293
1S0	1I6	6H5/2	O'1	216
1S0	3P2	6H5/2	4K11/2	-35
1S0	3P2	6H5/2	O'1	-692

Pr to Eu

The Pr to Eu transfer paths above include the initial state of Eu to be the ground state (7F_0), or the first excited manifold (7F_1). The 7F_1 is included because it is only 355 cm^{-1} above the ground state, and may be appreciably populated at lamp operating temperatures. The results show a total of 15 viable transfer paths. All paths lead to Pr emission from the 3P_0 level. All of the Eu final states are in the 5D_3 level or above, and will lead to efficient red emission from the 5D_0 . These factors make Eu an excellent candidate for converting the first Pr photon into the visible. The drawback with Eu lies in the fact that in some hosts it has a charge transfer absorption band at low energies.

Table B-36
Pr to Eu Transfer Paths

Pr (Initial)	Pr (Final)	Eu (Initial)	Eu (Final)	Energy Mismatch (cm-1)
7F_0 initial Eu level				
1S0	1D2	7F0	F1	1978
1S0	3P0	7F0	5D3	1651
1S0	1D2	7F0	G1	1497
1S0	3P1	7F0	5D3	1060
1S0	3P0	7F0	5L6	843
1S0	1I6	7F0	5D3	827
1S0	3P1	7F0	5L6	252
1S0	1I6	7F0	5L6	19
1S0	3P2	7F0	5D3	-81
1S0	3P0	7F0	B1	-166
1S0	3P0	7F0	C1	-589
1S0	3P1	7F0	B1	-757
1S0	3P2	7F0	5L6	-889
1S0	1I6	7F0	B1	-990
7F_1 initial Eu level				
1S0	1D2	7F1	G1	1852
1S0	3P1	7F1	5D3	1415
1S0	3P0	7F1	5L6	1198
1S0	1I6	7F1	5D3	1182
1S0	3P1	7F1	5L6	607
1S0	1I6	7F1	5L6	374
1S0	3P2	7F1	5D3	274
1S0	3P0	7F1	B1	189
1S0	3P0	7F1	C1	-234
1S0	3P1	7F1	B1	-402
1S0	3P2	7F1	5L6	-534
1S0	1I6	7F1	B1	-635
1S0	3P0	7F1	D1	-760
1S0	3P1	7F1	C1	-825

Pr to Gd

Due to the fact that the 1st excited state of Gd is at about 32,000 cm⁻¹, there are no viable transfer paths for Gd to convert the first photon of Pr into the visible region.

Pr to Tb

Table B-37
Pr to Tb Transfer Paths

Pr (Initial)	Pr (Final)	Tb (Initial)	Tb (Final)	Energy Mismatch (cm-1)
1S0	3P0	7F6	5D3	-242
1S0	3P0	7F6	5L10	-347
1S0	3P1	7F6	5D3	-833
1S0	3P1	7F6	5L10	-938

There are two viable transfer paths, both of which lead to Pr emission from the 3P_0 level. Also, both transfer paths result in Tb excitation to, or above, the 5D_3 manifold. At proper Tb concentrations, this leads to efficient green emission from 5D_4 manifold. That the two transfer paths both require energy to be absorbed from the lattice may be problematic. A host should be sought for which these energy mismatches are ≥ 0 . Also the low-lying 4f-5d band of Tb may compete with Pr for the exciting UV photon. Because it is such a strong emitter, and because there are some viable transfer paths, further work on Tb is warranted, albeit in a limited manner. Again the results will be very much host dependent.

Pr to Dy

Table B-38
Pr to Dy Transfer Paths

Pr (Initial)	Pr (Final)	Dy (Initial)	Dy (Final)	Energy Mismatch (cm-1)
1S0	1I6	6H15/2	4G11/2	1986
1S0	3P2	6H15/2	4G11/2	1078

There is only one viable transfer path, and for that path the energy mismatch is high enough so that it will have to be a phonon-assisted transfer in any host. In soft lattices such as fluorides, this transfer will involve more than one phonon, and so is not likely to be efficient. The Pr final state leads to emission from the 3P_0 level. The Dy final state leads to emission from the $^4F_{9/2}$ manifold at about $21,000\text{ cm}^{-1}$. This level emits anywhere from the blue-green to the infrared. Since Dy is not known as an efficient emitter in the visible, and because the transfer is likely to be inefficient, we do not consider Dy to be candidate for shifting the first Pr photon into the visible.

Pr to Ho

Table B-39
Pr to Ho Transfer Paths

Pr (Initial)	Pr (Final)	Ho (Initial)	Ho (Initial)	Energy Mismatch (cm-1)
1S0	3F4	5I8	3P2	1979
1S0	3F4	5I8	3L7	1961
1S0	3F3	5I8	3I7	1940
1S0	1D2	5I8	5G2	1897
1S0	1D2	5I8	3H6	1609
1S0	3F4	5I8	3I7	1518
1S0	3P1	5I8	5G5	1516
1S0	1I6	5I8	5G5	1283
1S0	1D2	5I8	5G3	1048
1S0	1D2	5I8	3L9	956
1S0	1G4	5I8	3F3	870
1S0	1G4	5I8	3F4	867
1S0	1G4	5I8	3H4	860
1S0	1G4	5I8	3F2	833
1S0	3P2	5I8	5G5	375
1S0	3P0	5I8	5G4	250
1S0	1G4	5I8	3G5	65
1S0	1D2	5I8	3K6	-28
1S0	3P0	5I8	3K7	-86
1S0	1D2	5I8	3F4	-170
1S0	3P1	5I8	5G4	-341
1S0	1I6	5I8	5G4	-574
1S0	3P1	5I8	3K7	-677
1S0	1D2	5I8	3D2	-878
1S0	1I6	5I8	3K7	-910

There are 13 viable transfer paths, but only four of them result in Pr emission from the 3P_0 level. The other paths result in emission from the 1G_4 (purely in the IR) or from the 1D_2 (IR and red), and so are of less use to the goal of visible emission. The Ho emission will be from any number of levels. The density of the Ho manifolds, however, is such that nonradiative decay is likely, so that Ho will not be an efficient visible emitter. This lack of visible emission from Ho and the fact

that 9 of the 13 transfer paths result in little or no visible emission from Pr lead us to conclude that Ho should not be explored further as an activator for Pr.

Pr to Er

Table B-40
Pr to Er Transfer Paths

Pr (Initial)	Pr (Final)	Er Initial	Er (Final)	Energy Mismatch (cm ⁻¹)
1S0	3P0	4I15/2	4G11/2	1994
1S0	3P1	4I15/2	4G11/2	1403
1S0	1I6	4I15/2	4G11/2	1170
1S0	3P0	4I15/2	2G9/2	979
1S0	3P0	4I15/2	2K15/2	724
1S0	1D2	4I15/2	2P3/2	695
1S0	3P1	4I15/2	2G9/2	388
1S0	3P2	4I15/2	4G11/2	262
1S0	1I6	4I15/2	2G9/2	155
1S0	3P1	4I15/2	2K15/2	133
1S0	1I6	4I15/2	2K15/2	-100
1S0	3P2	4I15/2	2G9/2	-753

There are 9 viable paths for energy transfer from Pr to Er. All of the transfer paths result in Pr emission from the 3P_0 level. All of the final levels of Er are above the green-emitting $^4S_{3/2}$ level, and non-radiative decay to the $^4S_{3/2}$ is an efficient process. (Note the $^2H_{9/2}$ may also emit in the green region.) A potential problem is that emission from the $^4S_{3/2}$ level is not 100% efficient due to nonradiative decay to the $^4F_{9/2}$ level, which sits about 3100 cm⁻¹ below the $^4S_{3/2}$. Also the $^4S_{3/2}$ emits to the $^4I_{13/2}$, with a corresponding wavelength of over 800 nm, useless to our goal of producing visible photons. The exact branching ratios of the Er levels involved will depend on the host. In summary, the number of transfer paths makes Pr to Er energy transfer likely. The main concern at this point is whether Er will emit efficiently in the visible. Since the first photon of Pr is basically useless in fluorescent lamp applications, any Er emission in the visible, even of modest efficiency, could result in quantum efficiencies above unity. We recommend, therefore, that Er be considered worthy of investigation as an activator to shift the first Pr photon.

Pr to Tm

Only one of the paths above is viable, and it results in no Pr emission in the visible. We recommend, therefore, against considering Tm as a candidate for shifting the first photon of Pr into the visible.

Table B-41
Pr to Tm Transfer Paths

Pr (Initial)	Pr (Final)	Tm (Initial)	Tm (Final)	Energy Mismatch (cm-1)
1S0	3F3	3H6	3P1	1348
1S0	1G4	3H6	3P0	1270
1S0	3F4	3H6	3P1	926
1S0	1G4	3H6	3P2	-718

Gd to REI Energy Transfer

We present the results of calculations of energy mismatches of the following transfer:



The final states of Gd and the REI can be any of a variety of $^{2S+1}\text{L}_J$ manifolds. The energy remaining with the Gd ion eventually leads to emission (or another transfer) from the $^6\text{P}_{7/2}$ level. The energy available to be transferred is less than about $17,000 \text{ cm}^{-1}$, and so at best will lead to the activator emitting in the orange-red spectral region. Listed in this appendix are only those transfer paths for which the energy mismatch is between 2000 cm^{-1} and -4000 cm^{-1} . A negative energy mismatch means that energy must be absorbed from the lattice in order to conserve energy. The energy levels used are of REI in LaCl_3 taken from Dieke's text, *Spectra and Energy Levels of Rare Earth Ions in Crystals*. (The Tm^{3+} energy levels are from the YCl_3 host.) Only the lowest level of each manifold was considered in these calculations. We show wide range of energy mismatches recognizing that the energy levels shift from host to host, are split by the crystal field, and that energy transfer can be efficient even if it is phonon-assisted. Somewhat arbitrarily, we term as 'viable' those transitions with an energy mismatch between 1200 cm^{-1} and -500 cm^{-1} .

Gd to Pr

Table B-42
Gd to Pr Transfer Paths

Gd (Initial)	Gd (Final)	Pr (Initial)	Pr (Final)	Energy Mismatch (cm-1)
6G7/2	6D7/2	3H4	3F4	1718
6G7/2	6P7/2	3H4	1D2	269
6G7/2	6D9/2	3H4	1G4	-270
6G7/2	6P5/2	3H4	1D2	-333
6G7/2	6P3/2	3H4	1D2	-913

There are three viable transfer paths. In two of these cases the Pr final state is the $^1\text{D}_2$ manifold, which emits both in the red and in the infrared. The quantum efficiency of emission in the visible will be host dependent. For the transfer path where the Pr final state is the $^1\text{G}_4$ manifold, the emission is entirely in the infrared. Thus, though Pr shows some potential for increased efficiency, it will depend on the branching ratios from the $^1\text{D}_2$ level and on the efficiency of the transfer. Although Pr may warrant some further investigation, it is not particularly promising as an activator for Gd.

Gd to Nd

Table B-43
Gd to Nd Transfer Paths

Gd (Initial)	Gd (Final)	Nd (Initial)	Nd (Final)	Energy Mismatch (cm-1)
6G7/2	6I7/2	4I9/2	4F3/2	1733
6G7/2	6P5/2	4I9/2	4F9/2	1592
6G7/2	6I9/2	4I9/2	4F3/2	1391
6G7/2	6I17/2	4I9/2	4F3/2	1336
6G7/2	6I11/2	4I9/2	4F3/2	1115
6G7/2	6P3/2	4I9/2	4F9/2	1012
6G7/2	6I15/2	4I9/2	4F3/2	997
6G7/2	6P7/2	4I9/2	2H11/2	993
6G7/2	6I13/2	4I9/2	4F3/2	962
6G7/2	6I7/2	4I9/2	4F5/2	699
6G7/2	6I7/2	4I9/2	2H9/2	621
6G7/2	6P5/2	4I9/2	2H11/2	391
6G7/2	6I9/2	4I9/2	4F5/2	357
6G7/2	6I17/2	4I9/2	4F5/2	302
6G7/2	6I9/2	4I9/2	2H9/2	279
6G7/2	6I17/2	4I9/2	2H9/2	224
6G7/2	6I11/2	4I9/2	4F5/2	81
6G7/2	6I11/2	4I9/2	2H9/2	3
6G7/2	6I15/2	4I9/2	4F5/2	-37
6G7/2	6I13/2	4I9/2	4F5/2	-72
6G7/2	6I15/2	4I9/2	2H9/2	-115
6G7/2	6I13/2	4I9/2	2H9/2	-150
6G7/2	6P3/2	4I9/2	2H11/2	-189
6G7/2	6P7/2	4I9/2	4G5/2	-195
6G7/2	6I7/2	4I9/2	4F7/2	-239
6G7/2	6P7/2	4I9/2	2G7/2	-329
6G7/2	6I7/2	4I9/2	2S3/2	-370
6G7/2	6I9/2	4I9/2	4F7/2	-581
6G7/2	6I17/2	4I9/2	4F7/2	-636
6G7/2	6I9/2	4I9/2	2S3/2	-712
6G7/2	6I17/2	4I9/2	2S3/2	-767
6G7/2	6P5/2	4I9/2	4G5/2	-797
6G7/2	6I11/2	4I9/2	4F7/2	-857
6G7/2	6P5/2	4I9/2	2G7/2	-931
6G7/2	6I15/2	4I9/2	4F7/2	-975
6G7/2	6I11/2	4I9/2	2S3/2	-988

There are 23 viable transfer paths. The final states of Nd all lead to visible emission, but only weakly so. The close spacing of the Nd manifolds make nonradiative decay to the $^4F_{3/2}$ the dominant decay process. The $^4F_{3/2}$ emits only in the infrared, so we do not recommend Nd as an activator for Gd.

Gd to Sm

Table B-44
Gd to Sm Transfer Paths

Gd (Initial)	Gd (Final)	Sm (Initial)	Sm (Final)	Energy Mismatch (cm-1)
6G7/2	6I15/2	6H5/5	6F11/2	1972
6G7/2	6I13/2	6H5/5	6F11/2	1937
6G7/2	6D9/2	6H5/5	6F7/2	1593
6G7/2	6D7/2	6H5/5	6F5/2	1372
6G7/2	6D7/2	6H5/5	6F7/2	548
6G7/2	6D9/2	6H5/5	6F9/2	416
6G7/2	6D7/2	6H5/5	6F9/2	-629
6G7/2	6P7/2	6H5/5	4G5/2	-950
6G7/2	6D9/2	6H5/5	6F11/2	-985

There are two viable transfer paths, neither of which lead to emission from Sm. Therefore, Sm should not be considered as an activator for Gd.

Gd to Eu

Table B-45
Gd to Eu Transfer Paths

Gd (Initial)	Gd (Final)	Eu (Initial)	Eu (Final)	Energy Mismatch (cm-1)
6G7/2	6P7/2	7F0	5D0	-367
6G7/2	6P5/2	7F0	5D0	-969

There is only one viable transfer path. If the transfer occurs, the emission from Eu will be very efficient. Because there is only one transfer and because in LaCl_3 it requires absorption of a phonon from the lattice, we expect the transfer efficiency to depend strongly upon the host lattice. Since this transfer has been observed, and since the payoff in visible emission could be large, it is worth investigating Eu as a potential activator for Gd.

Gd to Tb

There were no viable paths found that could transfer the energy associated with the first Gd photon to Tb. Tb should not be considered in the role of activator for Gd.

Gd to Dy

Table B-46
Gd to Dy Transfer Paths

Gd (Initial)	Gd (Final)	Dy (Initial)	Dy (Final)	Energy Mismatch (cm-1)
6G7/2	6I9/2	6H15/2	6F7/2	1902
6G7/2	6D9/2	6H15/2	6H9/2	1872
6G7/2	6D9/2	6H15/2	6F11/2	1866
6G7/2	6I17/2	6H15/2	6F7/2	1847
6G7/2	6I11/2	6H15/2	6F7/2	1626
6G7/2	6I15/2	6H15/2	6F7/2	1508
6G7/2	6I13/2	6H15/2	6F7/2	1473
6G7/2	6I7/2	6H15/2	6F5/2	841
6G7/2	6D7/2	6H15/2	6H9/2	827
6G7/2	6D7/2	6H15/2	6F11/2	821
6G7/2	6D9/2	6H15/2	6H7/2	527
6G7/2	6D9/2	6H15/2	6F9/2	512
6G7/2	6I9/2	6H15/2	6F5/2	499
6G7/2	6I17/2	6H15/2	6F5/2	444
6G7/2	6I11/2	6H15/2	6F5/2	223
6G7/2	6I15/2	6H15/2	6F5/2	105
6G7/2	6I13/2	6H15/2	6F5/2	70
6G7/2	6I7/2	6H15/2	6F3/2	43
6G7/2	6I9/2	6H15/2	6F3/2	-299
6G7/2	6I17/2	6H15/2	6F3/2	-354
6G7/2	6D7/2	6H15/2	6H7/2	-518
6G7/2	6D7/2	6H15/2	6F9/2	-533
6G7/2	6I11/2	6H15/2	6F3/2	-575
6G7/2	6D9/2	6H15/2	6H5/2	-660
6G7/2	6I15/2	6H15/2	6F3/2	-693
6G7/2	6I13/2	6H15/2	6F3/2	-728

There are 13 viable transfer paths, none of which lead to Dy emission in the visible. For this reason, Dy should not be considered as an activator for Gd.

*Gd to Ho***Table B-47**
Gd to Ho Transfer Paths

Gd (Initial)	Gd (Final)	Ho (Initial)	Ho (Final)	Energy Mismatch (cm-1)
6G7/2	6I7/2	5I8	5I5	1971
6G7/2	6I9/2	5I8	5I5	1629
6G7/2	6I17/2	5I8	5I5	1574
6G7/2	6P7/2	5I8	5F5	1441
6G7/2	6I11/2	5I8	5I5	1353
6G7/2	6I15/2	5I8	5I5	1235
6G7/2	6I13/2	5I8	5I5	1200
6G7/2	6P5/2	5I8	5F5	839
6G7/2	6D9/2	5I8	5I6	827
6G7/2	6P3/2	5I8	5F5	259
6G7/2	6I7/2	5I8	5I4	-29
6G7/2	6D7/2	5I8	5I6	-218
6G7/2	6I9/2	5I8	5I4	-371
6G7/2	6I17/2	5I8	5I4	-426
6G7/2	6I11/2	5I8	5I4	-647
6G7/2	6I15/2	5I8	5I4	-765
6G7/2	6I13/2	5I8	5I4	-800

There are eight viable paths to transfer the energy of the first Gd photon to Ho. None of these paths, however, lead to Ho emission in the visible. Therefore, Ho is a poor candidate as an activator for Gd.

Gd to Er

There are eight viable paths to transfer the energy of the first Gd photon to Er. The Er emission, however, will be almost entirely in the infrared. (The $^4F_{9/2}$ level emits slightly in the red, but mainly in the IR, while the $^9I_{9/2}$ level emits only in the IR.) Therefore, Er should not be considered as an activator for Gd.

Table B-48
Gd to Er Transfer Paths

Gd (Initial)	Gd (Final)	Er (Initial)	Er (Final)	Energy Mismatch (cm ⁻¹)
6G7/2	6D7/2	4I15/2	4I13/2	1870
6G7/2	6P7/2	4I15/2	4F9/2	1648
6G7/2	6P5/2	4I15/2	4F9/2	1046
6G7/2	6I7/2	4I15/2	4I9/2	764
6G7/2	6P3/2	4I15/2	4F9/2	466
6G7/2	6I9/2	4I15/2	4I9/2	422
6G7/2	6I17/2	4I15/2	4I9/2	367
6G7/2	6I11/2	4I15/2	4I9/2	146
6G7/2	6I15/2	4I15/2	4I9/2	28
6G7/2	6I13/2	4I15/2	4I9/2	-7
6G7/2	6D9/2	4I15/2	4I11/2	-743

Gd to Tm

Table B-49
Gd to Tm Transfer Paths

Gd (Initial)	Gd (Final)	Tm (Initial)	Tm (Final)	Energy Mismatch (cm ⁻¹)
6G7/2	6P7/2	3H6	3F2	1924
6G7/2	6P5/2	3H6	3F3	1875
6G7/2	6P5/2	3H6	3F2	1322
6G7/2	6P3/2	3H6	3F3	1295
6G7/2	6D9/2	3H6	3H5	1234
6G7/2	6P3/2	3H6	3F2	742
6G7/2	6I7/2	3H6	3F4	639
6G7/2	6I9/2	3H6	3F4	297
6G7/2	6I17/2	3H6	3F4	242
6G7/2	6D7/2	3H6	3H5	189
6G7/2	6I11/2	3H6	3F4	21
6G7/2	6I15/2	3H6	3F4	-97
6G7/2	6I13/2	3H6	3F4	-132

There are eight viable paths to transfer the energy of the first Gd photon to Tm. None of the Tm final states, however, lead to Tm emission in the visible region. As a consequence, we do not recommend Tm as an activator for Gd.

Task 11: Two-Photon Emission from Hg 254 nm Excitation

Task Leader: Charles Struck
 Task Members: Kailash Mishra
 Madis Raukas
 Roger Hunt, Jr.

Goal

The goal for Task 11 is a phosphor absorbing 253.7 nm Hg discharge emission and, for each absorption, emitting two visible photons useful for general lighting.

Quantum Cutting by Energy Transfer

Introduction

In the following discussion, we recognize three functions such a phosphor must perform:

1. to absorb strongly the 253.7 nm radiation,
2. to transfer this energy to a quantum cutter , i.e., to an impurity which can store the energy and in sequence transfer portions of this energy to two activators, and
3. to receive each portion of the transferred energy in an activator which emits a desired visible photon.

Limitations Imposed by the Physics of Energy Cascade Processes

The following discussion was suggested by K. Mishra.

In general, transfer transitions rates can be written as proportional to some squared matrix element:

$$W_{AB} = K \langle A^* B | 1/r_{ij} | AB^* \rangle^2. \quad [B-1]$$

Since $r_{ij} = r_i + R_{AB} - r_j$, where r_i is the distance between an electron and one nucleus and r_j is the distance between an electron and the other nucleus, and since both r_i and r_j are both much less than the inter-ionic distance R_{AB} , $1/r_{ij}$ can be expanded in a series of terms in $r_i^m r_j^n / R_{AB}^{m+n+1}$. The lowest term giving nonzero R_{AB} in Equation B-1 is that with $m=n=1$. This term yields a factor $1/R_{AB}^6$ in W_{AB} in Equation B-1. It also leads to the product of one-electron matrix elements $\langle A^* | r_i | A \rangle \langle B | r_j | B^* \rangle$. This product contains terms that also are in the matrix elements for optical absorption.

One therefore has a selection process for host-donor-activator systems which exhibit a particular energy transfer. If some energy transfer process will take place, then that host singly doped with the donor and that host singly doped with the acceptor will both exhibit allowed optical transitions between the electronic states involved in the energy transfer. How strong an emission is seen depends on the competition with nonradiative depopulation of the emitting state. Indeed, the initial state may be so strongly depopulated nonradiatively that the emission is not detectable with the apparatus at hand, but it is in principle there at some level. The lifetime of these optical transitions is the time available for the proposed energy transfer process.

In reality, the one electron matrix elements are themselves products of electronic and vibrational matrix elements. We have been considering only the electronic matrix element. The vibrational matrix element must also be non-zero. Riseberg and Moos have given an empirical exponential dependence of the transition rate on the energy gap to the next lower electronic state. Struck and Fonger [203] have shown that this transition rate depends on three parameters, the energy gap, the energy offset in the vibrational configurational coordinate, and the value of the electronic parameter. They have argued that the observed exponential dependence has no direct physical significance but is rather evidence of an underlying but as yet unexplored correlation between offset and the electronic factor.

Absorption of Excitation

Excitation is at $253.7 \text{ nm} = 39400 \text{ cm}^{-1} = 4.885 \text{ eV}$. Such absorption must be relatively strong, with absorption lengths smaller than 3 microns, i.e., absorptivities in the range of $3 \cdot 10^3 - 10^4$. A weaker absorption might allow detectable two-photon emissions but will not serve as a potential lamp phosphor.

Two possible absorbing processes are considered, namely, host lattice absorption and dopant absorption.

For a host in which each host-lattice band-to-band absorption at $253.7 \text{ nm} = 39400 \text{ cm}^{-1} = 4.885 \text{ eV}$ leads with good quantum efficiency to two visible photons, one has two possibilities. The first possibility is one in which an impurity level is near the middle of the band gap and in which electron capture and hole capture are radiative in the visible.

If we wish, for example, a photon at 480 nm and another at 620 nm, there is room for in total $2400 \text{ cm}^{-1} = 0.3 \text{ eV}$ Franck-Condon stabilization energy after electron capture plus after hole capture. We have no suggestions at all for such a host-impurity system. The second possibility is one in which band gap radiation leads to a host excitonic state which transfers energy to the quantum cutter and through the quantum cutter ultimately to two activators emitting the desired visible photons.

For dopant absorption, one needs a very wide bandgap material with some dopant supplying the allowed (e.g., $f^n \rightarrow f^{n-1}d$) absorption at 39400 cm^{-1} .

Host Excitonic Absorptions

One of the long-standing mysteries in cathodoluminescence is the 20% watt per watt efficiency of ZnS:Tm. This is the second most efficient phosphor known in cathodoluminescence and it is also the only rare-earth doped ZnS phosphor with an efficiency above 1%. The emission is blue and I believe is from 1D_2 . Excitation into 1D_2 is very close to the band gap energy, no more than a few tenths of an eV lower. There must be some as yet unknown mechanism for collecting hole-electron pairs efficiently by the Tm center.

If we could find a host with its bandgap near 253.7 nm which exhibits this same mechanism for electron hole recombination through Tm into 3P_2 , we would have a viable candidate for a two photon emitter, as we will develop below.

Quantum Cutter Schemes Involving Energy Transfer

The ideal choice for a quantum cutter would be one which has only one energy level somewhere between $17000\text{ cm}^{-1} = 588.2\text{ nm} = 2.11\text{ eV}$ and $20000\text{ cm}^{-1} = 500\text{ nm} = 2.48\text{ eV}$ and has a second energy level near $39400\text{ cm}^{-1} = 253.7\text{ nm} = 4.885\text{ eV}$. Nd^{3+} , Ho^{3+} , Er^{3+} and Tm^{3+} are shown [202] with energy levels near 39400 cm^{-1} and near 20000 cm^{-1} . The most promising one is Tm^{3+} . The others have a clutter of lines near 40000 cm^{-1} or near 20000 cm^{-1} which would likely prevent emission of either the first or the second photon or both.

The cascade of energy transfers envisaged here is from $\text{Tm}^{3+} ^3P_2$, $\text{Eu}^{3+} ^7F_0$ with energy $(38191+0=38191\text{ cm}^{-1})$ to $\text{Tm}^{3+} ^1G_4$, $\text{Eu}^{3+} ^5D_0$ with energy $(21216+16900=38116\text{ cm}^{-1})$ and from $\text{Tm}^{3+} ^1G_4$, $\text{Tb}^{3+} ^7F_6$ with energy $(21216+0=21216\text{ cm}^{-1})$ to $\text{Tm}^{3+} ^3H_6$, $\text{Tb}^{3+} ^5D_4$ with energy $(400+20800=21200\text{ cm}^{-1})$. This second step ends on a vibrationally excited state of $\text{Tm}^{3+} ^3H_6$ for energy conservation.. The second step might also involve Eu^{3+} , relying on the thermal population of $\text{Eu}^{3+} ^7F_1$: from $\text{Tm}^{3+} ^1G_4$, $\text{Eu}^{3+} ^7F_1$ with energy $(21216-400=20816\text{ cm}^{-1})$ to $\text{Tm}^{3+} ^3H_6$, $\text{Eu}^{3+} ^5D_2$ with energy $(0+20800=20800\text{ cm}^{-1})$.

This cascade is shown in Figure B-18.

If this active transferring level were $\text{Tm}^{3+} ^3P_2$ (39190 cm^{-1}), it might relax to 3P_1 (36413 cm^{-1}) and even to 3P_0 (35519 cm^{-1}) before it has time to transfer its energy to $\text{Eu}^{3+} ^5D_0$. These levels are included in Figure B-18 but without labels. Any such relaxations from $\text{Tm}^{3+} ^3P_2$ reduce the energy stored in the quantum cutter so that the first transfer in this cascade creating $\text{Eu}^{3+} ^5D_0$ would become energetically impossible.. Whether such relaxations are so fast as to be totally damaging can be determined only by experimental observation. Pappalardo gives the emission decay time from $\text{Tm}^{3+} ^3P_2$ in fluorides as 16 microseconds. One would have to have the Eu^{3+} close enough that transfer occurs within about a tenth of this time. We have no documented evidence that any particular energy transfer has been observed to occur within a microsecond. We have no evidence that it cannot occur this fast, either. We would look at the concentration quenching of rare earth emissions for such evidence.

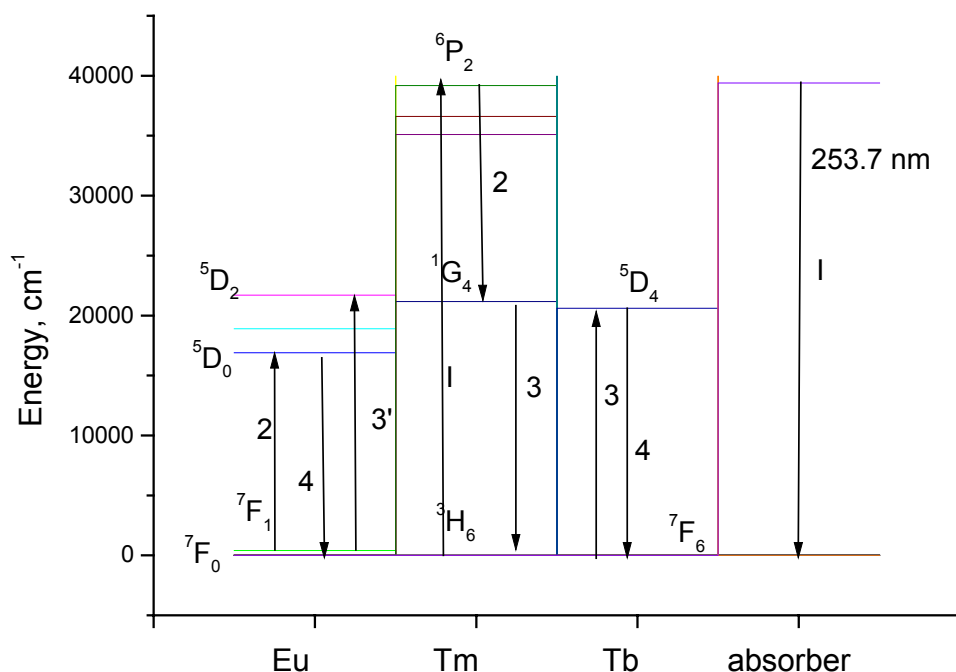


Figure B-18

Another important complication is that absorption into the Eu^{3+} charge transfer state (CTS) cannot serve both as the absorber of the 253.7 nm Hg radiation and also as a transfer sensitizer to populate $\text{Tm}^{3+} {}^3\text{P}_2$. The Eu^{3+} CTS would feed into a ladder of Eu^{3+} states about 8000 cm^{-1} lower and would therefore by-pass the quantum cutting process and yield only one visible photon from the emitting $\text{Eu}^{3+} {}^5\text{D}_j$ states. One seems therefore to be led logically to a host in which the Eu^{3+} CTS is higher than 39000 cm^{-1} , i.e., to a high bandgap material with another dopant chosen capable of absorbing the Hg radiation.

Even here, however, one seems to be led to somewhat contradictory requirements: a strong absorption implies a large Franck-Condon shift, while feeding $\text{Tm}^{3+} {}^3\text{P}_2$ from the state reached by this absorption requires a small Franck-Condon shift.

This difficulty is illustrated in Figure B-19.

Figure B-19 should not be misinterpreted. In this figure, the feeding state is shown with its absorption centered at 40600 cm^{-1} and with 39400 cm^{-1} simultaneously being in the wings of the feeding state absorption and of course also at the narrow Tm^{3+} absorption. Only the ground state and the offset state belong to the absorber. Separated from the absorber in space but close enough to interact with it, there is a Tm^{3+} with its own configurational coordinate. The ground state and the two states without offsets belong to the Tm^{3+} system. The two systems are shown in one rather than in two graphs to demonstrate the delicacy of the energy match which must exist for effective energy transfer.

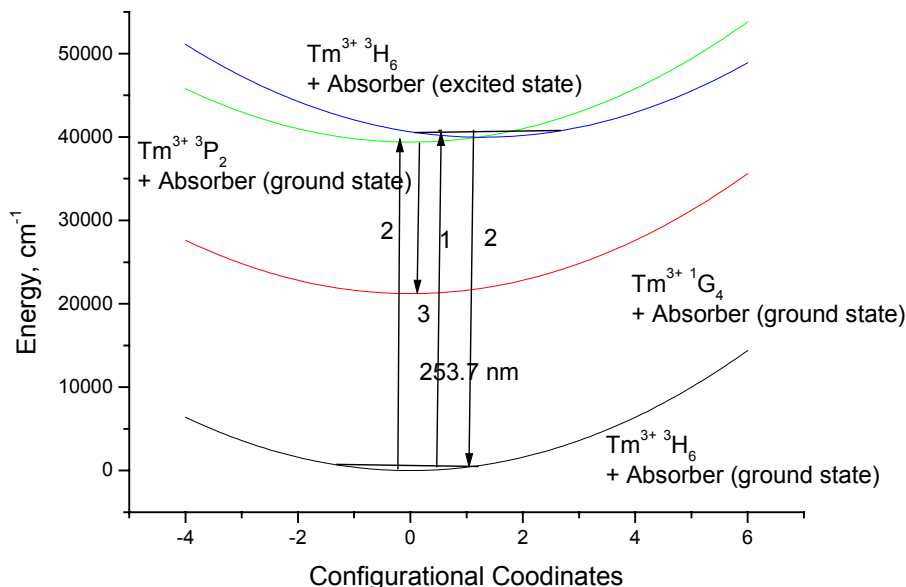


Figure B-19

The first transition, labeled 1, is the absorption of the 253.7 nm = 39400 cm⁻¹ Hg emission in the absorber, in the wings of its absorption band. The second transition, labeled 2, is the energy transfer at 38191 cm⁻¹, which is simultaneously the center of the emission band of the absorber and the narrow line position of the Tm³⁺ ³P₂ state. The third transition, labeled 3, is the Tm³⁺ contribution to the first energy transfer to Eu³⁺, i.e., to the first step in quantum cutting.

We deem the conflicting demands as quantitative rather than logically contradictory. It may possibly be that some fd state might have small enough Franck-Condon offsets from its ground state, that it might be placed in energy near 39400 cm⁻¹, and that it might transfer its energy to the Tm³⁺ ³P₂ state before its being depopulated by some other process.

It is quantitative competition such as this that we are fighting. For example, Dorenbos places the fd bands of Ce³⁺ in LiBaF₃ at 248 nm and its emission at 312 nm. This is a total Franck-Condon relaxation energy of 8271 cm⁻¹. If this number were 2000 cm⁻¹ and if the absorption were at 253 nm, we would have a very promising candidate for the absorber. But even then one would have to have the Ce near enough to Tm to allow transfer in 10-100 nanoseconds. These values bracket the expected lifetime of Ce emissions in these hosts.

We have searched, unsuccessfully, using Table 3 together with Table 1 in Dorenbos's second paper [201], for some other rare earth ion whose lowest fd state might be near 254 nm in some host and which might be expected to transfer its energy to Tm³⁺ ³P₂. Nevertheless, this scheme remains possible as a provider of the required strong absorption of 253.76 nm Hg radiation.

Organic materials sometimes have strong absorptions in sharp lines. Perhaps there is an organic material with its first sharp absorption precisely at 39400 cm⁻¹, into which we might put a chelating agent surrounding Tm³⁺, plus a chelating agent surrounding Eu³⁺, plus perhaps a chelating agent surrounding Tb³⁺. A potential danger here is that the chelating cage may separate the quantum cutter Tm³⁺ spatially from the two visible photon emitters Eu³⁺ and Tb³⁺ and thereby prevent efficient energy transfer.

There is a rich literature in organometallic compounds involving rare earth ions. We have several hundred citations for such organometallics, plus a book dating from the 1960s. None as best we can see address organometallics with their lowest strong absorption near 40000 cm^{-1} . There are indeed organic materials with bandgaps near 40000 cm^{-1} : tetracene is one. It would require a search by an organic chemist plus a physicist team to evaluate the potential of this process.

Throughout this discussion, we have not addressed the requirement that energy transfer will in fact dominate over all other mechanisms for depopulating Tm^{3+}P_2 . The Section below will show that one will have to search for a special host in which this transfer does in fact dominate over nonradiative depopulations of this state.

Recommendations for Approach Using Energy Transfer

A search for a host with a band gap near 253.7 nm should be pursued, together with the development of a theoretical understanding of the mechanism by which ZnS:Tm attains its high cathodoluminescence efficiency.

There is a chance that some ion might be found with an absorption and an emission band with only a 2000 cm^{-1} Franck-Condon shift, and which will transfer its excitation energy to Tm^{3+}P_2 within its lifetime. If so, the sequence of energy transfers involved in Figure B-19 seem to be achievable.

There is a chance that an organic system might be found which will absorb Hg emissions at 253.7 nm and emit two visible photons. What is needed is an organic compound or polymer with a strong narrow absorption precisely at 253.7 nm , into which one can incorporate organometallic (chelates) compounds containing the desired rare earth quantum cutter and the desired rare earth activators. One would hope for small chelating agents so that the quantum cutter remains close enough to the emitters to allow efficient energy transfer.

There are some less far reaching goals which are of value for knowledge's sake. We might confirm that in high band gap such as LaPO_4 materials and at some threshold concentrations of the dopants to be determined, one does see Tm^{3+}P_2 in the excitation spectrum of Eu^{3+} emissions, and one does see Tm^{3+}G_4 in the excitation spectrum of Tb^{3+} emissions. One might look also for Dy^{3+} , Ho^{3+} , Er^{3+} and Sm^{3+} emissions from Tm^{3+}P_2 .

General Bibliography for Section I

Spectroscopy, Theory

1. Wegh, Meijerink, A., Lamminmaki, R-J, and Holsa, J.,
J. Luminescence 87-89(2000)1002-1004

Band Gap Compilations

1. Rodnyi, P. A., Sov. Phys. Solid State 34(1992)1053-1066
2. Bakcerzyk, M., Gontarz, Z., Moszynski, M., and Kapusta, M.,
J. Luminescence 78-89 (2000)963-966
3. Strehlow, W. H. and Cook, E.L., J. Phys. Chem. Ref. Data 2(1973)163-192

Mishra. 12-13-01 Tm^{3+} as an Activator or Sensitizer Ion for Designing Multi-Photon Phosphors for 254 nm Emission

Introduction

Tm^{3+} as a cascading ion to split a ultraviolet photon to two visible photons was initially considered by Pappalardo. Because of its electronic configuration, $4f^{12}$, its energy level diagram is similar to that of Pr^{3+} ($4f^2$). The energy level diagram of Tm^{3+} is expected to be sparse and the $^1\text{S}_0$ level was expected to provide the initial state for cascading transition via transitions to the group of energy levels $^1\text{I}_6$ and $^3\text{P}_j$ states (Figure B-20.)

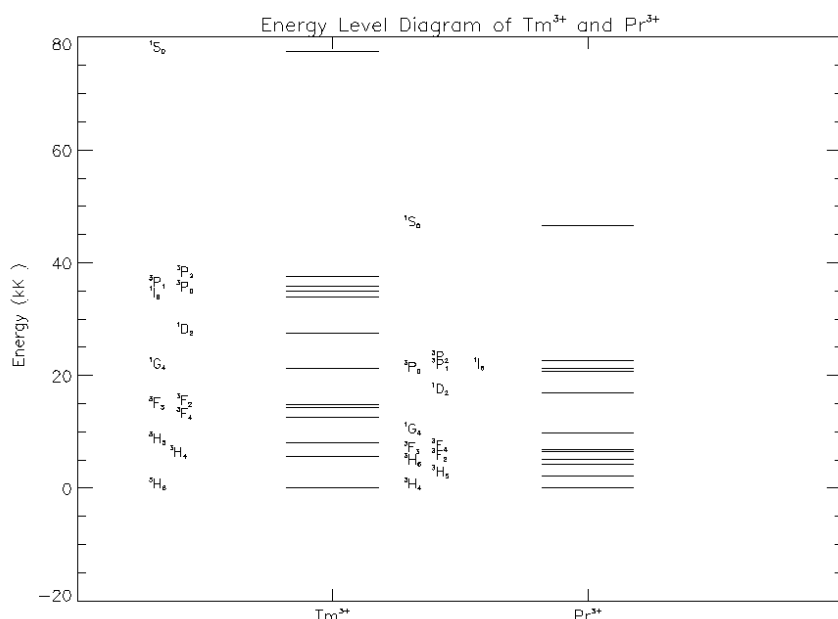


Figure B-20

Energy Level Diagram of Tm^{3+} in Y_2O_3 and Pr^{3+} in LaF_3 . Since the Energy Levels of Pr^{3+} in Y_2O_3 are not well Resolved, those in LaF_3 are used.

The energy level diagram of Tm^{3+} (Figure B-20) exhibits a number of interesting differences from that of Pr^{3+} :

1. The energy levels associated with the f^{12} manifold of Tm^{3+} spans over a larger energy range, $\sim 80\text{kK}$.
2. The $^1\text{S}_0$ level from predictions based on observed energy levels in different hosts appears at $> 75 \text{ kK}$ above the ground state, and is less likely to be observed in an oxide lattice. Thus, $^1\text{S}_0$ state of Tm cannot be the starting energy level for cascading transition as in Pr^{3+} .
3. The states $^3\text{P}_j$ and $^1\text{I}_6$ are not as crowded as in Pr^{3+} . The $^1\text{I}_6$ level appears below the $^3\text{P}_j$ states, not in the midst of $^3\text{P}_j$ states as in Pr^{3+} .
4. The $^3\text{P}_2$ state is separated by more than 2000 cm^{-1} from the $^3\text{P}_1$ state. Thus, the probability of non-radiative relaxation from $^3\text{P}_2$ to $^3\text{P}_1$ is less likely. (11863 sec^{-1} Tm^{3+} compared to 312250 sec^{-1} for Pr^{3+} , estimates from Pappalardo).

5. The 3P_2 state appears at 37638.9 cm^{-1} (265.7 nm) above the ground state, 3H_6 in Y_2O_3 , at an energy comparable to 254 nm radiation from the Hg-discharge. Additionally, it is separated from the 1G_4 level (21324 cm^{-1}) by 612 nm which is in the region where Eu^{3+} emission ($^5D_0 \rightarrow ^7F_2$) transition occurs.

Although Tm^{3+} was initially investigated as a candidate for cascading transitions because of its similarity in electronic structure to that of Pr^{3+} , the scheme of cascading transition from 1S_0 level was immediately abandoned because of the energetic position of this level. Most likely due to the proximity of the groups of levels due to the 3P and 1I_6 levels to 254 nm radiation. Pappalardo investigated the possibility of photo cascading emission (PCE) originating from these states. The Judd-Ofelt parameters used in this study were similar to those of Pr^{3+} in LaF_3 . He concluded that the quantum yield for this phosphor will not exceed 50%. However, it can be seen from Table 1 that the Judd-Ofelt parameters for Tm^{3+} in LaF_3 is very different from those used by Pappalardo. Since the cascading transition is originating from nonzero J levels, particularly for the 3P_2 , it is not necessary to satisfy the condition, $\Omega_6 \ll \Omega_4, \Omega_2$ for PCE. It is therefore we reexamined the possibility of PCE from the 3P_2 level.

Multi-Photon Scheme for Tm^{3+}

The PCE scheme for Tm^{3+} considered in this preliminary study is based on sequential transitions from the 3P_2 state to the 1G_4 state and then from the 1G_4 state to the 3H_6 or $3H_j$ states. The latter transitions (N band) have been observed in Y_2O_3 and occurs around 480 nm (blue). The important question is whether the $^3P_2 \rightarrow ^1G_4$ transition will occur efficiently. There cannot be any magnetic dipole transition between these two levels. In the case of forced dipole transition, the intensity of emission depends strongly on the Ω_2 parameter (see Figure B-21.), because of the linear dependence of transition probability on the Judd-Ofelt parameters, the slopes being determined by the square of reduced matrix elements of the unit tensors, U^k . These latter parameters were taken from Pappalardo for intermediate coupling and do not change very much for observed variations in the crystal field parameters. The reduced matrix elements of the unit tensors, U^2 , U^4 and U^6 are 0.7754, -0.0312 and 0.3242 respectively. For Y_2O_3 , the quantum efficiency of this transition is estimated to be 0.18 based on nonradiative transition probabilities listed by Pappalardo.

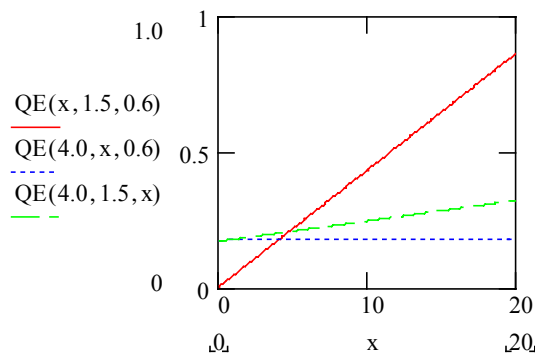


Figure B-21

**Variation of Quantum Efficiency (QE) for the 3P_2 to 1G_4 Transition with Ω_2 , Ω_4 and Ω_6
Note the Strong Dependence of QE on Ω_2 (Red Line)**

The strength of this transition depends on values of Ω_2 . The Ω parameters for several crystalline hosts are listed in Table B-50. The value of Ω_2 as large as $15.95 \times 10^{-20} \text{ cm}^2$ has been observed in zinc sodium sulfate glass. It is conceivable that in host systems with large Ω_2 , this transition can be utilized to generate a multi-photon system at excitation energies less than 254 nm either through a direct PCE or energy transfer to another rare earth ion.

Table B-50
Judd-Ofelt Parameters (in 10^{-20} Cm^2) for Tm3+

Host	Ω_2	Ω_4	Ω_6
LaF_3	0.52	0.59	0.22
Y_2O_3	4.0	1.5	0.6
YAl_2O_3	0.67	2.30	0.7
$\text{Y}_3\text{Al}_5\text{O}_{12}$	0.7	1.2	0.5
$\text{Tm}(\text{C}_2\text{H}_5\text{SO}_4) \cdot 39\text{H}_2\text{O}$	0.6	2.25	1.25
K7(TmW10O35)	1.58	5.78	0.83
$\text{LiYF}_4\text{Y}_2\text{SiO}_5$	2.79	0.45	0.98
Y_2SiO_5	2.43	1.74	0.66

Conclusion

We considered a PCE scheme originating from the $3P_2$ level of Tm3+. Our conclusions are as follows:

1. Tm^{3+} could provide a new case of cascading transitions originating at an energy level, $3P_2$ that can be excited by radiations at wavelengths $> 254 \text{ nm}$. The signature of this PCE will be in the characteristic 612 nm emission line.
2. The most important Judd-ofelt parameter driving this transition is Ω_2 . This parameter depends strongly on the host lattice. It is possible that a crystalline host can be found where this parameter is large enough to make this transition very efficient.
3. The proposed scheme for PCE from Tm^{3+} differs from that Pr^{3+} in the fact that it originates from a group of crowded levels, 3P_j and 1I_6 . Similar cases could possibly be found from other rare earth ions at different excitation energies.

Recommendation

We know that there are many hurdles before a new PCE phosphor can be designed based on Tm^{3+} . Our calculations are in no way comprehensive. We would like to make following recommendation for the further studies:

The possibility of PCE from Tm^{3+} originating at 3P_2 level should be investigated thoroughly from a theoretical perspective along with simultaneous experimental search for evidence of $^3P_2 \rightarrow ^1G_4$ transition in the emission spectrum. If both the experimental and theoretical studies result in positive indications, a thorough search for new host lattices with gap larger than 4.9 eV, and new activator ions that could be sensitized by this transition should be initiated.

Bibliography

Theory

1. R. Pappalardo, J. Luminescence 14, 159 (1976).

Spectroscopy

1. W. K. Krupke, Phys. Rev. 145, 325 (1966).
2. W. T. Carnall, P. R. Field, J. Morrison, and R. Sarup, J. Chem. Phys. 52, 4054 (1970).
3. J. B. Gruber, M. D. Seltzer, M. E. Hills, S. B. Stevens and C. A. Morrison, J. Appl. Phys. 73, 1929 (1993).
4. J. B. Gruber, W. F. Krupke and J. M. Poindexter, J. Chem. Phys. 41, 3363 (1964).

Judd-Ofelt Parameters

1. A. Morrison and R. P. Leavitt, Handbook on the Physics and Chemistry of Rare Earth Ions, Vol. 5 (ed. K. A. Gschneidner, Jr. and L. Eyring, North Holland, 1982).
2. C. G  ller-Walrand and K. Binnemans, Handbook on the Physics and Chemistry of Rare Earth Ions, Vol.2 5 (ed. K. A. Gschneidner, Jr. and L. Eyring, Elsevier Science, 1998).

Raukas MPP for 254 nm Emission from Hg-Discharge: Experimental

Discussion

We investigated the suitability of Tm^{3+} as a ‘quantum cutter’ in $\text{Y}_2\text{O}_3:\text{Tm}$ using spectroscopic measurements. We found no evidence of quantum cutting in the visible spectral region of emission from this relatively large Ω_2 ($=4.0$) material even at temperatures down to 22K. Emission from $^1\text{I}_6$ as the first step of quantum cutting was observed in the far red region at 771, 778 and 780 nm. These emissions end in $^1\text{G}_4$, as we would like emissions from $^3\text{P}_2$ to do.

Thulium ions (in the form of hydrous nitrate) were doped into Y_2O_3 matrix (purity of both 99.99% relative to RE elements, Alfa Aesar) by solid-state diffusion at 1500C and the powder was thereafter studied under Xe-lamp excitation at both room and liquid helium temperatures. From the discussions with K. Mishra we had determined the goal of such a study as to look for the emission of the ‘first’ photon in the desirable two-step radiative relaxation from the $^3\text{P}_2$, $^3\text{P}_1$, $^3\text{P}_0$ and $^1\text{I}_6$ levels of Tm^{3+} upon excitation into $^3\text{P}_2$ level or higher. Most of the transitions and energy levels in the visible spectral range described by Gruber et al. [204] are indeed observed upon excitation at around 360 nm ($^3\text{H}_6\text{-}^1\text{D}_2$ transition, 27800 cm^{-1}) and at around 261/264 ($^3\text{H}_6\text{-}^3\text{P}_2$, 37800 cm^{-1}), 277 ($^3\text{H}_6\text{-}^3\text{P}_1$, 36100 cm^{-1}), 283 ($^3\text{H}_6\text{-}^3\text{P}_0$, 35200 cm^{-1}) and 290 nm ($^3\text{H}_6\text{-}^1\text{I}_6$, 34300 cm^{-1}). Groups of lines corresponding to the radiative relaxation from $^1\text{D}_2$ to $^3\text{H}_4$ and $^3\text{H}_5$ manifolds, from $^1\text{I}_6$ to $^3\text{F}_4$, $^3\text{F}_3$ and $^3\text{F}_2$ and from $^1\text{G}_4$ to $^3\text{H}_6$ manifolds appear in the recorded spectra (by tentative identification using energy values). In addition to these, more lines that by the same tentative criteria could belong to $^3\text{F}_2$ to ground state or $^1\text{D}_2$ to $^3\text{F}_4$ (649-663 nm or about 15400-15820 cm^{-1}), $^3\text{F}_3$ to ground state (679-685 nm or about 14700-14600 cm^{-1}) and $^1\text{I}_6$ to $^3\text{H}_4$ (346-361 nm or about 28900-27680 cm^{-1}) relaxation were detected. Unlike some other sharp spectral features observed, they possess the characteristic excitation spectra of the Tm^{3+} f-f transitions.

However, the thrust behind this investigation was showing the existence of photons emitted in the spectral range of 578-634 nm (17290 to 15770 cm^{-1}) that would appear for excitation into $^3\text{P}_2$ but not into $^1\text{D}_2$ levels. Energy of such photons would correspond to transitions from $^3\text{P}_2$ level to $^1\text{G}_4$, the necessary first step in cascade emission. Alternatively, expecting photons from $^3\text{P}_1$ or $^3\text{P}_0$ requires monitoring the range of 652-707 nm (15330 to 14140 cm^{-1}). Despite the efforts, no such emissions could be identified even at temperatures around 22K. However, we were successful to observe spectral lines under 264 nm excitation (into $^3\text{P}_2$) and at liquid helium temperatures at 771, 778 and 780 nm that disappeared when the sample was excited at 360 nm ($^1\text{D}_2$). The presence of the lines at room temperature was nearly undetectable. At 22K, their total intensity was more than an order of magnitude lower than for $^1\text{D}_2$ - $^3\text{H}_4$. Out of many, these three lines had the characteristic Tm^{3+} excitation spectrum at 22K with the transitions into ^3P and ^1I manifolds but no $^1\text{D}_2$ excitation peak (see Figure B-22). Based on that and the corresponding energies of the emissions of 12970, 12850 and 12820 cm^{-1} we assign them to the transitions from $^1\text{I}_6$ to $^1\text{G}_4$ levels and not to relaxation from the $^3\text{F}_4$ manifold to the ground state. Despite the close match in energy, there is no immediate explanation why emission from $^3\text{F}_4$ (to the ground state) should occur under higher (into ^3P , ^1I) and not lower (^1D) energy excitation since all upper levels ($^3\text{P}_J$, $^1\text{I}_6$, $^1\text{D}_2$, $^1\text{G}_4$) are expected to feed $^3\text{F}_4$ [205]. Thus, although useless for the lighting applications, we believe the emission of two cascading photons has been demonstrated by observing simultaneous emissions at 771 (778, 780) nm and around 480-490 nm upon excitation into ^3P and ^1I multiplets. A complete proof would follow from more detailed measurements with counting the photons in various spectral lines under the two excitations in question.

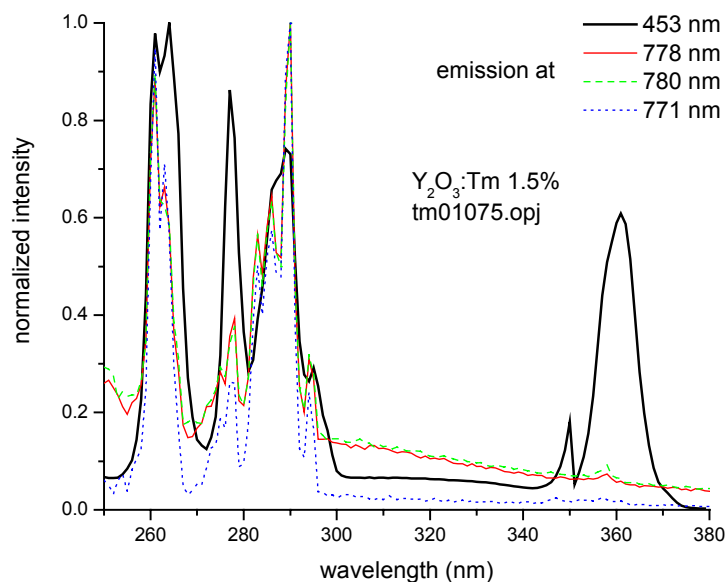


Figure B-22
Excitation Spectra of $\text{Y}_2\text{O}_3:\text{Tm}$ for 453, 771, 778 and 780 nm Emissions at 22K

Utilizing Tm^{3+} as a quantum cutter seems to be complicated by more general considerations. Tm^{3+} is known by its blue emission around 450 nm. This emission, observed in a number of host materials as the strongest among all its visible lines, is a result of $^1\text{D}_2$ to $^3\text{H}_4$ transition rather than $^1\text{G}_4$ to ground state relaxation. The latter path would be desirable for the quantum cutting action where the first step is due to radiative relaxation to the $^1\text{G}_4$ level. The emission of photons from this level results in spectral lines at 480-490 nm and is typically weaker than the $^1\text{D}_2$ - $^3\text{H}_4$ radiative transition. In Y_2O_3 , the peak intensities are found to differ by a factor of 1000 [204]. We estimate the ratio of total integrated intensities of these transitions to be around an order of magnitude for different excitation energies (possibly contains unidentified emission peaks). Clearly, Y_2O_3 as a host-activator system may not happen to be good for cascading emission. However, we chose Y_2O_3 due to relatively large Ω_2 value of 4.0 that is expected to maximize the $^3\text{P}_2$ - $^1\text{G}_4$ transition probability (see the contribution to this task from K. Mishra). According to the values of unity tensor $U^{(k)}$ matrix elements [205], large Ω_2 should provide preferential population of $^1\text{G}_4$ over $^1\text{D}_2$. Unfortunately, they also promote the domination of the $^1\text{D}_2$ blue emission. For $\Omega_2 \ll \Omega_4, \Omega_6$ the transition strengths of the two emissions should become comparable. Due to the lack of sufficient data available in the literature, it is presently hard to say precisely how prevailing $^1\text{D}_2$ emission actually is.

On the other hand, yttrium oxide has a relatively higher phonon cut-off frequency (560 cm^{-1}) than for example fluorides (e.g. MnF_2 350 cm^{-1} , LaF_3 450 cm^{-1}) or perhaps bromides, and thus favors faster multiphonon relaxation from $^3\text{P}_2$ that bridges the gap of about 2000 cm^{-1} to $^3\text{P}_1$. This is indeed observed when comparing the relative integrated efficiencies of $^3\text{P}_2$, $^3\text{P}_1$ and $^3\text{P}_0 + ^1\text{I}_6$ excitation bands for the $^1\text{I}_6$ - $^3\text{F}_2$ emission at room temperature. There is only about 30% loss of efficiency when excited into the highest level ($^3\text{P}_2$) compared to direct excitation into $^1\text{I}_6$ from where the emission occurs, i.e. the two levels are well connected. Alternatively, such relaxation can be facilitated by the nearby Tm^{3+} charge-transfer state but no evidence of it was found below the bandgap absorption. A host material with low phonon frequencies is desirable for higher likelihood of observing $^3\text{P}_2$ - $^1\text{G}_4$ radiative transition.

The lack of evidence for radiative $^3\text{P}_2$ - $^1\text{G}_4$ transition in $\text{Y}_2\text{O}_3:\text{Tm}$ does not completely rule out Tm^{3+} as a quantum cutter. Energy transfer processes over short distances that compete with the nonradiative decay can in principle make use of even weakly occurring transitions. The efficiency of such cascading transitions of Tm^{3+} in different hosts and/or the energy transfer to more efficient emitters remains to be checked.

Recommendations

We recommend:

Modeling of potential PCE/stepwise transfer in other RE ions like Er^{3+} and Ho^{3+} (to be repeated in Tm^{3+}), somewhat analogous to [205];

Experimental study of Tm^{3+} (Er^{3+} , Ho^{3+}), both separately and pair wise with Eu^{3+} or Tb^{3+} in some host of low phonon frequencies and with the location of Eu^{3+} CT band at higher energies than 250-260 nm to minimize the interference effects under Tm-excitation;

Finding theoretical and experimental evidence for initiating a broad search for a suitable host material in organic compound domain.

Additional Bibliography Regarding Tm^{3+}

1. W.T. Carnall, P.R. Fields, J. Morrison, R. Sarup, J.Chem.Phys. 52 (1970), 4054.
2. W.T. Carnall, H. Crosswhite, J.Less-Comm.Met. 93 (1983), 127.
3. R. Reisfeld, Y. Eckstein, J.Chem.Phys. 63 (1975), 4001.
4. W.F. Krupke, Phys.Rev. 145 (1966), 325.
5. C.A. Morrison, R.P. Leavitt, J.Chem.Phys.71 (1979), 2366.
6. R.P. Leavitt, C.A. Morrison, J.Chem.Phys.73 (1980), 749.
7. K. Hirao et al., J.Appl.Phys. 78 (1995), 3445.
8. R.J. Thrash, L.F. Johnson, J.Opt.Soc.Am.B 11 (1994), 881.
9. A.W. Kueny et al. J.Opt.Soc.Am.B 10 (1993), 1834.
10. J.B. Gruber et al. J.Appl.Phys. 81 (1997), 6585.
11. D.C. Yeh et al. Phys.Rev.B 39 (1989), 80.
12. S. Tanabe et al. Phys.Rev.B 47 (1993), 2507.

Task 12: Phosphor Synthesis and Processing

Task Leader: Joanna McKittrick

Task Members: Arun Dutta
Roger Hunt
Doug Keszler

Conclusions from Original Objectives

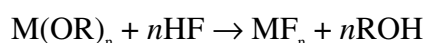
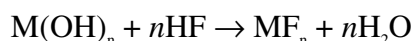
- Identify fluoride-host phosphor synthesis via literature searching
 - 11 articles identified, 9 published since 1995
 - Newer articles report on chemical synthesis techniques, older articles report on fluorination of oxides or solid state reactions
 - No reports on oxygen contamination studies
- Determine manufacturing pitfalls for using these phosphors
 - Cost (chemical synthesis) and toxicity of precursors (fluorination)
- Identify candidate materials for coating the fluoride-based phosphors as a hedge if surface stability remains the limiting factor
 - Coating must be VUV transparent with a band gap > 6.5 eV
 - Candidates are simple oxides such as MgO , SiO_2 and Al_2O_3
- Determine weight loss of candidate phosphors in manufacturing solutions
 - pH, conductivity and electrokinetic properties of AlF_3 and CaF_2 measured in aqueous solutions, drying experiments in progress

Recommendations of Promising Research Topics

- Identify fluoride-host phosphor synthesis via literature searching
 - Fluoride phosphors can be synthesized without HF gas or liquid
 - Sol gel and (trifluoroacetic acid)
 - Hydrothermal and chemical precipitation (ammonium hydrogen fluoride)
 - These methods should be tried, oxygen contamination identified
- Determine manufacturing pitfalls for using these phosphors
 - Cost of phosphor synthesis should not be ignored
- Identify candidate materials for coating the fluoride-based phosphors as a hedge if surface stability remains the limiting factor
 - Aging experiments must be done on degradation of fluoride-based phosphors with and without coatings in a VUV environment
- Determine weight loss of candidate phosphors in manufacturing solutions
 - Experiments should continue

Background

Synthesis of complex metal fluorides can be accomplished by a variety of techniques. The most elementary is through solid state reaction of the unary metal fluorides which is carried out under flowing HF gas at temperatures above 1000°C. The dense body that results must be ground or milled into a fine powder; a step that introduces contamination [206]. Fluorination of organic or inorganic oxides is a much cleaner technique [207]. The oxides, which are prepared through solution chemistry, have starting particle sizes in the sub-micron range. These high surface area, powders can be converted into fluorides under flowing HF gas at temperatures around 500°C within hours [208, 209]. The basic chemical reactions are:



Where M = metal ion and R = H, CH₃, C₂H₅, etc. The reaction rates are controlled by the temperature, partial pressures of the gases and how quickly the water or alcohol can be evacuated from the reaction chamber. Complex compositions such as ZrF₄-BaF₂-LaF₃-AlF₃-NaF (ZBLAN) glasses have been formed by this technique [208, 210]. Various other fluorine containing gases such as F₂ or NF₃ and can be used.

There are three newer techniques that look promising and do not involve using fluorinated gases. The first involves a chemical precipitation method, the second is a hydrothermal synthesis technique and the third is through sol gel chemistry. ScF₃ was prepared by a low temperature liquid technique [211]. Fine particle size Sc(OH)₃, freshly precipitated, was suspended in a solution containing NH₄HF₂, ammonium hydrogen fluoride. A complex salt, NH₄ScF₄ crystallized, complete after three weeks. The powder was filtered, washed and decomposed under an IR lamp for one week. The resulting powder was not contaminated by N or H. Hydrothermal synthesis was carried out for the formation of LiErF₄ using both oxide and fluoride precursors [212]. The starting materials, LiF, Er₂O₃ and NH₄HF₂, were added to water and sealed in a stainless steel autoclave and heated to 240°C for 3-5 days. The resulting washed and dried powder was single phase LiErF₄. Sol gel methods were used to form powders and films of SrAlF₃ and BaMgF₄ [213]. The starting materials were strontium, barium or magnesium acetate [M(CH₃COO)₂] and aluminum ethoxide [Al(OC₂H₅)₃]. The desired molar ratios were dissolved in IPA and trifluoroacetic acid, CF₃COOH. The solution was stirred for 2-4 hours and dried at 80°C for 2 days to form a gel. The gels crystallized into the complex fluoride phase at temperatures < 400°C. However, trace amounts of unary fluorides were found, even after heating the powders to 800°C. The powders remained stable to these temperatures.

Other papers on synthesis

A.V. Goryunov, A.I. Popov, N.M. Khajdukov and P.P. Fedorov, 'Crystal Structure of Lithium and Yttrium Complex Fluorides,' Mat. Res. Bull., 27, 213-220 (1992).

Largeau, M. El-Ghozzi and D. Avignant, 'Synthesis and Crystal Structure of a New Mixed-Valence Terbium Fluoride, KTb^{III}Tb₂F₁₂, and Related KLn^{III}M₂F₁₂ Compounds (M^{IV} = Tb, Zr, Hf; Ln^{III} = Ce-Lu),' J. Solid State Chem., 139, 248-258 (1998).

M.A. Subramanian, R.H. Harlow, V.N.M. Rao, 'New [Ru(NH₃)₆]MF₆ Phases: Precursors to Catalysts for Halogenation Reactions,' *Mat. Res. Bull.*, 35, 1587-1592 (2000).

M.G. Zhiyahin, A.V. Olenov, F.M. Spiridonov, L.N. Komissarova and O.G. D'yachenko, 'Hydrothermal Synthesis and Crystal Structure of a New Sodium Yttrium Fluoride Phosphate NYFPO₄,' *J. Solid State Chem.*, 157, 8-12 (2001).

Multiple Task Report: Los Alamos National Laboratory

P. Jeffrey Hay and Joel D. Kress

The work initiated at Los Alamos impacts Tasks 2 (Bulk and Surface Defects in Fluorides), Task 6 (Modeling) and Task 7 (Sugano-Tanabe diagrams). At a meeting held at OSI (Beverly, Mass.) on October 30, 2001, Modeling and Simulation Needs for Multi-Photon Phosphors (MPPs) were identified and priorities assigned to each need (see Table B-51). From this list of needs, Los Alamos has started work on Need #1 (Pr³⁺, Tm³⁺ .multiplet structures in oxide lattices), Need #4 (calculations of Dq for 2nd and 3rd row transition metals d² ions in oxide lattices) and Need #5 (Limited CI calculations on d-manifold configurations) . A brief survey of existing capabilities for Need #6 (Total energy calculations for fluorides with oxygen defects) is also provided below.

Task 2: Bulk and Surface Defects in Fluorides

In this section we address Need #6 in Table B-51 (Modeling and Simulation Needs). One recommendation from Part II, Section 6 from the final report for Task 2 is "These (experimental) studies could be complemented by calculations using ab initio quantum computation methods." Simulations based on both ab initio and empirical molecular mechanics-type descriptions of the interatomic potential between atoms are routinely used to study both bulk and surface defects in ionic lattices. (Examples studied by researchers at Los Alamos include UO₂, SrZrO₃, silicates, zeolites, and radiation damage in pyrochlores.) The basic strategy is to construct a lattice in a simulation cell containing N_{ion} total number of cations and anions. Periodic boundary conditions (PBCs) are enforced so that the simulation cell represents an infinitely extended bulk solid (3-dimensional PBCs) or surface (2-dimensional PBCs). Defects (e.g., vacancies, substitutionals, interstitials) are introduced into the simulation cell and energies and heats of formation and migration are computed. The crucial ingredient for obtaining meaningful properties from such an atomistic simulation is an accurate description of the interatomic forces. The trade-off between empirical potentials and ab initio calculations is accuracy vs. speed of computation. The speed of computation of the present ab initio methods limits the simulation size to N_{ion} ~ few hundred ions, whereas for the classical methods, N_{ion} ~ 1000 ions can be treated. The size of the simulation cell (number of ions used) is important in terms of limiting the (artificial) interaction of a defect with its periodic image. Although empirical potentials are not "ab initio", they can be quite accurate, since parameters in the potentials are carefully fit to experimental and ab initio information (such as lattice constant, cohesive energy, bulk modulus, etc.) Finite-sized cluster models, constructed from the defect structures predicted by the modeling with PBCs, can be used as input for ab initio calculations of the electronic states (e.g., optical properties , excitation spectra) of defects (see discussion below on Multiplet States in Fluoride and Oxide Lattices).

Finally, if empirical classical potentials do not exist for the ions of interest, ab initio calculations are an attractive option; fitting new empirical potentials can take from anywhere between a man-month up to man-years of work.

Empirical Potential Modeling

A successful empirical interatomic potential for ionic solids is based on a Born description of an ionic lattice, where the interatomic forces consist of a long-range Coulomb term and a short-range radial terms. The polarizability of the ions is realized through a shell model. Popular shell model computer codes are GULP for bulk systems [214] and MARVIN for surfaces [215]. Recent examples of this type of simulation include oxygen migration in La_2NiO_4 [216] and the structure of LaMnO_3 and Mn_2O_3 [217]. Since Born-type potentials exist to describe many of the demonstrated and potential oxide hosts identified in Table II of the final report for Task 3, defect states of these hosts could be calculated with the empirical approach.

Ab Initio Simulations

Ab initio quantum electronic structure calculations for simulation cells with periodic boundary conditions are efficiently carried out using (1) planewaves to expand the valence electronic wavefunctions and (2) pseudopotentials (PPs) to represent the core electrons of each ion. This approach is commonly used by solid-state physicists to study the electronic band structure and cohesive energies (binding energies) of solids and surfaces. To carry out a simulation for a given ionic lattice, an accurate and efficient PP must be specified for each kind of atom in the lattice. The calculation is ab initio (a Schrodinger equation is solved for the electron-electron and electron-ion interactions) once the ionic positions in the lattice and PPs are specified. One such total energy band structure computer code is VASP (Vienna ab initio Simulation Package) [218]. PPs for the main group elements, transition metals, and La and Ce are provided with VASP. Therefore, defect structures for most of the demonstrated and potential oxides hosts identified in Table B-52 in the final report for Task 3 could be calculated with an ab initio band structure approach. Also, the effect of impurity and dopant atoms can be studied. (Note there are limitations on the concentration of point defects due to the limited number of total ions in the simulation cell.) Numerous examples of defect calculations in ionic lattices by ab initio methods exist in the literature; we list here a review [219] and a calculation of planar defects in SrTiO_3 and BaTiO_3 [220]. Finally, radiation-induced defects in silicon and silicon carbide have been studied at Los Alamos with ab initio methods. [221] During a radiation damage event, the irradiating particle transfers recoil energy to an atom in the lattice (so-called primary knock-on atom, PKA). If the recoil energy exceeds the material-dependent displacement-threshold energy (E_d), the PKA leaves its original lattice site and creates a Frenkel defect pair. E_d for the main symmetry directions in Si and SiC was calculated using ab initio methods. These calculations provided the first ab initio benchmarks for determining the accuracy of commonly-performed simulations based on empirical potentials.

Tasks 6 and 7: Multiplet States of Transition Metal and Lanthanide Ions in Fluoride and Oxide Lattices

In this section we assess the use of quantum chemistry methods employing cluster models to provide information on the electronic states of transition metal and lanthanide ions in crystal environments. This addresses the Needs #1, #4 and #5 in Table B-51 (Modeling and Simulation Needs). The following cases are considered: a Ni^{2+} ($3d^8$) ion at an octahedral site in a fluoride lattice (KNiF_3), a Nb^{3+} ($4d^2$) ion at an octahedral site in an oxide lattice, Nb^{3+} at a 7-coordinate site in the oxide La_2O_3 , and Pr^{3+} ($4f^2$) at a 7-coordinate site in La_2O_3 . Results are compared with experimental spectroscopic studies. The basic approach will involve Hartree-Fock calculations plus limited configuration interaction (CI) among the d (or f) manifold to obtain the full set of dⁿ (or fⁿ) states in the surrounding field of the oxide (or fluoride) neighbors. While more extensive CI calculations are quite feasible than the results reported here, the overall goal in this initial assessment is to provide some indication of the relative merits of this approach for representative lattice sites. The programmatic needs can determine the proper balance between carrying out higher accuracy calculations on particular systems on the one hand and screening a variety of combination of ions and lattices on the other.

There is an extensive literature on the use of cluster calculations to examine local properties in ionic solids. Typically studies of optical spectra, such as transition metals in oxides, employ Hartree-Fock based techniques supplemented by configuration interaction [222, 223] but recent studies have also included density functional approaches [224].

Details of the Calculation

Cluster Models

For a transition metal or lanthanide (M^{q+}) ion at a substitutional lattice site in an oxide or fluoride crystal, a simple cluster model is employed consisting of the M^{q+} ion, the first coordination shell of anions (X), and the second coordination shell of cations (A). Much more realistic descriptions of the Madelung potential in the vicinity of the MX_n arising from the effects of the lattice can be achieved by using more elaborate point charges arranged about the cluster, as has been reported in the literature by other investigators including our colleagues. For the purposes of this survey only the first two coordination shells have been considered, and K^+ ions are chosen to represent the second shell of cations (A) to keep the overall charge on the cluster as close to neutral as possible. For Ni^{2+} in a 6-fold fluoride site in KNiF_3 , a NiF_6K_8 cluster is used with the Ni^{2+} at the center of a cube, the F⁻ ions on the faces (at a bond distance of 2.0 Å and the K^+ ions on the vertices. A similar NbO_6K_8 cluster is used to represent Nb^{3+} in a 6-fold oxide site as in a perovskite ABO_3 structure with Nb-O bond distances of 2.1 Å. For Nb^{3+} or Pr^{3+} in a 7-fold oxide site (La_2O_3) where there are 12 cations in the second coordination shell a MO_7K_{12} cluster is used. There are three distinct M-O bond lengths, which are taken from La_2O_3 , one O at 2.46 Å three O at 2.36 Å and three O at 2.73 Å.

Basis Sets and Effective Core Potentials

Standard 6-31G contracted gaussian basis sets are used in the calculations for the O and F ions which permit a flexible “double zeta” description of the valence 2s and 2p orbitals. For Ni and Nb “small core” effective core potentials by Hay and Wadt [225] are used to replace the core electrons and, in the case of Nb, to incorporate relativistic effects. For Ni^{2+} the outer 3s, 3p, 3d (and formally unoccupied 4s and 4p) electrons are explicitly treated with the contracted gaussian basis. Analogously for Nb^{3+} the outer 4s, 4p, 4d (and 5s, 5p) electrons are treated as valence electrons. For Pr^{3+} the small core potentials of Dolg et al. [226] are used to replace the $[\text{Ar}] 3d^{10}$ core.

Self-Consistent Field and Configuration Interaction Calculations

Restricted open-shell Hartree-Fock calculations are performed on the high-spin ground state of the metal complex. For the d^2 (Nb^{3+}) and f^2 (Pr^{3+}) cases, the remaining d or f orbitals are obtained using the improved virtual orbital technique. A configuration interaction (CI) calculation is carried out including all possible d^n or f^n states. For the d^2 case this corresponds to 10 triplet and 15 singlet states. Spin-orbit coupling effects are not included at this point in the calculations. All calculations were carried out using the MESA electronic structure code [227].

Results

Ni^{2+} in 6-Fold Fluoride Site (KNiF_3)

The calculated results are summarized and compared to the experimentally observed spectra [228] in Table B-52. The agreement for the lowest 3T_2 and 3T_1 transitions is quite good. The crystal field splitting $10Dq$, which in this case corresponds to the ${}^3A_2 - {}^3T_2$ excitation energy, is calculated to be 7180 cm^{-1} compared to 7250 cm^{-1} experimentally. At higher energies the experimental energies are overestimated considerably. This reflects in part the fact that no orbital relaxation effects have been included in the small CI calculations.

Nb^{3+} in 6-Fold Oxide Site (ABO_3) and 7-Fold Oxide Site (La_2O_3)

The analogous case for the d^2 ion Nb^{3+} in an octahedral oxide field as would arise by doping in a ABO_3 perovskite lattice is presented in Table B-53. The lowest singlet states are found at 9840 cm^{-1} (1E) and $10\,500 \text{ cm}^{-1}$ (1T_2) above the ground 3T_1 state. The lowest excited triplet state (3T_2) arises at $26\,100 \text{ cm}^{-1}$. In the familiar six-fold site, the $e_g - t_{2g}$ splitting of the 4d orbitals is represented by the $10Dq$ parameter. From fitting selected levels approximate values are obtained for $10Dq = 28\,400 \text{ cm}^{-1}$ and Racah parameters $B = 742 \text{ cm}^{-1}$ and $C = 2794 \text{ cm}^{-1}$.

For the lower symmetry C_{3v} situation where Nb^{3+} is doped into a seven-coordinate substitutional site in La_2O_3 , the 4d orbitals are split into three sets (1e, a and 2e). This results in a more complex set of levels as shown in Table B-53. Instead of 11 levels for the six-fold case there are now 17 levels for the seven-fold case. The lowest spin-allowed excited triplet state (3A) now occurs at $17\,000 \text{ cm}^{-1}$, considerably lower compared to the 6-fold oxide site case.

Pr³⁺ in 7-Fold Oxide Site (La₂O₃)

The levels for the f² Pr³⁺ ion are shown in Table B-54 as calculated according to the scheme discussed above. Comparison with the recent experiment observations by Moune *et al.* [16] of Pr³⁺ in La₂O₃ are also made in Table B-54. For lanthanide ions in oxide and fluoride lattices, the splittings of the 4fⁿ states decrease in the order multiplet effects > spin-orbit effects > ligand field effects. The calculated multiplet families fall in similar energy ranges as observed experimentally. The highest ¹S state is greatly overestimated at this level of calculation. Since spin-orbit coupling effects are not included in the calculations, a detailed comparison with the experimental triplet states is problematic at this stage. We note that the calculated states for the ³F multiplet nonetheless are found between 6277 and 7023 cm⁻¹ as compared to the range of 5165 to 7243 cm⁻¹ observed experimentally for the ³F₂, ³F₃ and ³F₄ submultiplets.

The first 11 triplet states from the CI calculations of the ground state ³H multiplet lie between 0 to 1492 cm⁻¹, which arise from the ligand field splittings. These ligand field splittings in lanthanides are an order of magnitude smaller compared to transition metal ions. It is actually quite reassuring that the overall magnitude of these small effects is reasonably given in the relatively simple CI calculations. For the singlet states, where the comparison is more meaningful without spin-orbit effects, we note that the ligand field splittings in the ¹G multiplet are calculated to be ~ 800 cm⁻¹ as compared to ~600 cm⁻¹ observed experimentally.

Discussion

At this point we have carried out a survey of configuration interaction (CI) calculations of the full dⁿ or fⁿ manifold of states for representative transition metal and lanthanide ions in fluoride and oxide lattice sites using cluster models. The calculations were carried out at a consistent but not computationally demanding level. The cases considered thus far are as follows: Ni²⁺ (3d⁸) ion at an octahedral site in a fluoride lattice (KNiF₃), Nb³⁺ (4d²) ion at an octahedral site in an oxide lattice, Nb³⁺ at a 7-coordinate site in the oxide La₂O₃, and Pr³⁺ (4f²) at a 7-coordinate site in La₂O₃. From this survey, the qualitative features of the multiplets and the ligand field splittings were reproduced with relatively good agreement with experiment for the lower states and larger differences for higher states. From a first principles approach one does not anticipate achieving spectroscopic accuracy when compared to experiment or to ligand field models with a complete set of parameters. Rather the approach would be to compare the theoretical results to known experimental systems and then apply similar types of CI calculations to other combinations of metal dopants and lattice sites of potential interest. Depending on the programmatic needs, one could examine larger classes of lattice hosts at a particular level or concentrate on more accurate calculations on a smaller set of systems.

There are various options in terms of computer codes to perform such calculations on transition metal and lanthanide ions in oxide and fluoride lattices. The MESA code [227] that was developed at Los Alamos over 10 years ago was used for these studies, and it could be used to examine other lattices using clusters of similar size. For larger clusters to represent complex ligands such as sulfate and phosphate one would want to investigate more robust codes. While we have had extensive use of Gaussian98 in recent years, we would also want to investigate other possibilities including MOLPRO (Germany), COLUMBUS (Ohio State and Germany), GAMESS (Iowa State) and MOLCAS (Sweden) as potential options. The capabilities for

treating large numbers of excited electronic states and of including spin-orbit coupling effects would need to be assessed before embarking on such calculations. Based on the limited study to date the ab initio CI approaches appear to offer additional information to complement other approaches such as ligand field models.

Table B-51
Modeling & Simulation Needs for Multi-Photon Phosphors

	Impact	Priority
<i>Addressing MPP Task #6: Modeling I</i>		
1. Pr^{3+} , Tm^{3+} . . . multiplet structures in oxide lattices (cluster models)	1.a. Testing & extending Dicke diagram 1.b. Developing the capability for further testing of actuator/host combinations	1
2. Judd-Ofelt intensity parameters 2.a. Direct calculation or alternatives 2.b. Apply to example systems in 1. 2.c. Semi-empirical or different approach 2.d. Calculation of reduced matrix elements (e.g., Gd^{3+})	2.a. Helpful to identify cascading ions 2.b. Understanding the mechanisms causing different branching ratios (Ω_i 's)	2
3. 1 st -principles approach to the "Energy Gap Law"	3. Understanding the nonradiative decay rates	6
<i>Addressing MPP Task #7: Sugano-Tanabe Diagram for Transition Metal Candidates</i>		
Calculations of Dq for 2 nd & 3 rd row transition metals d^2 ions (Zr, Nb, Mo) in oxide lattices (cluster models)	4. Identifying cascading ions among the transition metals	3
5. Limited CI calculations on (t_{2g}^m , e_g^n) configurations	5. Identify activators to be sensitized by Pr^{3+} or Gd^{3+}	5
<i>Addressing MPP Task #12: Synthesis & Chemical Stability of Fluorides</i>		
6. Total energy calculations for fluorides with oxygen defects (F_i^- , O_i^{2-} , . . .)	6. Lamp manufacturing, phosphor synthesis and maintenance issues	4

Table B-52
Electronic States of Ni^{2+} (d^8) in Octahedral site in KNiF_3

State	Energy (10^3 cm^{-1})	
	Calc	Exptl ^a
3A2	0.0	0.0
3T2	7.18	7.25
3T1	12.4	12.5
1E	19.0	15.5
1T2	25.2	20.9
3T1	28.5	23.8
1A1	29.9	---
1T1	32.3	---
1E	36.5	---
1T2	37.3	---
1A1	70.8	

^a Ref. 15.

Table B-53
Calculated Electronic States of Nb^{3+} (d^2) in Six-Fold Oxide Site in ABO_3 Perovskite and in Seven-Fold Oxide Site in La_2O_3

Six-Fold Site		Seven-Fold Site	
	Energy (10^3 cm^{-1})	State	Energy (10^3)
3T1	0.00	3A	0.00
1E	9.84	1E	11.3
1T2	10.5	3A	17.0
1A1	23.5	1A	17.3
3T2	26.1	3E	19.0
3T1	35.0	3A	23.1
1T2	37.3	3E	25.4
1T1	39.2	1E	26.8
3A2	54.2	1A	27.3
1E	64.1	1A	28.8
1A1	75.8	1E	30.1
		3A	36.9
		3E	43.7
		1E	44.1
		1E	48.8
		1A	53.6
		1A	75.9

Table B-54
Results of $\text{Pr}^{+3} (f^2)$ in 7-Fold Oxide Site (C_{3v} Symmetry) in La_2O_3

Calc	Calc	Expt ^a
State w/o spin-orbit	Energy (cm^{-1})	Energy Range (cm^{-1}) w spin-orbit
	w/o Spin-Orbit	w/Spin-Orbit
^3E (^3H multiplet)	0	
^3A	395	
^3A	439	$^3\text{H}_4$ 0 - 404
^3A	505	$^3\text{H}_5$ 2215 – 2676
^3E	636	$^3\text{H}_6$ 4292 – 4 916
^3E	878	
^3E	1492	
^3A (^3F multiplet)	6277	
^3E	6387	$^3\text{F}_2$ 5165 – 5272
^3A	6584	$^3\text{F}_3$ 6479 - 6612
^3E	6848	$^3\text{F}_4$ 6949 - 7243
^3A	7023	
^3E (^3P multiplet)	27 895	$^3\text{P}_0$ 20 274
^3A	28 949	$^3\text{P}_1$ [20 723]
^1G multiplet	7 045 – 7 879	9 771 – 10 364
^1D multiplet	20 653 - 22 035	16 365 – 16 930
^1I multiplet	24 472 – 27 017 017 017	20 701 – 21 953
^1S multiplet	62 035	[46 608]

^a Ref. 16

References

1. C.R. Ronda, J. Alloys and Compounds **225** (1995) 534.
2. A.M. Srivastava, D.A. Doughty and W.M. Beers, J. Electrochem. Soc. **143** (1996) 4113.
3. A.M. Srivastava and W.M. Beers, J. Lumin. **171** (1997) 285.
4. L. van Pieterse, M. Heeroma, E. de Heer, and A. Meijerink, J. Lumin. **91** (2000) 177.
5. H.E. Hoefdraad, J. Solid State Chem. **15** (1975) 175.
6. H.G. Craighead, J.C. White et al. J. Vac. Sci. Technology B **1** (1983) 1186.
7. W. Hayes and A.M. Stoneham, 'Crystals with the fluorite structure', Ed. W. Hayes (Clarendon, Oxford, 1974), p.185.
8. T. Williams, K.S. Song, W.L. Faust and C.H. Leung, Phys. Rev. B **33** (1986) 7232.
9. K. Tanimura, T. Katoh and N. Itoh, Phys. Rev. B **40** (1989) 1282.
10. R.T. Wegh, H. Donker, A. Meijerink, J. Holsa, R.-J. Lamminmaki, Phys. Rev. B **56** (1997) 13841.
11. K.H. Yang and J.A. DeLuca, Phys. Rev. B **17** (1978) 4246.
12. D.A. Patterson and R.G. Fuller, Phys. Rev. Lett. **18** (1967) 1123.
13. B.G. Gorshkov, S. Epifanov et al., Kvant Electron. (Moscow) **6** (1979) 2415 [Sov. J. Quantum Electron. **9** (1980) 1420].
14. K. Vogler, I. Kluft, T. Schroeder et al., Proc. SPIE-Int. Soc. Opt. Eng. **4102** (2000) 255.
15. V. Liberman, M. Rotschild, J.H. Sedlacek et al., Proc. SPIE-Int. Soc. Opt. Eng. **4000** (2000) 488.
16. R.C. Preston, C. Brookes, F.W.J. Clutterbuck, J. Phys. E **13** (1980) 1206.
17. O.O. Glazunov, Khim. Fiz. **13** (1994) 141.
18. T.S. Lyubarskaya, A.M. Pukhov, Zh. Prikl. Spectrosk. **48** (1988) 484.
19. H. Hosono, M. Mizuguchi et al., J. Appl. Phys. **85** (1999) 3038.
20. A. Bohun, L. Roskocova, M. Svantner and J. Foldvari, Czech. J. Phys., Sect. B **28** (1978) 795.

21. V.A. Arhangelskaya, V.M. Reiterov, L.M. Trofimov, Zhurnal Prikl. Spectrosk. **32** (1980) 103.
22. R. Rauh, E. Liebold, Phys. Stat Sol. A **64** (1981) K165.
23. C. Feldmann, T. Juestel, C.R. Ronda, D.U. Wiechert, J. Lumin. **92** (2001) 245.
24. J.A. Groenink and G. Blasse, J. Solid State Chemistry **32** (1980) 9.
25. V. Denks, T. Savikhina and V. Nagirnyi, Appl. Surf. Science **158** (2000) 301.
26. P.W. Levy, J.A. Kierstead, C. Woody, NIST Spec. Publ. **775** (1989) 49.
27. R.T. Wegh, Thesis Utrecht University, 1999.
28. A.M. Stoneham, *Theory of Defects in Solids*. Oxford, Clarendon Press (1975).
29. B.R. Sever, N. Kristianpoller, F.C. Brown, Phys.Rev.B 34, (1986) 1257.
30. N. Kristianpoller, A. Rehav, M. Israeli, phys.stat.sol. (b) 74, (1976) 245.
31. F.C. Brown, B.R. Sever, N. Kristianpoller, Phys.Scripta 35, (1987) 582.
32. W.A. Runciman, B. Srinivasan, D.D. Richardson, Aust.J.Phys. 38, (1985) 741.
33. A. Clark, J.L. Marin, R. Rodriguez, C. Ruiz-Mejia, Cryst.Latt.Def. and Amorph. Mat. 10, (1984) 185.
34. Ch. Lushchik, J. Kolk, A. Lushchik, N. Lushchik, phys.stat.sol. (a) 86, (1984) 219.
35. P. Kofstad, *Nonstoichiometry, Diffusion, and Electrical Conductivity in Binary Metal Oxides*. New York-London-Sidney-Toronto, Wiley-Interscience (1978), p.55-58.
36. G. Pacchioni, Sol.State Sciences 2, (2000) 161.
37. J.M. Bunch, Phys.Rev.B 16, (1977) 724.
38. M.V. Nikanovich, A.P. Shkadarevich, Yu.S. Tipenko, D.S. Umreiko, J.Appl. Spectr. 58, (1993) 187.
39. N. Kristianpoller, B. Trieman, J.Physique C 41, (1980) C6-109.
40. I Nuritdinov, K. Turdanov, N.M. Mirinoyatova, V.M. Reiterov, Opt.Spectr. 81, (1996) 392.
41. J.M. Flaherty, J.Electrochem.Soc. 128, (1981) 131.
42. W. Tews, U. Vater, G. Kunzler, U. Sasum, A. Kloss, phys.stat.sol. (a) 130, (1992) K131.

43. O. Tada, K. Tominaga, T. Kondo, Y. Kondo, J.Electrochem.Soc. 131, (1984) 1365.
44. F.M. Ryan, J.Lumin. 24/25, (1981) 827.
45. W. Lehmann, J.Electrochem.Soc. 130, (1983) 426.
46. D.V. McCaughan, R.A. Kushner, V.T. Murphy, Phys.Rev.Lett. 30, (1973) 614.
47. W. Lehmann, F.M. Ryan, A.S. Manocha, W. McAllister, J.Electrochem.Soc. 130, (1983) 171.
48. S. Mrowec, *Defects and Diffusion in Solids* (Materials Science Monographs, 5). Elsevier, Amsterdam-Oxford-New York (1980), pp. 110-113.
49. M. J. Gillan, Phil.Mag. A 43, (1981) 301.
50. N.N. Greenwood, *Ionic Crystals, Lattice Defects and Nonstoichiometry*. London, Butterworths (19??), pp.76-85.
51. R.J.D. Tilley, *Principles and Applications of Chemical Defects*. Stanley Thornes (Publishers) Ltd. (1998), p. 12.
52. D. Pooley, Sol.St.Comm. 3, (1965) 241; H.N. Hersh, Phys.Rev. 148, (1966) 928.
53. K. Schwartz, Nucl.Instr.Methods in Phys.Res.B 107, (1996) 128.
54. B. Trieman, N. Kristianpoller, phys.stat.sol. (b) 105, (1981) 739.
55. M.N. Kabler, R.T. Williams, Phys.Rev.B 18, (1978) 1948.
56. C.R.A. Catlow, M.J. Norgett, J.Physique C 34, (1973) C9-45.
57. E.K. Zavadovskaya, A.T. Ovcharov, M.I. Kalinin, V.M. Lisitsyn, Sov.Phys.J. n5, (1972) 129.
58. N. Kristianpoller, Nucl.Instr.Methods in Phys.Res.B 1, (1984) 198.
59. N. Kristianpoller, Phys.Scripta 36, (1987) 179.
60. J.L. Allen, N. Seifert, Y. Yao, R.G. Albridge, A.V. Barnes, N.H. Tolk, A.M. Strauss, R.C. Linton, R.R. Kamenetzky, J. A. Vaughn, M.M. Finckenor, *LDEF: 69 Months in Space*. Third Post-Retrieval Symposium, part 3. Nat.Aeronautics and Space Administration, Hampton, VA, Langley Res.Center (1995), pp.1131-1145.
61. D.F. Heath, P.A.Sacher, Appl.Opt. 5, (1966) 937.
62. W. Hayes, R.F. Lambourn, phys.stat.sol. (b) 57, (1973) 693.
63. P.J. Call, W. Hayes, J.P. Scott, A.E. Hughes, J.Phys.C:Sol.State Phys. 7, (1974) 2417.

64. G. Baldacchini, ENEA Frascati Research Center, Roma, Italy (private communications).
65. G. Pacchioni, P. Pescarmona, *Surf.Sci* 412/413, (1998) 657.
66. M.M. Mikhailov, N.Ya. Kuznetsov, L.E. Ryabchikova, *Inorg.Mat.* 24, (1988) 1136.
67. G.K. Walters, T.L. Estle, *J.Appl.Phys.* 32, (1961) 1854.
68. U. Vater, W. Tews, U. Sasum, *phys.stat.sol. (a)* 130, (1992) K221.
69. L.N. Aleksandrov, V.D. Zolotov, U.S. Mordyuk, *Inorg.Mat.* 12, (1976) 1639.
70. P.H. Holloway, T.A. Trottier, B. Abrams, C. Kondoleon, S.L. Jones, J.S. Sebastian, W.J. Thomas, H. Swart, *J.Vac.Sci.Technol. B* 17, (1999) 758.
71. K. Li, D. Wang, F. Wu, T. Xie, T. Li, *Mat.Chem.Phys.* 64, (2000) 269.
72. M.R.V. Sahyun, R.G. Brisbois, *J.Appl.Phys.* 59, (1986) 2189.
73. C.H. Seager, *Appl.Phys.Lett.* 73, (1998) 85.
74. Swart, H.C., J.S. Sebastian, T.A. Trottier, S.L. Jones, and P.H. Holloway (1996) Degradation of zinc sulfide phosphors under electron bombardment. *J. Vacuum Sci. Technol. A* **14**, 1697-1703.
75. Sebastian, J.S., H.C. Swart, T.A. Trottier, S.L. Jones, and P.H. Holloway (1997) Degradation of ZnS field-emission display phosphors during electron-beam bombardment. *J. Vacuum Sci. Technol. A* **15**, 2349-2353.
76. Abrams, B.L., T.A. Trottier, H.C. Swart, E. Lambers, and P.H. Holloway (1998) Electron beam degradation of sulfide-based thin film phosphors for field emission flat panel displays. *Mater. Res. Soc. Symposium Proc.* **508**, 261-267.
77. Darici, Y., P.H. Holloway, J. Sebastian, T. Trottier, S. Jones, and J. Rodriguez (1999) Electron beam dissociation of CO and CO₂ on ZnS thin films. *J. Vacuum Sci. Technol. A* **17**, 692-697.
78. Holloway, P.H., T.A. Trottier, J. Sebastian, S. Jones, X.-M. Zhang, J.-S. Bang, B. Abrams, W.J. Thomes, and T.-J. Kim (2000) Degradation of field emission display phosphors. *J. Appl. Phys.* **88**, 483-488.
79. Abrams, B.L. W. Roos, P.H. Holloway and H.C. Swart (2000) Electron beam-induced degradation of zinc sulfide-based phosphors. *Surface Science* **451**, 174-181.
80. Z. Yang, J. H. Lin, and M. Z. Su, Photon cascade emission of Pr³⁺ in LnBaB₉O₁₂ (Ln = La, Y), *Science in China Series B-Chemistry* 44, 1 (2001).
81. A. M. Svivastava, D. A. Doughty, and W. W. Beers, On the vacuum-ultraviolet excited luminescence of Pr³⁺ in LaB₃O₆, *J. Electrochem. Soc.* 144, L190 (1997).

82. A. M. Srivastava, D. A. Doughty, and W. W. Beers, Photon cascade luminescence of Pr^{3+} in $\text{LaMgB}_5\text{O}_{10}$, *J. Electrochem. Soc.* 143, 4113 (1996).
83. A. M. Srivastava and W. W. Beers, Luminescence of Pr^{3+} in $\text{SrAl}_{12}\text{O}_{19}$: observation of two photon luminescence in oxide lattice, *J. Lumin.* 71, 285 (1997).
84. X.J. Wang, S. Huang, L. Lu, W.M. Yen, A.M. Srivastava, A.A. Setlur, ‘Energy transfer in Pr^{3+} - and Er^{3+} -codoped $\text{CaAl}_{12}\text{O}_{19}$ crystal” *Opt. Commun.* 195, 405 (2001).
85. E. van der Kolk, P. Dorenbos, C.W.E van Eijk, ‘Vacuum ultraviolet excitation of $^1\text{S}_0$ and $^3\text{P}_0$ emission of Pr^{3+} in $\text{Sr}_{0.7}\text{La}_{0.3}\text{Al}_{11.7}\text{Mg}_{0.3}\text{O}_{19}$ and SrB_4O_7 ”, *J. Phys-Cond. Matter*, 13 5471 (2001).
86. Inorganic Crystal Structure Database, Gmelin Institut, Fachinformationszentrum, Karlsruhe (1998).
87. B. Rupp, B. Smith and J. Wong, SEXIE - a microcomputer program for the calculation of coordination shells and geometries, *Computer Physics Communications* 67, 543 (1992), A.E. Tabor-Morris and B. Rupp, SEXIE 3.0-an updated computer program for the calculation of coordination shells and geometries, *Computer Physics Communications* 82, 23 (1994).
88. P. Dorenbos, ‘The $4f^n \rightarrow 4f^{n-1} 5d$ transitions of the trivalent lanthanides in halogenides and chalcogenides”, *J. Lumin.* 91, 91 (2000).
89. P. Dorenbos, ‘The 5d level positions of the trivalent lanthanides in inorganic compounds,” *J. Lumin.* 91, 155 (2000).
90. J. M. F. van Dijk and M F. H. Schuurmans, ‘On the nonradiative and radiative decay rates and a modified exponential energy gap law for $4f-4f$ transitions in rare-earth ions”, *J.Chem. Phys.* 78, 5317 (1983).
91. M F. H. Schuurmans and J. M. F. van Dijk, ‘On radiative and non-radiative decay times in the weak coupling limit”, *Physica* 123B, 131 (1984).
92. S. A. Payne and C. Bibeau, ‘Picosecond nonradiative processes in neodymium-doped crystal and glasses: Mechanisms for the energy gap law”, *J. Lumin.* 79, 143 (1998).
93. A. A. Setlur, H. A. Comanzo, A. M. Srivastava, et al., Advances in the development of quantum splitting phosphors, MRS Symposium *Luminescence and Luminescent Materials* (to be published).
94. A. A. Kaminskii, *Crystalline Lasers: Physical Processes and Operating Schemes*, CRC Press, Boca Raton, FL (1996).
95. W. W. Piper, J. A. DeLuca, and F. S. Ham, ‘Cascade fluorescent decay in Pr^{3+} -doped fluorides: achievement of quantum yield greater than unity for emission of visible light”, *J. Lumin.* 8, 344 (1974).

96. E. van der Kolk, ‘Vacuum ultraviolet phosphors for lamps and displays, photon cascade emission of Pr^{3+} and optimisation of Mn^{2+} based phosphors,’ Ph.D. dissertation, Delft University of Technology (2001).
97. C. Gorller-Walrand and K Binnemans, ‘Spectral Intensities of f-f Transitions,’ in *Handbook of the Physics and Chemistry of Rare Earths, Vol 25*, ed. K.A. Gschneidner Jr. and L. Eyring, (Elsevier, Amsterdam, 1998) p. 101-264.
98. C.K. Jorgensen and R. Reisfeld, *J. Less Common Metals*, **93**, 107 (1983).
99. A.F. Kirby and R.A. Palmer, *Inorg. Chem.*, **20** 1030, 4219 (1981).
100. F.S. Richardson, *Chem. Phys. Lett.*, **86**, 47 (1982).
101. R. Reisfeld, G. Katz, C. Jacoboni, R. DePape, M.G. Drexhage, R.N. Brown and C.K. Jorgensen, *J. Solid State Chem.* **48**, 323 (1983).
102. M. Arai, N Matsuda and M. Tametami, *J. Alloys Comp.* **192** 45 (1993).
103. C. de Mello Donega, A. Meijerink and G. Blasse, *J. Phys. Chem. Sol.* **56**, 673 (1994).
104. E. G. Reut and A.I. Ryskin, *Phys. Stat. Sol.* **A17**, 47 (1973).
105. R.T. Wegh, H. Donker, K.D. Oskam and A. Meijerink, *Science* **283** (1999) 664.
106. R.T. Wegh, H. Donker, K.D. Oskam and A. Meijerink, *J. Lumin.* **82** (1999) 93.
107. R.T. Wegh, E.V.D. van Loef and A. Meijerink, *J. Lumin.* **90** (2000) 111.
108. K.D. Oskam and A. Meijerink, to be published.
109. C. Feldmann, T. Juestel, C. R. Ronda, D.U. Wiechert, *J. Lumin.* **92** (2001) 245.
110. W. Barendswaard, J.H. van der Waals, *Molec. Phys.* **59** (1986) 337.
111. C.K. Jorgensen, *Progr. Inorg. Chem.* **12** (1970) 101.
112. G. Blasse, *Structure and Bonding* **42** (1980) 1.
113. C.W. Struck, W.H. Fonger, *Phys. Rev. B* **4** (1971) 22.
114. H.E. Hoefdraad, *J. Solid State Chem.* **15** (1975) 175.
115. C.W. Struck, W.H. Fonger, in: ‘Optical properties of Excited States in Solids, NATO ASI Ser. B (1992) 301.
116. E. Nakazawa, *Chem. Phys. Lett.* **56** (1978) 161.
117. E. Nakazawa, *J. Lumin.* **18/19** (1979) 272.

118. L. van Pieterse, M. Heeroma, E. de Heer, A. Meijerink, J. Lumin. **91** (2000) 177.
119. L. van Pieterse, A. Meijerink, J. Alloys and Compounds **300-301** (2000) 426.
120. N. Guerassimova, N. Garnier, C. Dujardin, A.G. Petrosyan, C. Pedrini, Chem. Phys. Lett. **399** (2001) 197.
121. A. Ranfagni, D. Mugnai, M. Bacci, G. Viliani, M.P. Fontana, Adv. Physics **32** (1983) 823.
122. G. Blasse, Progress in Solid State Chem. **18** (1988) 79.
123. A. Fukuda, Phys. Rev. B **1** (1970) 4161.
124. H. H. Folkerts, M.A. Hamstra, G. Blasse, Chem. Phys. Lett. **246** (1995) 135.
125. K.P. Oboth, F.J. Lohmeier, F. Fischer, Phys. Stat. Sol. (b) **154** (1989) 789.
126. Z. Hao, Y. Yang, X. Yin, B. Yu, Z. Guan, J. Lumin. **40/41** (1988) 700.
127. K.D. Oskam, R.T. Wegh and A. Meijerink, to be published.
128. M. Messori, A. Scacco, Solid State Comm. **76** (1990) 5.
129. P. Dorenbos, J. Lumin. **91** (2000) 155.
130. A. Ellens, A. Meijerink, G. Blasse, J. Lumin. **59** (1994) 293.
131. T. Hoshina, S. Kuboniwa, J. Phys. Soc. Jpn. **31** (1971) 828.
132. J. Rubio O., J. Phys. Chem. Solids **52** (1991) 101.
133. E. Loh, Phys. Rev. **147** (1966) 332.
134. L.R. Elias, Wm.S. Heaps, W.M. Yen, Phys. Rev. B **8** (1973) 4989.
135. T. szczurek and M. Schlesinger, in: Proceedings of the International Symposium of Rare Earth Spectroscopy, edited by B. Jezowska-Trzebiatowska, J. Legendziewicz and W. Strek (World Scientific, Singapore, 1985) p. 309.
136. K.H. Yang and J.A. deLuca, Appl. Phys. Lett. **29** (1976) 499.
137. L.I. Devyatkova, O.N. Ivanova, K.B. Seirenyan, S.A. Tamazyan, S.P. Chernov, Sov. Phys. Dokl. **30** (1985) 687.
138. E. Sarantopoulou, A.C. Cefalas et al., Optics. Commun. **107** (1994) 104.
139. J.C. Krupa and M. Queffelec, J. Alloys and Compounds **250** (1997) 287.
140. J. Becker, J.Y. Gesland, et al., J. Lumin. **78** (1998) 91.

141. P. Dorenbos, Phys. Rev. B **62** (2000) 15640.
142. P. Dorenbos, Phys. Rev. B **62** (2000) 15650.
143. P. Dorenbos, Phys. Rev. B **64** (2001) 125117/1.
144. R.T. Wegh, W. van Klinken and A. Meijerink, Phys. Rev. B P. Dorenbos, Phys. Rev. B **64** (2001) 045115/1.
145. L. van Pieterse, R. T. Wegh, A. Meijerink and M.F. Reid, J. Chem. Phys. **115** (2001) 9382.
146. G. Blasse and B.C. Grabmaier, Luminescent Materials (Springer Verlag, Berlin, 1994), p.45.
147. L. van Pieterse, M.F. Reid, R.T. Wegh, S. Soverna and A. Meijerink, Phys. Rev. B. **65** (2002) 045113/1.
148. L. van Pieterse, M.F. Reid, G.W. Burdick and A. Meijerink, Phys. Rev. B, Phys. Rev. B **65** (2002) 045114/1.
149. R.T. Wegh and A. Meijerink, to be published.
150. B. Henderson and G.F. Imbusch, Optical Spectroscopy of Inorganic Solids, (Clarendon Press, Oxford, 1989).
151. R.T. Wegh, H. Donker and A. Meijerink, Phys. Rev. B **56** (1998) R13841.
152. M.F. Reid, L. van Pieterse, R.T. Wegh and A. Meijerink, Phys. Rev. B **62** (2000) 14744.
153. L. van Pieterse, M.F. Reid and A. Meijerink, Phys. Rev. Lett., in press.
154. M. Bredol, J. Merikhi and C. Ronda, Ber. Bunsenges. Phys. Chem. **96** (1992) 1770.
155. C. Pedrini, M. Moine et al., Chem. Phys. Lett. **206** (1993) 470.
156. Strehlow and Cook, J. Phys. Chem. Ref. Data, **2** (1973) 163.
157. J.H. Beaumont, W. Hayes, D. Kirk, G.P. Summers, Proc. Roy. Soc., Ser. A **315** (1970) 69-97.
158. Dorenbos, P. J. Luminescence 91(2000) 91-106, and 155-176.
159. Yang, et al., Photon cascade luminescence of Gd³⁺ in GdBaB₉O₁₆, J. Alloys and Compounds 308, 94 (2000).
160. Van Pieterse, L., J. Luminescence 91(2001)177.

161. C. Göller-Walrand and K. Binnemans, Spectral intensities of f-f transitions, *Handbook on the Physics and Chemistry of Rare Earths*, vol. 25 (1998), p. 101, and references cited therein.
162. See, for example, Yu. V. Orlovskii, T. T. Basiev, I. N. Vorob'ev, et al., Temperature dependencies of excited states lifetimes and relaxation rates of 3-5 phonon (4-6 μm) transitions in the YAG, LuAG and YLF crystals doped with trivalent holmium, thulium, and erbium, *Opt. Mater.* 18, 355 (2002).
163. J. M. F. van Dijk and M F. H. Schuurmans, On the nonradiative and radiative decay rates and a modified exponential energy gap law for 4f-4f transitions in rare-earth ions, *J. Chem. Phys.* 78, 5317 (1983).
164. M F. H. Schuurmans and J. M. F. van Dijk, On radiative and non-radiative decay times in the weak coupling limit, *Physica* 123B, 131 (1984).
165. S. A. Payne and C. Bibeau, Picosecond nonradiative processes in neodymium-doped crystal and glasses: Mechanisms for the energy gap law, *J. Lumin.* 79, 143 (1998).
166. Burns, R.G. (1993) *Mineralogical Applications of Crystal Field Theory*. Cambridge University Press, Cambridge.
167. Moore, C.E. (1952) Atomic energy levels. National Bureau of Standards Circular 467, Vol. II.
168. Sugano, S., Y. Tanabe, and H. Kamimura (1970) *Multiplets of Transition-Metal Ions in Crystals*. Academic Press, New York, p. 107.
169. X.-J. Wang, S. Huang, L. Lu, W.M. Yen, A.M. Srivastava, A.A. Setlur, *Opt. Commun.* **195**, 405 (2001).
170. D. L. Dexter, *J. Chem. Phys.* **21**, 836, 1953.
171. T. Kushida, *J. Phys. Soc. (Japan)* **34**, 1334 (1973).
172. R. T. Wegh, H. Donker, K.D. Oskam, A. Meijerink, *J. Lumin.* **82**, 93 (1999).
173. R.T. Wegh, E.V.D. van Loef, and A. Meijerink, *J. Lumin.* 90, 111 (2000) (see also E. van der Kolk, "Vacuum ultraviolet phosphors for lamps and displays, photon cascade emission of Pr^{3+} and optimisation of Mn^{2+} based phosphors," Ph.D. dissertation, Delft University of Technology (2001).
174. R.S. Meltzer and R.L. Cone, *Phys. Rev. B* **13**, 2818 (1976).
175. Z. Yang, J.H. Lin, and M.Z. Su, 'Photon cascade emission of Pr^{3+} in $\text{LnBaB}_9\text{O}_{16}$ ($\text{Ln}=\text{La}, \text{Y}$)', *Science in China Series B-Chemistry* **44**, 1 (2001).
176. A.M. Srivastava, D.A. Doughty, and W.W. Beers, 'Photon cascade luminescence of Pr^{3+} in $\text{LaMgB}_5\text{O}_{10}$,' *J. Electrochem. Soc.* **144**, 4113 (1996).

177. A.M. Srivastava, D.A. Doughty and W.W. Beers, "On the vacuum-ultraviolet excited luminescence of Pr^{3+} in LaB_3O_6 ," *J. Electrochem. Soc.* **144**, L190 (1997).
178. K.C. Mishra and K.H. Johnson, "The design of multi-photon phosphors via modified cascade emission from first-principles electronic structure calculation," Osram Sylvania Technical Report TR95-R/NL20024-ED (1995).
179. J.C. Slater, *The self-consistent field for molecules and solids*, Vol. 4 (McGraw Hill, NY) 1974.
180. S. Sugano, Y. Tanabe and H. Kamimura, *Multiplets of transition metal ions in crystals* (Academic Press, New York), 1970.
181. H. Sambe and R.H. Felton, *International J. of Quantum Chemistry* **10**, 155 (1976).
182. R.D. Shannon, *Acta Cryst.* **A32**, 751 (1976).
183. J.C. Slater, *Quantum Theory of Molecules and Solids*, Vol. 2 (McGraw Hill, New York) 1965.
184. F. A. Kröger, *Some aspects of the luminescent studies* (Elsevier, 1948).
185. K. H. Butler, *Fluorescent lamp phosphors* (Pennsylvania State University Press, 1980).
186. G. H. Dieke, *Spectra and energy levels of rare earth ions in crystals* (Interscience, 1968).
187. C. A. Morrison and R. P. Leavitt, *Handbook on the Physics and Chemistry of Rare Earth Ions*, Vol. 5 (ed. K. A. Gschneidner, Jr. and L. Eyring, North Holland, 1982).
188. G. H. Blasse and B. C. Grabmaier, *Luminescent materials* (Springer-Verlag, 1994).
189. S. Shinoya and W. M. Yen, *Phosphor Handbook* (CRC, 1999).
190. K. C. Mishra and K. H. Johnson, OSI Technical Reports TR-95-R/NLS0024-ED and TR-95-R/NLS0051-CH.
191. M. Zachau, OSI Internal Report, EC/L-M 10/96).
192. Berlman, I.B., *Handbook of Fluorescence Spectra of Aromatic Molecules*, Academic Press, New York, 1965.
193. Pappalardo, R., "Intersystem Crossing in Complex Molecules", and Jortner, J., "Electronic Relaxation in Large Molecules", in *Radiationless Processes*, ed. B. Di Bartolo, Plenum Press, New York, 1980.
194. *Molecular Luminescence*, Lim, E.C., ed., W. A. Benjamin Press, Inc. New York, 1969.
195. S. Singh, R.G.Smith, and L.G. Van Uitert, "Stimulated Emission Cross Section And Fluorescent Quantum Efficiency Of Nd^{3+} In Yttrium Aluminum Garnet At Room Temperatures," *Phys. Rev. B* 2566-2572 (1974).

196. B.M. Walsh, N.P. Barnes, and B. Di Bartolo, 'Branching Ratios, Cross Sections, And Radiative Lifetimes Of Rare Earth Ions In Solids; Application To Tm^{3+} And Ho^{3+} ,' *J. Appl. Phys.* **83** 2772-2787 (1998).
197. N.P. Barnes, E.D. Filer, C.A. Morrison, and C.J. Lee, 'Ho:Tm Lasers I: Theoretical,' *IEEE J. Quant. Elect.* **QE-32** 92-101 (1996).
198. Dieke, G.H., *Spectra and Energy Levels of Rare Earth Ions in Crystals*, Crosswhite and Crosswhite, eds., Interscience Press, New York, 1968.
199. See Multiphoton Phosphor Feasability Research Project, Session 1, notes from Prof. Meijerink's talk in May, 2001.
200. Pappalardo, R., *J. Luminescence* **14**, 159, 1976.
201. Dorenbos, P. *J. Luminescence* **91**(2000) 91-106, and 155-176.
202. Meijerink, A. and Wegh, R. T., Proceedings of IREC'98, Freemantle, Australia, 'VUV Spectroscopy of Lanthanides: Extending the Horizons'.
203. C. W. Struck and W. H. Fonger, 'Understanding Luminescence Spectra and Efficiency using W_p and Related Functions', Springer Verlag, Heidelberg, 1991, Chapter 12 and references therein.
204. J.B. Gruber, W.F. Krupke, J.M. Poindexter, *J.Chem.Phys.* **41**, (1964) 3363.
205. R. Pappalardo, *J.Lumin.* **14** (1976) 159.
206. O. Greis and J.M. Haschke, 'Rare Earth Fluorides,' *Handbook on the Physics and Chemistry of Rare Earths*, ed. K.A. Gschneider, Jr. and L. Eyring, North-Holland, 1982.
207. R. Lebullenger and M. Poulain, 'Room Temperature Synthesis of Fluoride Glasses,' *J. Non-Cryst. Sol.*, **184**, 166-171 (1995).
208. A. Konishi, R. Kanno and Y. Kawamoto, 'Synthesis of ZrF_4 - BaF_2 - LnF_3 Glasses (Ln = La, Ce, Pr, Nd or Eu) by Combined Process of Sol-Gel and Fluorination,' *J. Alloys and Comp.*, **232**, 53-59 (1996).
209. N. Dupont, A. De Kozak, P.. Gredin and M. Samouel, 'The Crystal Structure of $\text{Ba}_2\text{Cu}_2\text{AlF}_{11}$: a New Structure Type in Copper Fluoride Crystal Chemistry,' *Z. anorg. allg. Chem.*, **624**, 331-334 (1998).
210. M. Saad and M. Poulain, 'Flouride Glass Synthesis by Sol-Gel Process,' *J. Non-Cryst. Sol.*, **184**, 352-355 (1995).
211. P. Melnikov, M. Nalin and Y. Messaddeq, 'Scandium Fluorides,' *J. Alloys and Comp.*, **262-263**, 296-298 (1997).


212. X. Xun, S. Feng and R. Xu, 'Hydrothermal Synthesis of Complex Fluorides LiHoF_4 and LiErF_4 with Scheelite Structures under Mild Conditions,' *Mater. Res. Bull.*, **33** [3] 369-375 (1998).
213. S. Fujihara, S. Ono, Y. Kishiki, M. Tada and T. Kimura, 'Sol-gel Synthesis of Inorganic Complex Fluorides Using Trifluoroacetic Acid,' *J. Fluor. Chem.*, **105**, 65-70 (2000).
214. GULP program, J. D. Gale, 'General Utility Lattice Program,' Royal Institution and Imperial College, London, 1992 –1994.
215. D. H. Gay and A. H. Rohl, *J. Chem. Soc. Faraday Trans.* **91**, 925 (1995).
216. L. Miniverni, R. W. Grimes, J. A. Kilner, and K. E. Sickafus, *J. Materials Chem.* **10**, 2349 (2000).
217. S. M. Woodley, P. D. Battle, C. R. A. Catlow, and J. D. Gale, *J. Phys. Chem. B* **105**, 6824 (2001).
218. G. Kresse and J. Furthmuller, *Computational Materials Science* **6**, 15 (1996) and references therein.
219. G. Pacchioni, *Sol. State. Sciences* **2**, 161 (2000).
220. T. Suzuki and M. Fujimoto, *J Appl. Phys.* **89**, 5622 (2001).
221. W. Windl, T. J. Lenosky, J. D. Kress, and A. F. Voter, *Nuclear instruments and Methods in Physics Research B* **141**, 61 (1998).
222. E. Lorda, F. Illas and P. S. Bagus, *Chem. Phys. Lett.* **256**, 377 (1996).
223. C de Graaf, R. Broer and W. C. Niewpoort, *Chem. Phys.* **208**, 35 (1996).
224. K. Wissing, M. T. Barriuso, J. A. Arambur and M. Moreno, *J. Chem. Phys.* **111**, 10217 (1999).
225. P. J. Hay and W. R. Wadt, *J. Chem. Phys.* **82**, 299 (1985).
226. W. Liu and M. Dolg, *Phys. Rev. A* **57**, 1721 (1998).
227. MESA program, P.W. Saxe, R. L. Martin, M. Page and B. H. Lengsfeld III, 1990.
228. K. Knox, R. G. Shulman and S. Sugano, *Phys. Rev.* **130**, 512 (1963).
229. O. K. Moune, M. D. Faucher, C. K. Jayasankar and A. J. Lejus, *J. Luminesc.* **85**, 59 (1999).

About EPRI

EPRI creates science and technology solutions for the global energy and energy services industry. U.S. electric utilities established the Electric Power Research Institute in 1973 as a nonprofit research consortium for the benefit of utility members, their customers, and society. Now known simply as EPRI, the company provides a wide range of innovative products and services to more than 1000 energy-related organizations in 40 countries. EPRI's multidisciplinary team of scientists and engineers draws on a worldwide network of technical and business expertise to help solve today's toughest energy and environmental problems.

EPRI. Electrify the World

© 2003 Electric Power Research Institute (EPRI), Inc. All rights reserved. Electric Power Research Institute and EPRI are registered service marks of the Electric Power Research Institute, Inc. EPRI. ELECTRIFY THE WORLD is a service mark of the Electric Power Research Institute, Inc.

 Printed on recycled paper in the United States of America

I007799